UNDERSTANDING CALCIUM SIGNALING PATHWAY MEDIATED BY CALMODULIN AND RELATED PROTEINS IN *NEUROSPORA CRASSA*

A

thesis submitted in partial fulfilment of the

requirements for the award of the degree of

DOCTOR OF PHILOSOPHY

by

VIJYA LAXMI

Roll No. 11610614

Department of Biosciences and Bioengineering

Indian Institute of Technology, Guwahati

Guwahati-781 039, Assam, India

December 2016

भारतीय प्रौद्योगिकी संस्थान गुवाहाटी
INDIAN INSTITUTE OF TECHNOLOGY GUWAHATI
Department of Biosciences and Bioengineering
Guwahati – 781 039

DECLARATION

I do hereby declare that the content embodied in this thesis entitled **"Understanding Calcium Signaling Pathway Mediated by Calmodulin and Related Proteins in *Neurospora crassa*"** is the result of investigations carried out by me in the Department of Biosciences and Bioengineering, Indian Institute of Technology Guwahati, Guwahati-781039, Assam, India, for the award of degree of *Doctor of Philosophy in Biosciences and Bioengineering*, under the supervision of **Dr. Ranjan Tamuli** and **Prof. Utpal Bora**. The research work presented in this thesis is original and has not been submitted in part or full for any degree or diploma to any institute or university to the best of my knowledge and belief.

Guwahati
December, 2016

VIJYA LAXMI
Roll - 11610614

भारतीय प्रौद्योगिकी संस्थान गुवाहाटी
INDIAN INSTITUTE OF TECHNOLOGY GUWAHATI
Department of Biosciences and Bioengineering
Guwahati – 781 039

CERTIFICATE

This is to certify that the research work in this thesis entitled **"Understanding Calcium Signaling Pathway Mediated by Calmodulin and Related Proteins in *Neurospora crassa*"** has been carried out at the Indian Institute of Technology Guwahati, Guwahati-781039, Assam, India, by **Ms. Vijya Laxmi** (Roll No. 11610614), for the award of degree of *Doctor of Philosophy in Biosciences and Bioengineering* under our supervision. The outcome of the research work presented in this thesis is original and has not been submitted in part or full for any degree or diploma to any other university or institute.

Main Supervisor: **Dr. Ranjan Tamuli**
Associate Professor
Department of Biosciences and Bioengineering
IIT Guwahati

Guwahati
December, 2016

Co-Supervisor: **Prof. Utpal Bora**
Professor
Department of Biosciences and Bioengineering
IIT Guwahati

To

my loving parents

Mrs. Anita Keshri

&

Mr. Anjani Keshri

	Pages
Table of Contents	**i-v**
List of Figures	**vi-ix**
List of Tables	**x-xi**
List of Abbreviations	**xii-xiv**
Acknowledgments	**xv**
Synopsis	**xvi-xix**
Chapter 1: An introduction to *Neurospora crassa*, calcium signaling and calmodulin	1-24
1.1 The biology of *Neurospora crassa*	1
1.2 The life cycle of *N. crassa*	1-3
1.3 Gene silencing mechanisms in *N. crassa*	4-9
1.3.1 Quelling	4-5
1.3.2 Repeat-induced point mutation	6
1.3.3 Meiotic silencing	7-9
1.4 Calcium signaling in *N. crassa*	9-16
1.5 Calmodulin: the ubiquitous Ca^{2+} sensor protein	17-24
1.5.1 *Saccharomyces cerevisiae* and *Schizosaccharomyces pombe*	18-19
1.5.2 *Aspergillus nidulans*	19
1.5.3 *Candida albicans*	20
1.5.4 *Cryptococcus neoformans*	20-21
1.5.5 *Ceratocystis ulmi*	21
1.5.6 *Magnaporthe grisea*	21-22
1.5.7 *Colletotrichum trifolii* and Colletotrichum sp.	22
1.5.8 *Cochliobolus miyabeanus*	22
1.5.9 *Fusarium oxysporum* and Fusarium sp.	22-23
1.5.10 *Neurospora crassa*	23-24
1.6 Objectives of this study	24

Chapter 2: Materials and Methods 25-51
2.1 Materials 25-38
2.1.1 Chemicals and other materials 25
2.1.2 Bacterial strains 30
2.1.3 Plasmid vectors 30-32
2.1.4 Bacterial media, antibiotics and commonly used solutions 32-36
2.1.5 Solutions for growth, maintenance and crossing of Neurospora strains 36-38
2.2 Methods 39-51
2.2.1 Growth conditions 39
2.2.2 Crosses, fertility and ascospores collection 39
2.2.3 Stock management 39-40
2.2.4 Growth rate experiments 40
2.2.5 Dry weight analysis 41
2.2.6 Aerial hyphae development analysis 41
2.2.7 Hyphal morphology 41
2.2.8 Conidial cell count 41
2.2.9 Carotenoids estimation 41-42
2.2.10 Isolation of sterols and analysis by UV spectrophotometry 42
2.2.11 Assay for calcium sensitivity 42
2.2.12 Assay for UV sensitivity 42-43
2.2.13 Thermotolerance analysis 43
2.2.14 Assay for meiotic silencing 43
2.2.15 Scoring for antibiotic resistance 44
2.2.16 Preparation of competent cells 44
2.2.17 Transformation of competent *E. coli* cells by heat shock 44
2.2.18 Isolation of plasmid DNA from bacterial culture 44-45
2.2.19 Transformation of the *N. crassa* strain by electroporation 45-46
2.2.20 Neurospora genomic DNA isolation 46
2.2.21 Neurospora RNA isolation 46-47
2.2.22 Quantitation of nucleic acids 47
2.2.23 Polymerase Chain Reaction 47-48
2.2.24 Reverse-transcriptase PCR 48

2.2.25 Real-Time PCR 48
2.2.26 Digestion of DNA with restriction endonuclease 48-49
2.2.27 Ligation reactions 49
2.2.28 Site-directed mutagenesis 49
2.2.29 Agarose gel electrophoresis 49-50
2.2.30 Purification of DNA fragments from agarose gels 50
2.2.31 Sequence analysis 50
2.2.32 Databases and softwares used 50-51

Chapter 3: Understanding cellular role of calmodulin and related calcium signaling proteins in *Neurospora crassa* 52-89
3.1 Introduction 52-55
3.2 Results 55-86
3.2.1 NCU04120, NCU04898 and NCU04736 genes encode *cmd*, *trm-9* and *nca-2*, respectively and contain conserved domains 55-63
3.2.2 Effect of the CaM antagonists TFP and CPZ in *N. crassa* 63-71
3.2.3 Generation of the Δ*trm-9*Δ*nca-2* double mutant strain 71-73
3.2.4 The Δ*trm-9*Δ*nca-2* double mutant showed novel colony morphology and reduced conidiation 73-76
3.2.5 The Δ*trm-9*Δ*nca-2* double mutant has a slow growth phenotype and less in dry weight content 77-79
3.2.6 The slow growth phenotype of the Δ*trm-9*Δ*nca-2* mutant strain was not due to a defect in ergosterol biosynthesis 79-80
3.2.7 Carotenoid accumulation in Δ*trm-9*Δ*nca-2* double mutant strain 80-83
3.2.8 The Δ*trm-9*Δ*nca-2* mutant displayed an increased sensitivity to Ca^{2+} and UV stress and reduced viability in the acquisition of thermotolerance 84-86
3.3 Discussion 87-89

Chapter 4: Identification of important amino acid residues of calmodulin and its role in sexual development 90-128

4.1 Introduction 90

4.2 Results 91-126

4.2.1 Construction of the $P_{tcu\text{-}1}$*::cmd::5xGly::V5::gfp* plasmid 91-94

4.2.2 Generation of *cmd*^{RIP} mutant strains 95-112

4.2.3 The *cmd*^{RIP} (26) mutant shows a defect in vegetative growth, aerial hyphae development and carotenoid accumulation 113-118

4.2.4 The *cmd*^{RIP} (26) mutant showed a severe defect ultraviolet survival 118-120

4.2.5 CaM in *N. crassa* is required during meiosis for full fertility 120-126

4.3 Discussion 127-128

Chapter 5: Site-directed mutational analysis of calcium/calmodulin-dependent kinase-2 and expression studies of selected calcium signaling genes 129-174

5.1 Introduction 129-138

5.2 Results 138-172

5.2.1 Site-directed mutational analysis of Ca^{2+}/CaMK-2 138-149

5.2.2 Transformation of pRK-2, pVL-2, pVL-3 and pVL-4 constructs into the Δ*camk-2::hph* strain and confirmation of transformants 150-151

5.2.3 Site-directed mutational analysis of Ca^{2+}/CaMK-2 revealed two important residues serine 247 and threonine 267 152-159

5.2.4 Expression studies of the *cmd*, *trm-9* and *nca-2* gene in selected Ca^{2+}-signaling knockout mutant strains 159-162

5.2.5 Expression studies of selected Ca^{2+}-signaling genes in the Δ*trm-9* and Δ*nca-2* knockout mutant 162-163

5.2.6 Expression studies of *cmd*, *trm-9* and *nca-2* gene in double mutant strains 163-165

5.2.7 Expression profile of selected genes in wild-type, Δ*trm-9*, Δ*nca-2* and Δ*trm-9*Δ*nca-2* strains in response to Ca^{2+} and UV stress 165-172

5.3 Discussion 172-174

Additional data 175-179

Conclusion and Future perspectives 180-181

References 182-211

Publications 212

List of Figures **Pages**

Figure 1.1: The life cycle of *N. crassa* 3

Figure 1.2: Gene silencing pathways in Neurospora 5-6

Figure 1.3: Current model of meiotic silencing in *N. crassa* 8-9

Figure 1.4: Overview of calcium signaling system in *N. crassa* 10

Figure 2.1: Schematic of the pBARGEM7-1 vector 31

Figure 2.2: Schematic of the pRS426PVG/p*tcu-1* vector 32

Figure 2.3: Schematic view of a race tube 40

Figure 3.1 Strategy to generate deletion constructs for generating the *N. crassa* knockout mutants 52

Figure 3.2: Structure of the calmodulin antagonists 53

Figure 3.3: Genomic organization of NCU04120 and NCU04898 genes 56

Figure 3.4: Domain organization of the CaM and TRM-9 proteins 57-58

Figure 3.5: Sequence alignment of CaM and TRM-9 homologues 58-60

Figure 3.6: Phylogenetic analysis of the CaM and TRM-9 proteins 60-62

Figure 3.7: Promoter analysis of *cmd* and *trm-9* genes of *N. crassa* 62-63

Figure 3.8: Effect of TFP and CPZ on apical growth of *N. crassa* 65

Figure 3.9: Effect of TFP and CPZ on hyphal morphology of *N. crassa* 66

Figure 3.10: Effect of TFP and CPZ on growth of aerial hyphae in *N. crassa* 66-67

Figure 3.11: Analysis of carotenoids content of *N. crassa* in the presence of TFP and CPZ 68-69

Figure 3.12: Expression studies of *cmd* gene in the presence of CaM inhibitors 70

Figure 3.13: Effect of TFP and CPZ on sexual development of *N. crassa* 71

Figure 3.14: Construction of Δ*trm-9*Δ*nca-2* double knockout mutant 72

Figure 3.15: PCR analysis for double mutant confirmation. 73

Figure 3.16: Colony morphology of wild-type, Δ*trm-9*, Δ*nca-2* and Δ*trm-9*Δ*nca-2* strains 74

Figure 3.17: Hyphal morphology of wild-type, Δ*trm-9*, Δ*nca-2* and Δ*trm-9*Δ*nca-2* strains 74

Figure 3.18: Aerial hyphae culture of the wild-type, Δ*trm-9*, Δ*nca-2* and Δ*trm-9*Δ*nca-2* strains 75

Figure 3.19: Conidial cell count of wild-type, Δ*trm-9*, Δ*nca-2* and Δ*trm-9*Δ*nca-2* strains 76

Figure 3.20: Apical growth rate of wild-type, Δ*trm-9*, Δ*nca-2* and Δ*trm-9*Δ*nca-2* strains 77

Figure 3.21: Dry weight assay of wild-type Δ*trm-9*, Δ*nca-2* and Δ*trm-9*Δ*nca-2* strains 78

Figure 3.22: Ergosterol is present in the wild-type, Δ*trm-9*, Δ*nca-2* and Δ*trm-9*Δ*nca-2* strains 80

Figure 3.23: Carotenoid accumulation of wild-type, Δ*trm-9*, Δ*nca-2* and Δ*trm-9*Δ*nca-2* strains 81-82

Figure 3.24: Carotenoids accumulation of wild-type, Δ*trm-9*, Δ*nca-2* and Δ*trm-9*Δ*nca-2* strains during Ca^{2+} stress 82

Figure 3.25: Ca^{2+} sensitivity analysis of wild-type, Δ*trm-9*, Δ*nca-2* and Δ*trm-9*Δ*nca-2* strains 85

Figure 3.26: UV spot-test analysis of wild-type, Δ*trm-9*, Δ*nca-2*, Δ*trm-9*Δ*nca-2* and the *upr-1* mutant strain 86

Figure 3.27: Thermotolerance measurement of wild-type, Δ*trm-9*, Δ*nca-2* and Δ*trm-9*Δ*nca-2* strains in induced (44°C) and uninduced (30°C) conditions 86-87

Figure 4.1: Sequence of the *cmd* gene (locus NCU04120) and the primers used for generation and confirmation of the $P_{tcu\text{-}1}$*::cmd::5xGly::V5::gfp* construct 92-93

Figure 4.2: Schematics of generation and transformation of the $P_{tcu\text{-}1}$*::cmd::5xGly::V5::gfp* construct 94

Figure 4.3: PCR amplification of the *cmd* gene from the cmd^{RIP} mutants 99

Figure 4.4: Nucleotide sequence analysis of the endogenous cmd^{RIP} mutant alleles 103-106

Figure 4.5: Nucleotide sequence analysis of the ectopic *cmd*^{RIP} mutant alleles 107-110
Figure 4.6: Alignment of the CaM protein sequence of the wild-type and *cmd*^{RIP} mutant alleles 111-112
Figure 4.7: Expression of the CaM::V5::GFP protein under the P_{tcu-1} in *N. crassa* strains 112
Figure 4.8: Morphology of the *cmd*^{RIP} (26) mutant 113-115
Figure 4.9: The *cmd*^{RIP} (26) mutant showed a slow growth rate 115
Figure 4.10: Aerial hyphae growth of *cmd*^{RIP} (26) mutant 116
Figure 4.11: Carotenoids accumulation in the *cmd*^{RIP} (26) mutant 117
Figure 4.12: Fertility defect in cross homozygous of *cmd*^{RIP} mutant strains 118
Figure 4.13: UV survival assay of the *cmd*^{RIP} (26) mutant 119-120
Figure 4.14: Meiotic silencing assay of the *cmd* gene 121-122
Figure 5.1: Diagram depicting the sequence of events leading to the activation and autophosphorylation of CaMKII 130-131
Figure 5.2: Sequence analysis of the Ca^{2+}/CaM protein 131-132
Figure 5.3: Schematic representation of STRING network view of the cmd or CaM protein of *N. crassa* 134
Figure 5.4: Schematic representation of STRING network view of *trm-9* protein of *N. crassa* 135
Figure 5.5: Schematic representation of STRING network view of *nca-2* protein of *N. crassa* 136
Figure 5.6: Schematic representation site-directed mutation of *camk-2* 140
Figure 5.7: Clone reconfirmation of pRK-2 construct 141
Figure 5.8: Sequences selected for site-directed mutations 141-143
Figure 5.9: Primers locations of the *camk-2* gene for site-directed mutation 143-144
Figure 5.10: Confirmation of the S247A mutation in the pVL-2 construct 144-145
Figure 5.11: Confirmation of the T267A mutation in the pVL-3 construct 146-147

Figure 5.12: Confirmation of the mutation in the pVL-4 construct. 148-149

Figure 5.13: Confirmation of c*amk-2*, c*amk-2*^{S247A}, *camk-2*^{T267A} and *camk-2*^{L309D} transformants strains by PCR 151

Figure 5.14: Phenotype of crosses involving *camk-2*, *camk-2*^{S247A}, *camk-2*^{T267A} and the *camk-2*^{L309D} mutant strains 153

Figure 5.15: Fold change in expression of (A) *cmd*, (B) *trm-9* and (C) *nca-2* genes in selected Ca^{2+}-signaling knockout mutants 160-162

Figure 5.16: Fold change profile of selected Ca^{2+}-signaling genes in (A) Δ*trm-9* and (B) Δ*nca-2* knockout mutants 162-163

Figure 5.17: Fold change in expression profile of (A) *cmd*, (B) *trm-9* and (C) *nca-2* gene in the double knockout mutant strains 164-165

Figure 5.18: Fold change in expression profile of selected Ca^{2+}-signaling genes in (A) wild-type, (B) Δ*trm-9*, (C) Δ*nca-2* and (D) Δ*trm-9*Δ*nca-2* strains in response to Ca^{2+}-stress 167-169

Figure 5.19: Fold change in expression profile of *upr-1* and *cmd* gene in (A) wild-type, (B) Δ*trm-9*, (C) Δ*nca-2* and (D) Δ*trm-9*Δ*nca-2* strains in response to UV stress 170-172

List of Tables **Pages**

Table 1.1: Calcium signaling proteins in *N. crassa* 11-16

Table 2.1: *N. crassa* strains used in this study 26-30

Table 3.1: Apical growth rate of the wild type strain on addition of various amounts of TFP and CPZ in the Vogel's glucose agar medium 65

Table 3.2: Aerial hyphae height of the wild-type strain in the presence of various amounts of TFP and CPZ 68

Table 3.3: Carotenoids accumulation on addition of various amounts of TFP and CPZ 70

Table 3.4: Primers used for confirmation of knockout mutants by PCR 72

Table 3.5: Aerial hyphae height of wild-type, Δ*trm-9*, Δ*nca-2* and Δ*trm-9*Δ*nca-2* strains 76

Table 3.6: Apical growth of wild-type, Δ*trm-9*, Δ*nca-2* and Δ*trm-9*Δ*nca-2* strains 78

Table 3.7: Biomass accumulation of wild-type, Δ*trm-9*, Δ*nca-2* and Δ*trm-9*Δ*nca-2* strains 79

Table 3.8: Carotenoids content of wild-type, Δ*trm-9*, Δ*nca-2* and Δ*trm-9*Δ*nca-2* strains 83

Table 3.9: Carotenoid content of wild-type, Δ*trm-9*, Δ*nca-2* and Δ*trm-9*Δ*nca-2* strains during Ca^{2+} stress 83

Table 3.10: Average colony growth rate of the wild-type, Δ*trm-9*, Δ*nca-2* and Δ*trm-9*Δ*nca-2* strains at various concentrations of $CaCl_2$ 85

Table 4.1: Primers used for cloning of *cmd* gene 91

Table 4.2: Crosses to generate the $P_{tcu\text{-}1}$*::cmd::V5::gfp; mat A* and cmd^{RIP} mutant strains 97-98

Table 4.3: Sequence analysis of cmd^{RIP} mutant alleles 100-102

Table 4.4: Apical growth study of cmd^{RIP} (26) mutant strain 115

Table 4.5: Carotenoids accumulation of cmd^{RIP} (26) muatnt strain at 30°C 117

Table 4.6: Phenotypes of crosses involving strains inducing meiotic silencing of the *cmd* gene 122-126

Table 5.1: Functions of some of the important Ca^{2+}-signaling genes in *N. crassa* 137-138

Table 5.2: Primers used for site-directed mutation analysis 139

Table 5.3: Phenotype of crosses involving the *camk-2* mutant alleles 154-159

Table 5.4: Primers used for real-time PCR analysis 159-160

Appendix Table 1: Fold change in expression of *cmd*, *trm-9* and *nca-2* gene in selected knockout mutant strains 175

Appendix Table 2: Fold change in expression of selected Ca^{2+}-signaling genes in Δ*trm-9* and Δ*nca-2* knockout mutant strains 176

Appendix Table 3: Fold change in expression of *cmd*, *trm-9* and *nca-2* gene in double mutant strains 177

Appendix Table 4: Fold change in expression of selected genes in response to Ca^{2+} stress 178

Appendix Table 5: Fold change in expression of selected genes in strains in response to UV stress 179

List of Abbreviations

Å	angstrom
bar	basta or ignite resistance gene
BLAST	basic local alignment search tool for proteins
BCS	bathocuproinedisulfonic acid
bp	base pair
Ca^{2+}	calcium
CaM/*cmd*	calmodulin
Ca^{2+}/CaMK-2	calcium/calmodulin-dependent kinase-2
CNA	calcineurin
$CuSO_4$	copper II sulfate
CDD	conserved domain database
°C	degree Celsius
CPZ	chlorpromazine
cm	centimeter
cDNA	complementary DNA
DNA	deoxyribonucleic acid
dsRNA	double-stranded RNA
Da	dalton
E. coli	*Escherichia coli*
FGSC	Fungal Genetic Stock Centre
g	gram
GFP	green fluorescent protein
H_2O_2	hydrogen peroxide
hph	hygromycin B resistance gene
h	hour
HT	heterokaryotic transformant
HOP	homokaryotic progeny
J/m^2	joule per square meter
kb	kilobase

kV	kilovolt
LG	linkage group
MLCK	myosin light chain kinase
mRNA	messenger ribonucleic acid
MSUD	meiotic silencing by unpaired DNA
MEGA	molecular evolutionary genetics analysis
min	minute
ms	milliseconds
M	molar
mM	millimolar
mg	milligram
ml	milliliter
mm	millimeter
Mb	mega base pairs
mat A	mating type locus A
mat a	mating type locus a
NCU	*Neurospora crassa* unit
nat	nourseothricin
nm	nanometer
ng	nanogram
µg	microgram
µl	microlitre
Ω	ohms
OD_{600}	optical density at 600 nm
ORF	open reading frame
PMCA	plasma membrane Ca^{2+}-ATPase
P_{tcu-1}	copper-responsive promoter
pan-2	pantothenate-2
pH	potentia hydrogenica
PCR	polymerase chain reaction
psi	Pounds per square inch
qPCR	Quantitative real time polymerase chain reaction
rid-1	RIP-defective-1
RT-PCR	real-time / reverse transcriptase polymerase chain reaction

RNA	ribonucleic acid
RIP	repeat-induced point mutation
RISC	RNA-induced silencing complex
RNAi	RNA interference
RNAase	ribonuclease
rpm	revolutions per minute
siRNA	small interfering RNA
SCM	synthetic crossing medium
sec	second
Sad-1	suppressor of ascus dominance-1
SDM	site-directed mutagenesis
STRING	search tool for the retrieval of interacting genes/proteins
TFP	trifluoperazine
UV	ultraviolet
v/v	volume/volume
VGM	Vogel's glucose medium
VSM	Vogel's sucrose medium
V5	V5 peptide tag
w/v	weight/volume

Acknowledgements

First and foremost, I would like to pay my gratitude to my supervisor, Dr. Ranjan Tamuli, for his unwavering support and guidance throughout my PhD. I also thank him for his technical expertise, suggestions and endless patience in revising the thesis. I also thank my co-supervisor, Prof. Utpal Bora, for his mentorship and support throughout my research time at the IITG.

I would like to acknowledge all my doctoral committee members Prof. Ramesh Aiyagari, Dr. Nitin Chaudhary and Prof. Gopal Das for their constructive comments and suggestions on my work.

I am indebted to the present and previous Director of IITG and Head of the Biosciences and Bioengineering Department for providing all necessary facilities as well as MHRD for financial support.

I am grateful to Dr. D.P. Kasbeskar, CCMB, Hyderabad for providing Δ*Sad-1* strain.

I thank all my lab members, past and present, specially my seniors Rekha di and Ravi bhaiya and Upasana, Vishakha, Dibakar, Ajeet, Abhishek and Christy for helping me in countless ways.

I convey special acknowledgement to Shamsher, Saumya, Ziauddin, Himanshu, Yoganand, Amrendra, Anand, Mohit, Santosh, Gautam and all my friends at IITG for their endless support, care and encouragement during the entire journey. I will always treasure the friendship with Shruti, the sources of strength, warmth and entertainment during my stay in IITG.

This journey would not have been complete without my parents' blessings and support. I would like to pay my gratitude and love to Mummy, Papa, my brother Anand and my sister Neha for standing by me throughout this journey.

Vijya Laxmi

Synopsis

The model filamentous fungus *Neurospora crassa* is naturally found in tropical and subtropical regions in dead and decaying plants. *N. crassa* has been extensively used to understand complex biological processes, including the mechanism of calcium (Ca^{2+}) signaling. Ca^{2+} plays a central role as an intracellular signaling molecule in eukaryotes, yet, little is known about the Ca^{2+}-signaling process in fungi in comparison to animals and plants. *N. crassa* possesses a complex Ca^{2+}-signaling machinery that is a significant component of its signal transduction network (Borkovich *et al.* 2004). In *N. crassa*, Ca^{2+}-signaling is involved in regulating various functions such as vegetative growth, aerial hyphae development, hyphal branching, carotenoid accumulation, circadian rhythm, sexual development, ultraviolet (UV) survival, thermotolerance and oxidative stress tolerance (Deka *et al.* 2011; Tamuli *et al.* 2011; Kumar and Tamuli 2014). *N. crassa* has 48 Ca^{2+}-signaling genes, comprising of Ca^{2+}-channel proteins, Ca^{2+}/cation-ATPases, Ca^{2+}/H^{+} exchangers, Ca^{2+}/Na^{+} exchangers, phospholipase C-δ subtype, calmodulin and Ca^{2+} and/or CaM binding proteins and a single calmodulin (CaM), (Galagan *et al.* 2003; Borkovich *et al.* 2004; Zelter *et al.* 2004). However, most of the Ca^{2+}-signaling proteins have not been characterized and detailed relationship of CaM with other Ca^{2+} -signaling proteins remains to be established. In addition, *N. crassa* might possess novel intracellular Ca^{2+} release mechanism that remains to be identified and this might provide novel antifungal targets for drug discovery.

Chapter 1 describes briefly about the life cycle, overview of the genome defense mechanisms, and Ca^{2+}-signaling pathway in *N. crassa*. Furthermore, this Chapter also describes the brief description of our current knowledge about CaM in *N. crassa* and other fungi. Ca^{2+} binds to CaM via structural motifs called EF hands consisting of two α-helices joined by a 12 amino acid Ca^{2+}-binding loop in which conserved aspartate and glutamate residues chelate the Ca^{2+} ions (Gifford *et al.* 2007). The ability of CaM to act as a Ca^{2+} sensor lies in its ability to convert Ca^{2+} binding into the release of free energy. The structure and functions of CaM are largely conserved in pathogenic and non-pathogenic fungi, but the mechanisms of action have diverged (Chin and Means 2000; Kraus and Heitman 2003). CaM is involved in regulating numerous processes such as appressorium formation, bud formation, cellular morphogenesis, cell cycle control, cell wall formation, conidiation, cytokinesis, germ tube formation, germination, growth,

hyphal growth, mitotic spindle formation, pre-penetration morphogenesis, sexual development, stress responses, and virulence in fungi (Muthukumar and Nickerson 1984, 1986; Muthukumar *et al.* 1985; Roy and Datta 1987; Paranjape *et al.* 1990; Anraku *et al.* 1991; Lu *et al.* 1992; Geiser *et al.* 1993; Iida *et al.* 1995; Warwar and Dickman 1996; Sadakane and Nakashima 1996; Moser *et al.* 1997; Suresh and Subramanyam 1997; Lee and Lee 1998; Liu and Kolattukudy 1999; Kraus and Heitman 2003; Ahn and Suh 2007; Ding *et al.* 2014; Laxmi and Tamuli 2015). Disruption of the CaM was lethal in *Saccharomyces cerevisiae* (Davis *et al.* 1986), *Schizosaccharomyces pombe* (Takeda and Yamamoto 1987), *Aspergillus nidulans* (Rasmussen *et al.* 1990), *Cryptococcus neoformans* (Kraus *et al.* 2005), *Magnaporthe grisea* (Ma *et al.* 2009) and *N. crassa* (Laxmi and Tamuli 2015, 2016), indicating that CaM is an essential gene for viability in these fungi. Therefore, I studied cellular roles of CaM in *N. crassa* using CaM antagonists and utilizing two different gene silencing mechanisms, repeat-induced point mutation (RIP) and meiotic silencing. Moreover, I also studied some of the targets of CaM.

Chapter 2 describes materials and methods used in my thesis work. Growth and crosses of *N. crassa* strains were essentially as described previously (Westergaard and Mitchell 1947; Davis and de Serres 1970). The *N. crassa* strains were obtained from the Fungal Genetics Stock Center (FGSC, Manhattan, KS), and also generated in the laboratory. Cloning, site-directed mutagenesis, PCR, real-time PCR and other molecular biology experiments were performed by using the standard protocols essentially as described by Sambrook and Russell (2001) or manufacturers' protocols.

Chapter 3 describes the cellular role of CaM and two other Ca^{2+} -signaling genes in *N. crassa*. CaM is an essential gene; therefore, CaM antagonists trifluoperazine (TFP) and chlorpromazine (CPZ) were used to study its function. Addition of TFP and CPZ inhibit growth, aerial hyphae development, carotenoids accumulation, hyphal branching, and sexual development in *N. crassa.* I have also studied one of the important targets of CaM, *trm-9* and *nca-2* that encodes cation -ATPase and Ca^{2+}-ATPase respectively. I have also generated the Δ*trm-9*Δ*nca-2* double knockout mutants and studied phenotypes of the mutants. The Δ*trm-9*Δ*nca-2* double mutant strain showed a severe growth defect, less carotenoid accumulation, an increased sensitivity to $CaCl_2$, and reduced viability in

acquisition of thermotolerance induced by heat shock temperature. Thus, in this study, I have shown that *cmd*, *trm-9*, and *nca-2* genes play an important role in vegetative growth, pigmentation, and stress-tolerance in *N. crassa*.

Chapter 4 discussed generation and functional analysis of CaM mutant using the repeat-induced point (RIP) mutation, and the effect of CaM silencing by meiotic silencing during the sexual development. I generated *N. crassa* strains, Δ*rid-1::nat*; Δ*mus51::hph;* Δ*pan-2::bar::*P_{tcu-1}*::cmd::5xGly::V5::gfp; mat a*, which is duplicated for the CaM gene, with an endogenous *cmd* gene and an ectopic *cmd* copy cloned under the *tcu-1* promoter (Lamb *et al.* 2013; Tamuli *et al.* 2016) and subsequently used for generation of cmd^{RIP} mutant strains and to assay for meiotic silencing. I isolated eight cmd^{RIP} mutants containing both conventional (G-C to A-T) as well as non-conventional mutations (Kim and Nelson 2005). However, only one cmd^{RIP} mutant strain, Δ*pan-2::bar::*P_{tcu-1}*::*cmd^{RIP}; *mat A* (RIP-26) possess nonsynonymous mutations both in the endogenous and the ectopic copies of the *cmd* gene. The Δ*pan-2::bar::*P_{tcu-1}*::*cmd^{RIP}; *mat A* (26) strain contains D57Y and Q148H mutation in the endogenous copy and E8K mutation in the ectopic copy of the *cmd* gene. The other seven cmd^{RIP} mutant strains contain mutations only in the ectopic copy of the *cmd* gene. The cmd^{RIP} mutant stain, Δ*pan-2::bar::*P_{tcu-1}*::*cmd^{RIP}; *mat A* (RIP-26) showed a defect in growth, aerial hyphae development, carotenoid accumulation and a severe reduction in viability upon ultraviolet (UV) irradiation. Moreover, I performed crosses involving strains engineered for inducing meiotic silencing of CaM to understand its role in sexual development. Meiotic silencing of the *cmd* gene resulted in sterile phenotype of a cross, thereby, supporting its role in sexual development in *N. crassa*.

Chapter 5 describes site-directed mutational analysis of three important amino acid residues of CAMK-2 protein as well as expression analysis of CaM and some other selected Ca^{2+}-signaling genes through real-Time PCR. CaM interacts with various proteins and enzymes to amplify the Ca^{2+}-signaling cascade. Previous work in the laboratory had identified that the calcium/calmodulin-dependent kinase-2 (Ca^{2+}/CaMK-2) is necessary for full fertility in *N. crassa* (Deka *et al.* 2011; Kumar and Tamuli 2014). The *N. crassa* Ca^{2+}/CaMK-2 possess 11 conserved kinase domains, one putative CaM binding domain and nine putative phosphorylation sites and lacks conventional

phosphorylation sites of threonine and serine at positions 286 and 314 (Tamuli *et al.* 2011; Kumar and Tamuli 2014). I performed site-directed mutagenesis of important residues in the catalytic and Ca^{2+}/CaM binding domains of the *camk-2* by using the pRK-2 construct (P_{T7}*::camk-2::bar*; Kumar and Tamuli, 2014). I generated *N. crassa* strains with S247A and T267A mutations in the putative phosphorylation sites and L309D mutation in the CaM binding domain of the CaMK-2 protein. Crosses homozygous for the *camk-2*^{S247A} and *camk-2*^{T267A} mutants, or crosses involving these mutants with the *Δcamk-2* mutant showed an intermediate phenotype; however, crosses homozygous for the *camk-2*^{L309D} were fertile. Therefore, phosphorylation of serine at 247 and threonine at position 267 are important for fertility, however, leucine at position 309 might not be critical for CaM binding or CAMK-2 and CaM interaction is not essential for full fertility in *N. crassa*. In addition, I determined fold change expression levels of the *cmd*, *trm-9*, *nca-2* and some others Ca^{2+}-signaling genes through real-Time PCR in normal as well as in response to Ca^{2+} and UV stress, which indicated a complex interaction pattern among these genes.

Thus, in this study, I had determined functions of CaM both in vegetative and sexual phases of *N. crassa* using CaM antagonists. Furthermore, I had generated CaM mutants using RIP and their analysis revealed its critical amino acid residues. In addition, I found that CaM during meiosis is essential for full fertility. Moreover, I had also identified two critical amino acid residues of the *camk-2* gene and found a complex interaction patter among some of the Ca^{2+}-signaling genes. Therefore, this study revealed the functions of CaM and some of its related proteins both in vegetative growth and sexual development in *N. crassa*.

Chapter 1

An introduction to Neurospora crassa, calcium signaling and calmodulin

1.1 The biology of *Neurospora crassa*

Neurospora, named due to the nerve-like stripes found on its sexual spores, is the genus of a group of filamentous fungi. It was studied as a causative organism of orange mold infestation in French bakeries, and first reported in scientific literature in 1843 as *Oidium aurantiacum* (Payen 1843) and *Penicillium sitophilum* (Montagne 1843) independently. Thereafter, in 1927, Dodge and Shear studied the same bakery fungus and identified *Neurospora crassa* (Shear and Dodge 1927). Dodge identified the two mating types and demonstrated Mendelian segregation in individual asci (Perkins and Davis 2000). In addition, Lindegren reported the genetic map of the sex chromosome of *N. crassa* that was also the first map for a fungus chromosome (Lindegren 1936). Subsequent work on Neurospora by Beadle and Tatum introduced the concept of 'one gene, one enzyme' (Beadle and Tatum 1941) and awarded the Nobel Prize in "Physiology or Medicine" in 1958. These pioneering research work on *N. crassa* has been established as an ideal eukaryotic model organism, and extensively used in diverse field of biological research, such as the circadian rhythms, DNA methylation and repair, genome defense, mitochondrial protein import and post-transcriptional gene silencing (Galagan *et al.* 2003). As a heterotroph organism, *N. crassa* can use a carbon and nitrogen few simple salts, trace elements, and biotin, a single vitamin, for vigorous growth. *N. crassa* has a simple, heterothallic, haploid life cycle and its genome size is 43 Mb, which divided into seven linkage groups (LG I-VII, size ranges from 4 to 10.3 Mb each) that contain 10,082 protein coding genes (Davis and de Serres 1970; Perkins and Davis 2000; Galagan *et al.* 2003).

1.2 The life cycle of *N. crassa*

The life cycle of *N. crassa* (Figure 1.1) possesses a more complex process of vegetative or asexual and sexual reproduction than unicellular yeasts (Raju 1992; Springer 1993). The vegetative system of *N. crassa* is composed of multinucleate branched filaments or hyphae. The hyphae are segmented by incomplete cross-walls or septa that allow cytoplasm to flow along the hyphae usually in direction of the growth, carrying nuclei, mitochondria and other inclusions for some distance. A hyphal system is also called a mycelium. During vegetative growth, *N. crassa* produces two types of mitotic spores, multinucleate macroconidia and uninucleate microconidia (Davis and de Serres 1970). Macroconidia are used to inoculate vegetative cultures and they serve also as the fertilizing male parent in a sexual cross. During the growth process, microconidia are

lately formed by a process quite distinct from macro conidial formation. On the other hand, ascospores are formed at the end of the sexual process; they can survive for a long period in dormant stage at which genotypes may be isolated in the unambiguous pure form (Davis and de Serres 1970).

N. crassa is a heterothallic filamentous fungus that contains two nonswitching mating type, *A* and *a* in a sexual phase in its life cycle. Sexual development in *N. crassa* is induced by limiting nitrogen and carbon sources. In response to nutrient starvation, the hyphae of *N. crassa* undergo complex changes and develop to a protoperithecium, which is a spherical multicellular female reproductive structure. Special receptor hyphae, called trichogyne, emanate from the protoperithecium, and fuses with a male cell of opposite mating type that is typically a hyphal fragment, macroconidium, or microconidium. After fusion the male nucleus is transported to the protoperithecium that contains nuclei of opposite mating type recognize each other and initiates the development of the multicellular sexual apparatus called perithecium and results in plasmogamy. After plasmogamy, the nuclei derived from the male and the female parents coexist in a heterokaryotic tissue and undergoes mitotic divisions until they are sorted into dikaryotic tissue that contains only one nucleus of each mating type in each cell compartment. In the dikaryotic tissue, nuclei of opposite mating type do not fuse immediately, they undergo a synchronous mitosis to isolate two nuclei in the tip of a specialized hook-shaped cell structure called the crozier. During karyogamy, the nuclei fuse to form a diploid zygote nucleus and immediately undergoes the two meiotic divisions and a postmeiotic mitosis to yield eight sexual spores called ascospores within an eight-spore ascus in an order that reflects their lineage. The matured ascospores are ejected through ostiole, a pore at the tip of the perithecium. Ascospores are germinate following heat shock to activate and produce vegetative mycelia (Davis and de Serres 1970; Raju 1980, 1992; Springer 1993; Perkins and Davis 2000; Kim *et al.* 2012).

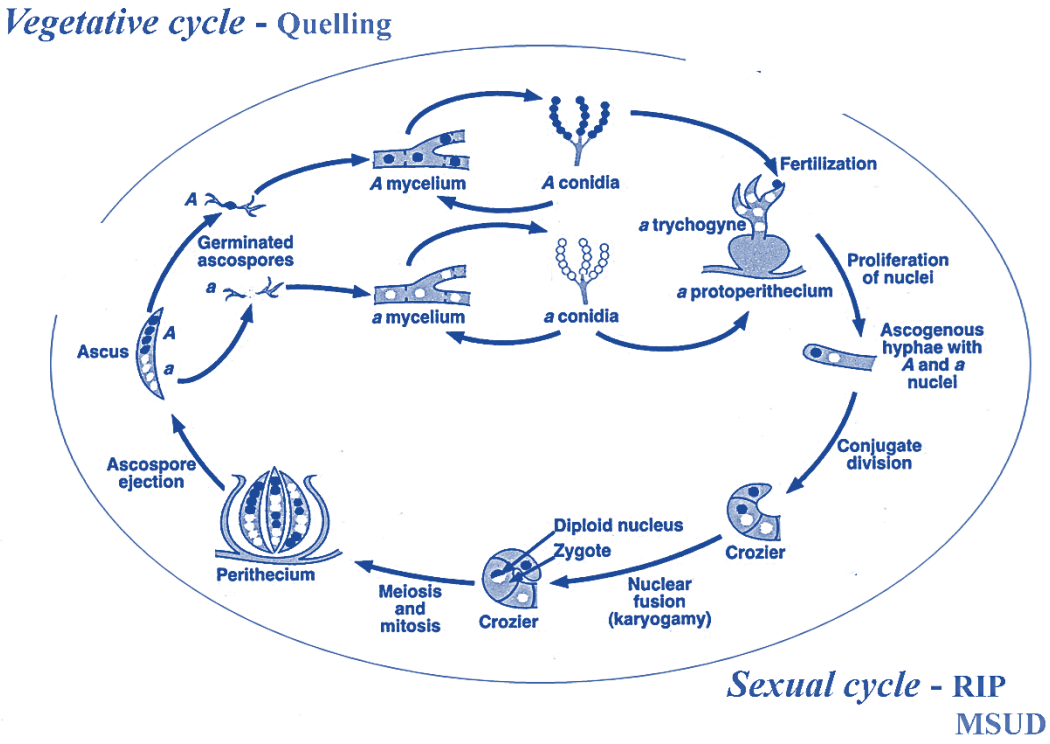

Figure 1.1: The life cycle of *N. crassa*. Mating occurs between strains of opposite mating type *mat A* and *mat a*. The haploid nuclei proliferate in the premeiotic ascogenous tissue, and after fertilization, resulting in the formation of asci within the developing ascocarp called perithecium. In the young ascus, the haploid nuclei derived from the *mat A* and *mat a* parents are fused. The diploid zygote nucleus immediately undergoes two meiotic divisions (meiosis I and II) and a post-meiotic mitosis in the same cytoplasm of the ascus. Subsequently, the eight haploid nuclei are sequestered in a linear order of eight spindle-shaped (american football-shaped) ascospores in the narrow ascus. About 200 asci are produced in each perithecium, and the maturing ascospores become multinucleate and pigmented. Stages of three different genome defense systems or gene silencing mechanisms; quelling, RIP (repeat-induced point mutation) and MSUD (meiotic silencing by unpaired DNA) are shown (Adapted from Shiu *et al.* 2001; Borkovich *et al.* 2004).

1.3 Gene silencing mechanisms in *N. crassa*

The maintenance of a relatively stable genome is paramount to the survival of an organism. *N. crassa* has been established as a unique paradigm for the study of gene silencing mechanisms, indeed its genome is protected from expansion of selfish nucleic acids by three different gene-silencing phenomena that have been found to operate in distinct phases of the Neurospora life cycle (Figures 1.1; Figures 1.2; Selker 1990; Catalanotto *et al.* 2006). In the vegetative phase, a reversible post-transcriptional gene-silencing (PTGS) mechanism known as 'quelling' (Romano and Macino 1992), and during the sexual phase, two other gene-silencing mechanisms that are RIP, a transcriptional gene-silencing (TGS) mechanism (Cambareri *et al.* 1989) and MSUD, a PTGS mechanism (Shiu *et al.* 2001) are discovered in *N. crassa*.

1.3.1 Quelling

Pandit and Russo in 1992 reported gene silencing mechanism in the vegetative phase of *N. crassa* (Pandit and Russo 1992), but the first report of silencing of both transforming DNA and homologous endogenous sequences was made by Romano and Macino, called "quelling" in *N. crassa* (Romano and Macino 1992). Quelling is a posttranscriptional event probably triggered by an aberrant RNA molecule in Neurospora, in which transgenes induces sequence specific mRNA degradation (Figures 1.2; Cogoni *et al.* 1996). The discovery of quelling-defective (*qde*) genes, in which transgene induced gene silencing is impaired, has been a milestone in the understanding the process of posttranscriptional gene silencing in *N. crassa* (Cogoni and Macino 1997). Transgene induced gene silencing has been termed quelling in *N. crassa* was similar to other silencing phenomena, such as co-suppression and RNA interference in animals and co-suppression in plants (Cogoni and Macino 1999a; Pickford *et al.* 2002; Catalanotto *et al.* 2004). Large repeated sequences can potentially form secondary structures including cruciform arrangements that can be recognized by a RecQ DNA helicase called QDE-3 (Cogoni and Macino 1999b). QDE-3 at the transgenic locus is able to attract QDE-1, an RNA-dependent RNA polymerase (Cogoni and Macino 1999a) and converts a single-stranded RNA into a double-stranded RNA (dsRNA) molecule that is subsequently processed into small interfering RNA (siRNA) of 21–25 nucleotides by one of two redundant DICER-like ribonuclease proteins, DCL-1 and DCL-2 (Catalanotto *et al.* 2004). These siRNAs are further incorporated into a multiprotein complex called RNA-induced silencing complex (RISC) containing an argonaute protein QDE-2 (Catalanotto

et al. 2002). The siRNAs are used by the RISC to guide degradation of complementary mRNA targets (Catalanotto *et al.* 2006).

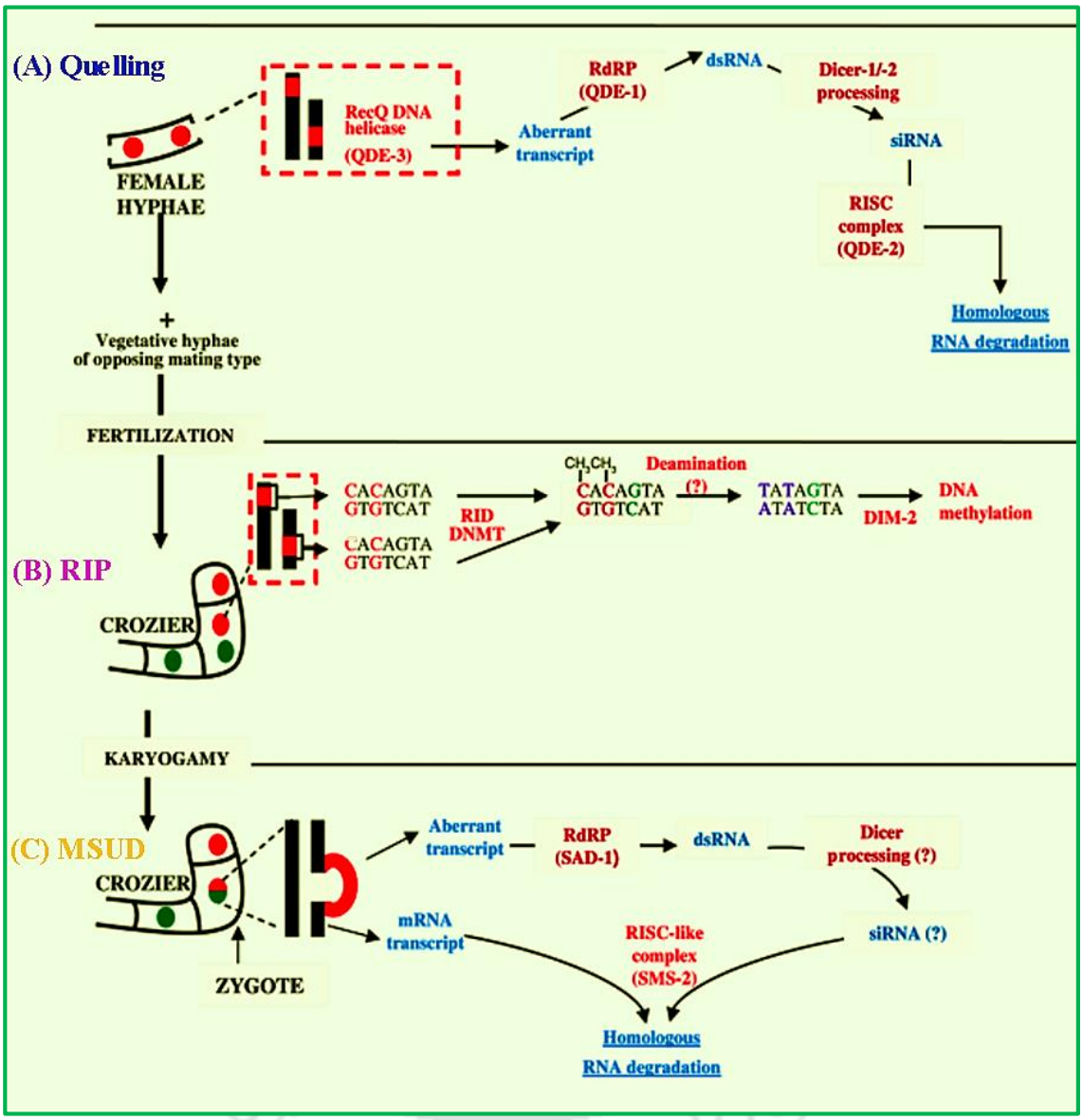

Figure 1.2: Gene silencing pathways in Neurospora. (A) Quelling occurs in the vegetative phase when Neurospora grows as a haploid mycelium. Two PTGS mechanisms have been identified in Neurospora: quelling and MSUD. (B) During plasmogamy, the haploid nuclei are confined in a specialized hook-shaped structure known as crozier, where RIP occurs on duplicated DNA sequences. Red C:G pairs represent targets of methylation by a putative DNA methyltransferase known as RID. Putative deamination of these pairs can lead to a T: A conversion (shown in blue), while

the unmutated C:G pairs (shown in green) are subsequently targeted by the DNA methyltransferase DIM-2. (C) After DNA replication, the fusion of the two nuclei (karyogamy) results in the formation of the zygote, where, unpaired DNA sequences are detected and silenced by the MSUD (Adapted from Catalanotto *et al.* 2006).

1.3.2 Repeat-induced point mutation

Repeat-induced point mutation (RIP) is a homology based process that recognizes and mutates repetitive DNA sequences and also causes epigenetic silencing of the mutated sequences through DNA methylation. RIP occurs before karyogamy and identifies DNA duplications that are greater than ~400 bp or ~1 kb in the case of unlinked duplications, and causes C:G to T:A mutations into both copies of the duplicated DNA. RIP identifies duplications that share greater than ~80% nucleotide identity in a single passage through the sexual cycle, and up to ~30% of the C:G pairs in duplicated sequences might be mutated. RIP occur preferentially in the CpA dinucleotides and the RIP-mutated sequences are frequent targets for DNA methylation (Figures 1.2). Thus, RIP is a process that mutates and often leads to epigenetic silencing of repetitive DNA (Galagan *et al.* 2003; Galagan and Selker 2004). RIP associated cytosine methylation spread to the flanking sequences of the duplication up to 4 kb (Foss and Selker 1991; Irelan *et al.* 1994; Perkins *et al.* 1997; Selker *et al.* 2003). Although not clear, it has been proposed that the mechanism of RIP involves cytosine deamination to uracil or deamination of 5-methylcytosine to thymine. These two pathways require a failure to repair lesions before subsequent rounds of DNA replication. The *rid-1* (*RIP-defective-1*) gene that encodes a putative DNA methyltransferase protein, is the only known molecular component of the RIP machinery till date (Freitag *et al.* 2002). In general, mutations by RIP are sufficient to completely inactivate affected sequences, however, the number and extent of mutations is variable (Selker 1990, 1997, 1999; Catalanotto *et al.* 2006). As a result of RIP, the *N. crassa* genome contains little repetitive DNA. Therefore, RIP possibly play a role in the inactivation of transposons that have already been duplicated more than once (Selker 1990, 1997). Some repeated sequences such as tandemly repeated rDNA sequences located within the nucleolus organizer and DNA sequences encoding 5S RNA and tRNA that are below the size threshold of the RIP machinery, are escaped from RIP.

1.3.3 Meiotic silencing

Meiotic silencing, which was previously called as MSUD, occurs after karyogamy. In *N. crassa*, if a gene is not paired with a homolog in meiotic prophase I, a signal will be generated resulting in transient silencing of all sequences homologous to the unpaired gene, including genes that are themselves paired, by the meiotic silencing process (Shiu *et al.* 2001; Shiu and Metzenberg 2002). Meiotic silencing was discovered via studies of a gene called *asm-1* (*Ascospore maturation-l*), required for mature melanised ascospores production. It was found that if any gene coding for any function required during meiosis is inserted ectopically into a wild-type or innocuously-marked strain and crossed it to the wild-type, the heterozygous cross showed a barren phenotype (Aramayo and Metzenberg 1996; Aramayo *et al.* 1996; Shiu *et al.* 2001). Detection of unpaired regions is not restricted to particular DNA sequences or chromosomal regions, rather, correlates with the size of the unpaired region as well as the degree of non-identity it shares with its homolog (Shiu *et al.* 2001; Lee *et al.* 2004). Meiotic silencing can detect even subtle amounts of sequence non-identity (~5% across 2 - 4 kb) and its sensitivity is further increased if the unpaired region carries DNA methylation marks, suggesting that besides DNA sequence, chromatin context may also contribute to detection of unpaired regions (Pratt *et al.* 2004; Dumesic and Madhani 2014).

The proteins that are found involved in meiotic silencing are SAD-1 (suppressor of ascus dominance-1); an RNA-directed RNA polymerase (Shiu *et al.* 2001; Shiu and Metzenberg 2002), SMS-2 (Suppressor of meiotic silencing-2); an argonaute-like protein (Lee *et al.* 2003), SMS-3 (Suppressor of meiotic silencing-3); dicer-like protein (Lee DW, McLaughlin M, Pratt RJ, Aramayo R, unpublished; Lee *et al.* 2004; Kelly and Aramayo 2007), SAD-2, a protein regulating SAD-1 localization (Shiu *et al.* 2006) and QIP (QDE-2 interacting exonuclease); an exonuclease (Lee *et al.* 2010). SAD-1 appears to be involved in the production of a single-stranded aberrant RNA from an unpaired segment. This RNA is exported to the perinuclear region where it acts as a template for the SAD-1 mediated dsRNA synthesis. DCL-1 then processes the dsRNA into siRNAs, which guides SMS-2 to identify and slice complementary mRNA (Figures 1.3).

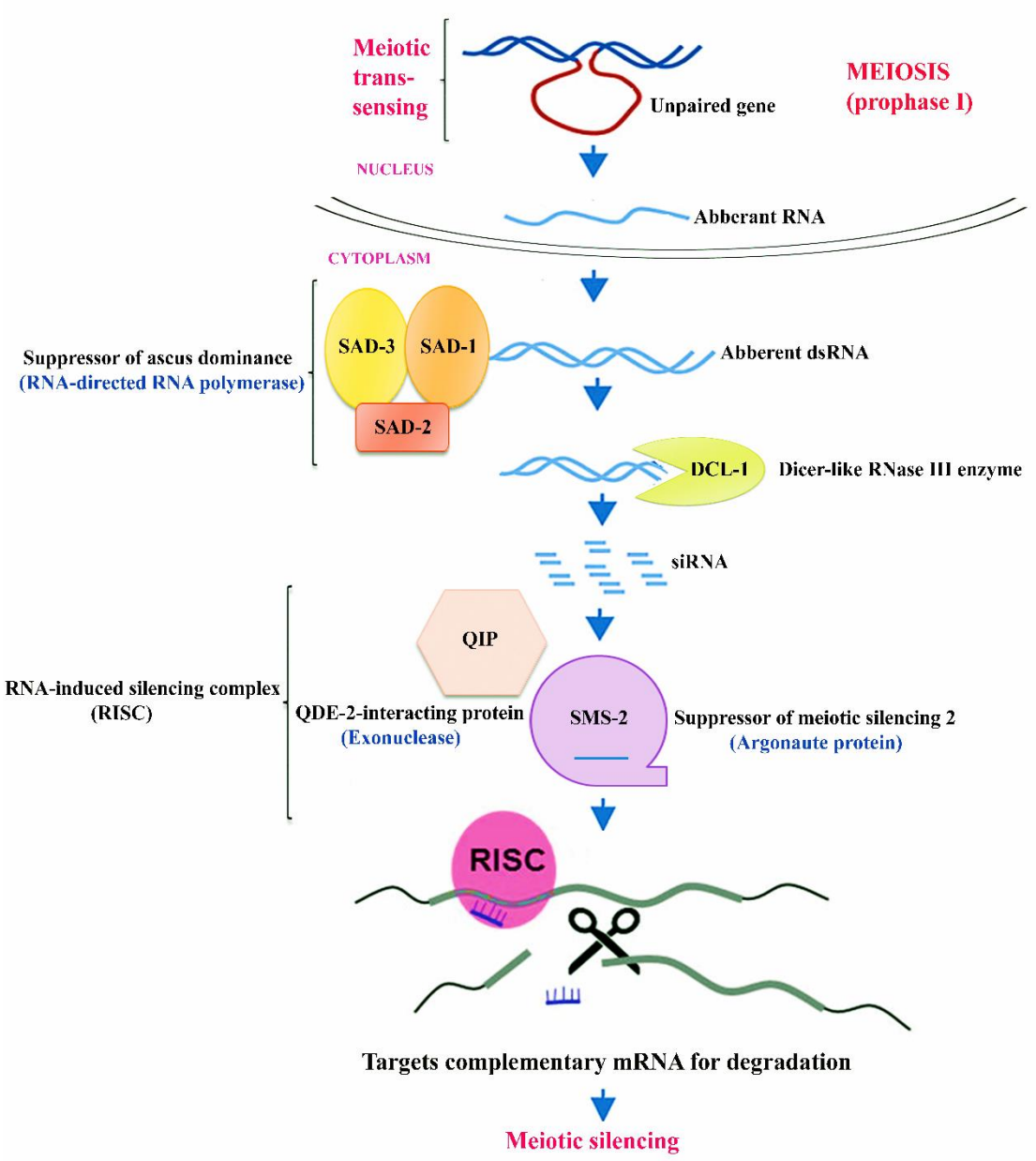

Figure 1.3: Current model of meiotic silencing in *N. crassa*. During the first meiotic prophase, an unpaired DNA triggers the transcription of aberrant RNAs from an unpaired DNA region. The RNA-directed RNA polymerase (RdRP), SAD-1 converts aberrant RNA into dsRNA, which are processed by DCL-1 into small RNAs, which are then loaded onto a RISC complex with the argonaute SMS-2 as the core component. The activation of the SMS-2 complex results in the silencing of homologous RNA. SAD-2 may function in the pathway by recruiting SAD-1 to its proper location to perform its activity (Adapted form Li *et al.* 2010; Chang *et al.* 2012).

In current working model of meiotic silencing, SAD-2 is a protein that interacts with SAD-1 and helps its transport to the perinuclear region; mutation of SAD-2 suppresses meiotic silencing. QIP is an exonuclease removes the passenger strand of a siRNAs duplex (Shiu *et al.* 2001, 2006; Shiu and Metzenberg 2002; Lee *et al.* 2004; Kelly and Aramayo 2007; Alexander *et al.* 2008; Li *et al.* 2010; Xiao *et al.* 2010). Meiotic silencing could be effective against sequences that are not established in homologous positions of both parents, i.e., that are not diploid when they should be. This silencing mechanism might be important in holding down the genetic load attributable to transposable elements that move during meiosis (Shiu *et al.* 2001). Meiotic silencing may provide insights into the function of genes necessary for meiosis, including genes for which a knockout construct would be lethal in vegetative life (Shiu *et al.* 2001; Shiu and Metzenberg 2002).

1.4 Calcium signaling in *N. crassa*

Neurospora possesses a wide range of signaling capabilities and therefore, serves as an outstanding model organism for investigations of the signaling pathway. The intracellular signaling pathways in *N. crassa* are involved mitogen-activated protein kinase (MAPK), histidine kinase (HK), response regulator (RR), G-protein-coupled receptors (GPCRs) and Ca^{2+}-signaling (Figure 1.4).

Ca^{2+} plays a central role as an intracellular signal in biological systems (Berridge *et al.* 1998; Sanders *et al.* 2002; Davies and Terhzaz 2009). Binding of Ca^{2+} changes protein confirmation and charge, which are the two universal signaling tools of signal transduction, and thus Ca^{2+} regulates protein functions (Bootman *et al.* 2001; Clapham 2007). The ubiquitous role of Ca^{2+} lies in its chemistry that involves its molecular structure, balance state, binding strength, ionization potential and kinetic parameters in the biological reactions. The Ca^{2+} ion has maximum affinity for carboxylate oxygen and interestingly, acidic amino acids like aspartic acid and glutamic acid that contain the carboxylate oxygen occur more frequently in proteins. The Ca^{2+} ion typically exhibits high coordination numbers (6–8) and can accommodate 4–12 oxygen atoms in its primary coordination sphere. The coordination geometry of Ca^{2+} is often irregular (i.e. protein induced) due to its favourable ionic radius (100–120 pm) and its electronic structure (Swain and Amma 1989; Carugo *et al.* 1993; Jaiswal 2001; Clapham 2007). The resting level of cytosolic free Ca^{2+} ($[Ca^{2+}]_c$) is very low (typically 50–100 nM), which is maintained by active Ca^{2+}-pumps and Ca^{2+}-transporter proteins, reaching values

close to 1 µM when the cell is stimulated by a variety of physiological stimuli, this large concentration gradient allows intracellular Ca^{2+} to work as a useful second messenger (Berridge *et al.* 1998).

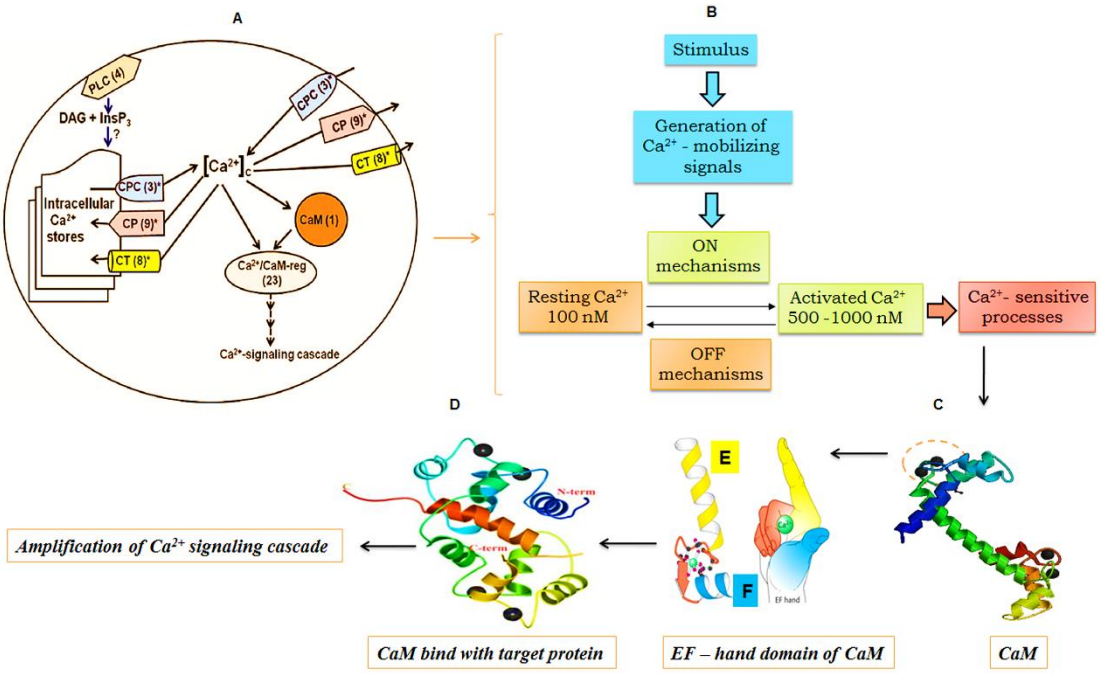

Figure 1.4: Overview of calcium signaling system in *N. crassa*. (A) CPC, Ca^{2+}-permeable channel; CA, Ca^{2+}-and cation–ATPases; CE, Ca^{2+}/H^{+} and Ca^{2+}/Na^{+} exchanger; CaM, calmodulin; Ca^{2+}/CaM-reg, calcium- and CaM regulated; PLC, phospholipase C; DAG, diacylglycerol; InsP3, inositol -1,4,5-trisphosphate (Adapted from Tamuli *et al.* 2013). (B) The average cytosolic concentration of free Ca^{2+} in resting cells ranges from 20 to 50 nm, reaching values close to 1000 nM when the cell is stimulated by a variety of physiological stimuli, while in the extracellular fluid this concentration is about 1 mM. This large concentration gradient allows intracellular Ca^{2+} to work as a useful second messenger. (C) Structure of CaM protein and its EF hand motif and (D) Binding of CaM with its target protein (Adapted from RCSB Protein Data Bank and Biochemistry by Stryer).

The filamentous fungus *N. crassa* has been established as an excellent eukaryotic model organism that can be utilized to investigate the complex Ca^{2+}-signaling processes. *N. crassa* has 48 Ca^{2+}-signaling proteins that comprises of three Ca^{2+}-channel proteins, nine Ca^{2+}/cation-ATPases, six recognizable Ca^{2+}/H^{+} exchangers, two novel putative Ca^{2+}/Na^{+} exchangers, four novel phospholipase C-δ subtype proteins, 23 Ca^{2+}/CaM regulated proteins and one CaM (Figure 1.4, Table 1.1; Borkovich *et al.* 2004). It is different from other animal and plant Ca^{2+}-signaling pathways as it has both Ca^{2+}/Na^{+} as well as Ca^{2+}/H^{+} exchangers whereas animals have only Ca^{2+}/Na^{+} exchangers and plants have Ca^{2+}/H^{+} exchangers, also it lacks receptors for second messengers such as inositol-1,4,5-trisphosphate, ryanodine and cyclic ADP ribose that are responsible for Ca^{2+} release from internal stores in other organisms (Berridge *et al.* 2000; Bootman *et al.* 2001; Sanders *et al.* 2002). However, detailed knowledge about the main components involved in any one Ca^{2+}-mediated signal responses pathway is still not clear for *N. crassa* or any other filamentous fungus (Galagan *et al.* 2003; Borkovich *et al.* 2004).

Table 1.1[a]: Calcium signaling proteins in *N. crassa*

Sl. no.	NCU no.	Name	Type of protein	Best overall[b] (*e*-value; organism; protein name; accession number)
1.	02762.7		Ca^{2+} permeable channel	0; *Verticillium dahliae* (cch1); EGY18507.1
2.	06703.7		Ca^{2+} permeable channel	2e-97; *Paracoccidioides brasiliensis* (MID1); EEH23338.1
3.	11680.7[c]		Ca^{2+} permeable channel	0; *Ajellomyces dermatitidis* (Yvc1); EGE78766.1
4.	03305.7	NCA1	Ca^{2+} -ATPase	0; *Trichophyton tonsurans* (SCA-1); EGD96734.1
5.	04736.7	NCA2	Ca^{2+} -ATPase	0; *Magnaporthe oryzae* (Plasma membrane calcium-transporting ATPase 3); EHA56671.1

6.	05154.7	NCA3	Ca^{2+} -ATPase	0; *Glomerella graminicola* (Calcium-translocating P-type ATPase); EFQ29373.1
7.	03292.7	PMR1	Ca^{2+} -ATPase	0; *Uncinocarpus reesii* (PMR1); XP_002541437.1
8.	08147.7	PH-7	Ca^{2+} -ATPase	0; *Glomerella graminicola* (Potassium/sodium efflux P-type ATPase); EFQ36596.1
9.	04898.7		Ca^{2+} -ATPase	0; *Cordyceps militaris* (Cation-transporting ATPase 4); EGX91104.1
10.	03818.7		Ca^{2+} -ATPase	0; *Verticillium dahliae* (Neo1p); EGY18069.1
11.	07966.7		Cation-ATPase	0; *Trichophyton tonsurans* (Cta3p); EGD97988.1
12.	10143.7[d]		Cation-ATPase	0; *Cordyceps militaris* (ATPase 14type 13A2); EGX92563.1
13.	07075.7	CAX	Ca^{2+} /H^{+} exchanger	0; *Glomerella graminicola* (Calcium/proton exchanger); EFQ30300.1
14.	00916.7		Ca^{2+} /H^{+} exchanger	2e-176; *Aspergillus fumigates* (Membrane bound cation transporter); XP_001481534.1
15.	00795.7		Ca^{2+} /H^{+} exchanger	1e-149; *Aspergillus niger* (Membrane bound cation transporter); XP_001400827.2

16.	06366.7		Ca^{2+} /H^{+} exchanger	0; *Sclerotinia sclerotiorum* (Ca^{2+} /H^{+} antiporter); XP_001589752.1
17.	07711.7		Ca^{2+} /H^{+} exchanger	4e-160; *Trichophyton tonsurans* (Vacuolar calcium ion transporter/H^{+} exchanger); EGD98067.1
18.	05360.7		Ca^{2+} /H^{+} exchanger	0; *Metarhizium anisopliase* (Calcium permease); EFY95914.1
19.	02826.7		Ca^{2+}/ Na^{+} exchanger	0; Verticillium albo-atrum (Sodium/calcium exchanger protein); XP_003004985
20.	08490.7		Ca^{2+}/ Na^{+} exchanger	1e-83; *Aspergillus niger* (Sodium/calcium transporter); XP_001397155.1
21.	01266.7		Phospholipase C	0; *Sordaria macrospora* (Phosphoinositide-specific phospholipase C); XP_003348116.1
22.	06245.7	PLC-1	Phospholipase C	0; *Glomerella graminicola* (Phosphatidylinositol-specific phospholipase C); EFQ28596.1
23.	11415.7[e]		Phospholipase C	0; *Glomerella graminicola* (Phosphatidylinositol-specific phospholipase C); EFQ31595.1
24.	02175.7		Phospholipase C	3e-125; *Botryotinia fuckeliana* (BcPLC2); CCD34776.1

25.	04120.7	CaM	Calmodulin	1e-103; Gibberella zeae (CaM); XP_382067.1
26.	03804.7	CNA-1	Calcineurin catalytic subunit	0; *Sordaria macrospora* (Serine/threonine-protein phosphatase 2B catalytic subunit protein); XP_003352213.1
27.	03833.7	CNB-1	Calcineurin regulatory subunit /variant	2e-119; *Trichoderma reesei* (Calcineurin, beta subunit); EGR44907.1
28.	09265.7		Calnexin	0; Sordaria macrospora (cnx1); XP_003347545.1
29.	05225.7[f]		Ca^{2+} and/or CaM binding protein	0; *Magnaporthe oryzae* (Mitochondrial NADH dehydrogenase); EHA47323.1
30.	02115.7		Ca^{2+} and/or CaM binding protein	0; *Magnaporthe oryzae* (EF hand domain-containing protein); EHA48778.1
31.	01564.7		Ca^{2+} and/or CaM binding protein	0; *Magnaporthe oryzae* (Calcium dependent mitochondrial carrier protein); EHA48778.1
32.	06948.7		Ca^{2+} and/or CaM binding protein	2e-54; *Mycosphaerella graminicola* (Calcium ion binding, calmodulin); EGP88834.1
33.	04379.7	NCS-1	Ca^{2+} and/or CaM binding protein	4e-126; *Grosmannia clavigera* (Neuronal calcium sensor 1); EFX03580.1

34.	02738.7	PEF-1	Ca^{2+} and/or CaM binding protein	2e-130; *Verticillium dahliae* (Peflin); EGY21808.1
35.	09871.7		Ca^{2+} and/or CaM binding protein	4e-33; *Verticillium dahliae* (Centrin-3); EGY16271.1
36.	01241.7		Ca^{2+} and/or CaM binding protein	0; *Trichoderma reesei* (Mitochondrial carrier protein); EGR44893.1
37.	06347.7		Ca^{2+} and/or CaM binding protein	0; *Sordaria macrospora* (Actin cytoskeleton-regulatory complex protein); XP_003350109.1
38.	06617.7	CAMK-3	Ca^{2+} and/or CaM binding protein	7e-93; *Verticillium albo-atrum* (Myosin regulatory light chain cdc4); XP_003009631.1
39.	03750.7		Ca^{2+} and/or CaM binding protein	8e-74; *Botryotinia fuckeliana* (Calmodulin); XP_001560827.1
40.	08980.7	NDE-1	Ca^{2+} and/or CaM binding protein	0; *Grosmannia clavigera* (Alternative NADH-dehydrogenase); EFX03867.1
41.	02283.7	CAMK-2	Ca^{2+} and/or CaM binding protein	0; *Sordaria macrospora* (Calcium/calmodulin-dependent protein kinase type I); XP_003344498.1
42.	09123.7	CAMK-1	Ca^{2+} and/or CaM binding protein	0; *Sporothrix schenckii* (Calcium/calmodulin-dependent kinase); AAV80434.1

43.	02814.7	PRD-4	Ca^{2+} and/or CaM binding protein	0; *Grosmannia clavigera* (Serine/threonine-protein kinase chk2); EFX01629.1
44.	09212.7		Ca^{2+} and/or CaM binding protein	0; *Verticillium dahliae* (Serine/threonine-protein kinase srk1); EGY15110.1
45.	06650.7		Ca^{2+} and/or CaM binding protein	3e-61; *Nectria haematococca* (Phospholipase A2); XP_003042542.1
46.	02411.7		Ca^{2+} and/or CaM binding protein	0; *Glomerella graminicola* (Microtubule associated protein); EFQ31793.1
47.	06177.7		Ca^{2+} and/or CaM binding protein	0; *Magnaporthe grisea* (CMKK2); ACM41720.1
48.	04265.7		Ca^{2+} and/or CaM binding protein	7e-85; *Bacillus megaterium* (Beta-fructosidase FruA); AEN90524.1

[a]Adapted from Tamuli *et al.* 2013

[b]BLASTP search (http://blast.ncbi.nlm.nih.gov/Blast.cgi; Altschul *et al.* 1990, 1997, 2005) with the default parameters for each of the 48 Ca^{2+}-signaling proteins against the non-redundant protein sequence databases at the NCBI has been indicated the respective best overall match in other organisms.

[c]Split from NCU07605.1.

[d]Split from NCU01437.1.

[e]Split from NCU09655.1; [f]NCU05225.5 (was indicated as NCU08980.1 in Borkovich *et al.* 2004).

1.5 Calmodulin: the ubiquitous Ca^{2+} sensor protein

Ca^{2+}-signaling is mediated by a number of proteins including a high affinity Ca^{2+}-sensor protein calmodulin (CaM). CaM regulates numerous cell functions in different organisms including the model filamentous fungus *N. crassa* (Tamuli *et al*. 2013; Laxmi and Tamuli 2015, 2016).

The name CaM was first suggested by W. Y. Cheung (Cheung 1970). CaM was discovered as an activator of cyclic nucleotide phosphodiesterase in brain and heart (Kakiuchi and Yamazaki 1970; Cheung 1970). The crystal structure of CaM in the Ca^{2+} -bound form shows a dumbbell-shaped molecule with two globular domains arranged in a trans configuration connected by a long central α-helix. Each lobe consists of two helix-loop-helix motifs (EF hands), which are joined by a short antiparallel β-sheet; bind with two Ca^{2+} ions (Babu *et al.* 1988; James *et al.* 1995; Zhang *et al.* 2012). Ca^{2+}-free CaM is referred to as apocalmodulin (ApoCaM), which is structurally different from Ca^{2+}-CaM. While most target proteins bind Ca^{2+}-CaM, certain proteins only bind to ApoCaM. CaM is a dynamic 17 kDa Ca^{2+} sensor protein, capable of responding to a wide range of Ca^{2+} concentrations (10^{-12} M –10^{-6} M) and uses different modes of Ca^{2+}-dependent interactions, which are responsible for generating high affinity as well as specificity for targets (Means and Dedman 1980; Chin and Means 2000). Interest in CaM is also attributed by its binding proteins that are not only more in numbers but also widely varied. Ca^{2+}-CaM binding domains in different target proteins show very little similarity in primary sequence. Instead, these binding sites are amphipathic α-helices, typically 20 residues in length, with basic and hydrophobic residues intermingled. In addition, one or more aromatic residues are also found near the amino-terminal end of this region, which are important to binding (Zvelebil and Thornton 1993; Jurado *et al.* 1999). Based upon their Ca^{2+} ion requirement for CaM binding, it is possible to classify CaM-binding proteins into three categories, Ca^{2+}-dependent, Ca^{2+}-independent and Ca^{2+}-inhibited. There are three recognition motifs for CaM interaction, IQ motif as a consensus for Ca^{2+}-independent binding and two related motifs for Ca^{2+}-dependent binding, termed 1-8-14 and 1-5-10 based on the position of conserved hydrophobic residues (Rhoads and Friedberg 1997). Thus, CaM can bind to at least 30 different target enzymes and proteins including Ca^{2+}-transport ATPase, phosphodiesterase, nitric oxide synthase and CaM-dependent protein kinases such as myosin light chain kinase (MLCK) and calcineurin (CNA). Therefore, CaM plays a central role in regulating a number of fundamental

cellular activities from fungi to mammals (Jurado *et al.* 1999; Zhang *et al.* 2012). Current understandings on CaM in some of the fungal species are discussed below.

1.5.1 *Saccharomyces cerevisiae* and *Schizosaccharomyces pombe*

Budding yeast *Saccharomyces cerevisiae* contains a single CaM gene (*cmd1*) with no intron. Deletion of *cmd1* gene are unable to grow in vegetative phase and from spores, indicating that CaM is an essential gene (Davis *et al.* 1986). Vertebrate CaM binds 4 Ca^{2+} ions whereas *S. cerevisiae* CaM binds only 3 Ca^{2+} (Luan *et al.* 1987; Matsuura *et al.* 1991; Starovasnik *et al.* 1993) and vertebrate CaM is able to complement the essential function of CaM in yeast (Davis and Thorner 1989; Ohya and Anraku 1989). The amino acid composition of yeast CaM was different from other lower eukaryotes CaM, in that it had no tyrosine, but more leucine and high ratio of serine to threonine (Ohya *et al.* 1987). CMD mutant allele that are completely defective for Ca^{2+}-binding sites does not abolish the ability of the protein to support growth, suggesting that this function independent to Ca^{2+}-binding in *S. cerevisiae* (Geiser *et al.* 1991; Nakashima *et al.* 2012). Cells deficient in CaM expression showed bud emergence and DNA synthesis, but did not accomplish nuclear division (Ohya and Anraku 1989). CaM performs essential functions including polarized cell growth accumulating at sites of cell growth in *S. cerevisiae* (Brockerhoff and Davis 1992) and regulating Myo2p (unconventional myosin) through a direct interaction (Brockerhoff *et al.* 1994). Interaction between CaM and spindle pole body component (Spc110p), an essential mitotic target of CaM, promotes mitotic spindle formation from the centrosome or spindle pole body (SPB) in *S. cerevisiae* (Sun *et al.* 1992; Geiser *et al.* 1993; Stirling *et al.* 1994). Several phenylalanine residues in yeast CaM are required to different extents in different combinations in order to carry out each of the several essential tasks (Ohya and Botstein 1994a). Examination of 14 temperature sensitive yeast mutants bearing one or more phenylalanine to alanine substitutions in the single CaM gene, revealed diverse essential functions of CaM in yeast (Ohya and Botstein 1994b). In *S. cerevisiae*, mutants lacking either N-terminal or C-terminal half of CaM and containing two EF hand motifs, bind Ca^{2+}, however, fail to fully acquire induced thermotolerance (Iida *et al.* 1995). In addition to these CaM also regulates cell cycle control in *S. cerevisiae* (Anraku *et al.* 1991) and functions in stress responses primarily through the activation of CaM-dependent protein kinases and phosphatase (Cyert 2001).

Similarly, fission yeast *Schizosaccharomyces pombe*, contains a single gene encoding CaM (*cam1*), which is essential for cell growth (Takeda and Yamamoto 1987). *S. pombe* CaM exhibits more homology to vertebrate CaM than to that of *S. cerevisiae* (Hubbard *et al.* 1982; Davis *et al.* 1986; Takeda and Yamamoto 1987). In *S. pombe*, Ca^{2+} binding to CaM is required for its essential function, and a mutant that is compromised for Ca^{2+} binding exhibits defects in function of spindle during mitosis (Moser *et al.* 1995, 1997). SPB assembly mechanism for Pcp1p (pole target of CaM), an Spc110p-related CaM target protein of the *S. pombe* distinct from budding yeast Spc110p (Flory *et al.* 2002).

1.5.2 *Aspergillus nidulans*

Similar to yeast, *Aspergillus nidulans* contains one CaM gene, disruption of the CaM gene by site-specific homologous recombination was lethal, indicating that CaM is essential (Rasmussen *et al.* 1990). CaM of *A. nidulans* is more homologous to vertebrate CaM (84% identity) than CaM from either *S. cerevisiae* (64%) or *S. pombe* (74%). In contrast to *S. cerevisiae*, *A. nidulans* CaM is able to bind four Ca^{2+} ions and requires Ca^{2+}-CaM for cell cycle progression. In *A. nidulans*, CaM mutated in the Ca^{2+}-binding sites do not support growth and division (Rasmussen *et al.* 1990, 1992). Raising the CaM concentration by inducing the alcA promoter not only causes the cells to enter the proliferative cycle more quickly and to grow faster, but also decreases the concentration of extracellular Ca^{2+} required to support growth by 10-fold, as compared with cells grown in non-inducing medium. Thus both the intracellular CaM and extracellular Ca^{2+} concentrations are important and interactive factors in regulating the nuclear division cycle of *A. nidulans* (Lu *et al.* 1993). Depletion of CaM causes a failure to progress from cell cycle between G2 and M in *A. nidulans* (Lu *et al.* 1992, 1993). CaM concentrates at the apex of growing hyphae and localizes to the spitzenkorper in *A. nidulans* (Wang *et al.* 2006). The localization of CaM fusion with GFP protein was found quite dynamic throughout the hypha and was concentrated to the active growing sites during germination, hyphal growth, cytokinesis, conidiation and depletion of CaM by alcA promoter repression induced the explicit abnormalities of germlings with the swollen germ tubes (Chen *et al.* 2010).

1.5.3 *Candida albicans*

Candida albicans undergoes yeast-mycelial conversion through the intermediary formation of a germ tube, this morphogenetic transformation has been implicated in the depelopment of pathogenicity of the fungus (Saltarelli *et al.* 1975; Bistoni *et al.* 1986). CaM encoding gene (*CMD1*) was also isolated and characterized from the dimorphic and pathogenic fungus *C. albicans* (Hubbard *et al.* 1982; Saporito and Sypherd 1991). CaM is important for the yeast to mycelial transition (Sabie and Gadd 1989) by differential protein phosphorylation in *C. albicans* (Paranjape *et al.* 1990; Datta 1992) or by regulating cAMP levels, or chitin synthase activity or by modulating syntheis, localization or polymerization of actin and microtubule organization (Datta 1992). In addition, two-fold higher *CMD1* activity levels were measured in hyphal cells of *C. albicans* (Paranjape *et al.* 1990). The CaM inhibitors trifluoperazine (TFP) and chlorpromazine (CPZ) inhibited the yeast-to-mycelial transition of *C. albicans* in vitro (Roy and Datta 1987; Buchan *et al.* 1993; Sato *et al.* 2004). TFP and the Ca^{2+} ionophore A23187 inhibit germ tube formation, also reduced the rate of phosphorylation that is important for germ tube formation, which indicated a possible involvement of Ca^{2+} and CaM in germ tube formation in *C. albicans* (Roy and Datta 1987; Paranjape *et al.* 1990; Datta 1992). CaM also plays an important role for the regulation of stress response and virulence via activation of CNA, a Ca^{2+}/CaM-dependent phosphatase (Blankenship *et al.* 2003; Kraus and Heitman 2003; Sanglard *et al.* 2003; Reedy *et al.* 2010) as well as Ca^{2+}/CaM-dependent protein kinases signaling cascade that are involved in the regulation of cell wall integrity and oxidative stress response in *C. albicans* (Ding *et al.* 2014).

1.5.4 *Cryptococcus neoformans*

In the opportunistic human pathogenic fungus *Cryptococcus neoformans*, CNA critically governs growth and virulence at 37°C (Odom *et al.* 1997; Cruz *et al.* 2001; Fox *et al.* 2001; Kraus *et al.* 2003) while in *C. albicans*, CNA is necessary for survival in serum and virulence (Blankenship *et al.* 2003). As disscused earlier, CaM can function in both Ca^{2+}-dependent and independent form in *S. cerevisiae* (Geiser *et al.* 1991; Cyert 2001; Nakashima *et al.* 2012). Similarly Ca^{2+}-free form of CaM and CNA share an essential function that governs cellular morphogenesis in *C. neoformans* (Kraus *et al.* 2003). The *CAM1* gene was demonstrated to be essential by using gene disruption approaches and *CAM1/cam1Δ* diploid strain in *C. neoformans*, as in other fungi. A unique temperature-

sensitive allele of the *CAM1* gene was isolated via insertional mutagenesis and found to confer temperature-sensitive growth by reducing but not abolishing CAM expression. The *cam1-ts* allele, a Ca^{2+}-independent CAM mutant in which the four Ca^{2+}-binding EF hands are mutated. In the absence of CNA function, the *cam1-ts* mutant displayed a severe morphological defect with impaired bud formation. Expression of a CaM-independent CNA mutant did not suppress the growth defect of the *cam1-ts* mutant at 37°C, indicating that CaM promotes growth at high temperature via CNA-dependent and -independent pathways. In addition, a Ca^{2+} binding defective allele of *CAM1* complemented the 37°C growth defect, FK506 hypersensitivity, and morphogenesis defect of the *cam1-ts* mutant. Thus CaM performs Ca^{2+} and CNA-independent and -dependent roles to govern morphogenesis and growth at 37°C in *C. neoformans* (Kraus *et al.* 2005).

1.5.5 *Ceratocystis ulmi*

Ascomycete *Ceratocystis ulmi* is the causative agent of Dutch elm disease (Kulkarni and Nickerson 1981). Similar to *C. albicans* and *C. neoformans,* Ca(II)-CaM is required for regulation of yeast-mycelium dimorphism in *C. ulmi* (Muthukumar and Nickerson 1984, 1985, 1986). Ca(II) ions, ethylene glycol-bis(O-aminoethyl ether)-N,N-tetraacetic acid, LaCl3, and six known CaM inhibitors (trifluoperazine, chlorpromazine, quinacrine, dibucaine, propranolol, and tetracaine) shifted the dimorphic potential of *C. ulmi* (Muthukumar and Nickerson 1984). In addition to this Ca(II)-CaM interaction is necessary for mycelial growth in *C. ulmi* and the absence of this interaction leads to the yeast phase (Muthukumar and Nickerson 1984). Similar to *A. nidulans*, CaM levels increased at the G1-S boundary of the cell cycle in *C. ulmi*. Moreover, CaM is also present buds or germ tubes of *C. ulmi* (Muthukumar *et al.* 1985).

1.5.6 *Magnaporthe grisea*

In the genome of *Magnaporthe grisea,* an ascomycete fungus, a single copy of CaM gene has been identified that contains five introns and highly homologous (90%) to plant and animal CaM (Liu and Kolattukudy 1999; Ma *et al.* 2009). Similar to other fungi, knock-out of CaM gene is lethal for *M. grisea* (Ma *et al.* 2009). *M. grisea* produces specialized infectious structures known as appressorium to infect its host, causing rice blast disease. Several Ca^{2+} modulators and CaM antagonists inhibited appressorium formation at the micromolar level, while conidia germination remained unaffected, thus Ca^{2+}/CaM -

dependent signaling system is involved in the infection process of *M. grisea* (Lee and Lee 1998). A GFP reporter gene under the CaM promoter was used to determine the CaM expression including the factors that affect its expression in *M. grisea*. GFP fluorescence reached a maximum at a fourfold level in 2 to 3 h of surface contact, suggests that CaM gene expressed early which precedes appressorium formation in *M. grisea* (Liu and Kolattukudy 1999).

1.5.7 *Colletotrichum trifolii* and Colletotrichum sp.

Similar to *M. grisea*, in phytopathogenic fungus *Colletotrichum trifolii* disturbance of Ca^{2+} homeostasis and CaM inhibition affect both germination and appressorium formation, implying that the Ca^{2+}/CaM signal transduction pathway plays an essential role in conidial germination and appressorium formation (Warwar and Dickman 1996). Similar conclusions were observed for *C. gloeosporioide, C. coccodes* and *C. dematium* (Kim *et al.* 1998; Ahn *et al.* 2003a; b). CaM gene is present as a single copy in the genome of *C. trifolii* and its predicted amino acid sequence shows considerable homology to other fungal CaM. The nucleotide sequence of the *C. trifolii* CaM gene suggested that it contain six introns while *A. nidulans* and *N. crassa* CaM have five introns. The relative importance of CaM expression during prepenetration development was studied by antisense expression using a conditional promoter from *N. crassa* and found that CaM is highly expressed during conidial germination and appressorium formation (Warwar *et al.* 2000).

1.5.8 *Cochliobolus miyabeanus*

Several inhibitors that act on various steps in the Ca^{2+}/CaM-dependent signaling pathway were used to elucidate the role of Ca^{2+}/CaM in the prepenetration morphogenesis of *Cochliobolus miyabeanus* (Ahn and Suh 2007a; b). In addition, maintenance of Ca^{2+} homeostasis within cells is also important for prepenetration development in *C. miyabeanus*, a pathogenic plant fungi (Ahn and Suh 2007a; b).

1.5.9 *Fusarium oxysporum* and Fusarium sp.

CaM from *Fusarium oxysporum* was similar to other fungal CaM. In contrast to *N. crassa*, *F. oxysporum* CaM contain 2 trimethyllysines residues (Cox *et al.* 1982; Hoshino *et al.* 1994). Primary structure of *F. oxysporum* CaM had high homology with *A. nidulans* CaM (Hoshino *et al.* 1994). CaM gene sequences was used for species specific

PCR based detection of the toxigenic species *F. proliferatum*, *F. oxysporum*, *F. verticillioides* and *F. subglutinans* from asparagus plants (Mulè *et al.* 2004a; b). The development of CaM specific primers for identification of Fusarium sp. should provide tools to prevent health risks caused by mycotoxin contaminated maize based food and feed, thus have a positive impact on plant, animal and human health (Mulè *et al.* 2004a; b). In addition, Ca^{2+} ionophore A23187 increased mean hyphal extension rate and hyphal growth unit length and this response was antagonized by low concentrations of CaM antagonist TFP. Thus Ca^{2+} and CaM involved in the regulation of hyphal extension and branching in *F. graminearum* A 3/5 (Robson *et al.* 1991).

1.5.10 *Neurospora crassa*

N. crassa has only one CaM that was isolated using affinity chromatography and identified based on its characteristic Ca^{2+} dependent shift in electrophoretic migration, activation of bovine heart cAMP – phosphodiesterase (PDE) and distinct peaks (located at 276, 268, 264, 258 and 252 nm) in an absorption spectrum that appears to be an essential gene for viability (Perez *et al.* 1981; Cox *et al.* 1982; Melnick *et al.* 1993; Galagan *et al.* 2003; Borkovich *et al.* 2004). The *N. crassa* CaM protein shows 59% homology to the yeast and 85% homology to the human CaM protein. The highest homology, however, is to CaM from *A. nidulans*, whose CaM protein sequence differs by only one amino acid (Rasmussen *et al.* 1990; Melnick *et al.* 1993). The *N. crassa* CaM encoding gene NCU04120 contains six exons and five introns that encodes a CaM protein of 149 amino acid residues with a predicted molecular weight of 16950 Da. Out of four EF-hand domains, one EF-hand is insensitive to Ca^{2+} ion. *N. crassa* CaM is slightly less acidic than its vertebrate counterpart, and its amino acid composition is typical to that of plant CaM with the exception that trimethyllysine is absent and content of serine is unusual high similar to *S. cerevisiae* (Cox *et al.* 1982; Ohya *et al.* 1987). *N. crassa* CaM is less potent in the activation of myosin light chain kinase than CaM from higher organisms (Cox *et al.* 1982). CaM activates soluble adenylate cyclase, protein kinase, cyclic AMP phosphodiesterase and protein phosphatase in *N. crassa* (Reig *et al.* 1984; Tuinen *et al.* 1984; Tellez-Inon *et al.* 1985; Higuchi *et al.* 1991). Inhibition of CaM by TFP and CPZ was shown to affect conidiation rhythm, light induced phase shifting, activation of chitin synthase enzyme, vegetative growth, hyphal development and sexual development in *N. crassa* (Suzuki *et al.* 1996; Sadakane and Nakashima 1996; Suresh and Subramanyam 1997; Laxmi and Tamuli 2015). In addition, CaM also play an

important role in carotenoid accumulation, ultraviolet (UV) survival and full fertility during meiosis in *N. crassa* (Laxmi and Tamuli 2016).

1.6 Objectives of this study

In this work, I studied cellular roles of CaM and some of its target proteins in *N. crassa.* Specifically, my objectives were as follows:

1. Understanding cellular role of calmodulin and related Ca^{2+}-signaling proteins in *N. crassa.*
2. Identification of important amino acid residues of CaM and its role in sexual development.
3. Site-directed mutational analysis of Ca^{2+}/CaMK-2 and expression studies of selected Ca^{2+}-signaling genes.

Chapter 2

Materials and Methods

Materials and Methods

2.1 Materials

2.1.1 Chemicals and other materials

Glucose, sorbose, fructose, sucrose, sorbitol, bacto-agar, sodium dodecyl sulphate (SDS), cetyltrimethyl ammonium bromide (CTAB), calcium chloride ($CaCl_2.H_2O$), sodium citrate dihydrate (Na_3 citrate.$2H_2O$), potassium phosphate monobasic (KH_2PO_4), potassium phosphate dibasic (K_2HPO_4), ammonium nitrate (NH_4NO_3), magnesium sulphate ($MgSO_4$), citric acid ($C_6H_8O_7.H_2O$), zinc sulphate heptahydrate ($ZnSO_4.7H_2O$), ferrous sulphate heptahydrate ($FeSO_4.7H_2O$), copper sulphate ($CuSO_4.5H_2O$), maganous sulphate ($MnSO_4.H_2O$), boric acid (H_3BO_3), sodium molybdate ($Na_2MoO_4.2H_2O$), potassium nitrate (KNO_3), sodium chloride, sodium hydroxide (NaOH), potassium acetate (CH_3COOK), Tris base ($C_4H_{11}NO_3$), ethylenediaminetetra acetic acid disodium salt (EDTA $C_{10}H_{14}N_2O_8Na_2.2H_2O$), skim milk, calcium D –pantothenate ($C_9H_{16}O_5N.1/2$ Ca), silica gel (6-12 mesh), hexane, acetone, Tween 80, glacial acetic acid, absolute ethanol, Phenol:Chloroform:Isoamyl mixture (25:24:1), β-mercaptoethanol, glycerol, chloroform, agarose, ethidium bromide, X-gal (5 bromo-4-chloro-3-indolyl-B-galactoside), IPTG (isopropylthio-β-d-galactoside) and other general laboratory chemicals and glass wares were procured from various manufacturers such as SRL (Mumbai, India), Merck (Mumbai, India), Himedia (Mumbai, India), Borosil (Mumbai, India), Tarsons (Kolkata, India) and Rankem reagents (Faridabad, India). Hygromycin, glufosinate ammonium sulphate (basta), biotin and Triazol reagent were purchased from the Sigma Aldrich, USA. All restriction enzymes, DNA size markers and Taq DNA polymerases for PCRs were purchased from New England Biolabs, USA. High fidelity Taq polymerases were purchased from Thermo Fisher Scientific, Finland. Custom oligonucleotide primers were purchased from Bioserve, Hyderabad, India as well as from Integrated DNA Technologies (IDT), USA. DNA purification kits were from Qiagen, USA. All other chemicals were purchased from local manufacturers and were of analytical grade.

Table 2.1: *N. crassa* strains used in this study

Sl. no.	Strain	Genotype	Reference
1.	74-OR23-IVA	Wild-type; *mat A*	FGSC 2489
2.	ORS-SL6 a	Wild-type; *mat a*	FGSC 4200
3.	74-OR23-1 A	Wild-type; *mat A*	FGSC 987
4.	OR8-1 a	Wild-type; *mat a*	FGSC 988
5.	NCU04120	[(*cmd; mat a*) + (Δ*cmd::hph; mat a*)] (heterokaryon)	FGSC 11618
6.	NCU04898	Δ*trm-9::hph; mat A*	FGSC 13040
7.	NCU04736	Δ*nca-2::hph; mat A*	FGSC 13071
8.	NCU09123	Δ*camk-1::hph; mat A*	FGSC 12547
9.	NCU09123	Δ*camk-1::hph; mat a*	FGSC 12548
10.	NCU02283	Δ*camk-2::hph; mat A*	FGSC 12449
11.	NCU02283	Δ*camk-2::hph; mat a*	FGSC 12448
12.	NCU06177	Δ*camk-3::hph; mat A*	FGSC 11536
13.	NCU06177	Δ*camk-3::hph; mat a*	FGSC 11537
14.	NCU09212	Δ*camk-4::hph; mat a*	FGSC 11545
15.	NCU06366	*cpe-1::hph; mat A*	FGSC 11408
16.	NCU06366	*cpe-1::hph; mat a*	FGSC 11407
17.	NCU06703	*mid-1::hph; mat A*	FGSC 11708
18.	NCU06703	*mid-1::hph; mat a*	FGSC 11707
19.	NCU06245	*plc1::hph; mat a*	FGSC 11411
20.	NCU06650	*splA2::hph; mat A*	FGSC 11247
21.	NCU06650	*splA2::hph; mat a*	FGSC 11246
22.	NCU04379	*ncs-1::hph; mat A*	FGSC 11404
23.	NCU04379	*ncs-1::hph; mat a*	FGSC 11403
24.	Δ*Sad-1*	Δ*Sad-1::hph; mat A*	FGSC 8741
25.	Δ*Sad-1*	Δ*Sad-1::hph; mat a*	FGSC 8740
26.	i-94-120	*erg-3; mat a*	Prakash *et al.* 1999

27.	34-97-3	*upr-1; mat a*	Tamuli *et al.* 2006
28.	17	Δ*camk-1::hph*Δ*camk-2::hph; mat a*	Kumar and Tamuli 2014
29.	21	Δ*camk-2::hph*Δ*camk-3::hph; mat A*	Kumar and Tamuli 2014
30.	51-IV-8a	Δ*rid-1::nat*; Δ*mus-51::hph; mat a*	Ouyang *et al.* 2015
31.	20	Δ*trm-9::hph; mat a*	Laxmi and Tamuli 2015
32.	23	Δ*nca-2::hph; mat a*	Laxmi and Tamuli 2015
33.	12	Δ*trm-9::hph*Δ*nca-2::hph; mat A*	Laxmi and Tamuli 2015
34.	19	Δ*trm-9::hph*Δ*nca-2::hph; mat a*	Laxmi and Tamuli 2015
35.	26-35-IV-8	[(Δ*rid-1::nat*; Δ*mus-51::hph; mat a*) + (Δ*pan-2::bar::*P_{tcu-1}*::cmd::5xGly::V5::gfp; mat a*)] (heterokaryon)	Laxmi and Tamuli 2016
36.	850	Δ*rid-1::nat*; Δ*pan-2::bar::* P_{tcu-1}*::cmd::V5::gfp; mat a*	Laxmi and Tamuli 2016
37.	851	Δ*rid-1::nat*; Δ*pan-2::bar::* P_{tcu-1}*::cmd::V5::gfp; mat a*	Laxmi and Tamuli 2016
38.	852	Δ*rid-1::nat*; Δ*pan-2:: bar::* P_{tcu-1}*::cmd::V5::gfp; mat a*	Laxmi and Tamuli 2016
39.	853	Δ*rid-1::nat*; Δ*pan-2::bar::* P_{tcu-1}*::cmd::V5::gfp; mat a*	Laxmi and Tamuli 2016
40.	854	Δ*rid-1::nat*; Δ*pan-2::bar::* P_{tcu-1}*::cmd::V5::gfp; mat a*	Laxmi and Tamuli 2016
41.	2	Δ*pan-2::bar::*P_{tcu-1}*:: cmd::V5 ::gfp; mat A*	Laxmi and Tamuli 2016

42.	4	Δ*pan-2::bar::*P$_{tcu-1}$*::cmd::V5 ::gfp; mat A*	This study
43.	12	Δ*pan-2::bar::*P$_{tcu-1}$*::cmd::V5 ::gfp; mat A*	This study
44.	13	Δ*pan-2::bar::*P$_{tcu-1}$*::cmd::V5 ::gfp; mat A*	This study
45.	15	Δ*pan-2::bar::*P$_{tcu-1}$*::cmd::V5 ::gfp; mat A*	This study
46.	16	Δ*pan-2::bar::*P$_{tcu-1}$*::cmd::V5 ::gfp; mat A*	This study
47.	17	Δ*pan-2::bar::*P$_{tcu-1}$*::cmd::V5 ::gfp; mat A*	This study
48.	24	Δ*pan-2::bar::*P$_{tcu-1}$*::cmd::V5 ::gfp; mat A*	Laxmi and Tamuli 2016
49.	28	Δ*pan-2::bar::*P$_{tcu-1}$*::cmd::V5 ::gfp; mat A*	This study
50.	30	Δ*pan-2::bar::*P$_{tcu-1}$*::cmd::V5 ::gfp; mat A*	This study
51.	31	Δ*pan-2::bar::*P$_{tcu-1}$*::cmd::V5 ::gfp; mat A*	This study
52.	34	Δ*pan-2::bar::*P$_{tcu-1}$*::cmd::V5 ::gfp; mat A*	This study
53.	41	Δ*pan-2::bar::*P$_{tcu-1}$*::cmd::V5 ::gfp; mat A*	This study
54.	RIP-26	Δ*pan-2::bar::*P$_{tcu-1}$*::cmd*^{RIP}*::V5 ::gfp; mat A*	Laxmi and Tamuli 2016
55.	RIP-38	Δ*pan-2::bar::*P$_{tcu-1}$*::cmd*^{RIP}*::V5 ::gfp; mat A*	Laxmi and Tamuli 2016
56.	RIP-3	Δ*pan-2::bar::*P$_{tcu-1}$*::cmd*^{RIP}*::V5 ::gfp; mat A*	Laxmi and Tamuli 2016
57.	RIP-6	Δ*rid-1::nat*; Δ*pan-2::bar::*P$_{tcu-1}$ *::cmd*^{RIP}*::V5::gfp; mat a*	Laxmi and Tamuli 2016

58.	RIP-9	Δ*pan-2::bar::*P$_{tcu-1}$*::cmd*^{RIP}*::V5 ::gfp; mat A*	Laxmi and Tamuli 2016
59.	RIP-35	Δ*rid-1::nat*; Δ*pan-2::bar::*P$_{tcu-1}$ *::cmd*^{RIP}*::V5::gfp; mat a*	Laxmi and Tamuli 2016
60.	RIP-50	Δ*rid-1::nat*; Δ*pan-2::bar::*P$_{tcu-1}$ *::cmd*^{RIP}*::V5::gfp; mat a*	Laxmi and Tamuli 2016
61.	RIP-55	Δ*pan-2::bar::*P$_{tcu-1}$*::cmd*^{RIP}*::V5 ::gfp; mat A*	Laxmi and Tamuli 2016
62.	HT-C6	[(Δ*camk-2::hph; mat A*) + (*camk-2::bar; mat A*)] (heterokaryon)	Laxmi and Tamuli 2016
63.	HT-S29	[(Δ*camk-2::hph; mat A*) + (*camk-2*^{S247A}*::bar; mat A*)] (heterokaryon)	Laxmi and Tamuli 2016
64.	HT-T23	[(Δ*camk-2::hph; mat A*) + (*camk-2*^{T267A}*::bar; mat A*)] (heterokaryon)	Laxmi and Tamuli 2016
65.	HT-L1	[(Δ*camk-2::hph; mat A*) + (*camk-2*^{L309D}*::bar; mat A*)] (heterokaryon)	Laxmi and Tamuli 2016
66.	HOP-102	Δ*camk-2::hph; camk-2::bar; mat a*	Laxmi and Tamuli 2016
67.	HOP-116	Δ*camk-2::hph; camk-2::bar; mat A*	Laxmi and Tamuli 2016
68.	HOP-119	Δ*camk-2::hph; camk-2::bar; mat a*	Laxmi and Tamuli 2016
69.	HOP-120	Δ*camk-2::hph; camk-2::bar; mat A*	Laxmi and Tamuli 2016
70.	HOP-17	Δ*camk-2::hph; camk-2*^{S247A} *::bar; mat A*	Laxmi and Tamuli 2016
71.	HOP-51	Δ*camk-2::hph; camk-2*^{S247A} *::bar; mat a*	Laxmi and Tamuli 2016

72.	HOP-12	Δ*camk-2::hph; camk-2*^{T267A} *::bar; mat a*	Laxmi and Tamuli 2016
73.	HOP-19	Δ*camk-2::hph; camk-2*^{T267A} *::bar; mat A*	Laxmi and Tamuli 2016
74.	HOP-4	Δ*camk-2::hph; camk-2*^{L309D} *::bar; mat A*	Laxmi and Tamuli 2016
75.	HOP-34	Δ*camk-2::hph; camk-2*^{L309D} *::bar; mat a*	Laxmi and Tamuli 2016
76.	HOP-36	Δ*camk-2::hph; camk-2*^{L309D} *::bar; mat a*	Laxmi and Tamuli 2016
77.	HOP-37	Δ*camk-2::hph; camk-2*^{L309D} *::bar; mat A*	Laxmi and Tamuli 2016

2.1.2 Bacterial strains

The *Escherichia coli DH5-α,* genotype is *SupE44* Δ*lacU169* (*ϕ80lacZ* Δ*M15*) *hsdR17 recA1 end A1 gyrA96 thi-1 relA1,* is a recombination-deficient amber suppressing strain used for growth of plasmids (Sambrook and Russell 2001). The *ϕ80 lacZ* Δ*M15* mutation permits α-complementation with the amino terminus of β-galactosidase encoded in pUC vectors. It was used for all routine transformations, plasmid isolation and selection of recombinants.

2.1.3 Plasmid vectors

1. pBARGEM7-1

The plasmid vector pBARGEM7-1 (Figure 2.1), 4.5 kb in size, carries the fungal selectable marker *bar*, polylinker and lacZ' sequence including the *T7* and *SP6* promoters, bacterial selectable marker ampicillin and pUC origin (Pall and Brunelli 1993). The expression of *bar* gene is under the control of *A. nidulans trpC* promoter. The *bar* gene encodes a phosphinothricin acetyl transferase that detoxifies the antibiotic basta present in the selection medium and therefore, serves as a selectable marker for fungal transformants. The polylinker region containing the lacZ' sequence is subcloned from pGEM7Zf (+) vector. Insertion of DNA fragments into the polylinker region disrupt

the function of the lacZ' gene and recombinant clone can be screened by blue-white selection on the concept of α-complementation (Ullmann *et al.* 1967).

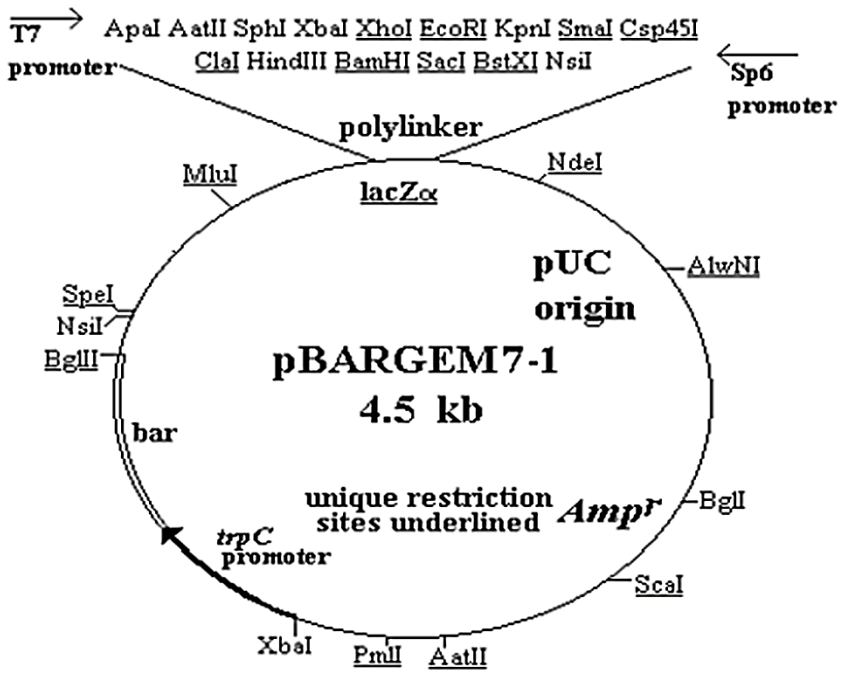

Figure 2.1: Schematic of the pBARGEM7-1 vector. The size of the vector is 4.5 kb. The unique restriction sites are underlined in the polylinker region of lacZ' sequence (Adapted from Pall and Brunelli 1993).

2. pRS426PVG/p*tcu-1*

Yeast/*E. coli* shuttle vector pRS426PVG (Ouyang *et al.* 2015) is the backbone for this constructs. The pRS426PVG/ptcu-1 vector (Figure 2.2) confer uracil prototrophy to *ura3* yeast mutants (URA3) and ampicillin resistance (Ap^R) in *E. coli*. In addition, the pRS426PVG/p*tcu-1*vector contains the copper-responsive promoter (P_{tcu-1}) of the *N. crassa* high affinity copper transporter (Korripally *et al.* 2010; Lamb *et al.* 2013), the 5' and 3' flanking regions for the *N. crassa pantothenate-2* (*pan-2*) ORF surrounding the P_{tcu-1} , a multiple cloning sequence (MCS), a 5-glycine linker (5xGly), a V5 peptide tag, the green fluorescent protein gene (GFP) and the *bar* gene, that confers resistance to phosphinothricin (other chemical names are glufosinate-ammonium, basta, ignite, or finale) in *N. crassa*. The 5' *pan-2* flank extends from 1 kb upstream to the sequence just before the ATG, whereas the 3' flank begins with the sequence just beyond the stop codon

and extends 1 kb downstream. In the pRS426PVG/p*tcu-1* vector, induction and repression of the cloned gene is regulated by the addition of a copper chelator called bathocuproinedisulfonic acid (BCS) and by availability of excess Cu^{2+} on addition of copper II sulfate ($CuSO_4$), respectively.

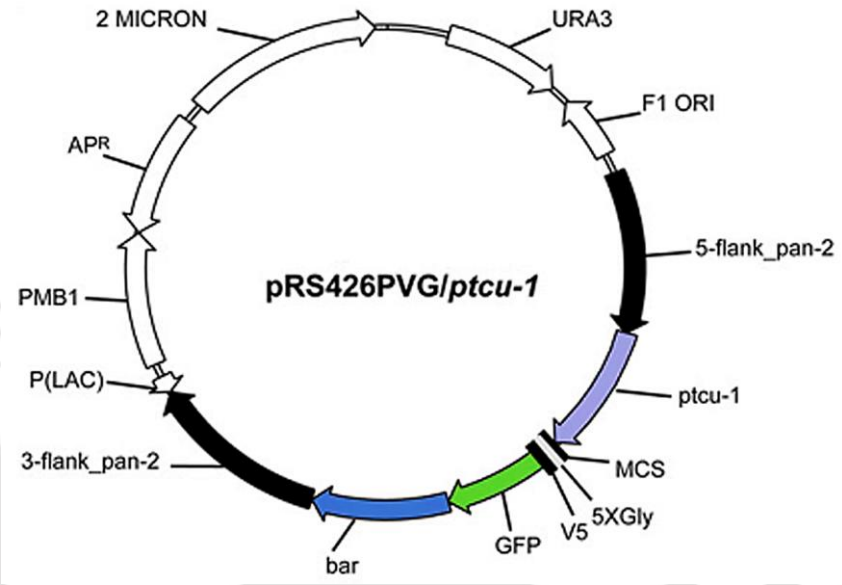

Figure 2.2: Schematic of the pRS426PVG/p*tcu-1* vector. The size of the vector is 10,602 bp. The pRS426PVG/p*tcu-1* vector contains the P_{tcu-1} (violet arrow), the 5' and 3' flanking regions for the *N. crassa pan-2* ORF (black arrows) surrounding the P_{tcu-1}, a MCS (black bar), a 5xGly linker (gray bar), a V5-Tag (black bar), a GFP gene (green arrow), and the *bar* gene (blue shading). The other abbreviations are: P(LAC), lac promoter; 2 MICRON, yeast 2 micron 2 origin of replication; and F1 ORI, origin of replication in *E. coli* (Adapted from Ouyang *et al.* 2015).

2.1.4 Bacterial media, antibiotics and commonly used solutions

Commonly used solutions, which are described below, were prepared essentially as described by Sambrook and Russell (2001).

1. Bacterial media: Luria Bertani (LB) broth, LB agar, terrific broth and SOC medium were purchased from Himedia (Mumbai, India) and prepared according to manufacture protocol and sterilized by autoclaving.

2. IPTG (isopropylthio-D-galactoside): A 20% solution of IPTG was prepared by dissolving 2 g of IPTG in 8 ml of sterile water. The volume of the solution was adjusted to 10 ml and sterilized by passing it through a 0.45-µm filter. The solution was dispensed into 1 ml aliquots and stored at -20ºC.

3. X-gal (5 bromo-4-chloro-3-indolyl-B-galactoside): A stock solution of 20 mg/ml X-gal was prepared in dimethylformamide in an amber eppendorf tube to prevent damage by light and stored at -20ºC.

4. 5 M NaCl: Dissolved 29.22 g of NaCl in 80 ml of distilled water and adjusted the volume to 100 ml. The stock was then sterilized by autoclaving and stored at room temperature.

5. 10 N NaOH: Dissolved 40 g of NaOH pellet slowly in 80 ml of distilled water, stirring continuously in a plastic beaker placed on ice, adjusted the volume to 100 ml and stored at room temperature.

6. 5 M $CaCl_2.2H_2O$: Amount of 73.5 g of $CaCl_2.2H_2O$ was dissolved in distilled water to a final volume of 100 ml. The solution was sterilized by autoclaving.

7. 0.1% DEPC: 0.1% DEPC (Diethylpyrocarbonate) solution was prepared in double autoclaved distilled water and sterilized by autoclaving.

8. 8 M LiCl: Amount of 33.9 g of LiCl was dissolved in a final volume of 100 ml of double autoclaved distilled water and sterilized by autoclaving.

9. 1 M glucose: Amount of 18.016 g of glucose was dissolved in a final volume of 100 ml of distilled water and sterilized by autoclaving.

10. 1 M Sorbitol: Amount of 18.21 g of sorbitol was dissolved in distilled water to a final volume of 100 ml and sterilized by autoclaving.

11. 5 M Sucrose: Amount of 85.575 g of sucrose was dissolved in distilled water to a final volume of 100 ml and sterilized by autoclaving.

12. Ampicillin: A 1000X stock solution of 100 mg/ml ampicillin was made in sterile water and stored at -20°C.

13. Hygromycin B (100 mg/ml): A stock solution of 100 mg/ml was prepared by dissolving an amount of 100 mg of hygromycin B in 1 ml of sterile water and stored at -20°C.

14. Glufosinate ammonium sulphate (basta; 100 mg/ml): A stock solution of 100 mg/ml was prepared by dissolving an amount of 100 mg of basta in 1 ml of sterile water and stored at -20°C.

15. Ethidium bromide (10 mg/ml): 50 mg of ethidium bromide was dissolved in 5 ml of distilled water to prepare 10 mg/ml stock.

16. 6X Gel-loading Buffer (Type III): A solution of 0.25% (w/v) bromophenol blue, 0.25% (w/v) xylene cyanol and 30% glycerol (v/v) was made in sterile water and stored at 4°C.

17. 10% SDS: Dissolved 10 g of SDS (Sodium dodecyl sulphate**)** in 90 ml of distilled water, heated to 60ºC and stirred with a magnetic stirrer to assist dissolution. The volume was adjusted to 100 ml and stored at room temperature.

18. 1 M Tris: Dissolved 121.1 g of Tris base in 800 ml of distilled water, adjusted pH to the desired value (7.5 or 8.0) by adding concentrated HCl. The volume was adjusted to 1 liter with distilled water and sterilized by autoclaving.

19. 0.5 M EDTA (pH 8.0): EDTA is disodium ethylenediaminetetra-acetate.2 H2O. 186.1 g of EDTA was dissolved in 800 ml of distilled water, adjusted pH to 8.0 by adding NaOH pellets. The volume was adjusted to 1 liter and sterilized by autoclaving.

20. RNAase A: Dissolved pancreatic RNAase (DNAase free, Sigma) at a concentration of 10 mg/ml in 10 mM Tris-Cl (pH 7.5), 15 mM NaCl and stored at -20°C.

21. Alkaline lysis Solution I: Amount of 50 mM glucose, 25 mM Tris-Cl (pH 8.0) and 10 mM EDTA (pH 8.0) was added from their stock solutions in a final volume of 100 ml distilled water. Sterilized by autoclaving and stored at 4ºC.

22. Alkaline lysis Solution II: Amount of 0.2 N NaOH and 1% SDS were added in a required volume. The solution was freshly prepared just prior to use.

23. Alkaline lysis Solution III: For a volume of 100 ml solution, 60 ml of 5 M potassium acetate, 11.5 ml of glacial acetic acid and 23.5 ml of distilled water were mixed together. The resulting solution is 3 M with respect to potassium and 5 M with respect to acetate. Sterilized by autoclaving and stored at 4ºC.

24. 50X TAE: The stock solution of 50X TAE for one liter contains 242 g Tris base, 57.1 ml of glacial acetic acid and 100 ml of 0.5 M EDTA (pH 8.0).

25. 1 X TE: The solution was prepared by adding 10 mM Tris-HCl (pH 8.0) and 1 mM EDTA (pH 8.0) from their respective stocks.

26. 10X MOPS electrophoresis buffer: MOPS is a 3 [N-Morpholino] Propanesulphonic acid. The stock solution of 10X MOPS for 1 liter contains 41.8 g of MOPS (0.2 M), 20 ml sodium acetate solution (20 mM) and 20 ml EDTA (10 mM). After dissolving, 41.8 g of MOPS in DEPC-treated water, pH was adjusted to 7.0 with 2 N NaOH and then added sodium acetate solution and EDTA in an indicated volume. Solution was filter sterilized using 0.45-µm millipore filter and stored at room temperature protected from light.

27. Lysis buffer for Neurospora genomic DNA isolation: The lysis buffer contains 10 mM Tris-HCl (pH 7.5), 0.5 M NaCl, 10 mM EDTA, 1% SDS and 1% CTAB.

39. Lysis buffer for Neurospora RNA isolation: The lysis buffer contains 100 mM Tris HCl (pH 8.0), 0.6 M NaCl, 10 mM EDTA (pH 8.0), 4.5% SDS and 2% β- mercaptoethanol.

40. 2 M KCl: Dissolved 14.9 g of KCl in a final volume of 100 ml of distilled water and stored at room temperature.

2.1.5 Solutions for growth, maintenance and crossing of Neurospora strains

Media for culturing Neurospora were prepared essentially as described in Davis and De Serres, 1970.

1. Biotin solution

5 mg of biotin was dissolved in 100 ml of 50% (v/v) ethanol and stored at 4^0C.

2. Trace element solution

Trace element solution was prepared by adding the following compounds successively, with stirring to 95 ml of distilled water.

Citric acid.$1H_2O$	5.00 g
$ZnSO_4.7H_2O$	5.00 g
Fe $(NH_4)_2$ $(SO_4)_2.6H_2O$	1.00 g
$CuSO_4.5H_2O$	0.25 g
$MnSO_4.1H_2O$	0.05 g
H_3BO_3	0.05 g
$Na_2MoO4.2H_20$	0.05 g

The final volume was adjusted to 100 ml; 1 ml of chloroform was added as a preservative and stored at room temperature.

3. Vogel's Medium N

Vogel's Medium N (VM; Vogel 1964) was prepared as a 50X-strength solution as follows: To 750 ml of distilled water, the following ingredients were added in order, dissolving each one prior to addition of the next.

Na_3 citrate.$5H_2O$	150 g
KH_2PO_4	250 g
NH_4NO_3	100 g
$MgSO_4.7H_2O$	10 g
$CaCl_2.2H_2O$	5 g
Biotin solution	5 ml
Trace element solution	5 ml

The volume of the solution was adjusted to 1 liter and 3 ml of chloroform was added as a preservative. $CaCl_2.2H_2O$ predissolved in 10 ml H_2O. VM stocks lacking ammonium (NH_4NO_3) but contain 0.5% L-proline was also used for basta selection.

4. Vogel's glucose medium (VGM)

Vogel's medium N	1X
Glucose	1.5 % (w/v)

5. Vogel's glucose agar medium

Vogel's medium N	1X
Glucose	1.5% (w/v)
Agar	2.0% (w/v)

6. Vogel's sucrose medium (VSM)

Vogel's medium N	1X
Sucrose	2 % (w/v)

7. 4X Synthetic crossing medium

4X strength synthetic crossing medium (SCM) was prepared by adding the following compounds with stirring to 500 ml of water. After adding the following components, the solution was sterilized by autoclaving.

KNO_3	2.0 g
K_2HPO_4	1.4 g
KH_2PO4	1.0 g
$MgSO_4.7H_2O$	1.0 g
$CaCl_2$	0.2 g
NaCl	0.2 g
Biotin solution	0.2 ml
Trace element solution	0.2 ml

8. SCM agar

SCM	1X
Glucose	1.5% (w/v)
Agar	2.0% (w/v)

9. 10X FGS

Fructose	0.5% (w/v)
Glucose	0.5% (w/v)
Sorbose	20% (w/v)

10. Vogel's sorbose agar medium

FGS	1X
Vogel's medium N	1X
Agar	2.0% (w/v)

11. Top agar

FGS	1X
Vogel's medium N	1X
Agar	2.8% (w/v)

12. Skim milk: Sterile milk was prepared by suspending 3.5 g milk powder in 50 ml of deionized water and stored at 4°C.

13. Media supplements (http://www.fgsc.net/methods/stanford.html)

Ca-pantothenate: 1 ml per 100 ml medium from a stock of 1mg/ml in distilled H_2O. Ca-pantothenate supplement stock solution was autoclaved and stored at 4°C.

14. Sterilization

All glassware and plastic ware were sterilized by autoclaving at a steam pressure of 15 psi at 120°C for 20 min. Solutions were prepared in double-distilled water and generally sterilized by autoclaving. Heat-sensitive solutions were sterilized by filtering through a sterile 0.45 µm nitrocellulose filter (Millipore). For RNA isolation, all glass wares were first treated with 0.1 % DEPC solution for overnight, dried in oven at 80ºC and sterilized by autoclaving.

2.2 Methods

2.2.1 Growth conditions

Growth and maintenance of the Neurospora strains were essentially as described in Davis and De Serres (1970).

2.2.2 Crosses, fertility and ascospores collection

Crosses between *N. crassa* strains were essentially as described previously (Westergaard and Mitchell 1947; Davis and de Serres 1970). Crosses were performed by confrontation between opposite mating type mycelia inoculated as plugs on SCM agar medium either in 55 mm diameter petri dishes or 100 mm long glass tubes. The crosses were incubated at 22°C in a low temperature incubator (usually BOD incubator) for 3 to 4 weeks; ascospores began to be shot after 14-16 days. In addition, strains were also crossed to opposite mating type as either the female (protoperithecia) or male (fertilizing) parent to detect mating-specific defects. Dilute conidial suspensions of the male parent were applied directly to 7 days old SCM cultures of opposite mating type strain, containing fully differentiated protoperithecia. Development of perithecia were examined microscopically and images were photographed. For analysis of rosette formation in the perithecia, single perithecium (15-21 days old cross) was dissected by using needle on glass slide containing 10-20 µl of water and observed under microscope (Carl Zeiss, Germany) at 20X magnification. The phenotypes of the crosses were examined on the petri plate lid under a microscope after 25 days and based on the total ascospores produced in a plate culture, the phenotypes of the crosses were scored as fertile (produced thousands of ascospores), intermediate (produced few hundred ascospores) or barren (produced exceptionally few ascospores). Ascospores were harvested by washing the lids with ~1 ml of sterile H_2O after 20-30 days. They are then plated on sorbose agar plate, activated by heat shock at 65°C for 30-60 min in a shaking water bath and picked. Picking was done under dissection microscope by cutting out a small block of agar below the ascospore and transferring it to a slant with minimal or selective media followed by incubation at 30°C for growth.

2.2.3 Stock management

Silica stocks were prepared for storage purpose. Strains were grown in a tube on Vogel's glucose agar slant for seven to ten days. Silica (6-12 Mesh, Grade 40) was sterilized by

autoclaving and dried for 2-3 days at 60°C and cooled to room-temperature before use. Silica was filled in cryos tube (4.5 ml) and kept in ice for 30 min. For each strain, one ml of autoclaved skim milk was added to the culture tube and vortexed vigorously. Spore suspension was drawn up into a pasteur pipette and dispensed into the pre-chilled silica gel and vortexed vigorously for five minutes, breaking up any clumps in the process. Tubes were vortexed regularly for 8-10 days. After a week or more, stocks were frozen at –20°C.

2.2.4 Growth rate experiments

Growth was initially measured by placing either conidia or a plug of agar containing mycelium in the center of a petri dish containing Vogel's glucose agar medium and incubated at 30ºC. Colony growth was circled after 12 h from inoculation point with an interval of 3 h over a period of 24 h to obtain radial growth rate. Strains that show lower growth rate on petri dish were further analyzed by using standard race tube assay (Figure 2.3; Ryan *et al.* 1943). The race tube was partially filled with a 13 ml of Vogel's glucose agar medium and inoculated with either conidia or mycelial plug at one end and incubated at 30°C for 3 days. The apical growth rate of *N. crassa* was determined by measuring the mycelial extension rates at every 12 h intervals in race tube and the distance of the hyphal growth front from the inoculation point was measured and plotted against time. Radial and apical growth rates were calculated as cm h^{-1}.

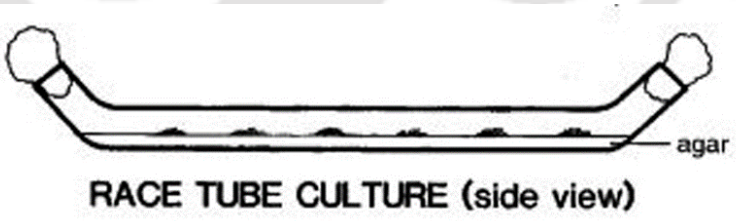

Figure 2.3: Schematic view of a race tube. A race tube is a hollow glass tube (40 cm long, 1.2 to 1.4 cm in diameter) bent upward at the both ends
(Adapted from http://www.fgsc.net/2000compendium/2000compendF.html).

2.2.5 Dry weight analysis

For growth yield, ~1 X 10^6 conidia cells/ml of *N. crassa* strains were inoculated in VGM at 30ºC with shaking at 200 rpm for growth. Mycelia were collected in every 24 h by filtration, dried and weighed over a period 96 h.

2.2.6 Aerial hyphae development analysis

For aerial hyphae growth, ~1 X 10^6 conidia cells/ml were inoculated in VSM and grown for 3 days at 30 °C in dark and 4 days in constant light at room temperature. Height of aerial hyphae was measured and photographed.

2.2.7 Hyphal morphology

For analysis of hyphal morphology, strains were grown for 12-16 h on a thin layer of Vogel's glucose agar medium on glass slide and observed under microscope at 20X magnification.

2.2.8 Conidial cell count

For conidial cell count, ~1 X 10^6 conidia cells/ml of each strain were inoculated in Vogel's glucose agar medium at 30ºC for 2 days in dark, followed by 24 h illumination. Conidial cells were harvested after 72 h of growth using sterile water followed by counting using a haemocytometer under a Trinocular Phase Contrast Microscope count was done after 72 h of growth.

2.2.9 Carotenoids estimation

For measured carotenoid content, ~1 X 10^6 conidia cells/ml of *N. crassa* strains were inoculated into VSM supplemented with 0.2% tween 80, used as a wetting agent to prevent conidiation (Zalokar 1954) and kept for growth at 30°C for two days in dark, followed by 24 h illumination at 30°C. After that mycelia were filtered, lyophilized and powdered. Carotenoids were extracted from 50 mg lyophilized powder by using 1ml of acetone and rotated in a cell mixer for 5 h after that the samples were centrifuged at 12,000 rpm for 10 min. The supernatant was taken out in 1.5 ml fresh eppendorf tube and kept at -80°C for 2 h. Then the tubes were incubated for 8 to 12 h at 30°C until acetone got evaporated. After that 1 ml hexane was added and mixes well. Crude carotenoids extract was scanned in the visible range (400 – 600 nm) by using Cary 100 Bio UV-

visible spectrophotometer (Agilent technologies, US). Hexane was used as reference for scanning. Total carotenoids content was calculated by measuring the maximum absorbance value at 470 nm and using formula: Total carotenoid content (µg/g) = [Total absorbance x Total volume of extract (1ml) x 10^4] / [Absorbance coefficient (2500) x Sample weight (g)] (Rodriguez-Amaya and Kimura 2004).

2.2.10 Isolation of sterols and analysis by UV spectrophotometry

The *N. crassa* strain of interest was grown in VGM at 30°C for 3 days. The mycelial mass was harvested by vacuum filtration and lyophilized. The dried mycelia mass was grinded by using mortar and pestle. About 50 mg of the fine powdered mycelia was taken in a 2 ml microfuge tube and 750 µl each of methanol and chloroform was added to the tube and rotated in a cell mixer for 10-12 h; centrifuged at 12,000 rpm for 10 minutes. The chloroform-methanol extract which contains the lipids was washed with 0.9 % NaCl (500 µl) and centrifuged at 12,000 rpm for 10 minutes. After that supernatant was discarded (white color) and extract was washed twice with 2 M KCl (500 µl); the aqueous and organic phases were separated by centrifugation at 12,000 rpm for 10 minutes. This step separates the saponifiable lipids from non-saponifiable lipids like sterols. The organic phase, which contains the sterols was air-dried at 30°C for 3 hrs. Sterols were dissolved in about 40 µl of chloroform. This sample was diluted 1: 1000 in ethanol and scanned in the UV range (200 – 350 nm), by using Cary 100 Bio UV-visible spectrophotometer (Agilent technologies, US). Absolute ethanol was used as reference for scanning.

2.2.11 Assay for calcium sensitivity

Calcium sensitivity test was performed with conidia grown on Vogel's glucose agar medium at 30°C for 72 h. Conidia was placed in the center of petri dishes containing Vogel's glucose agar media supplemented with 0.0 M, 0.2 M, 0.3 M and 0.4 M $CaCl_2$, incubated at 30ºC and colony diameter was measured after 12 h with an interval of 3 h over a period of 24 h. Radial growth rate was calculated as cm h^{-1}.

2.2.12 Assay for UV sensitivity

For UV sensitivity was assay, strains were grown in flasks containing Vogel's glucose medium at 30°C for 3 days in dark followed by three days under constant light at room

temperature. Strains were harvested, washed with sterile water and finally re-suspended in sterile water. For qualitative assay, conidial cell suspension of ~1 X 10^6 conidia cells/ml were further diluted and ~ 10^5, 10^4, 10^3, 10^2 and 10^1 conidia were spotted on Vogel's sorbose agar medium and irradiated with UV (253 nm wavelength) doses of 50, 100, 150 and 200 J/m^2 in a UVC 500 cross linker (Hoefer, UK). Plates were scanned after 48 h incubation at 30°C. For quantitative analysis, ~1000 conidia cells were plated on Vogel's sorbose agar medium and irradiated with the same UV doses. The plates were incubated at 30°C in the dark for 24-48 h and number of colonies on each plate counted.

2.2.13 Thermotolerance analysis

For measuring thermotolerance, three days old conidia were inoculated into liquid Vogel's glucose media at a concentration of ~1 X 10^6 cells/ml and germinated for 2 h with shaking at 200 rpm at 30°C. These germlings were exposed to different heat treatment condition in two sets; one set was held at 30°C for uninduced condition and the other set at 44°C for induced condition for 30 min, then one set of each were given a lethal heat shock at 52°C for 20 min (Yang and Borkovich 1999; Kumar and Tamuli 2014). After that these conidia were spread on Vogel's sorbose agar medium and incubated at 30°C for 2 days. Percent survival was obtained by dividing the number of viable colonies on plates subjected to heat treatment by the number of viable colonies on plates held at 30°C (control) and multiplying by 100.

2.2.14 Assay for meiotic silencing

The meiotic silencing was assayed using the crosses involving tester strains in which an extra copy of gene was introduced ectopically. The ectopic copy gene remains unpaired in meiosis in crosses of the testers with the wild-type strain of opposite mating type and induces the synthesis of siRNA that silences it as well as its paired native homologs via a gene silencing process called meiotic silencing (Shiu *et al.* 2001; Hammond *et al.* 2013; Nagasowjanya *et al.* 2013). In homozygous tester (tester A × tester a) crosses or in crosses of the testers with the Δ*Sad-1* (suppressor of meiotic silencing), meiotic silencing does not occur and the asci develop normally (Shiu *et al.* 2001; Nagasowjanya *et al.* 2013).

2.2.15 Scoring for antibiotic resistance

Antibiotic resistance was scored by streaking conidia onto 1.5% agar plate containing Vogel's sorbose medium and supplemented with the antibiotic. The antibiotics used were hygromycin B (220 µg/ml), basta (400 µg/ml) and nourseothricin (50 µg/ml).

2.2.16 Preparation of competent cells

Competent cells were prepared by inoculating a single colony of *E. coli* DH5α into 5 ml of LB broth and incubated at 37°C at 200 rpm for 12 h. One ml of this overnight culture was inoculated into 100 ml of LB broth and incubated at 37°C at 180 rpm for one and half hour or till the OD_{600} reached 0.3-0.4. The culture was chilled on ice and centrifuged at 2,710 g for 10 min at 4°C to pellet the cells. For each 50 ml culture pellet were then gently resuspended in 30 ml of ice cold autoclaved transformation buffer (TB: 80 mM $MgCl_2$ and 20 mM $CaCl_2$) and incubated on ice for 10 min. The centrifugation was repeated and for each 50 ml culture pellet cells were resuspended in 2 ml of 0.1 mM $CaCl_2$ containing 10% glycerol (1800 µl of 0.1 mM $CaCl_2$ and 200 µl of absolute glycerol) and distributed into 100 µl aliquots and stored at -80°C.

2.2.17 Transformation of competent *E. coli* cells by heat shock

Competent cells were removed from the -80°C freezer and thawed on ice. Ligated DNA sample (~50 ng -100 ng) was added to the competent cells and mixed gently. The cells were incubated on ice for 30 min, following which they were subjected to heat shock at 42°C in water bath (Julabo GmbH, Germany) for 90 sec. After heat shock 800 µl of SOC media was added to the cells and the tube was incubated at 37°C with shaking at 200 rpm for 1 h. The culture was centrifuged at 8000 rpm for 5 min to pellet the cells. Supernatant was removed and pellet was resuspended 200 µl SOC broth. After that cells were plated on 90 mm LB agar plates containing 100 µg/ml of ampicillin. The plates were incubated at 37°C for 12-14 h growth.

2.2.18 Isolation of plasmid DNA from bacterial culture

Small-scale or minipreparation of plasmid was made by alkaline lysis with SDS (Sambrook and Russell 2001). Briefly, 5 ml of overnight bacterial culture was centrifuged in microfuge tube for 5 min at 6000 rpm and 4°C. Pellet was suspended in 200 µl alkaline lysis solution I to remove media component and centrifuged for 5 min at

6000 rpm and 4°C. Then supernatant was discarded and 100 µl alkaline lysis solution I was added to the pellet. Bacterial suspension was vortexed briefly and kept on ice for 10 min. After that pellet was resuspended in 200 µl alkaline lysis solution II, contents were mixed by inverting the tubes 4-5 times and kept up to 5 min, followed by further addition of 150 µl alkaline lysis solution III. Contents were mixed by inverting the tube 4-5 times and centrifuged for 10 min at 10,000 rpm and 4°C. The supernatant was transferred to the fresh microfuge tube and equal volume of chloroform (~400 µl) was added; centrifuged for 10 min at 10,000 rpm and 4°C. The aqueous phase was taken in a fresh microfuge tube (1.5 ml) and plasmid DNA precipitated by adding 1.5 volumes of absolute ethanol (~800 µl). The tube was gently inverted for few times and kept at 4°C for 3 hrs. DNA was pelleted by centrifuging the tube for 10 min at 10,000 rpm. The supernatant was discarded and the pellet was washed with 70% ethanol; centrifuged for 10 min at 12,000 rpm. Ethanol was discarded and tube was gently inverted on tissue paper for 5 min. The trace of ethanol was completely removed and the DNA pellet was allowed to dry at room temperature for 10 min. Finally, the pellet was dissolved in about 30 µl of 1X TE buffer (pH 8.0) or sterile H_2O and stored at -20ºC.

2.2.19 Transformation of the *N. crassa* strain by electroporation

The protocol was based on the method described by Margolin *et al.* (2000). The recipient strain was grown in three to four 250 ml conical flasks on Vogel's glucose agar medium for three days at 30°C in dark followed by two days under constant light at room temperature. The conidia cells were harvested in sterile water and separated from the mycelium by passing the suspension through cheesecloth attached to a 50 ml falcon tube (the mouth of a 50 ml falcon tube was covered with cheesecloth and sterilized by autoclaving beforehand). The conidial suspension was taken in a 50 ml falcon tube and centrifuged at 3000 rpm for 10 min at 4°C. The conidial mass was washed once with 50 ml water and twice with 1 M sorbitol. Conidial suspension was finally suspended in 1 M sorbitol at a concentration of ~$3x10^9$ cells/ml (concentrated solution of conidia). About 40 µl of the conidial suspension was mixed with the transforming DNA and the mixture was placed in a pre-chilled 0.2 cm sterile electroporation cuvette (BioRad Laboratories, Hercules, CA). Electroporation was performed using a BioRad Gene Pulser apparatus (BioRad Laboratories, Hercules, CA) and conditions for electroporation were 1.5 kV (voltage gradient), 25 µF (capacitance) and 600 Ω (resistance). The time constant varied from 13 to 15 ms. Immediately after the pulse, 1 ml of pre-chilled 1 M sorbitol was

added, kept in ice for 15 min and the transformant conidial suspension was mixed with top agar and plated on a Vogel's sorbose agar medium supplemented with appropriate antibiotic (basta was used at a concentration of 220 µg/ml for transformation). Transformants were pickable under a dissection microscope after 1-3 days. A control transformation was done without adding DNA to eliminate the possibility of any contamination (Margolin *et al.* 2000).

2.2.20 Neurospora genomic DNA isolation

The strain of interest was grown in VGM at 30°C for 2 to 3 days with shaking at 200 rpm. The mycelial mass was harvested by vacuum filtration and lyophilized. The dried mycelia were grinded using mortar and pestle to a fine powder. Approximately, 100 mg of the powdered mycelia was taken in a 2 ml microfuge tube and 1 ml of lysis buffer added to it. Complete mixing of the mycelia powder and lysis buffer was achieved using a pipette tip or a toothpick. The mixture was incubated at 65°C for 30 min and mycelial debris was removed by centrifugation at 12,000 rpm for 10 min. The supernatant was taken in a fresh microfuge tube and 600 µl of phenol:chloroform:isoamyl alcohol mixture (25:24:1) was added. The tube was rotated in a cell mixer for 30 min and centrifuged at 12,000 rpm for 10 min. The aqueous phase was taken in a fresh microfuge tube and washed with 600 µl of chloroform to remove the last traces of phenol. The aqueous phase was taken in a fresh tube and genomic DNA precipitated by adding 1 ml of pre-chilled absolute ethanol and kept at 4°C for one and half hour. Genomic DNA was pelleted by centrifuging the tube for 10 min at 10,000 rpm. The supernatant was discarded and the pellet was washed with 70% ethanol; centrifuged for 10 min at 10,000 rpm. The trace of ethanol was completely removed by gently inverting the tube on tissue paper for 5 min and the genomic DNA pellet was allowed to dry at room temperature for 10 min. Finally, the pellet was dissolved in about 30 µl of 1X TE buffer (pH 8.0) and stored at -20ºC. All centrifugations were carried out at 25ºC.

2.2.21 Neurospora RNA isolation

RNA from *N. crassa* was isolated as described previously (http://www.fgsc.net/fgn37/sokol.html). The strain of interest was grown in 250 ml conical flasks in VGM at 30°C with shaking at 180 rpm for 16 h. The mycelial mass was harvested by vacuum filtration and immediately frozen in liquid nitrogen. The frozen tissue was grinded to a fine powder using mortar and pestle. The powder (~25 mg) was

immediately transferred into 2 ml microfuge tube containing 300 µl TRIzol reagent (Invitrogen, CA) to protect RNA from degradation by RNAase, followed by further addition of the mixture of 750 µl lysis buffer (0.6 M NaCl, 10 mM EDTA, 100 mM Tris HCl, pH 8.0, 4% SDS) and 750 µl phenol (saturated with 0.1 M Tris HCl, pH 8.0). The mixture was vortexed briefly for 10 min. The tube was rotated in a cell mixer for 20 min and centrifuged at 10,000 rpm for 10 min. The upper aqueous phase was carefully removed and transferred to a fresh 2 ml microfuge tube containing an equal volume of phenol (saturated with 0.1 M Tris HCl, pH 8.0). The mixture was vortexed for few seconds and centrifuged for 10 min at 10,000 rpm. The upper aqueous phase was transferred to a fresh 2 ml eppendorf tube then 750 µl of 8 M LiCl was added. The mixture was stored overnight at 4°C for 16-20 h. The next day mixture was vortexed briefly and centrifuged for 10 min at 10,000 rpm. The pellet was resuspended (which is not always visible) in 300 µl double autoclaved water, with 30 µl 3 M Na-acetate (pH 5.2) and 750 µl ethanol. The mixture was stored at -20°C for 2 h and centrifuged at 10,000 rpm and 4°C for 10 min. The supernatant was discarded and the precipitate was washed with 70% ethanol; centrifuged for 10 min at 10,000 rpm and 4°C. The RNA pellet was dried in room temperature for 5 to 10 min and dissolved in 30 µl DEPC treated or RNAase free water and stored at -80°C.

2.2.22 Quantitation of nucleic acids

The concentration of nucleic acids was estimated by measuring the OD at 260 nm in Nano drop spectrophotometer (Eppendorf, Germany). The following empirical relationships were used to calculate the concentrations. An OD of 1 corresponds to ~50 µg/ml for double-stranded DNA, ~40 µg/ml for RNA, ~33 µg/ml for single-stranded DNA and ~20-30 µg/ml for oligonucleotides. The purity of nucleic acids was estimated by calculating the OD_{260}/OD_{280} ratio. Pure DNA has an OD_{260}/OD_{280} ratio of ~1.8; pure RNA has an OD_{260}/OD_{280} ratio of ~2.0 (Barbas *et al.* 2007).

2.2.23 Polymerase Chain Reaction

Polymerase chain-reaction (PCR) was used to amplify specific DNA sequences from genomic DNA or cDNA for molecular purposes. All PCRs reaction were performed in the Arktik Thermal Cycler (Thermo Fisher Scientific, Finland) and by using Taq DNA polymerase (Cat no. M0273S, New England Biolabs, USA); according the manufacturer's protocol. Taq DNA polymerase isolated from *Thermus aquaticus* and

has no proofreading ability. For cloning and SDM purposes, Phusion High-Fidelity DNA Polymerase (Cat. no. F-530S, Thermo Scientific, USA) was used. Phusion High-Fidelity DNA Polymerase isolated from *Pyroccocus furiosus* and possesses proofreading activity (3'- 5' exonuclease activity). Ordinarily, the PCR conditions were varied with respect to the product size and annealing temperature of the primers.

2.2.24 Reverse-transcriptase PCR

For Reverse-transcriptase PCR (RT-PCR) based gene expression study, total RNA was isolated from the mycelia using the procedure as described in Neurospora RNA isolation. cDNA was synthesized from two µg of total RNA template using Thermo Scientific Verso cDNA synthesis kit (Cat no. AB-1453/A). The cycling condition for cDNA synthesis was 50ºC for 45 min followed by 95ºC for 2 min for one cycle. The cDNA template was further subjected to PCR cycling with gene specific primers to analyze the expression of gene. The PCR amplicons were analyzed in 1.2% agarose gel with 100 bp DNA ladder for size comparison of amplicons.

2.2.25 Real-Time PCR

Pure RNA preparation, isolated from *N. crassa* was used for real-time PCR (RT-PCR). One µg of total RNA was used to synthesize cDNA using Thermo Scientific Verso cDNA synthesis kit, as described previously. RT-PCR was performed in ABI 7500 Fast Real-Time PCR System (Applied Biosystems, USA) with the SYBR® select master mix (Applied Biosystems, USA) by using 100 ng of cDNA and 10 mM each of primer in a final reaction volume of 15 µl. In general, 15 µl reaction mixture contained 7 µl of cDNA (100 ng), 0.5 µl of forward and reverse primer and 7µl syber green. The PCR cycle was as follows: 95°C for 10 min followed by 40 cycles of 95 °C for 15 s and 60 °C for 1 min. The $2^{-\Delta\Delta C_T}$ quantification method was used to calculate the fold change expression of each gene, using the β-tubulin gene as an endogenous control and wild-type as calibrator (Livak and Schmittgen 2001).

2.2.26 Digestion of DNA with restriction endonuclease

For analytical and preparative purposes, plasmid DNA were digested with specific restriction endonucleases (New England Biolabs, USA). An aliquot of ~50 -100 ng of DNA was digested with 5 units of restriction endonuclease in a final volume of 30 µl. The reaction was carried out for 3 h using suitable buffers and assay conditions as

specified by the manufacturer's protocol. The digested DNA fragments were analyzed by agarose gel electrophoresis. Digestion with two enzymes was done after consulting the enzyme compatibility chart present in the New England Biolabs (NEB).

2.2.27 Ligation reactions

Ligation reactions were carried out using Quick Ligation TM Kit (NEB, Cat no. M2200S). The 20 µl ligation reaction volume contained ~50 ng of a linearized DNA vector, a 3-fold molar excess of insert, 10 µl of 2X ligation buffer (132 mM Tris-HCl, 20 mM MgCl2, 2 mM dithiothreitol, 2 mM ATP, 15% Polyethylene, glycol 6000) and 1 µl Quick T4 DNA ligase enzyme. The ligation was performed for 15-20 min at 25ºC in cooling water bath.

2.2.28 Site-directed mutagenesis

The procedure for generating the site-directed mutations was essentially as described in QuickChange® II site-directed mutagenesis protocol (Stratagene, CA, USA). The mutagenic primer for site-directed mutation was designed by using QuikChange® Primer Design software (http://www.genomics.agilent.com/primerDesignProgram.jsp?&_requestid=247130). Briefly, the mutational PCR reactions were performed using mutagenic primer pairs and Phusion™ High-Fidelity DNA Polymerase (Cat. no. F-530S, Thermo Scientific, USA) according to the manufacturer's protocol. The site-directed mutagenesis PCR generates a mutated plasmid containing staggered nicks. The PCR products were digested with *DpnI* restriction enzyme (Cat. no. R0176S) to digest the parental methylated and hemimethylated DNA template (unmutated) and then transformed into the *E. coli* DH5α competent cells for nick repair. The transformant colonies were selected on LB-ampicillin plate (100 µg/ml) and plasmids were isolated. The desired mutation in the respective plasmid construct was confirmed by DNA sequencing (SciGenom Labs, Cochin, India, and Eurofins Genomics India Pvt Ltd., Bangalore, India).

2.2.29 Agarose gel electrophoresis

The DNA samples were loaded with one-sixth the volume of 6X DNA loading dye (0.25% bromophenol blue, 0.25% xylene cyanol, 30% glycerol). Depending upon the size of the fragments to be resolved, the samples were loaded on 0.8% to 1% agarose gels cast on 1X TAE containing 0.5 µg/ml ethidium bromide. Electrophoresis was

carried out in 1X TAE at 5 V/cm. Standard DNA size markers were run alongside for estimation of DNA fragment sizes. The ethidium bromide stained DNA samples were visualized on a gel doc (Bio-Rad, Image 4.1). RNA samples were resolved in 1.2% to 1.5% agarose gel containing 2.2 M formaldehyde, 1X MOPS buffer and 0.5 µg/ml ethidium bromide.

2.2.30 Purification of DNA fragments from agarose gels

PCR-amplified DNA subsequently used for cloning, sequencing and transformation was purified from agarose gels using the QIAquick Gel Extraction Kit (Qiagen, Cat no. 28704). The sample containing DNA was resolved in 1% high purity agarose gel. The DNA bands were visualized on a gel doc (Bio-Rad, Image 4.1) and was excised and transferred to a weighed 1.5 ml eppendorf tube. DNA from the gel slice was eluted according to the manufacturer's protocol.

2.2.31 Sequence analysis

BLAST (Altschul *et al.* 1990, 1997) analysis was performed using software tools available from NCBI (http://blast.ncbi.nlm.nih.gov/Blast.cgi) and Conserved Domains Database (CDD; Marchler-Bauer and Bryant 2004; Marchler-Bauer *et al.* 2009) database was used to identify conserved domains in the protein. Protein sequences were aligned with Clustal X (Thompson *et al.* 1997) then transferred to GeneDoc for visualization (Nicholas *et al.* 1997). Phylogenetic tree (Felsenstein 1985; Rzhetsky and Nei 1992) was constructed from these alignments using the software Molecular Evolutionary Genetics Analysis version 5 (MEGA5; Tamura *et al.* 2011).

2.2.32 Databases and softwares used

1. *N. crassa* databases: Genome resource for *Neurospora* is available at http://fungidb.org. The web site for Fungal Genetic Stock Centre (FGSC) is http://www.fgsc.net

2. NCBI/EMBL: NCBI at http://www.ncbi.nlm.nih.gov/ or EMBL at http://embl.org/ is used to retrieve the primary sequence of proteins or nucleic acid.

3. BLAST: This was used for aligning nucleotide and amino acid sequences for searching sequence data bases. This is available at http://www.ncbi.nlm.nig.gov.BLAST

4. Clustal W: This software was used for multiple alignment of DNA and protein sequence. It is available at http://www.ebi.ac.uk./clustal or commonly used offline software is clustal X.

5. MEGA tool: It is used to depict the evolutionary relationship among the organisms or gene sequences. This is available at http://www.megasoftware.net/

6. ExPasy translate tool: This was used for translating DNA sequence to protein sequence. It is available at http://www.expasy.org/tools/DNA

7. Genomatix software: This is used for promoter analysis of Genomic DNA sequence. It is available at http://www.genomatix.de/cgi-bin//matinspector_prof/mat_fam

8. GeneDoc: This software was used for finding conserved domains among aligned sequences of DNA or protein. It is available at http://www.nrbsc.org/gfx/genedoc/

9. Conserved Domain Database (CDD): This was used to identify conserved domains in the proteins. This is available at http://www.ncbi.nlm.nih.gov/Structure/cdd/wrpsb.cgi

10. String : String version 10.0, available at http://string-db.org/, was used to predict functional protein association networks.

11. QuikChange® Primer Design: This was used for site-directed mutation (SDM) primer design. It is available at http://www.genomics.agilent.com/primerDesignProgram.jsp?&_requestid=247130

12. Site for reverse-complement: To convert a DNA sequence into reverse-complement counterpart, sequence manipulation suite (SMS) software package was used. It is available at http://www.bioinformatics.org/sms/index.html

13. Maps sites for restriction enzymes: This was used for restriction analysis of DNA sequences. It is available at http://www.restrictionmapper.org/

Chapter 3

Understanding cellular role of calmodulin and related calcium signaling proteins in Neurospora crassa

3.1 Introduction

The genome analysis of filamentous fungus *N. crassa* has identified ~10,082 protein coding genes including 48 Ca^{2+}-signaling genes that encode for Ca^{2+}-channel proteins, Ca^{2+}/cation-ATPases, Ca^{2+}/H^{+} exchangers, Ca^{2+}/Na^{+} exchangers, phospholipase C-δ subtype, CaM and Ca^{2+} and/or CaM binding proteins (Galagan *et al.* 2003; Borkovich *et al.* 2004). All Ca^{2+}-signaling knockout mutants were generated using a high-throughput gene knockout procedure developed by the *Neurospora* genome project (http://www.dartmouth.edu/~neurosporagenome/proj_overview.html; Colot *et al.* 2006) and obtained from the FGSC (Figure 3.1).

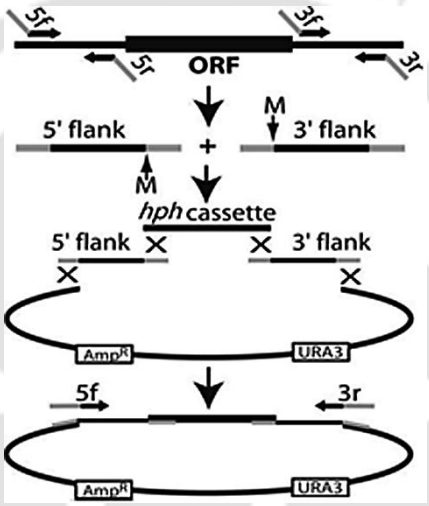

Figure 3.1 Strategy to generate deletion constructs for generating the *N. crassa* knockout mutants. The 5' and 3'-flanks of the target open reading frame (ORF) were amplified separately from wild-type with primers 5f with 5r and 3f with 3r. Primers 5r and 3f contained *MmeI* site (M) and 5' tails homologous to the *hph* cassette. In addition, tails of the primers 5f and 3r were homologous to the pRS426 vector. The *hph* cassette was separately PCR amplified from the pCSN44 vector (Staben *et al.* 1989) using specific primer pair. The two flanks, the *hph* cassette, and gapped yeast shuttle vector (pRS426) were co-transformed into the yeast strain FY834 (Winston *et al.* 1995) to generate the circular construct through homologous recombination. The pooled yeast DNA was used as template with primers 5f and 3r to PCR amplify final linear deletion cassette. The selectable marker *hph* is transcribed in the antisense direction relative to the direction of transcription of the target gene (Adapted from Colot *et al.* 2006).

The only CaM in *N. crassa* is encoded by the NCU04120 gene and CaM appears to be essential for viability (Galagan *et al.* 2003; Borkovich *et al.* 2004). Therefore, I studied the cellular role of CaM in *N. crassa* using two CaM antagonists TFP and CPZ. TFP (https://pubchem.ncbi.nlm.nih.gov/compound/trifluoperazine#section=Top) and CPZ (https://pubchem.ncbi.nlm.nih.gov/compound/chlorpromazine) are typical antipsychotic of the phenothiazine chemical class (Figure 3.2).

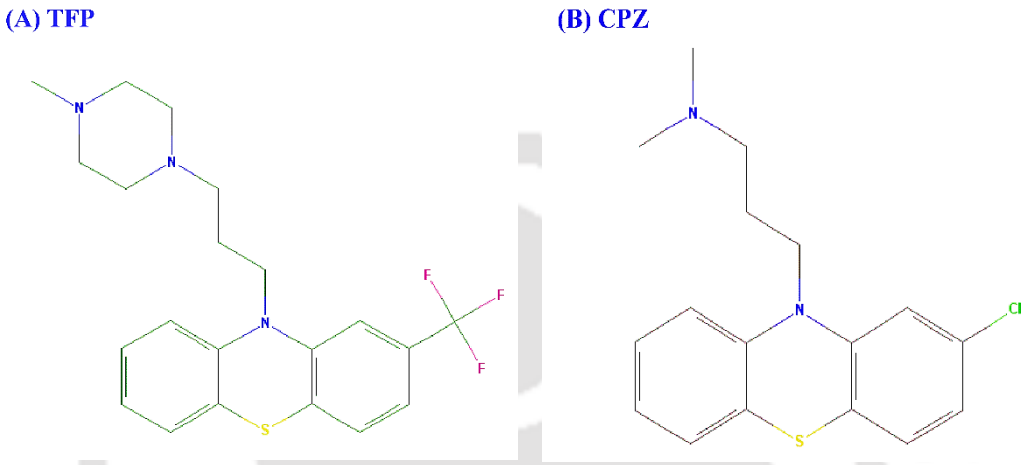

Figure 3.2: Structure of the CaM antagonists. (A) TFP and (B) CPZ (Adapted from PubChem).

The CaM antagonists compete with Ca^{2+} for binding to the CaM that consequently inhibit Ca^{2+}/CaM signaling (Ahn and Suh 2007a). In its activated (Ca^{2+}-bound) conformation, CaM exposes hydrophobic residues to the solvent, enabling binding to a target, either a protein or an inhibitor. The binding process itself requires a large conformational change involving the unfolding of the central helix in order to allow for rotation of the C-terminal domain to form the binding site. The binding of CaM antagonists, particularly the phenothiazine to the lipophilic domain of CaM is well documented, to elucidate the role of CaM in cellular regulation (Roufogalis 1985). The crystal structure of CaM bound to TFP has been determined and refined to a resolution of 2.45 Å (Cook *et al.* 1994), but the crystal structure of Ca^{2+}-CaM-TFP complex has been determined to 2 Å resolution in 1994 (Vandonselaar *et al.* 1994). Only one TFP is bound to CaM and that is sufficient to cause distortion of the central α-helix and juxtaposition of the N- and C-terminal domains as seen in CaM-polypeptide complexes (Cook *et al.* 1994). Inactivation of Ca^{2+}-CaM by TFP is possibly due to this major tertiary structural

alteration in Ca^{2+}-CaM that is initiated and stabilized by drug binding. The drug makes only a few contacts with one residue in the N-terminal domain and extensive contacts with residues in the C-terminal domain of CaM. Two hydrophobic binding pockets, created by amino acid residues adjacent to Ca^{2+}-coordinating residues, form the key recognition sites on Ca^{2+}-CaM for both inhibitors and target enzymes (Vandonselaar *et al.* 1994). In addition, CPZ is a phenothiazine with actions similar to TFP. The spin-labelled derivative of chlorpromazine (CPZSL) was used to probe the phenothiazine binding site of CaM by electron spin resonance (ESR) spectrometry. The completion of the spectroscopic changes requires the presence of 4 Ca^{2+} ions per CaM molecule. CPZSL has a high sensitivity to various effectors in the environment of the drug binding site (Rainteau *et al.* 1984). Both CaM activated muscle MLCK and pea NAD^{+} kinase act in a Ca^{2+}-dependent manner and these activities were inhibited by TFP or CPZ (Nakamura *et al.* 1984). TFP and CPZ were shown to affect different cell functions in *N. crassa*, such as shortening of period length of the conidiation rhythm, light induced phase shifting and activation of chitin synthase enzyme in *N. crassa* (Suzuki *et al.* 1996; Sadakane and Nakashima 1996; Suresh and Subramanyam 1997).

CaM interact with various proteins and enzymes to amplify the Ca^{2+}-signaling. One of the targets of CaM is the Ca^{2+} -ATPase, a Ca^{2+} pump that help in fine tuning of Ca^{2+} homeostasis in cells by pumping Ca^{2+} out of cells. CaM stimulates plasma membrane Ca^{2+}-ATPase (PMCA) activity by binding to an autoinhibitory domain of PMCA. The CaM-binding domain is located near the C-terminus of PMCA (Osborn *et al.* 2004; Giacomello *et al.* 2013). In *N. crassa*, nine ATPases have been identified and they possess conserved cation transporter/ATPase domain in the proteins (Galagan *et al.* 2003; Borkovich *et al.* 2004). Lack of the *nca-2* (NCU04736) gene, a Ca^{2+}-ATPase, results in slow growth, female sterility and accumulates more Ca^{2+} than the wild-type, indicating that it functions in the plasma membrane to pump Ca^{2+} out of the cell (Bowman *et al.* 2011). In addition, one of the cation-ATPase, *trm-9* (NCU04898) shows sequence homology to SPF1 ATPase of *S. cerevisiae*. SPF1 family ATPases genes conserved from yeast to human, however, the function of these ATPases is unclear. SPF1 is not essential for cell viability and its substrate specificity is unknown and loss of SPF1 may perturb homeostasis of ions that affects modification and sorting of proteins in the secretory pathway of yeast (Cronin *et al.* 2000; Suzuki 2001). However, mechanism of *trm-9* functions remains unknown in *N. crassa*. In order to understand *trm-9* functions

and its relation with other ATPases including the one encoded by the *nca-2* gene, I have studied their genetic interactions.

Thus, in this Chapter, I describe the cellular role of CaM based on the effect of TFP and CPZ and functions of *nca-2* and *trm-9* in *N. crassa*.

3.2 Results

3.2.1 NCU04120, NCU04898 and NCU04736 genes encode *cmd*, *trm-9* and *nca-2*, respectively, and contain conserved domains

Sequence analysis of NCU04120 and NCU04898 was performed by using information obtained from fungi genome database (http://fungidb.org). The NCU04120 gene is genetically mapped in supercontig five from position 4911110-4913296 (+ strand) at the right arm of linkage group V (LG VR) (Figure 3.3A) whereas NCU04898 gene is genetically mapped in supercontig four from position 665386-670016 (+ strand) at LG IVR (Figure 3.3B). The NCU04120 contains six exons and five introns (Figure 3.3C) and NCU04898 possess two exons and one intron (Figure 3.3D). The NCU04120 (GenBank accession number AAA33569.1) and NCU04898 (GenBank accession number XP_958407.1) sequence was used as a query sequence in a BLAST search to identify its homologues. BLAST (Altschul *et al.* 1990, 1997) analysis was performed using software tools available from NCBI (http://blast.ncbi.nlm.nih.gov/Blast.cgi) and the proteins were selected based on *E* value, % identities and gapes (Tamuli *et al.* 2011). The CDD (Marchler-Bauer *et al.* 2009) database was used to identify conserved domains in the protein (Figure 3.4). The homologue protein sequences were aligned with Clustal X (Thompson *et al.* 1997) and visualized using GeneDoc (Nicholas *et al.* 1997). The sequence analysis revealed that the NCU04120 gene encodes for CaM (http://fungidb.org/fungidb/app/record/gene/NCU04120), a highly conserved Ca^{2+}-signaling protein possessing four conserved EF hand motifs, in *N. crassa* (Figure 3.5A). Similarly, the NCU04898 gene, called *trm-9*, encodes a cation ATPases (http://fungidb.org/fungidb/app/record/gene/NCU04898) that possesses one conserved E_1-E_2 ATPases domain and one halo-acid dehalogenase like hydrolase domain (Figure 3.5B). Phylogenetic trees were constructed from the aligned homologue sequences of these proteins using the minimum evolution method (Rzhetsky and Nei 1992), 500 bootstrap replications as test of phylogeny (Felsenstein 1985) and the software MEGA5 (Tamura *et al.* 2011) revealed that CaM and TRM-9 are clustered with the homologues from the closely related fungi (Figure 3.6). In addition, promoter region was analyzed by

selecting ~2 kb sequences from upstream of the start codon of the ORF and transferred to MatInspector in Genomatix software (http://www.genomatix.de/cgi-bin//matinspector_prof/mat_fam) to predict transcription factor binding sites (Quandt *et al.* 1995). Promoter analysis revealed important putative regulatory elements involved in transcription of the *cmd* and *trm-9* genes (Figure 3.7). In addition, the NCU04736 gene was previously identified as *nca-2* that encodes a PMCA type Ca^{2+}-ATPase (Bowman *et al.* 2009, 2011).

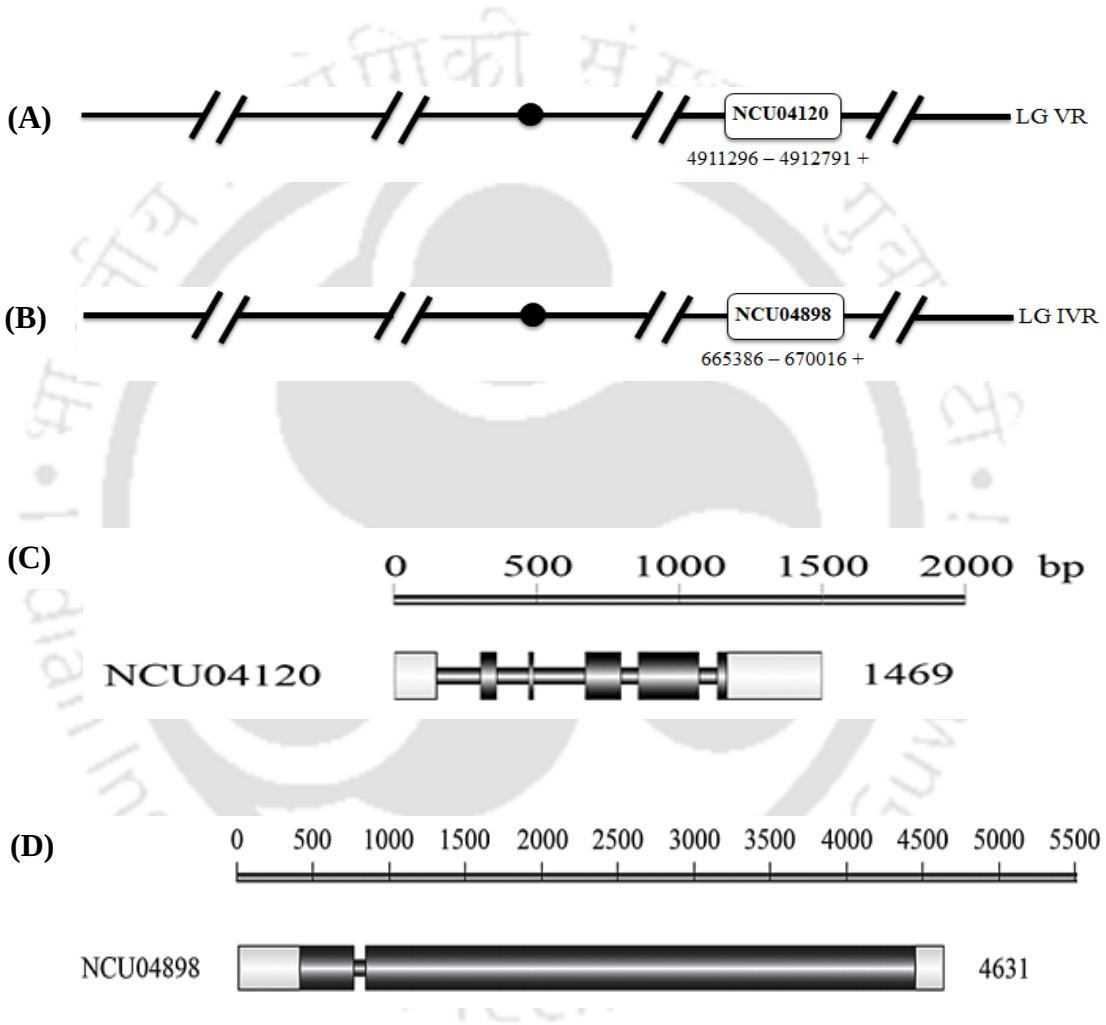

Figure 3.3: Genomic organization of NCU04120 and NCU04898 genes. Genomic location of the (A) NCU4120 and (B) NCU04898. Gene structure of the (C) NCU4120 and (D) NCU04898 gene. The relative positions of the exons (black bar), introns (black line) and untranslated regions (UTRs; light grey bar) are shown (Adapted from Tamuli *et al.* 2013).

(A)

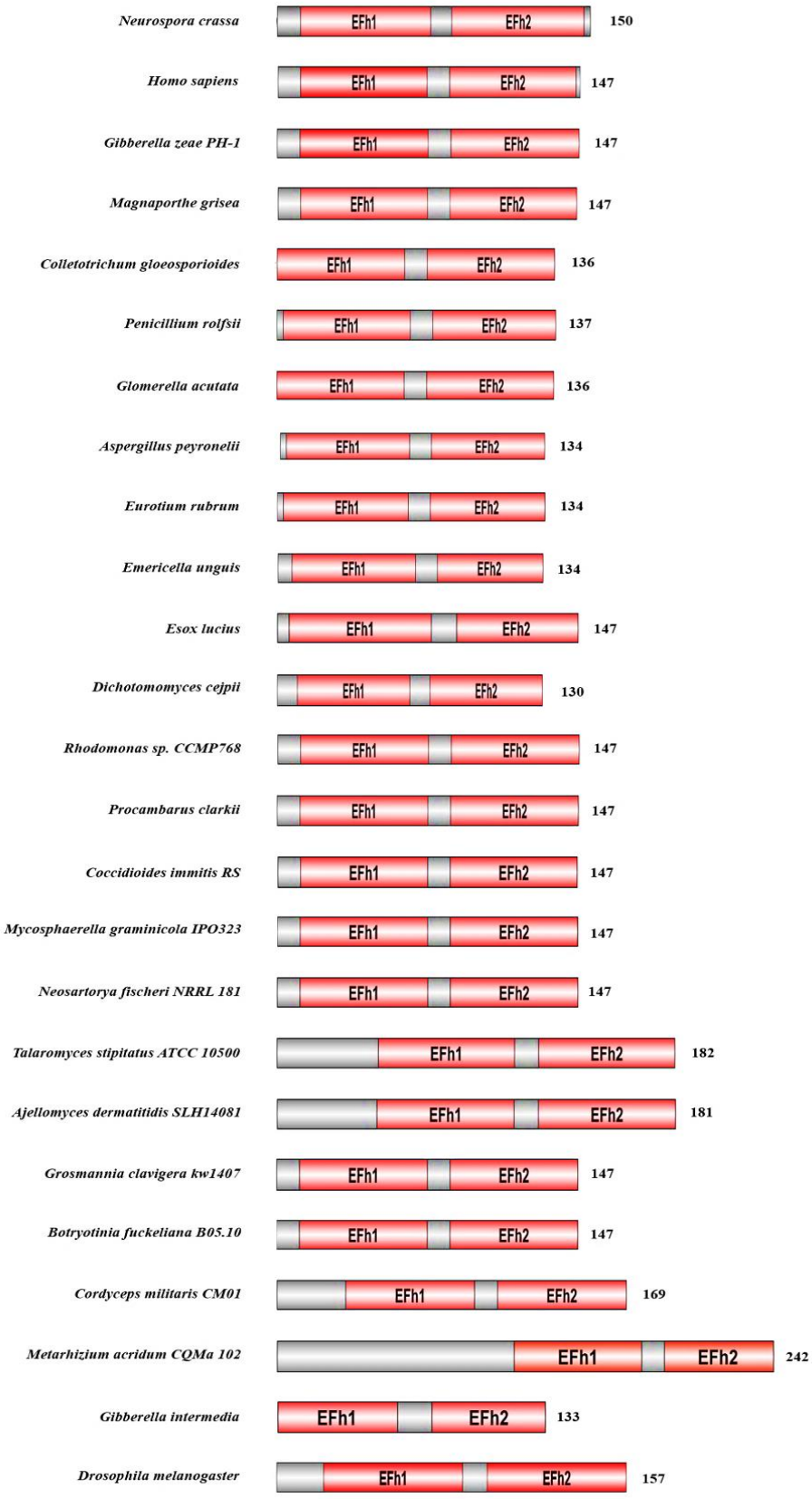

(B)

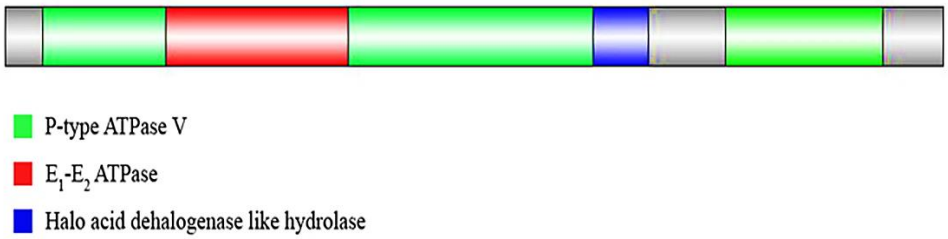

Figure 3.4: Domain organization of the CaM and TRM-9 proteins. (A) Domain comparison of the *N. crassa* CaM protein homologues. The motif depicted with red color represents the represents the EF-hand domain. (B) Domain organization of the TRM-9 protein of *N. crassa* as predicted using the CDD search of NCBI. TRM-9 possesses conserved three P-type ATPase V domain (green), one E_1-E_2 ATPases domain (red) and one halo-acid dehalogenase like hydrolase domain (blue). The domain figure was prepared using the software DOG 2.0.

(A)

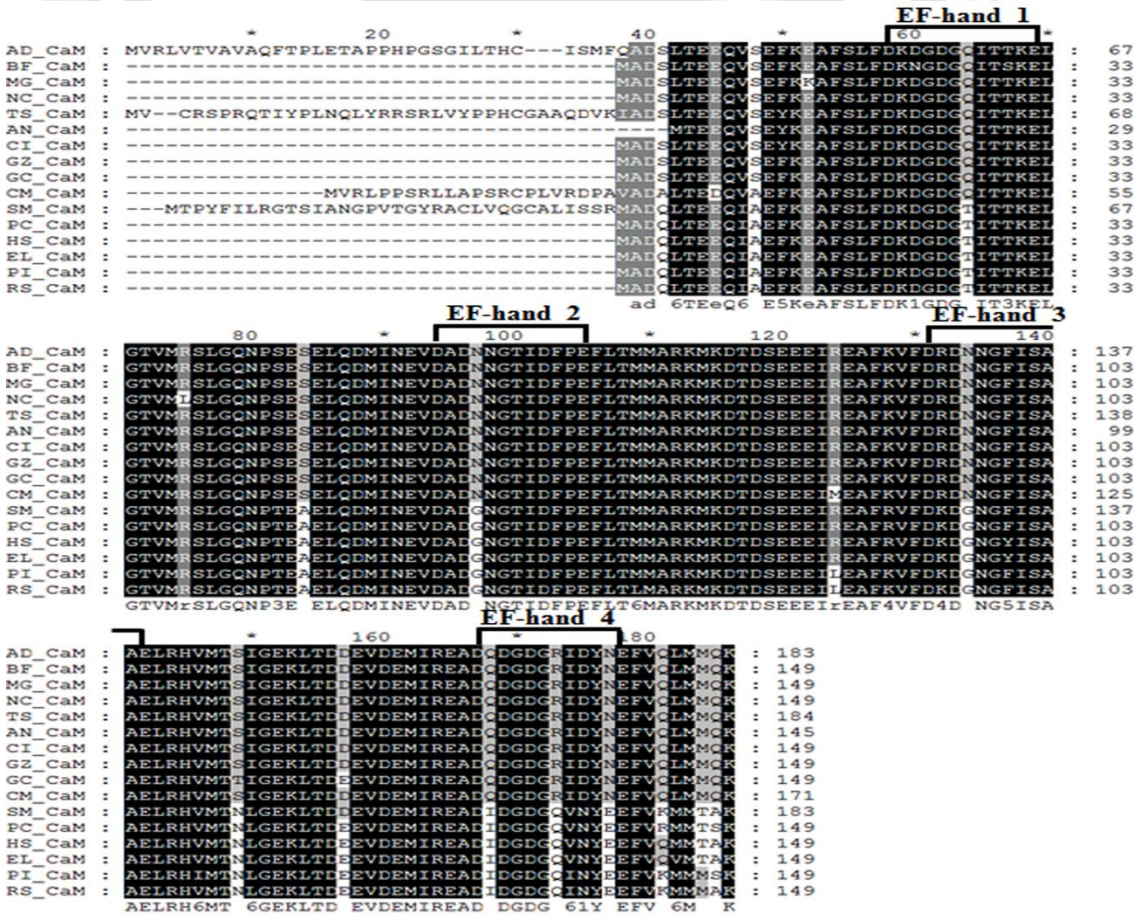

(B)

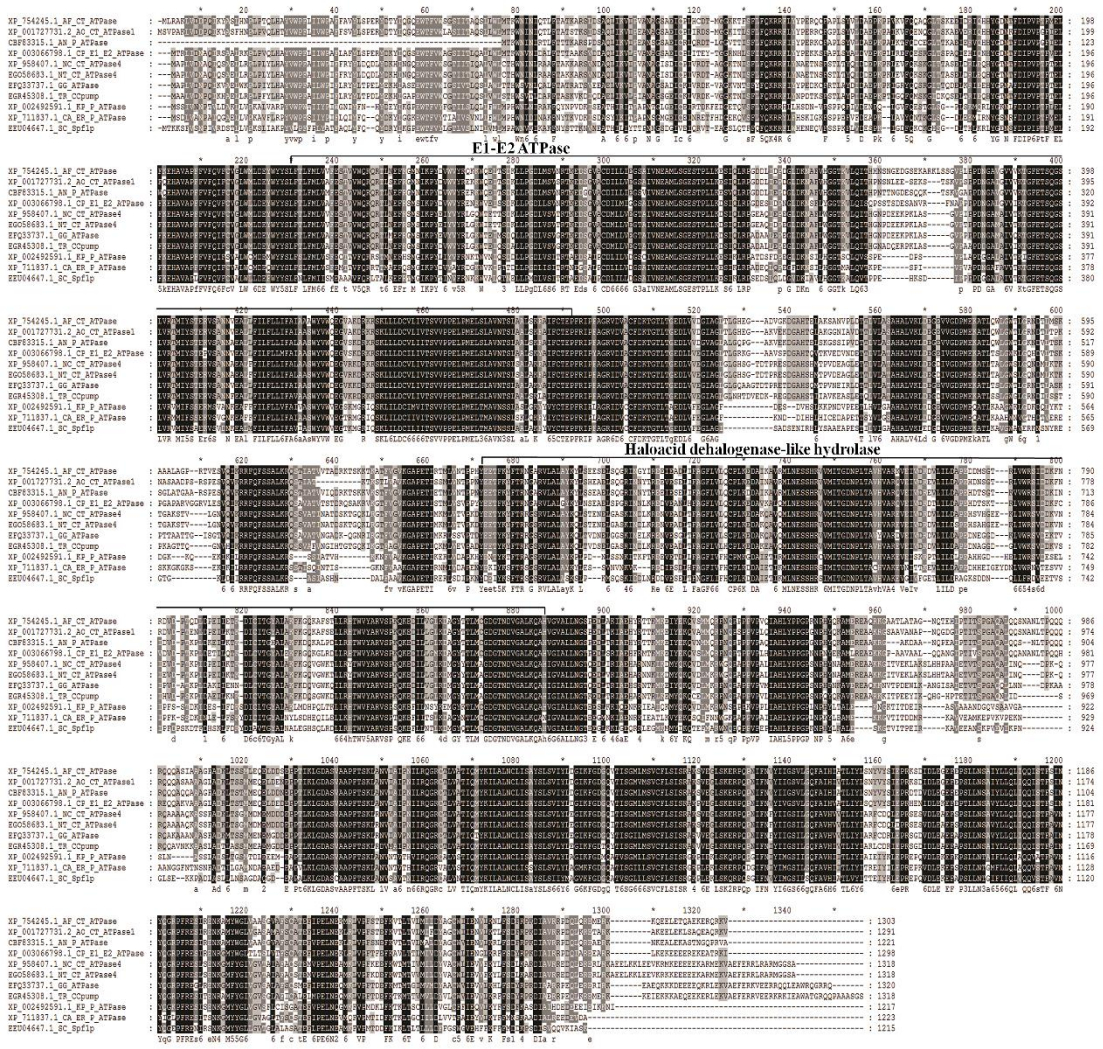

Figure 3.5: Sequence alignment of CaM and TRM-9 homologues. Sequence alignment of the *N. crassa* (A) CaM and (B) TRM-9 homologues. Conserved amino acids are indicated in black (100%), dark gray (>80%) and light gray (>60%). (C) Phylogenetic analysis of CaM homologues. The homologue sequences used for the sequence analysis are from *Ajellomyces capsulatus* (AC), *Ajellomyces dermatitidis SLH14081* (AD), *Aspergillus fumigatus* (AF), *Arthroderma gypseum* (AG), *Aspergillus nidulans FGSC A4* (AN), *Aspergillus kawachii* (AK), *Aspergillus nidulans* (AN), *Aspergillus oryzae* (AO), *Botryotinia fuckeliana B05.10* (BF), *Candida albicans* (CA), *Coccidioides immitis* (CI), *Cordyceps militaris CM01* (CM), *Coccidioides posadasii* (CP), *Dichotomomy cescejpii* (DC), *Drosophila melanogaster* (DM), *Exophiala dermatitidis* (ED), *Esox lucius* (EL), *Eurotium rubrum* (ER), *Emericella unguis* (EU),

Grosmannia clavigera kw1407 (GC), *Glomerella graminicola* (GG),*Gibberella zeae PH-1* (GZ), *Homo sapiens* (HS), *Komagataella pastoris* (KP), *Metarhizium anisopliae* (MA), *Magnaporthe grisea* (MG), *Neurospora crassa* (NC), *Neurospora tetrasperma* (NT), *Ogataeapara polymorpha* (OP), *Paracoccidioides brasiliensis* (PB), *Procambarus clarkii* (PC), *Puccinia graminis f. sp. Tritici* (PG), *Phytophthora infestans T30-4* (PI), *Penicillium rolfsii* (PR), *Pyrenophora tritici-repentis* (PT), *Rhodomonas sp. CCMP768* (RS), *Saccharomyces cerevisiae* (SC), *Saccharomyces cerevisiae RM11-1a* (SC RM11), *Saccharomyces cerevisiae* (SCSK), *Schistosoma mansoni* (SM), *Sordaria macrospora* (SM), *Spathaspora passalidarum* (SP), *Scheffersomyce sstipitis* (SS), *Trichophyton equinum* (TE), *Trichoderma reesei* (TR), *Talaromyces stipitatus ATCC 10500* (TS) and *Verticillium albo-atrum* (VA; Adapted from Laxmi and Tamuli 2015).

(A)

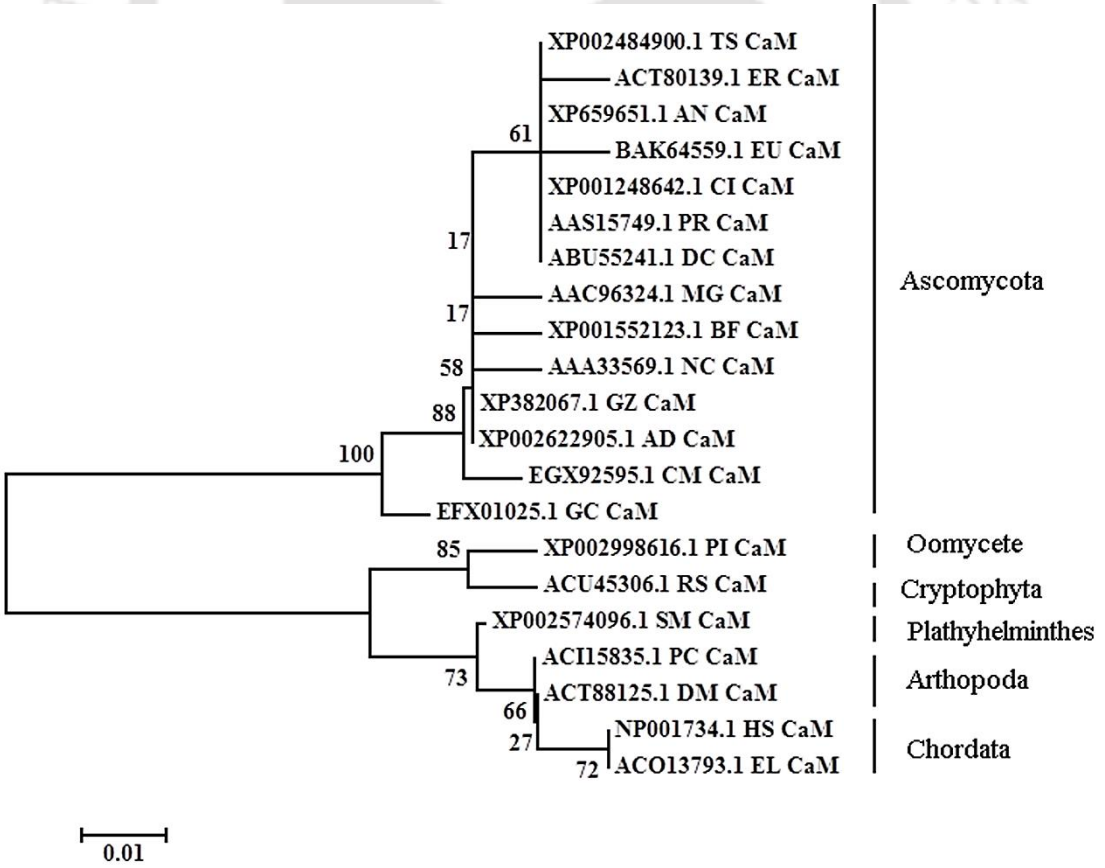

(B)

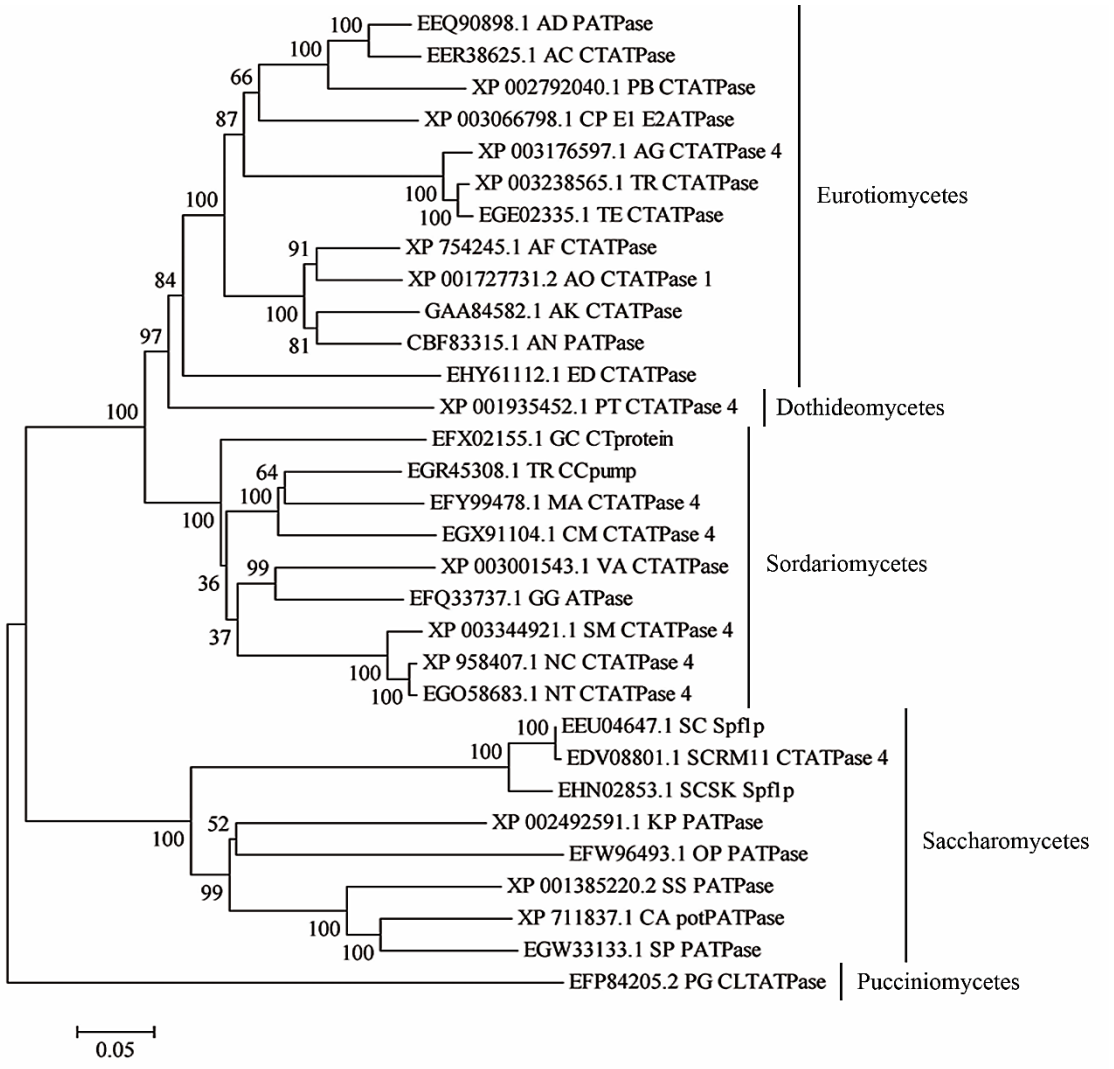

Figure 3.6: Phylogenetic analysis of the CaM and TRM-9 proteins. Protein sequences are described using GenBank accession numbers, phylum is indicated at major clades, and bar indicates scale of genetic distances. Phylogenetic analysis of TRM-9 homologues. A phylogenetic analysis with a subset of (A) CaM and (B) TRM-9 proteins from fungi to mammals revealed that the *N. crassa* CaM and TRM-9 protein clustered with the Ascomycota and Sordariomycetes clade respectively. The homologue sequences used for the sequence analysis are from *Ajellomyces capsulatus* (AC), *Ajellomyces dermatitidis SLH14081* (AD), *Aspergillus fumigatus* (AF), *Arthroderma gypseum* (AG), *Aspergillus nidulans FGSC A4* (AN), *Aspergillus kawachii* (AK), *Aspergillus nidulans* (AN), *Aspergillus oryzae* (AO), *Botryotinia fuckeliana B05.10* (BF), *Candida albicans* (CA), *Coccidioides immitis* (CI), *Cordyceps militaris CM01*

(CM), *Coccidioides posadasii* (CP), *Dichotomomy cescejpii* (DC), *Drosophila melanogaster* (DM), *Exophiala dermatitidis* (ED), *Esox lucius* (EL), *Eurotium rubrum* (ER), *Emericella unguis* (EU), *Grosmannia clavigera kw1407* (GC), *Glomerella graminicola* (GG), *Gibberella zeae PH-1* (GZ), *Homo sapiens* (HS), *Komagataella pastoris* (KP), *Metarhizium anisopliae* (MA), *Magnaporthe grisea* (MG), *Neurospora crassa* (NC), *Neurospora tetrasperma* (NT), *Ogataeapara polymorpha* (OP), *Paracoccidioides brasiliensis* (PB), *Procambarus clarkii* (PC), *Puccinia graminis f. sp. Tritici* (PG), *Phytophthora infestans T30-4* (PI), *Penicillium rolfsii* (PR), *Pyrenophora tritici-repentis* (PT), *Rhodomonas sp. CCMP768* (RS), *Saccharomyces cerevisiae* (SC), *Saccharomyces cerevisiae RM11-1a* (SC RM11), *Saccharomyces cerevisiae* (SCSK), *Schistosoma mansoni* (SM), *Sordaria macrospora* (SM), *Spathaspora passalidarum* (SP), *Scheffersomyce sstipitis* (SS), *Trichophyton equinum* (TE), *Trichoderma reesei* (TR), *Talaromyces stipitatus ATCC 10500* (TS) and *Verticillium albo-atrum* (VA; Adapted from Laxmi and Tamuli 2015).

(A)

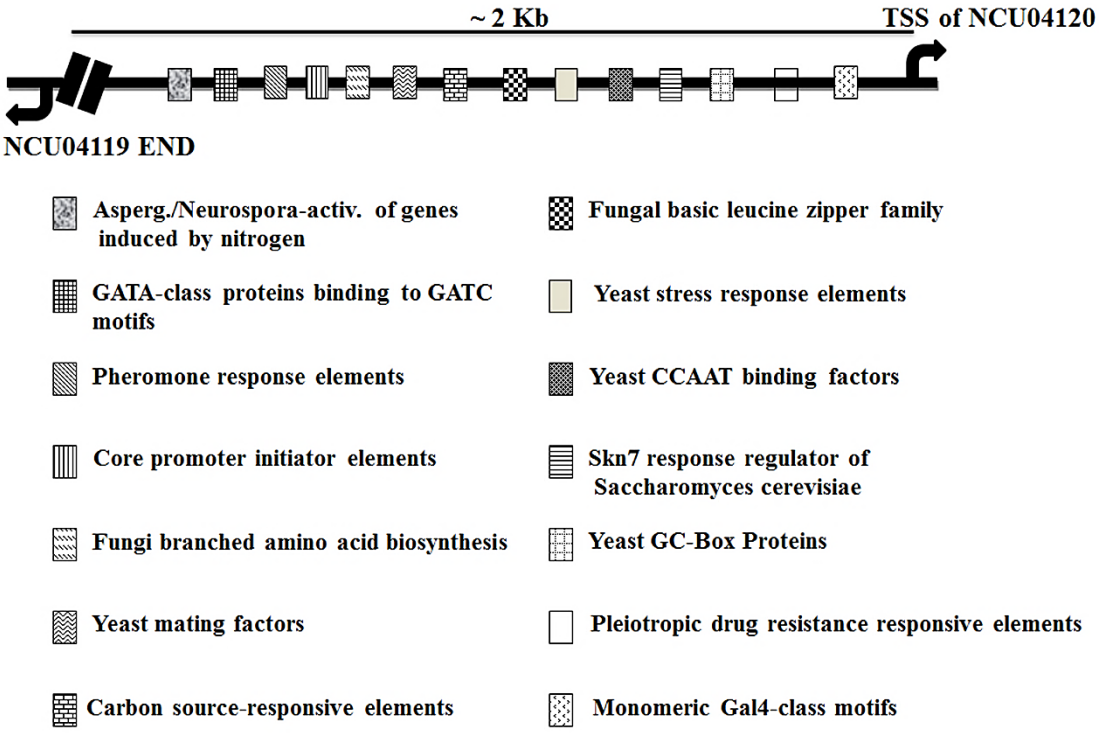

(B)

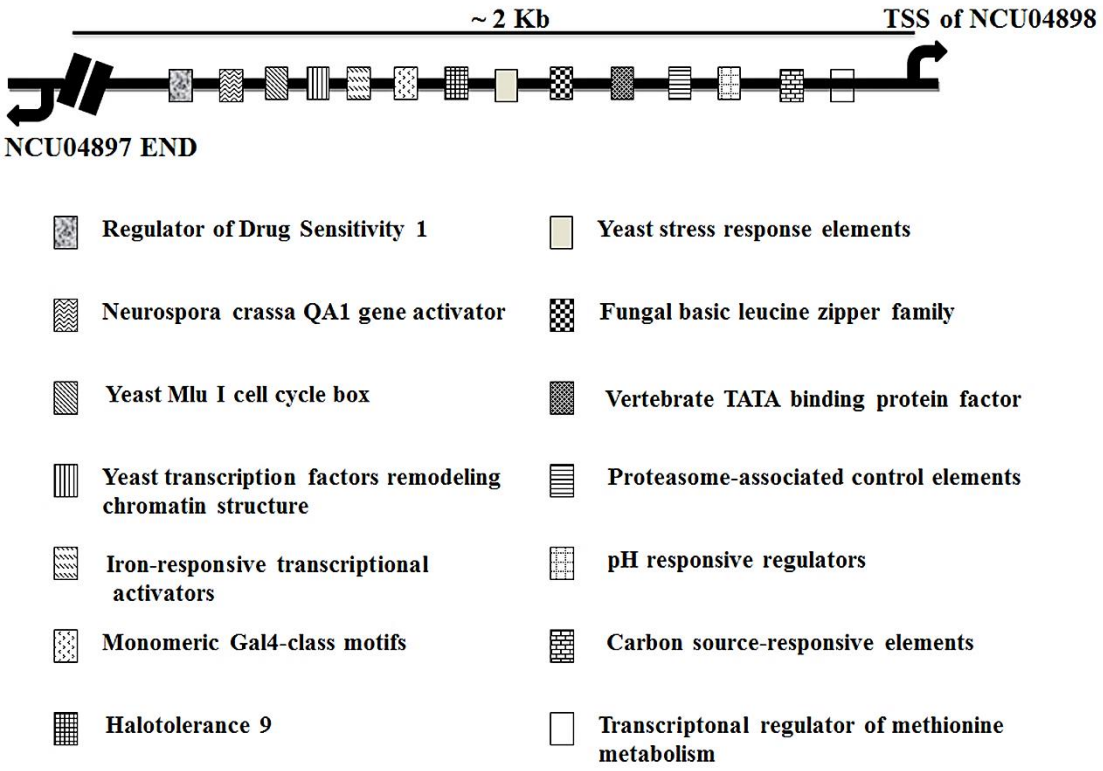

Figure 3.7: Promoter analysis of *cmd* and *trm-9* genes of *N. crassa*. The predicted regulatory elements in the promoter sequences of (A) *cmd* (B) *trm-9* from *N. crassa*. Some of the regulatory sequences (grey pattern boxes) near the transcription start sites (TSS) for each gene are shown. These regulatory sequences could further support the involvement of both genes in specific cell functions (Adapted from Laxmi and Tamuli 2015).

3.2.2 Effect of the CaM antagonists TFP and CPZ in *N. crassa.*

The Δ*cmd::hph* homokaryotic strain could not be isolated from the initial heterokaryotic knockout strain (*cmd;* Δ*cmd::hph*), suggesting that the *cmd* gene might be essential for viability. Therefore, I used CaM antagonists TFP (Sigma Aldrich-T6062) and CPZ (Sigma Aldrich- C8138) to investigate the cellular role of CaM in *N. crassa* (as described in materials and methods). Addition of TFP and CPZ in different concentrations (10, 20, 40, 60, 80 and 100 µM) inhibit growth (Figure 3.8; Table 3.1), hyphal branching (Figure 3.9) and development of aerial hyphae (Figure 3.10; Table 3.2) in *N. crassa*.

I also analyzed carotenoid accumulation in *N. crassa* in the presence of TFP and CPZ to investigate the role of CaM in carotenoid accumulation. Carotenoids are the most ubiquitous and widespread natural pigment, characteristic for organisms of all major taxa and play vital roles in key biological processes such as photosynthesis, vision and the quenching of free radicals and singlet oxygen (Vershinin 1999). The orange pigmentation of the fungus *N. crassa* is due to the accumulation of the xanthophyll neurosporaxanthin and precursor carotenoids (Díaz-Sánchez *et al.* 2011). Carotenoids were extracted as described in materials and methods. The carotenoid profile of the wild-type strain in presence of the inhibitors followed the order wild-type > 10 µM CPZ > 20 µM CPZ >10 µM TFP > 20 µM TFP (Figure 3.11; Table 3.3). Therefore, these results indicate the CaM protein might modulate carotenoid accumulation in *N. crassa*. The difference of carotenoids accumulation in presence of TFP and CPZ might be due to the difference of mechanism of inhibition mediated by TFP and CPZ. In addition, the *cmd* transcript level was found to be decreased in the presence of TFP and CPZ as revealed by the real time PCR analysis (as described in materials and methods; Figure 3.12).

To answer whether *cmd* gene play a role in sexual development in *N. crassa*, I set up crosses homozygous for wild-type strain (as described in materials and methods), which showed a defect in perithecia formation and results in a sterile phenotype on addition of TFP or CPZ in the SCM agar, which otherwise form normal perithecia and produce thousands of ascospores in control cross (Figure 3.13). These results suggest that CaM play a role in vegetative growth, hyphal development and sexual development in *N. crassa*.

Therefore, CaM antagonists TFP and CPZ affect growth, aerial hyphae development, carotenoids accumulation and sexual development in *N. crassa.*

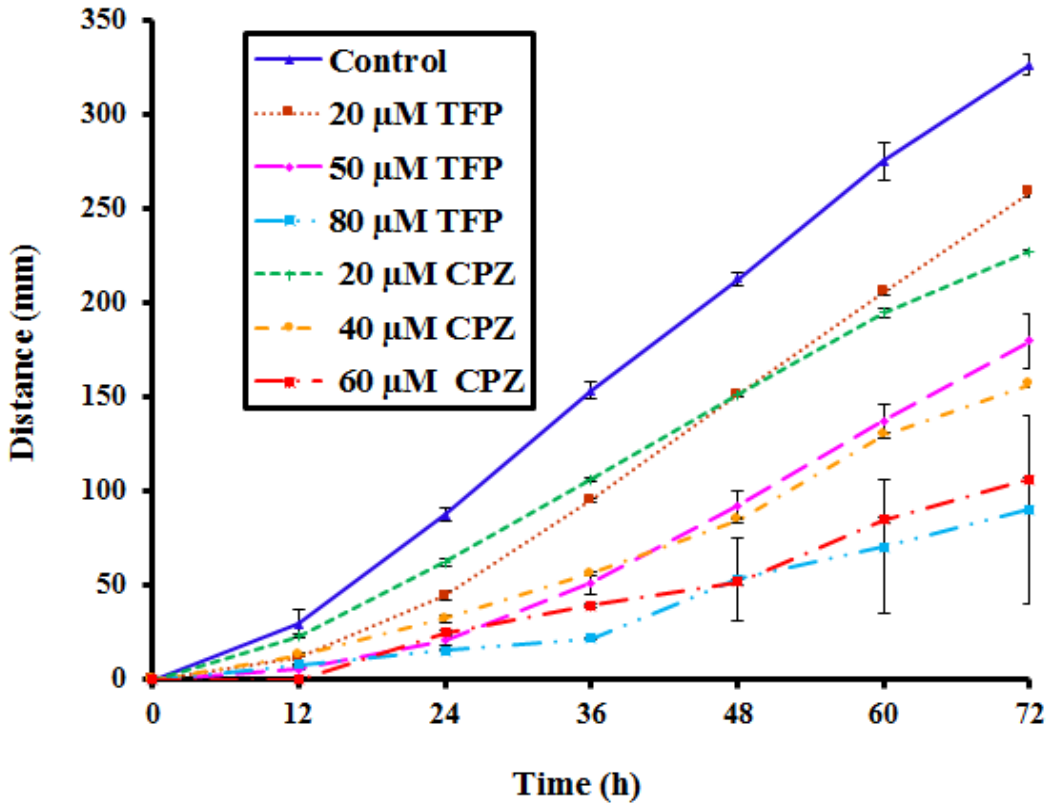

Figure 3.8: Effect of TFP and CPZ on apical growth of *N. crassa*. Wild-type strain of *N. crassa* was grown in the presence of TFP and CPZ and rate of apical growth was measured at regular interval and plotted against time. Error bars indicate the standard errors calculated from the data for three independent experiments (Adapted from Laxmi and Tamuli 2015).

Table 3.1: Apical growth rate of the wild-type strain on addition of various amounts of TFP and CPZ in the Vogel's glucose agar medium

Sl. no.	Amount of TFP and CPZ	Growth rate (cm h^{-1})
1.	None (Control)	0.37 ± 0.21
2.	20 µM TFP	0.25 ± 0.06
3.	50 µM TFP	0.15 ± 0.12
4.	80 µM TFP	0.08 ± 0.28
5.	20 µM CPZ	0.28 ± 0.04
6.	40 µM CPZ	0.16 ± 0.04
7.	60 µM CPZ	0.11 ± 0.03

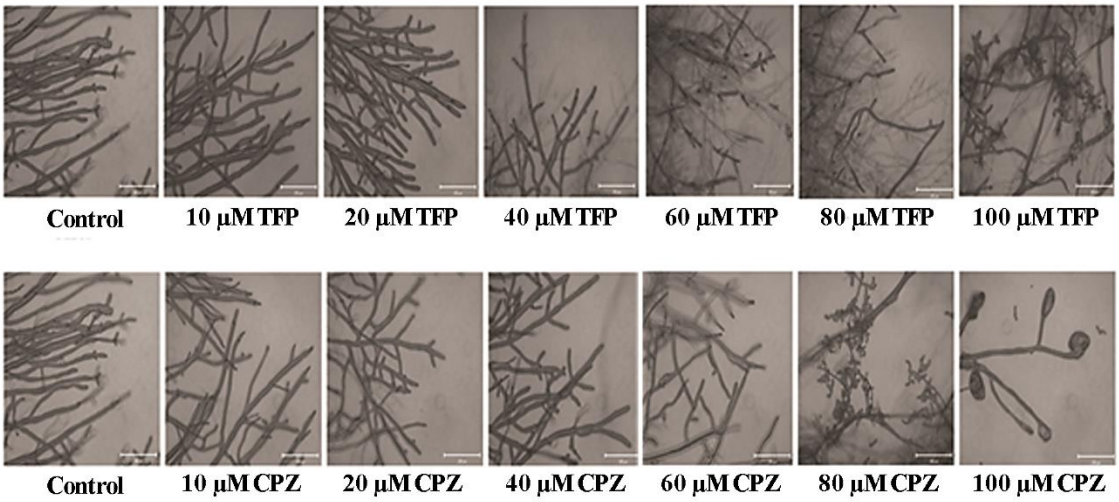

Figure 3.9: Effect of TFP and CPZ on hyphal morphology of *N. crassa*. Wild-type strain of *N. crassa* was grown on a thin layer of Vogel's glucose agar medium supplemented with various concentrations of TFP and CPZ on a glass slide for 12 h and observed under a microscope at 20X magnification.

(A)

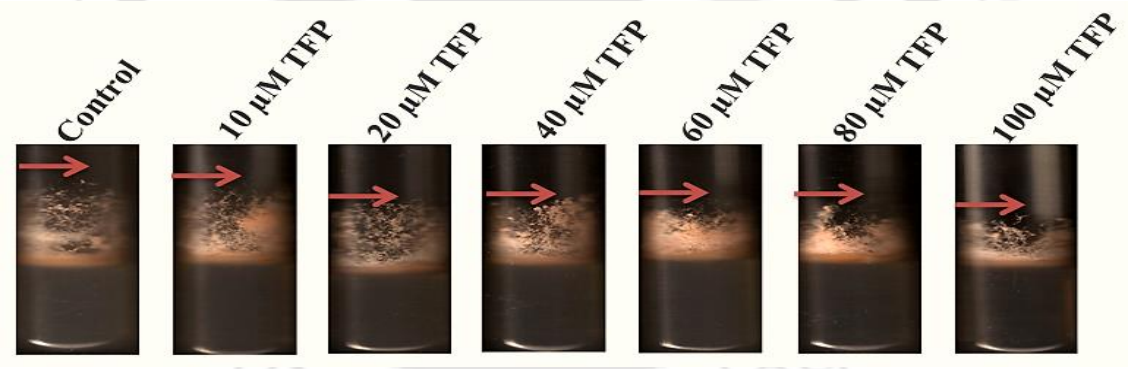

(B)

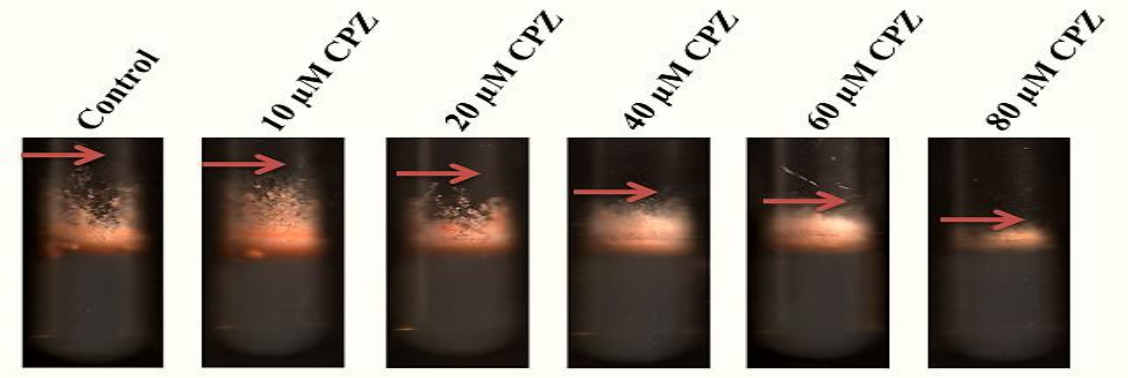

(C)

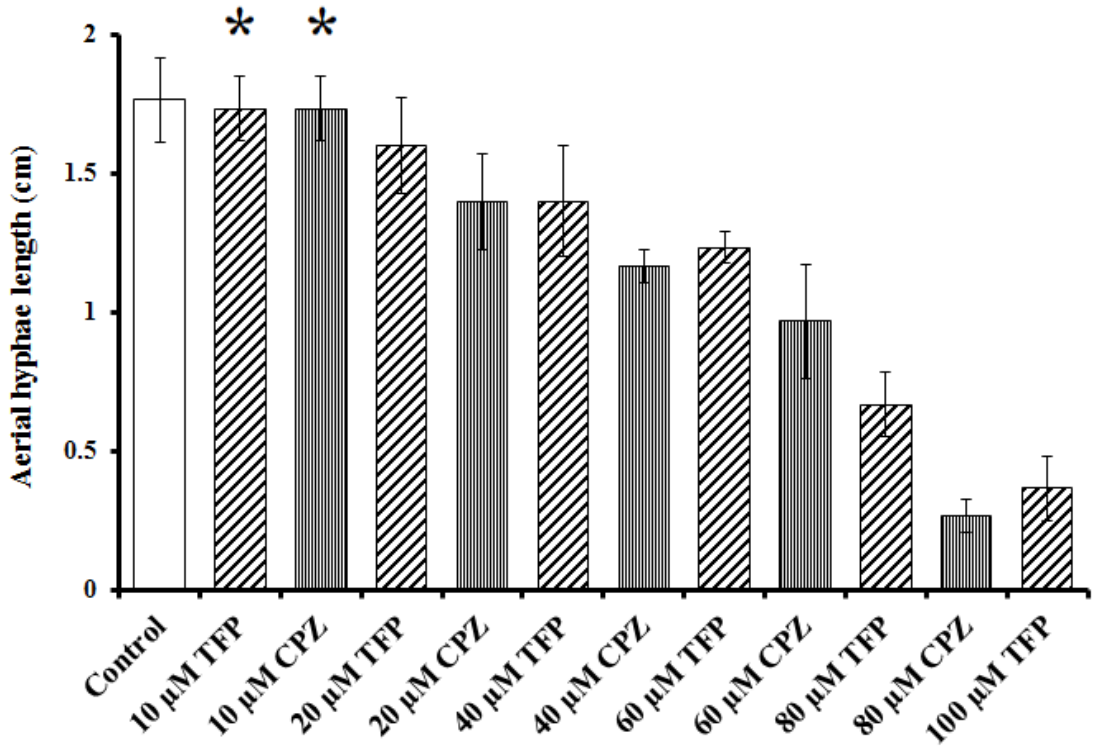

Figure 3.10: Effect of TFP and CPZ on growth of aerial hyphae in *N. crassa*. Aerial hyphae growth of the wild-type strain in the presence of (A) TFP and (B) CPZ. Cultures were grown on Vogel's glucose agar medium for three days at 30°C in dark and four days in constant light at room temperature and photographed. The edges of aerial hyphae were indicated by red arrows. (C) Aerial hyphae length of cultures grown on VSM at 30ºC in various concentrations of TFP and CPZ for three days at 30°C in dark and four days in constant light at room temperature. Statistically significant values are indicated by asterisks, *P < 0.05 (Adapted from Laxmi and Tamuli 2015).

Table 3.2: Aerial hyphae height of the wild-type strain in the presence of various amounts of TFP and CPZ

Sl. no.	Amount of TFP or CPZ	Height (cm)
1.	None (Control)	1.76 ± 0.15
2.	10 µM TFP	1.73 ± 0.11
3.	20 µM TFP	1.60 ± 0.17
4.	40 µM TFP	1.40 ± 0.20
5.	60 µM TFP	1.23 ± 0.05
6.	80 µM TFP	0.66 ± 0.11
7.	100 µM TFP	0.36 ± 0.11
8.	10 µM CPZ	1.73 ± 0.11
9.	20 µM CPZ	1.40 ± 0.17
10.	40 µM CPZ	1.16 ± 0.05
11.	60 µM CPZ	0.96 ± 0.20
12.	80 µM CPZ	0.26 ± 0.05

(A)

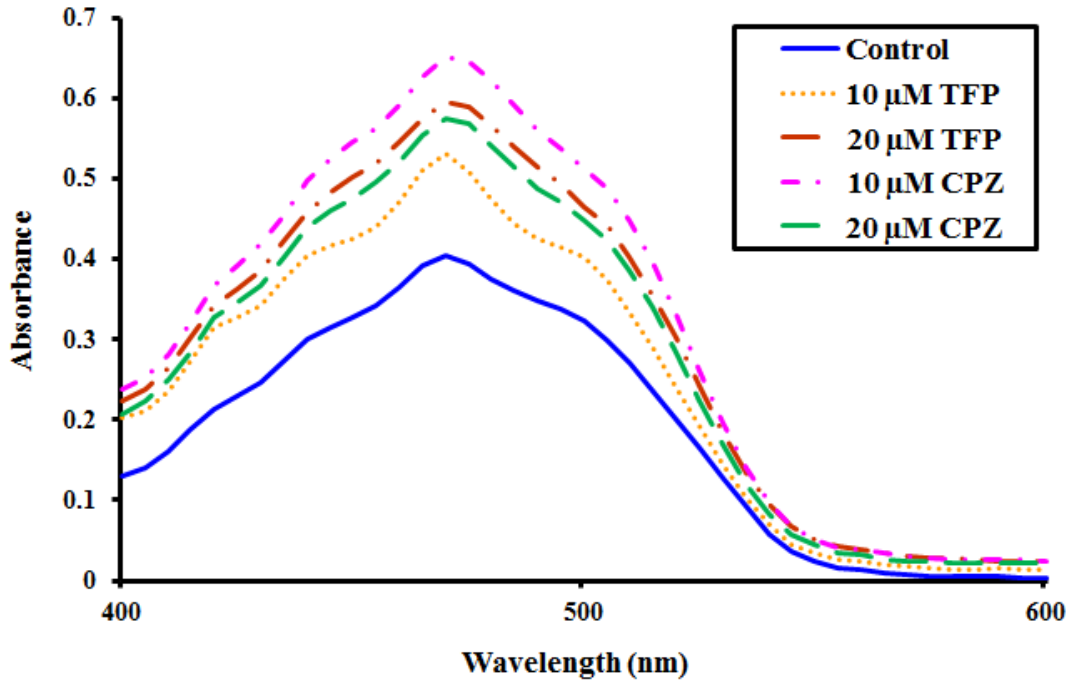

(B)

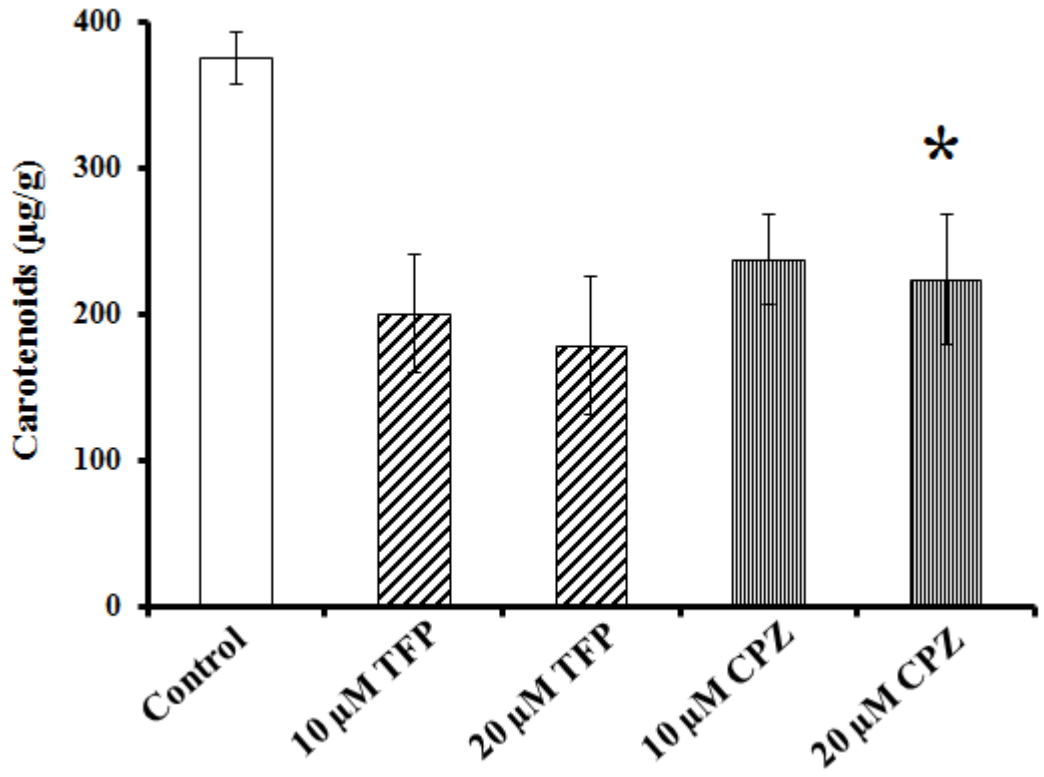

Figure 3.11: Analysis of carotenoids content of *N. crassa* in the presence of TFP and CPZ. (A) Absorption spectra profile of crude carotenoids samples obtained from wild-type strain grown in the presence of TFP and CPZ employed for carotenoids estimation. Maximal absorption is at 470 nm. (B) Carotenoid content of wild-type strain in the presence of CaM antagonist TFP and CPZ. Carotenoids were extracted and estimated in µg carotenoids per g of dry weight. Standard errors calculated from the data for three independent experiments are shown using error bars. Statistically significant values are indicated by asterisks, *P < 0.05. The strains were grown for two days in dark at 30°C, followed by 24 h under light at 30°C (Adapted from Laxmi and Tamuli 2015).

Table 3.3: Carotenoids accumulation on addition of various amounts of TFP and CPZ

Sl. no.	Amount of TFP or CPZ	Carotenoid (µg/g dry mycelial powder)
1.	None (Control)	375.59 ± 17.89
2.	10 µM TFP	200.11 ± 40.11
3.	20 µM TFP	178.56 ± 47.33
4.	10 µM CPZ	237.45 ± 30.52
5.	20 µM CPZ	223.59 ± 44.12

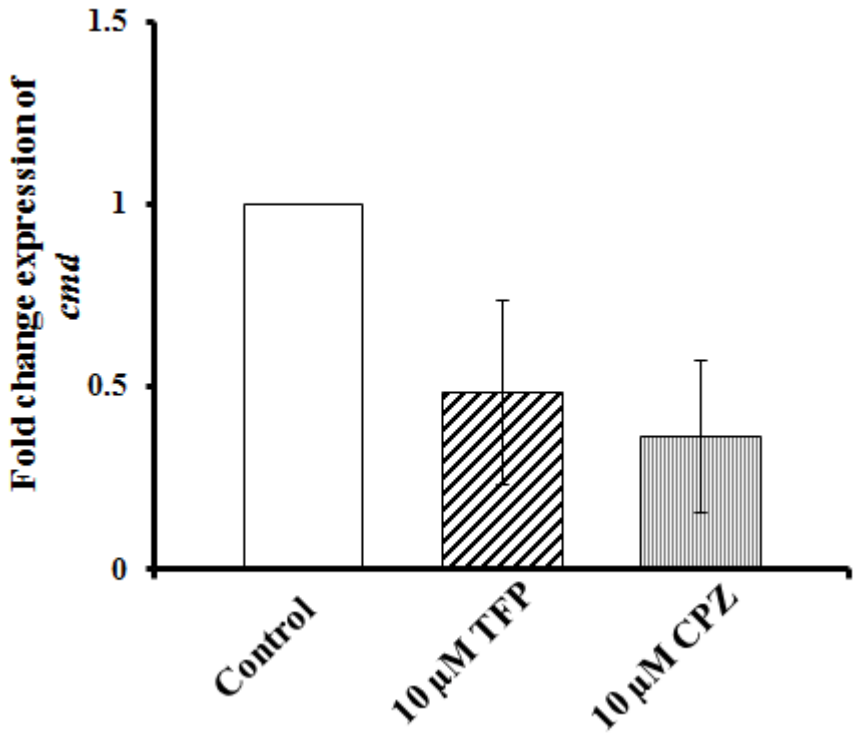

Figure 3.12: Expression studies of *cmd* gene in the presence of CaM inhibitors. Fold change in expression was calculated by $2^{-\Delta\Delta C_T}$ method (Livak and Schmittgen 2001), using wild-type and β-tubulin as calibrator and endogenous control respectively. Standard errors calculated from the data for two independent experiments are shown using error bars (Adapted from Laxmi and Tamuli 2015).

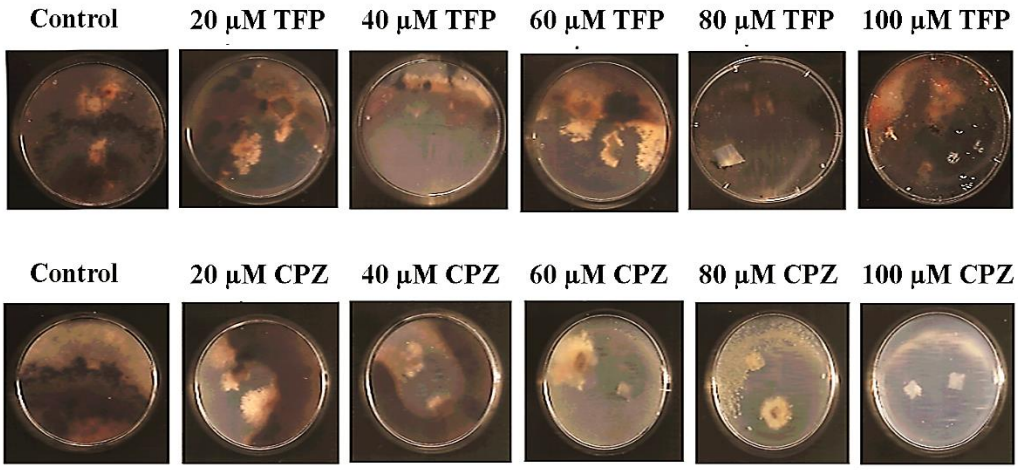

Figure 3.13: Effect of TFP and CPZ on sexual development of *N. crassa*. Addition of TFP and CPZ in SCM agar at various concentrations causes defect in perithecia formation of crosses involving the wild-type strain of opposite mating type.

3.2.3 Generation of the Δ*trm-9*Δ*nca-2* double mutant strain

The *N. crassa* Δ*trm-9* and Δ*nca-2* single knockout mutants were generated by the *N. crassa* genome project (http://www.dartmouth.edu/~neurosporagenome/proj_overview.html) and also studied previously (Colot *et al.* 2006; Bowman *et al.* 2011; Deka and Tamuli 2013; Laxmi and Tamuli 2015). To generate the Δ*trm-9*Δ*nca-2* double mutant, I crossed the Δ*trm-9* and the Δ*nca-2* single mutants of opposite mating type (Figure 3.14). The ascospores were harvested after 21 days, germinated on Vogel's sorbose agar plate after heat shock and the well germinated individual progeny strains were transferred to Vogel's glucose agar medium for growth at 30ºC for 3 days and screened for hygromycin resistance (hyg^R). DNA was isolated from hyg^R progenies and PCR analysis was performed to identify the double mutants. The forward primers NCU04898-5F and NCU04736-5F that are specific for upstream of the 5'flank of the genes *trm-9* and *nca-2* respectively, were used with the common reverse primer 5HPHR that is specific for the *hph* cassette used to generate the knockout mutants (Table 3.4). Amplification of PCR products of size ~1.2 and ~1.018 kb verified the presence of the *trm-9* and *nca-2* knockout alleles, respectively, in the mutants (Figure 3.15).

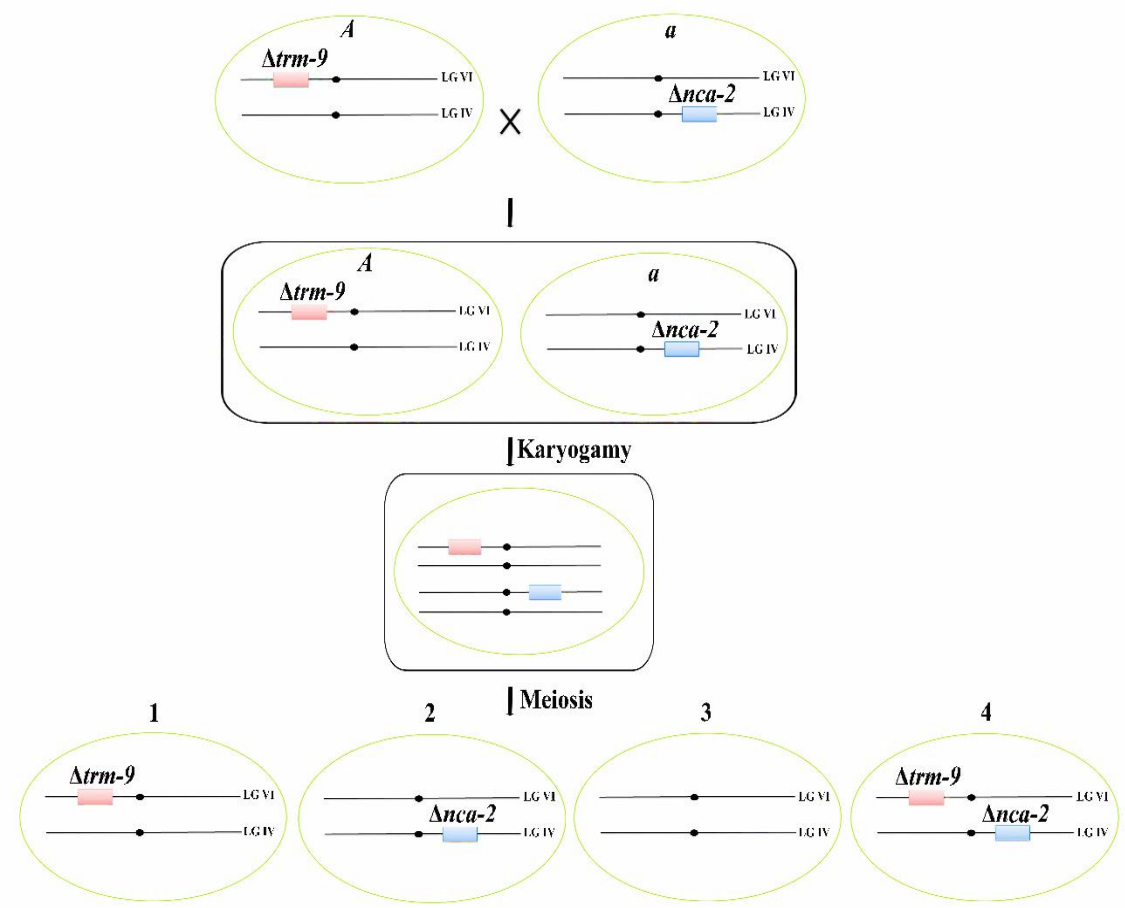

Figure 3.14: Construction of Δ*trm-9*Δ*nca-2* double knockout mutant. Strategy to generate the double knockout mutant by crossing the Δ*trm-9* and Δ*nca-2* single mutants of opposite mating type. After fertilization, karyogamy and meiosis event, four types of progeny strains; (1) mutant bearing the *trm-9* allele, (2) mutant bearing *nca-2* allele (3) wild-type and (4) double mutant bearing Δ*trm-9* and Δ*nca-2* allele (1:1:1:1 segregation ratio) are produced.

Table 3.4: Primers used for confirmation of knockout mutants by PCR

Sl. no.	Primer	Sequence (5'→ 3')
1.	NCU04898-5F	GGTTAGTGAGCTTTGAGTCG
2.	NCU04736-5F	TACACTGGTAATGGACCACG
3.	5HPHR	ATCCACTTAACGTTACTGAAATC

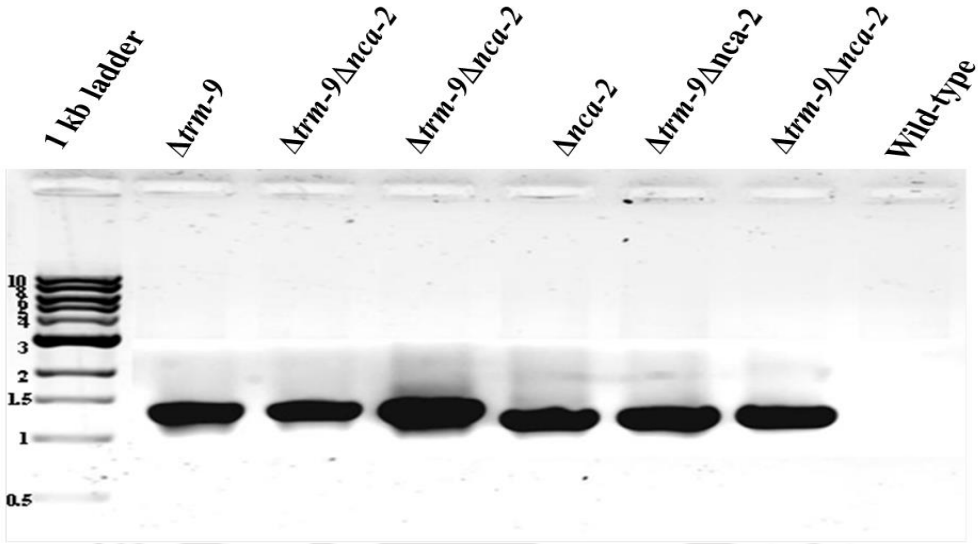

Figure 3.15: PCR analysis for double mutant confirmation. The Δ*trm-9*Δ*nca-2* double mutants were verified by using the forward primers NCU04898-5F and NCU04736-5F specific for upstream of the ORF of genes *trm-9* and *nca-2*, respectively and with the common reverse primer 5HPHR that is specific for the *hph* cassette used to generate the knockout mutants (Colot *et al.* 2006; Deka *et al.* 2011). Amplification of PCR products of size ~1.2 and ~1.018 kb indicate the presence of the Δ*trm-9* and Δ*nca-2* knockout alleles, respectively. The wild-type was used as negative controls for the knockout alleles (indicated in the parenthesis) using the allele specific primer pairs. PCR products were visualized in a 0.8% agarose gel with 1 kb DNA ladder (Adapted from Laxmi and Tamuli 2015).

3.2.4 The Δ*trm-9*Δ*nca-2* double mutant showed novel colony morphology and reduced conidiation

For colony morphology study, wild-type, Δ*trm-9*, Δ*nca-2* and Δ*trm-9*Δ*nca-2* strains were grown at 30ºC for three days followed by three days under constant light at room temperature. The Δ*trm-9*Δ*nca-2* double mutant that showed distinct colony morphology with matty-like colony growth and this phenotype was different from either of the parental single mutants and the wild-type (Figure 3.16). In addition, I also studied the hyphal morphology and aerial hyphae growth of Δ*trm-9*Δ*nca-2* mutant (as described in materials and methods). The Δ*trm-9*Δ*nca-2* double mutant also showed profuse and less-

branched hyphae (Figure 3.17) and reduced aerial hyphae development (Figure 3.18; Table 3.5) as compared to the wild-type and their parental strain. In addition Δ*trm-9*Δ*nca-2* double mutant also produced very few conidia (asexual spores). The effect of mutation on conidiation process was studied by calculating conidial count (as described in materials and methods). Conidial count percentage of Δ*trm-9*Δ*nca-2* double mutant was found to be more than that of wild-type (Figure 3.19).

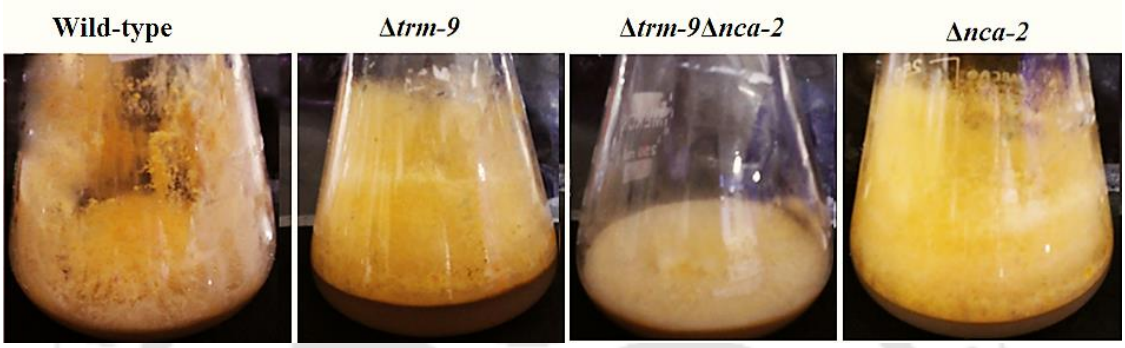

Figure 3.16: Colony morphology of wild-type, Δ*trm-9*, Δ*nca-2* and Δ*trm-9*Δ*nca-2* strains. The Δ*trm-9*Δ*nca-2* double mutant strain showed matty-like growth and reduced pigmentation (Adapted from Laxmi and Tamuli 2015).

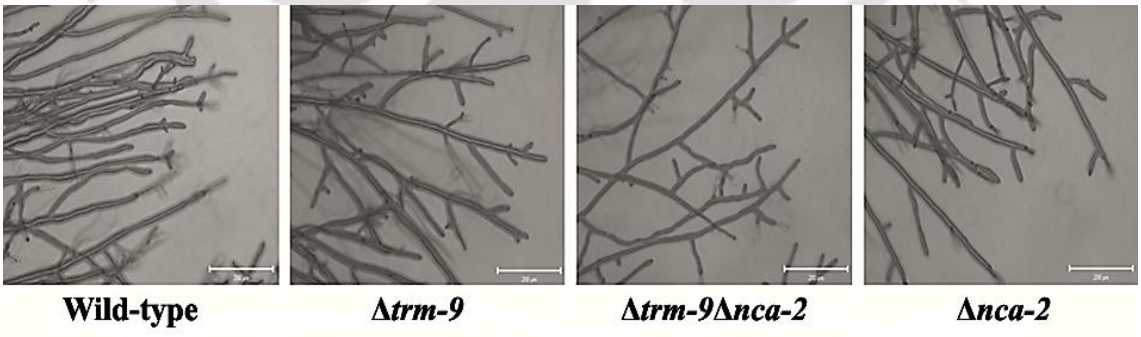

Figure 3.17: Hyphal morphology of wild-type, Δ*trm-9*, Δ*nca-2* and Δ*trm-9*Δ*nca-2* strains. Strains were grown at 30°C for 12 h on a thin layer of Vogel's glucose agar medium on glass slide and observed under microscope at 20X magnification.

(A)

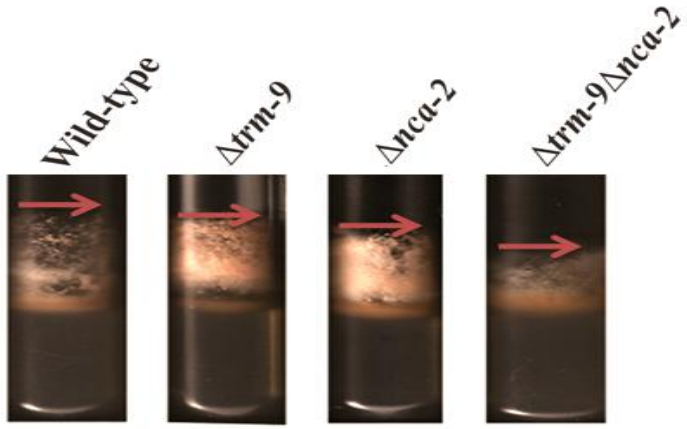

(B)

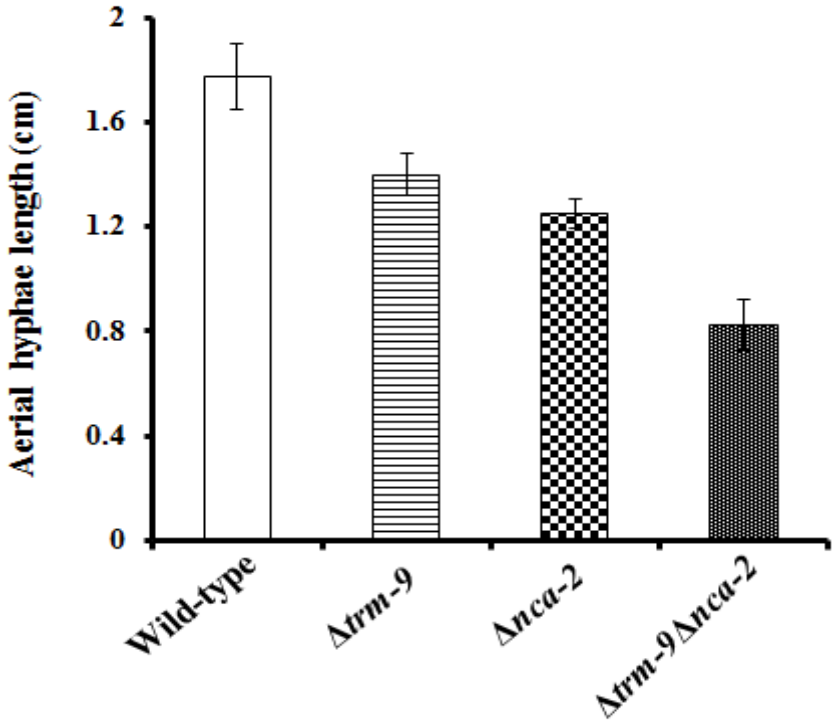

Figure 3.18: Aerial hyphae culture of the wild-type, Δ*trm-9*, Δ*nca-2* and Δ*trm-9*Δ*nca-2* strains. (A) Strains were grown on Vogel's glucose agar medium at 30°C for three days and photographed and edges of aerial hyphae were indicated by arrows. (B) Aerial hyphae length of cultures grown on VSM for three days at 30°C in dark and four days in constant light at room temperature The aerial hyphae growth of Δ*trm-9*Δ*nca-2* double mutant strain was less than as compared to parental single mutants and wild-type strain (Adapted from Laxmi and Tamuli 2015).

Table 3.5: Aerial hyphae height of wild-type, Δ*trm-9*, Δ*nca-2* and Δ*trm-9*Δ*nca-2* strains

Sl. no.	Strain	Height (cm)
1.	Wild-type	1.77 ± 0.12
2.	Δ*trm-9*	1.40 ± 0.08
3.	Δ*nca-2*	1.25 ± 0.05
4.	Δ*trm-9*Δ*nca-2*	0.82 ± 0.09

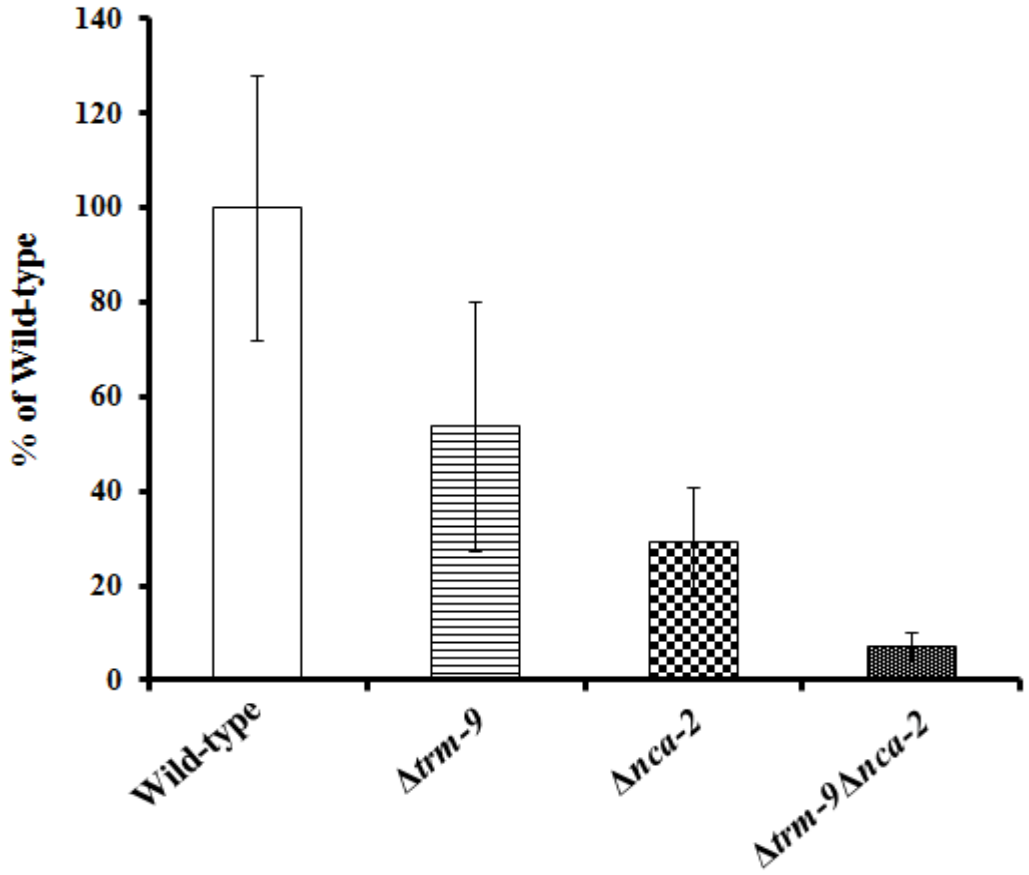

Figure 3.19: Conidial cell count of wild-type, Δ*trm-9*, Δ*nca-2* and Δ*trm-9*Δ*nca-2* strains. Conidia count of wild-type and mutant strains are plotted with relative counting with respect to wild-type. Error bars indicate the standard errors calculated from the data for three independent experiments. Conidial cell count of Δ*trm-9*Δ*nca-2*double mutant strain was less than the parental single knockout mutant strains and wild-type.

3.2.5 The Δ*trm-9*Δ*nca-2* double mutant has a slow growth phenotype and less in dry weight content

The apical growth rate and dry weight content of the double mutant strain was studied as described in materials and methods. Growth rate for Δ*trm-9*Δ*nca-2* double mutant was lower than their parental single mutants and the wild-type (Figure 3.20; Table 3.6). In addition, the dry weight of the strains followed the order wild-type >Δ*nca-2*>Δ*trm-9*>Δ*trm-9*Δ*nca-2* (Figure 3.21; Table 3.7).

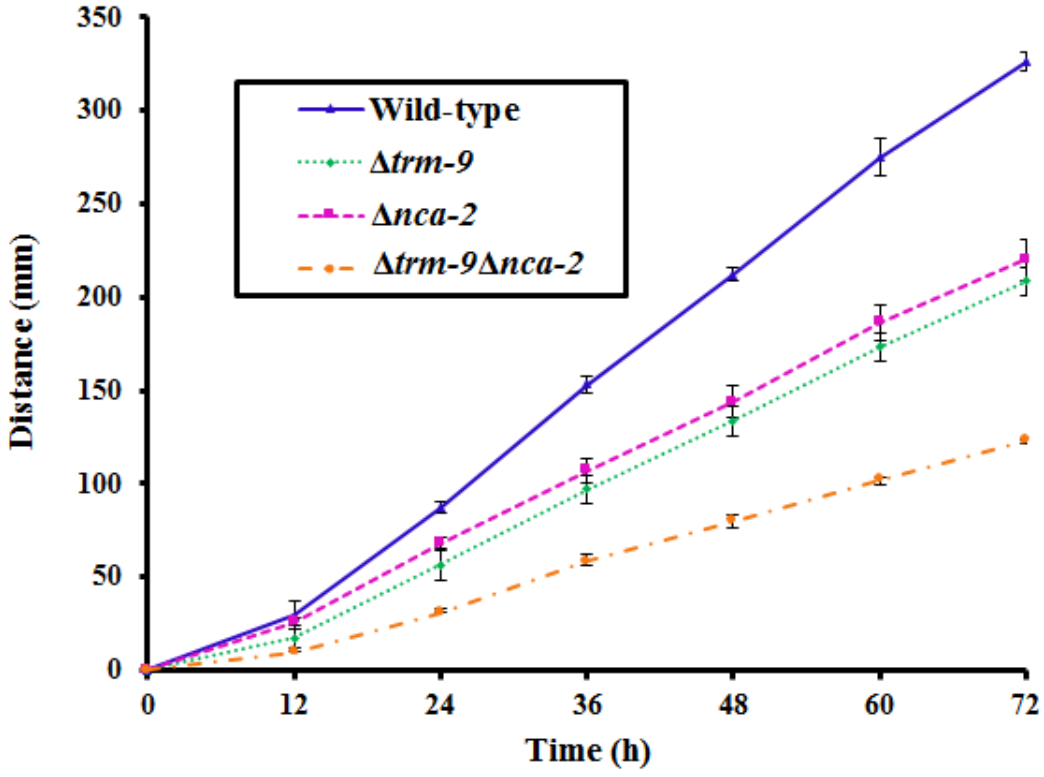

Figure 3.20: Apical growth rate of wild-type, Δ*trm-9*, Δ*nca-2* and Δ*trm-9*Δ*nca-2* strains. Rate of apical growth rate of the wild-type, Δ*trm-9* and Δ*nca-2*, Δ*trm-9*Δ*nca-2* strains were measured using race tubes. Growth rate of Δ*trm-9*Δ*nca-2* double mutant strain was lesser as compared to parental single mutants and wild-type strain (Adapted from Laxmi and Tamuli 2015).

Table 3.6: Apical growth of wild-type, Δ*trm-9*, Δ*nca-2* and Δ*trm-9*Δ*nca-2* strains

Sl. no.	Strain	Growth rate (cm h^{-1})
1.	Wild-type	0.37 ± 0.21
2.	Δ*trm-9*	0.24 ± 0.24
3.	Δ*nca-2*	0.28 ± 0.15
4.	Δ*trm-9*Δ*nca-2*	0.14 ± 0.03

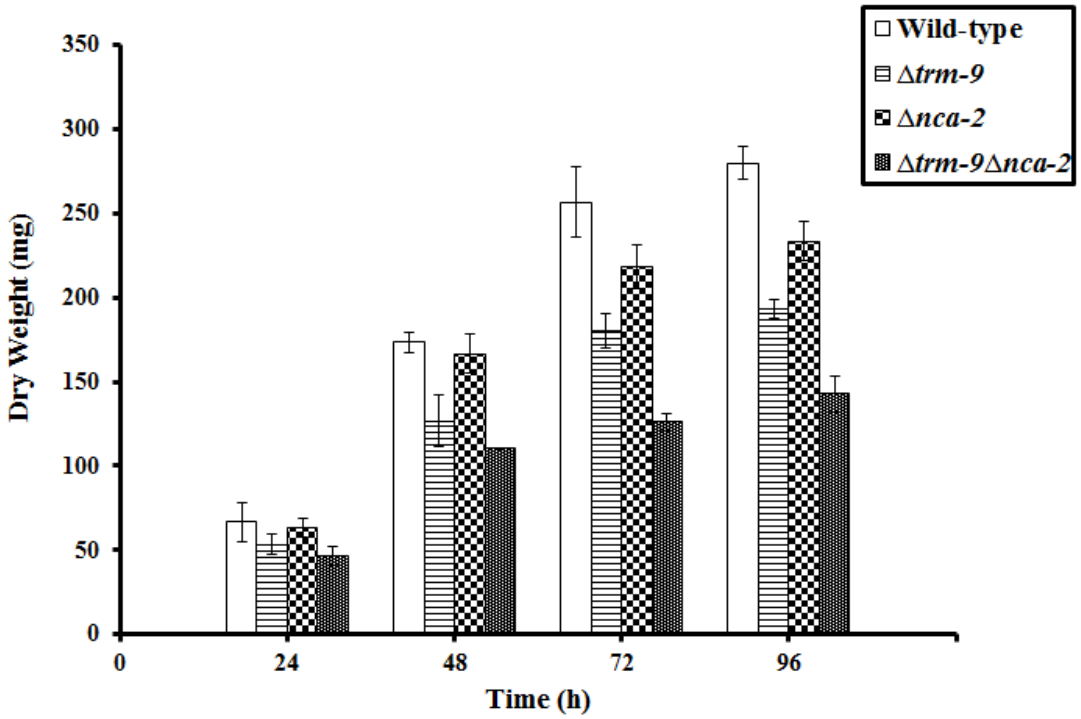

Figure 3.21: Dry weight assay of wild-type Δ*trm-9*, Δ*nca-2* and Δ*trm-9*Δ*nca-2* strains. Dry weight yield of Δ*trm-9*Δ*nca-2* double mutant strain was less than parental single mutants and the wild-type (Adapted from Laxmi and Tamuli 2015).

Table 3.7: Biomass accumulation of wild-type, Δ*trm-9*, Δ*nca-2* and Δ*trm-9*Δ*nca-2* strains

Sl. no.	Strain	24 h	48 h	72 h	96 h
		Dry weight (mg)			
1.	Wild-type	66.66 ± 11.54	173.33 ± 5.77	256.66 ± 20.81	280.00 ± 10.00
2.	Δ*trm-9*	53.33 ± 5.77	126.66 ± 15.27	180.00 ± 10.00	193.33 ± 5.77
3.	Δ*nca-2*	63.33 ± 5.77	166.66 ± 11.54	218.33 ± 12.58	233.33 ± 11.54
4.	Δ*trm9*Δ*nca-2*	46.66 ± 5.77	110.33 ± 0.57	126.00 ± 5.29	142.66 ± 11.01

3.2.6 The slow growth phenotype of the Δ*trm-9*Δ*nca-2* mutant strain was not due to defect in ergosterol biosynthesis

The *trm-9* gene is the *N. crassa* homolog of *spf1* gene of *S. cerevisiae* and it was found that absence of *spf1* gene causes lack of control of HMG- CoA reductase enzyme degradation in sterol production (Cronin *et al.* 2000). Ergosterol is a major constituent of fungal plasma membrane synthesized from a central metabolite acetyl CoA (Parks and Casey 1995). The ergosterol biosynthesis pathway is catalyzed by several enzymes. In *N. crassa*, *erg-3* gene encodes sterol C-14 reductase that catalyzes the reduction of the $\Delta^{14,15}$ double bond in intermediates in the sterol biosynthesis pathway using NADPH as a cofactor. The RIP induced *erg-3* mutant grows slowly due to a defect in ergosterol biosynthesis. Ergosterol has UV absorption maxima at 272, 282 and 293 nm whereas the *erg-3* mutant sterols absorb maximally at ~250 nm, typical of Δ8, 14 sterols, indicating absence of ergosterol in the *erg-3* mutant (Prakash *et al.* 1999). To test if the slow growth phenotype of the Δ*trm-9*Δ*nca-2* double mutant was due to a defect in ergosterol biosynthesis I analyzed the ergosterol profiles (as described in materials and methods). UV spectra analysis of sterols isolated from the wild-type, Δ*trm-9*, Δ*nca-2* and Δ*trm-9*Δ*nca-2* double mutant strain showed intense peak at 272, 282 and 293 nm, which showed there is no defect in sterol biosynthesis (Figure 3.22). Thus, it was concluded that slow growth phenotype of the Δ*trm-9*Δ*nca-2* double mutant strain is not due to a

defect in ergosterol biosynthesis and *trm-9* gene is not involved in ergosterol biosynthesis pathway.

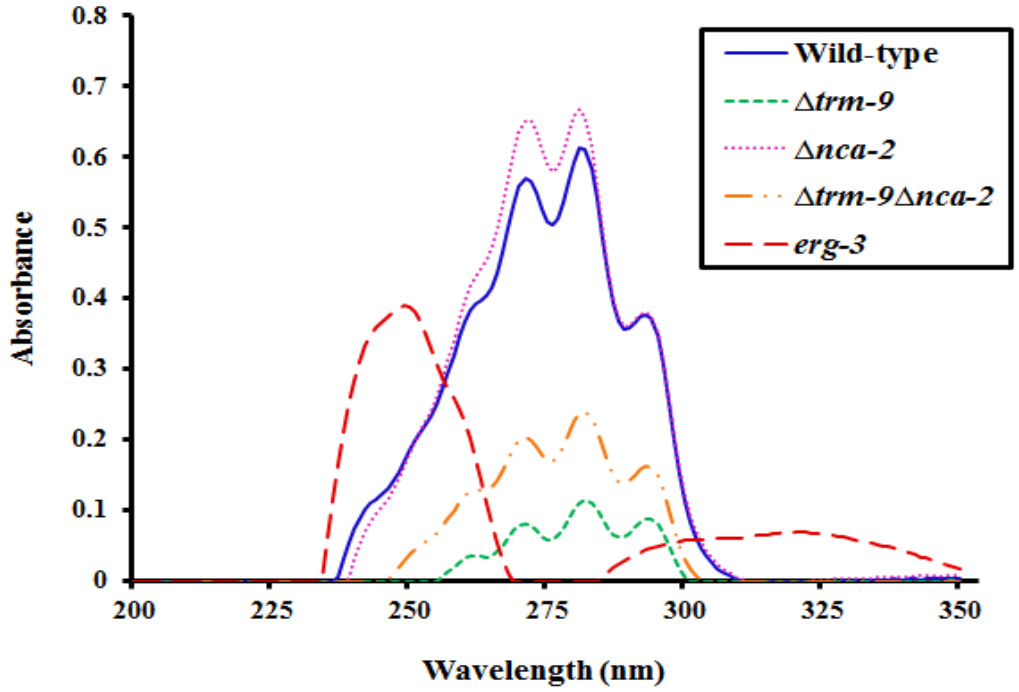

Figure 3.22: Ergosterol is present in the wild-type, Δ*trm-9*, Δ*nca-2* and Δ*trm-9*Δ*nca-2* strains. Profile of the sterols extracted from the wild-type, Δ*nca-2* mutant, Δ*trm-9*, Δ*trm-9*Δ*nca-2* and the *erg-3* mutant were analyzed by UV spectrophotometer (Adapted from Laxmi and Tamuli 2015).

3.2.7 Carotenoid accumulation in Δ*trm-9*Δ*nca-2* double mutant strain

The Δ*trm-9*Δ*nca-2* double mutant strain showed reduced pigmentation, therefore, I measured its carotenoid content (as described in materials and methods). The carotenoid profile of the Δ*trm-9*Δ*nca-2* double mutant was lower than either of the parental single mutant strains (Figure 3.23; Table 3.8) and reduced further on medium supplemented with high concentrations of $CaCl_2$ (Figure 3.24; Table 3.9). Thus, the role of *trm-9* and *nca-2* genes suggested involvement of Ca^{2+}-signaling pathway in modulating carotenoid biosynthesis. In addition, the Δ*nca-2* mutant was unable to grow on medium supplemented with 0.3 M $CaCl_2$ or more and consequently, carotenoids accumulation was not detected; however, accumulation of carotenoids in the Δ*trm-9* was similar to the

wild-type (Figure 3.24). Therefore, these results suggested that *nca-2* plays a role in carotenoids biosynthesis.

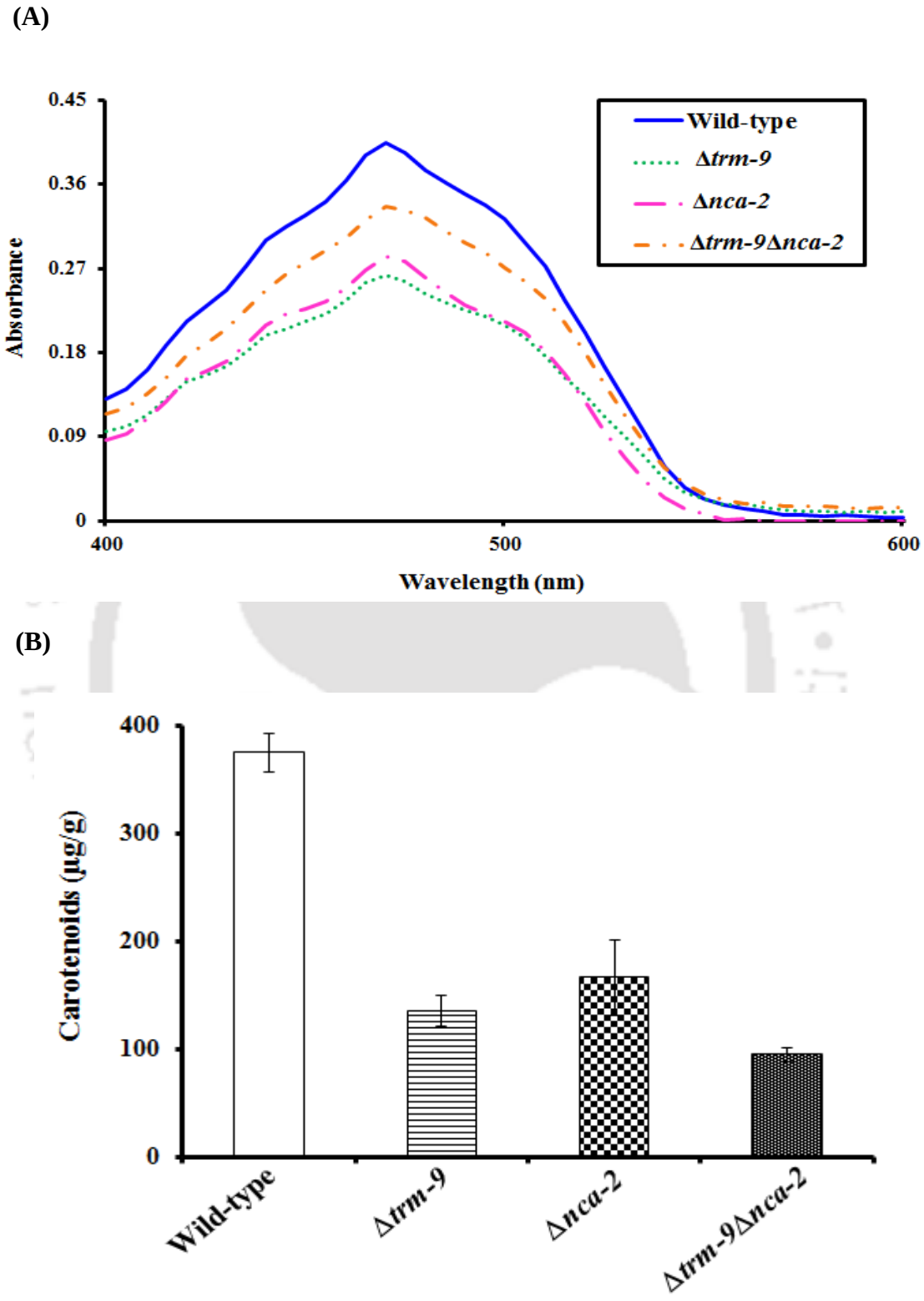

Figure 3.23: Carotenoid accumulation of wild-type, Δ*trm-9*, Δ*nca-2* and Δ*trm-9*Δ*nca-2* strains. (A) Absorption spectra and (B) Carotenoids content obtained from

wild-type *trm-9*, Δ*nca-2* and Δ*trm-9*Δ*nca-2* strains. Carotenoids were extracted and estimated in µg carotenoids per g of dry weight. Carotenoid content of Δ*trm-9*Δ*nca-2* double mutant is lower as compared to parental single mutants and wild-type strain. Error bars show the standard errors calculated from the data for three independent experiments.

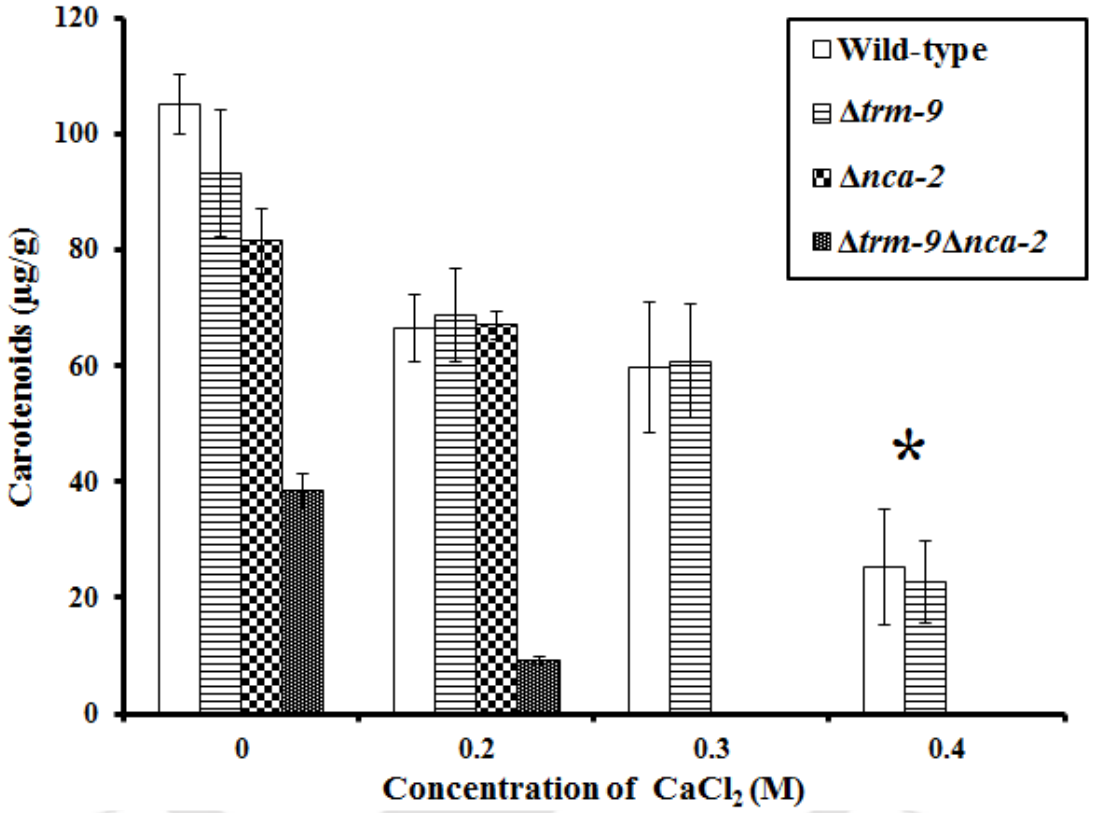

Figure 3.24: Carotenoids accumulation of wild-type, Δ*trm-9*, Δ*nca-2* and Δ*trm-9*Δ*nca-2* strains during Ca^{2+} stress. Carotenoids extracted from these strains grown in VGM without $CaCl_2$, supplemented with various concentrations of $CaCl_2$. Carotenoids were extracted and estimated in µg carotenoids per g of dry weight. Error bars show the standard errors calculated from the data for three independent experiments. Statistically significant values are indicated by asterisks, *P < 0.05 (Adapted from Laxmi and Tamuli 2015).

Table 3.8: Carotenoids content of wild-type, Δ*trm-9*, Δ*nca-2* and Δ*trm-9*Δ*nca-2* strains

Sl. no.	Strain	Carotenoid (µg/g dry mycelial powder)
1.	Wild-type	375.59 ± 17.89
2.	Δ*trm-9*	135.11 ± 14.25
3.	Δ*nca-2*	166.50 ± 35.54
4.	Δ*trm-9*Δ*nca-2*	95.58 ± 6.46

Table 3.9: Carotenoid content of wild-type, Δ*trm-9*, Δ*nca-2* and Δ*trm-9*Δ*nca-2* strains during Ca^{2+} stress

Sl. no.	Strain	Carotenoid (µg/g dry mycelial powder)			
		$CaCl_2$			
		0 M	0.2 M	0.3 M	0.4 M
1.	Wild-type	105.22 ± 5.10	66.57 ± 11.03	59.67 ± 5.67	25.29 ± 2.92
2.	Δ*trm-9*	93.20 ± 5.75	68.76 ± 7.99	60.86 ± 2.49	22.78 ± 0.69
3.	Δ*nca-2*	81.59 ± 11.23	67.08 ± 9.87	0	0
4.	Δ*trm9*Δ*nca-2*	38.47 ± 9.98	9.26 ± 6.98	0	0

3.2.8 The Δ*trm-9*Δ*nca-2* mutant displayed an increased sensitivity to Ca^{2+} and UV stress and reduced viability in the acquisition of thermotolerance

The sensitivity of the Δ*nca-2* mutant to Ca^{2+} stress was shown previously (Bowman *et al.* 2011; Deka *et al.* 2011). To test if Ca^{2+} stress tolerance is affected by the interactions of *nca-2* and *trm-9*, I studied effect of Ca^{2+} on the growth of Δ*trm-9*Δ*nca-2* double mutant strain (as described in materials and methods). The cytosolic free Ca^{2+} ($[Ca^{2+}]_c$) and the Ca^{2+}gradient in fungal hyphae plays an important role in establishing and maintaining apical organization, morphogenesis and growth (Jackson and Heath 1993). I performed the growth analysis on medium supplemented with various concentrations of $CaCl_2$. The average colony growth rate was calculated by plotting colony growth rate against different concentrations of $CaCl_2$. The Δ*trm-9*Δ*nca-2* double mutant showed more severe growth defect than *nca-2* knockout mutant on medium supplemented with 0.2 M and 0.3M $CaCl_2$ (Figure 3.25; Table 3.10), suggesting the requirement of these two genes in Ca^{2+} stress tolerance. It is possible that the *trm-9* gene might be involved in decreasing $[Ca^{2+}]_c$ by active pumping of Ca^{2+} into internal stores or efflux of Ca^{2+} from the cell.

Carotenoids, known to quench free radicals and possess a UV protective role (Luque *et al.* 2012), was reduced in the Δ*trm-9*Δ*nca-2* double mutant and the sensitivity of the Δ*nca-2* mutant to UV irradiation was previously reported (Bowman *et al.* 2011; Deka *et al.* 2011). Therefore, I assayed UV-sensitivity of the Δ*trm-9*Δ*nca-2* double mutant (as described in materials and methods). The results of the spot test revealed that the UV sensitivity of the Δ*trm-9*Δ*nca-2* double mutant was comparable to the parental single mutants (Figure 3.26). There is an interrelation of heat shock, oxidative stress and thermotolerance in *N. crassa* (Kapoor *et al.* 1990). Therefore, I also studied the ability of the Δ*trm-9*Δ*nca-2* double mutant in the acquisition of induced thermotolerance (as described in materials and methods). The Δ*trm-9*Δ*nca-2* double mutants showed decreased survival in induced thermotolerance as compared to parental single mutants. The survival in induced heat shock temperature followed the order Δ*nca-2*>Δ*trm-9*>Δ*trm-9*Δ*nca-2*>wild-type (Figure 3.27). Therefore, lack of both *nca-2* and *trm-9* had a negative effect in the acquisition of induced thermotolerance.

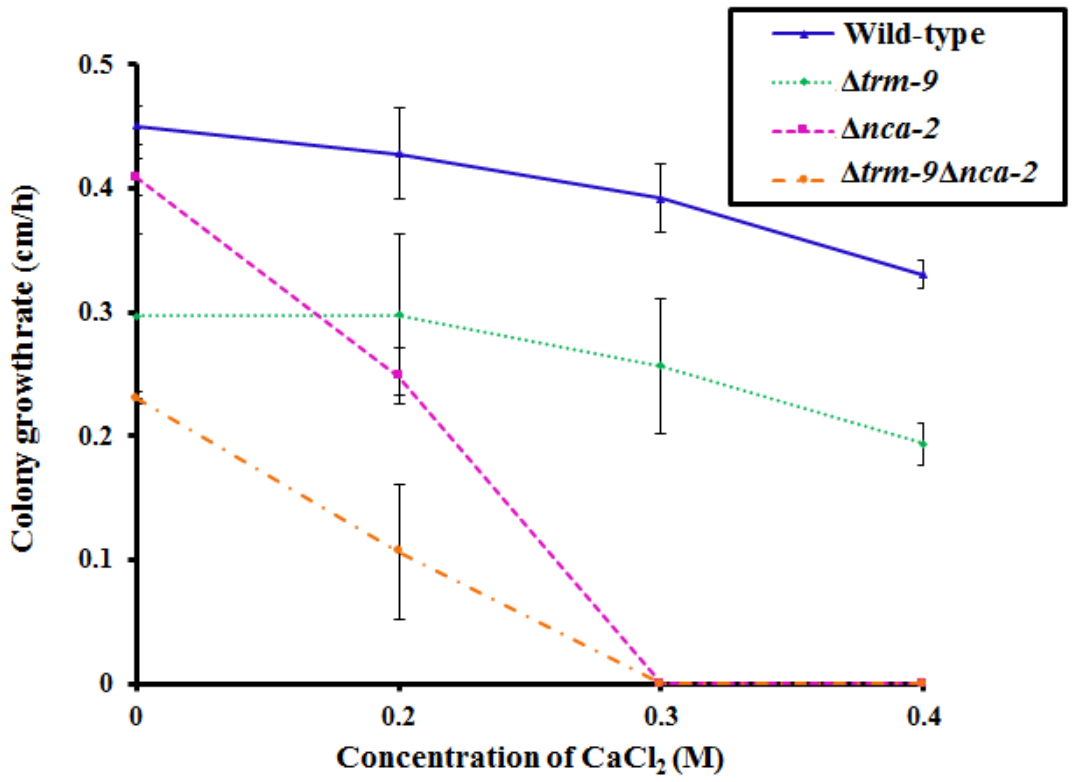

Figure 3.25: Ca^{2+} sensitivity analysis of wild-type, Δ*trm-9*, Δ*nca-2* and Δ*trm-9*Δ*nca-2* strains. Colony diameter (cm h^{-1}) of the strains was measured at regular intervals and plotted against various concentrations of $CaCl_2$. Standard errors calculated from the data for three independent experiments are shown using error bars (Adapted from Laxmi and Tamuli 2015).

Table 3.10: Average colony growth rate of the wild-type, Δ*trm-9*, Δ*nca-2* and Δ*trm-9*Δ*nca-2* strains at various concentrations of $CaCl_2$

Sl. no.	$CaCl_2$ (M)	Growth rate (cm h^{-1})			
		Wild-type	**Δ*trm-9***	**Δ*nca-2***	**Δ*trm9*Δ*nca-2***
1.	0	0.45 ± 0.01	0.29 ± 0.06	0.40 ± 0.01	0.23 ± 0.00
2.	0.2	0.42 ± 0.03	0.29 ± 0.06	0.24 ± 0.02	0.10 ± 0.05
3.	0.3	0.39 ± 0.02	0.25 ± 0.05	0	0
4.	0.4	0.33 ± 0.01	0.19 ± 0.01	0	0

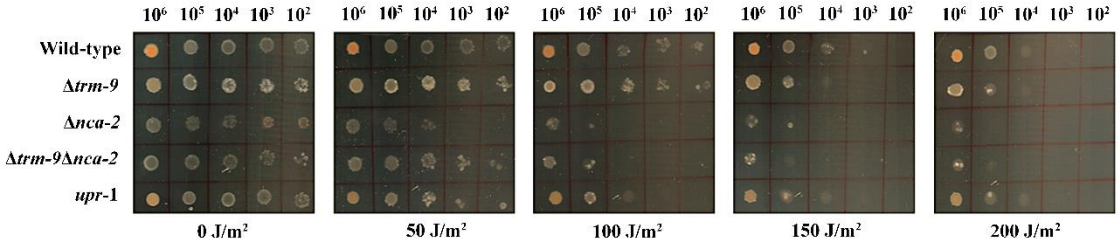

Figure 3.26: UV spot-test analysis of wild-type, Δ*trm-9*, Δ*nca-2*, Δ*trm-9*Δ*nca-2* and the *upr-1* mutant strain. Strains were grown on Vogel's glucose medium at 30°C for 3 days in dark followed by three days under constant light at room temperature. The *upr-1* mutant strain (Tamuli *et al.* 2006) was used to compare the relative UV sensitivity phenotypes (Adapted from Laxmi and Tamuli 2015).

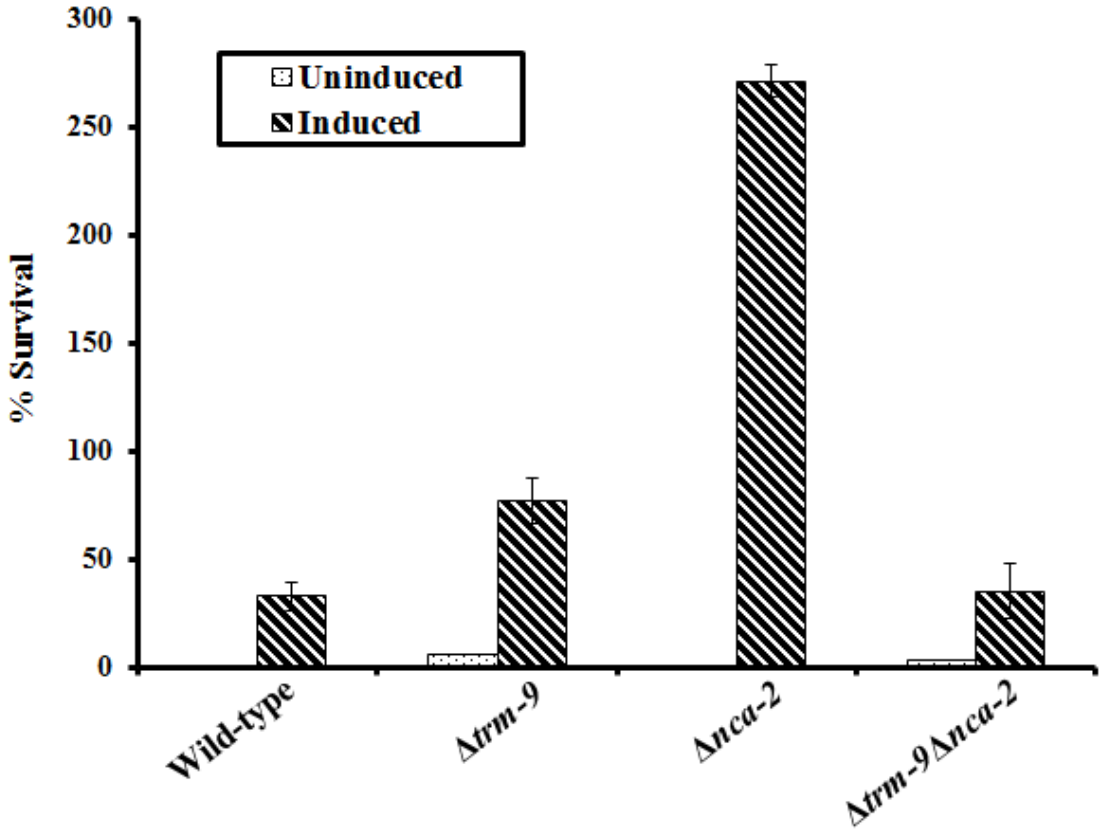

Figure 3.27: Thermotolerance measurement of wild-type, Δ*trm-9*, Δ*nca-2* and Δ*trm-9*Δ*nca-2* strains in induced (44°C) and uninduced (30°C) conditions. Each data

point represents the mean of three independent experiments. Uninduced (30°C) and induced (44°C) germlings were exposed to lethal heat shock at 52°C for calculating percent survival (Adapted from Laxmi and Tamuli 2015).

3.3 Discussion

The genes *cmd*, *trm-9* and *nca-2* encode for a CaM, a cation ATPases and a PMCA type Ca^{2+}-ATPase that possesses conserved domains (Figures 3.3-3.7). I studied the CaM role in growth of *N. crassa* using its antagonists TFP and CPZ. The CaM antagonists TFP and CPZ affected growth, hyphae morphology, aerial hyphae development, carotenoids accumulation and sexual development in *N. crassa* (Figures 3.8-3.11; Figure 3.13; Tables 3.1-3.3). The crystal structure of mammalian CaM has been refined at 2.2 Å, which shows dumbbell shaped molecule connected by a seven-turn α-helix, with an overall length of 65 Å. CaM also contains four Ca^{2+}-binding loops and two short, double-stranded antiparallel β-sheets between pairs of adjacent Ca^{2+}-binding loops referred to as EF-hand structures. In addition, X-ray structure of CaM also shows a large hydrophobic cleft in each half of the molecule, which is responsible for interaction with many of the pharmacological agents known to bind to CaM (Babu *et al.* 1988). Various naturally occurring compounds isolated from a wide variety of natural sources, including many fungi and plants has CaM-inhibitory properties, belonging to different structural classes such as alkaloid and peptide (Martínez-Luis *et al.* 2007; Mata *et al.* 2014). Among the most potent anti-CaM substances, however, the first class of drugs shown to demonstrate this property was the phenothiazines (Levin and Weiss 1976). Inhibition of CaM function by a phenothiazines first demonstrated by Levin and Weiss, and the effect of TFP inhibition on CaM activated enzymes can also be overcome by excess CaM (Levin and Weiss 1976, 1977). These different pharmacological compounds share many common structural features and display a large hydrophobic region, consisting of two or three aromatic rings and a side-chain amino group that is at least four atoms removed from the ring structure (Weiss *et al.* 1982). Interactions of drugs with CaM appear to involve two kinds of attachments, a hydrophobic interaction between lipophilic portions of the drug and non-polar regions of CaM and an electrostatic interaction occurs between a positively charged amino group on the drug and a negatively charged acidic residue on CaM (Weiss *et al.* 1982). The mode of action of phenothiazines are not specific for CaM protein (Mori *et al.* 1980; Wise *et al.* 1982; Hait and Lee 1985). The phenothiazine, TFP and CPZ, inhibited the CaM-induced activation of the

(Ca^{2+}+Mg^{2+})-ATPase of erythrocyte membranes (Raess and Vincenzi 1980; Roufogalis 1981). CPZ is about one-fourth less potent an inhibitor of CaM than TFP (Levin and Weiss 1976; Roufogalis 1981; Weiss *et al.* 1982). This could explain more potent effect of the TFP than CPZ on carotenoid accumulation in *N. crassa* (Figure 3.11; Table 3.3). The effect of the CaM antagonists TFP and CPZ in *N. crassa* was further supported by the reduced expression of the *cmd* gene (Figure 3.12).

In *N. crassa*, nine ATPases including seven Ca^{2+}-and cation-ATPases and two cation-ATPases have been identified (Benito *et al.* 2000). The *trm-9* gene encodes a cation-ATPases, homolog of the yeast *spf1* gene. The *spf1* gene encodes a novel P-type ATPase of *S. cerevisiae*. Replacement of aspartic acid at 487 position to asparagine leads to compete loss of function of *spf1* gene, which suggested that this residue plays an important role as an acceptor of the terminal phosphate of ATP during ATP hydrolysis and energy transduction. The *pmr1* gene, which encodes a yeast golgi ion pump, is functionally related to *spf1*. The *spf1* mutant shares many phenotypic features with the *pmr1* mutant. Moreover, absence of *spf1* gene causes lack of control of HMG-CoA reductase enzyme degradation in sterol production (Cronin *et al.* 2000; Suzuki 2001). In addition, the PMCA type Ca^{2+}-ATPase, NCA-2 plays a major role in pumping Ca^{2+} out of the cell and the Δ*nca-2* knockout mutant shows sensitivity to high concentration of extracellular Ca^{2+}, slow growth and female sterility phenotype (Bowman *et al.* 2011).

In this work, I generated the Δ*trm-9*Δ*nca-2* double mutant and studied its phenotype (Figures 3.14,-3.15). The Δ*trm-9*Δ*nca-2* double mutant showed novel colony morphology with less-branched hyphae (Figures 3.16-3.17). The Δ*trm-9*Δ*nca-2* double mutant displayed reduced aerial hyphae, slow growth rate, reduced carotenoid accumulation, increased sensitivity to Ca^{2+} and UV stress and reduced viability in the acquisition of thermotolerance induced by heat shock temperature (Figures 3.18-3.21; Figures 3.23-3.27; Table 3.5-3.10). However, the slow growth rate of the Δ*trm-9*Δ*nca-2* mutant strain was not due to a defect in ergosterol biosynthesis (Figure 3.22).

In *N. crassa*, growth is manifested by an increase in colony diameter and hyphal front, development of aerial hyphae and biomass accumulation. Hyphae extend at its tip, which is measured as apical growth and radial growth. Biomass is the amount of living matter in at a given time and measured in terms of the dried organic mass, since more than half is constituted by water. Hyphal branching is necessary for efficient colonization and utilization of the substrate upon which *N. crassa* grows. Aerial hyphae are hyphal

extensions which project above water-air interface and bear the asexual spores (conidia) that are hydrophobic in nature due to the presence of hydrophobin protein. In addition, the characteristic orange pigmentation of *N. crassa* is due to accumulation of xanthophyll neurosporaxanthin and variable amounts of carotenoids precursors (Harding *et al.* 1969; Harding and Turner 1981; Díaz-Sánchez *et al.* 2011). The *albino* (*al*) genes *al-1*, *al-2* and *al-3* loci found to be structural genes coding for a phytoene dehydrogenase, phytoenesynthetase and GGPP synthetase enzyme and regulated by the *white collar-1* (*wc-1*) required for carotenoid biosynthesis in *N. crassa* (Harding and Turner 1981). I found here that the *cmd*, *trm-9* and *nca-2* play an important role in growth and pigmentation in *N. crassa*. UV irradiation damages DNA by inducing formation of cyclobutane-pyrimidine dimers (CPDs) and 6-4 photoproducts and cells possess a molecular mechanism to protect DNA from this damage (Sinha and Häder 2002; Cadet *et al.* 2005). Carotenoids also possess a protective role against oxidative stress by quenching reactive oxygen species (Vershinin 1999). There is an interrelation of heat shock, oxidative stress and thermotolerance in *N. crassa*. There is a substantial increase in free radicals. O_2 in heat-shocked cells compared with non-shocked controls. Exposure of cells to $.O_2$ generating agents results in the induction of proteins specifically required for defense against oxidative damage that leads to production of H_2O_2 catalyzed by the multiple isoforms of *N. crassa* superoxide dismutase. H_2O_2, a deleterious agent, also generates -OH, an even more potent species, via the Haber-Weiss reaction (Kapoor *et al.* 1990). I found that genetic interaction of *trm-9* and *nca-2* play an important role in cell survival under Ca^{2+} and UV stress and exposure to heat-shock temperature in *N. crassa*. Thus, in this study, I have shown that *cmd*, *trm-9* and *nca-2* genes play an important role in growth, pigmentation and stress-tolerance in *N. crassa*.

A part of this chapter was published in Genomics and Applied Biology (Laxmi and Tamuli 2015) and presented in "4th Meeting of the Asian Forum of Chromosome and Chromatin Biology on Epigenetic Mechanisms in Development and Disease, 2012" held at Centre for Cellular and Molecular Biology, Hyderabad, India, "8th International Conference on Yeast Biology, 2013" held at Institute of Microbial Technology, Chandigarh, India and International Conference on Disease Biology and Therapeutics, 2014" held at Institute of Advanced Study in Science and Technology, Guwahati, India.

Additional functions of the *cmd* gene have been discussed in the next Chapter.

Chapter 4

Identification of important amino acid residues of calmodulin and its role in sexual development

4.1 Introduction

In the previous Chapter, I described the role of the *cmd*, *trm-9* and *nca-2* genes in growth, pigmentation and stress-tolerance in *N. crassa.* I determined functions for both the *trm-9* and *nca-2* genes using their knockout mutants. However, the functions of the *cmd* gene was determined using the antagonists CPZ and TFP, since *cmd* is an essential gene for which no knockout is available. Therefore, to investigate the functions of the *cmd* at the molecular level, I had utilized two gene silencing mechanisms identified in *N. crassa* for silencing the *cmd* gene. In this Chapter, I describe the effect of the silencing of the *cmd* gene using RIP and meiotic silencing mechanism in *N. crassa*.

In *N. crassa*, three gene silencing mechanisms, namely, quelling, RIP and meiotic silencing have been discovered. These gene silencing mechanism are involved in regulation of the amplification of unwanted sequences such as transposons and viruses. Quelling, which is similar to co-suppression in plants and RNA interference in animals, is a posttranscriptional gene silencing in the vegetative phase in *N. crassa* (Cogoni *et al.* 1996; Cogoni and Macino 1999; Pickford *et al.* 2002; Catalanotto *et al.* 2004).

Another gene silencing process called RIP occurs before karyogamy and consists of a genome-wide scan for duplicated sequences. Unlike quelling, RIP is an irreversible a gene silencing mechanism that causes multiple G:C to A:T mutations and methylation of remaining cytosine residues within the duplicated DNA sequences, acting only during the sexual cycle (Cambareri *et al.* 1989). The RIP associated cytosine methylation can also spread into the adjacent flanking regions (Selker *et al.* 1993; Irelan and Selker 1997). As with mammals and plants, methylation has been shown to cause gene silencing in *N. crassa*. Thus, RIP is a process that mutates and frequently leads to epigenetic silencing of repetitive DNA (Galagan *et al.* 2003; Galagan and Selker 2004).

In contrast to quelling, which targets foreign sequences present in multiple genomic copies, the meiotic silencing pathway can recognize even a single copy sequence as foreign sequence. In this system, genes unpaired during the pairing stage in meiotic prophase I, as well as any homologous copies found in the zygote, are transiently silenced during the sexual phase via degradation of sequence-specific target mRNA (Shiu *et al.* 2001; Shiu and Metzenberg 2002).

Since *cmd* is an essential gene, so I used RIP mediated gene disruption mechanism to generate *cmd* mutants. In addition, to determine if *cmd* gene is necessary during the meiosis, I tested the effect of meiotic silencing of the *cmd* gene in sexual development of *N. crassa.*

4.2 Results

4.2.1 Construction of the P_{tcu-1}::*cmd*::5xGly::V5::*gfp* plasmid

To generate *cmd*^{RIP} mutants, I cloned the *cmd* gene under the P_{tcu-1} promoter, which is induced and repressed, respectively, by the addition of BCS that is a copper chelator, and by addition of $CuSO_4$ that results in excess Cu^{2+} (Figure 2.2; Korripally *et al.* 2010; Lamb *et al.* 2013). The oligonucleotide primer pairs CMD-A-FOR and CMD-A-REV-GFP (Figure 4.1; Table 4.1) were used to PCR amplify a fragment of 1016 bp of CaM ORF from the wild-type strain and cloned into the *Pac*I and *Sma*I restriction sites of pRS426PVG (P_{tcu-1}::*5xGly::V5::gfp*) vector (Figure 4.2; Ouyang *et al.* 2015) using the yeast strain FY834 and recombination cloning method as described previously (Colot *et al.* 2006; Tamuli *et al.* 2016). The recombinant plasmid DNA isolated from the transformed yeast was further used for transformation into *E. coli* DH5α ultra-competent cells and recombinant plasmids isolated form these cells were confirmed by sequencing (Genomics Core, University of California Riverside).

Table 4.1: Primers used for cloning of *cmd* gene

Sl. no.	Primer	Sequence (5'→ 3')
1.	[a]CMD-A-FOR	ttcgcacacacatccccaaccaaccATGGTATGCTCATTC CTTATCTCGG
2.	[b]CMD-A-REV-GFP	gttagggataggctttccgccGCCTCCGCCCTTCTGCAT CATGAGCTGGACGAAC
3.	CaM-RIP-FP-1	ACCTCCATATCTACCACTTC
4.	CaM-RIP-FP-2	TCATCCACCACCAAGTTAGC
5.	CaM-RIP-RP	GATCCCTTCACATCCGAATG
6.	P_{tcu}-CaM-RIP-FP-3	TTGAGAACGAATCCTTCATC
7.	GFP-RV	AACTTGTGGCCGTTTACGTC

[a,b]Sequences in lowercase in the primers CMD-A-FOR and CMD-A-REV-GFP are homologous to the sequences of P_{tcu-1} and the *5xGly::V5::gfp*, respectively, in the pRS426PVG/ptcu-1 vector (Ouyang *et al.* 2015).

(A)

GATGGGATAGAGAGAATGGCCGTTGGCCGTTGGATGTCGAGCGAGCCAGGCAAATTGAAGTCGGGGTTTATGTT
AGGTGCCCTGCCCTTGTTTTGCGTGTGGTAGTTGGTGGCTGGCTGTTGGTAAAGTTGTTATTGTTGTTTCGTTGCC
CGGTAATTCTATAACCTGTTGTCGAGATGATTCAAACTCATTGTCGAGGCGGAAAAGGGAATGGATATAACAAGT
GGAAGTTTCAATGTTCCACCCCGGAAAACAACCGGTCGACTCGATCAAAAAAGTCATAACAACCGGACCTCGCGT
CGCTTGCTGCCCCGGTAGCTCCAGTCCCTAGAGGTATCGATCTTGAACAAGCCCCGTGTTCTGGAATCTCCAAAAA
GAAAACGAAACGGATCCGATTGCGTGTTTGAGTTGGTTTCACATCGCCGGGGTTCGACCACGGCGGGCACGGTG
TGGAGCGCCGAGAAAGTTGAGCAAGTTTCCATTGCAACGGTGTTCGTTTCCCTGGTTGCTGACTCCTTGTCGCCAT
CGGATCCAGAACATCACTCATCTTCAACAATATAGTGTTCCGTGAGCCGGAAACCGCCTCTCATTGCCTGTTTGGT
GTTCAATCCCCCCCTCCCCTTCAGTTTTTTTTCCATTTTTTATACTCCATTGGTTCCCACCGGGTGAGCATGTTTTTGG
CTTGGCTGTATATCATGCCACTGCAGAATTTGCCTTCATTCCCGGCCTTCTCGGTCATGCCATCGAGAGAATTTGA
GTGTTTATTCTATCTCGGAAAGGGGGGCCAGAGAGAAACGATATGACGCTAGAGTCTGGACACAGCTGCAGTGG
TTGAGCATCTTTGAGCACGTTTTTTTGCAATCAACAGTGGAGTGACGGTGTAACGTAAGGTCGTGTTTCGGCCACT
TCGGCGTGGTGTGTGGACCCTACAAATGGGGAAGTACTCGCTTTTCATTGGATGATTGAAACAATTGACCCAGGT
ACTCGGGGCTTCAACCCCCCCCCTAAACATGATGGGATGGAGGCGAGACGAGCTCCCCGTTCGGCGCGGCGCGC
TCATATTCCAGGCGAACGACACTCGGCCGGGAAACCGTCATGATGTCCCCGATTTGATGACATTGGTGATATCCA
TAGCGGACGGAGAGCTACGTACCGACGATTGACCCCTGAATCATCTCCAGAGATTCGTCGTTGATGGCGAGGCT
GGACGGAACATCTCGTGAACAAGAAGGTTTTCATCCGAGATTCCAACTCATACCTGCTCATTCACTCAGTCACTAC
CCATTGACACTTTTCTCCCTCTTTCCCGCTCTTTTCCCCTCATCTCCTGCCTCTTTTGTACGCTATCTAGCCTCACGAA
TGGAACCATAACCGTCCTCTTGCATTACTTGACTCCAAGCTAGTAGCTGCTGGGTTAGGGAACCCAACAATTGGTC
CTTGTCCTACCCGTTGGACCAAGTAGTGTGACTGAGAAGGTTTTCAAATACCCAATTACATAGACTACGGACATCG

P_{tcu}-CaM-RIP- FP-3 →

AAAGGAGTCGTCGTCAAGAAACGAGCTCAAAGACGAGGCTAAA**TTGAGAACGAATCCTTCATC**TTTTCTCTCACA
AACCGCCATCACTATTCAAGCACCAAGCCGACTCCAGCTTCACCCCTTACCCTTTTTTTTTT

CMD-A-FOR →

TTCGCACACACATCCCCAACCAACCATGGTATGCTCATTCCTTATCTCGGTGCCTCCCGGTCGAATCTGTTTGAGC
GCAACAAGAACCCCGCGGGTTAGCTCGAGGGGCTGCGGCCGGGCTGCGAACATACGATGATGGCTGGAAAGGA
GACGGGTGACTGACAAGGCTATCAACAACAGGCGGACTCCCTTACTGAAGAGCAGGTCTCTGAGTTCAAGGAGG
CCTTCTCCCTTTTTGTAAGTTGTTTTTCTTGCGCCGAGCTTCCTTGTCGCCTATGCTCAATCCCCTGTGTCGCCGTTT
GGCGCAAATCGTGCGAGCCTGATGACTGACCCGACACAACGTGACACAGGACAAGGACGGTGATGGTTAGTCTT

CaM-RIP-FP-2 →

CCGAAACCCTACCCCCCCAGATATCCGAAT**TCATCCACCACCAAGTTAGC**GGCAAGCGCCTTGGATCATAGTAGTT
GCGACGCACCCAACGCTTCTCACCGCCCGCCCCTGAACCGAGTTGCGATGTGAATACGAGCCCTACCGTAATGCA
CGCATACTGAACAGCAGCTAGGCCAAATCACCACCAAGGAGCTCGGTACCGTCATGCGCTCGTTGGGCCAGAACC
CCTCCGAGTCTGAGCTTCAGGACATGATCAACGAGGTCGATGCCGACAACAACGGCACCATTGACTTCCCTGGTA
TGATATAAACATTTCGGACTATGGACCTGCCAGCTCGCCGCTGACAATAGCCTATAGAGTTCCTTACCATGATGGC
CAGAAAGATGAAGGATACCGACTCCGAGGAGGAGATCCGTGAGGCCTTCAAGGTGTTCGATCGCGACAACAACG
GCTTCATCTCCGCTGCCGAGCTCCGTCACGTCATGACCTCCATCGGCGAGAAGCTCACTGATGACGAGGTTGATG
AGATGATCCGTGAGGCCGACCAGGACGGCGATGGGCGTATCGACTGTACGTCTTCAATTCATGCGACTCAGCCTG
GGTATAGCTTACTAACACCTTGTTTCCAAACAGACAACGA

CMD-A-REV-GFP ←

GTTCGTCCAGCTCATGATGCAGAAGGGCGGAGGCGGCGGAAAGCCTATCCCTAACCCTCTCCTCGGTCTCGATT
CTACGATGGTGAGCAAGGGCGAGGAGCTGTTCACCGGGGTGGTGCCCATCCTGGTCGAGCTGGACGGC

GFP-RV ←

GACGTAAACGGCCACAAGTTCAGCGTGTCCGGCGAGGGCGAGGGCGATGCCACCTACGGCAAGCTGACCCTGA
AGTTCATCTGCACCACCGGCAAGCTGCCCGTGCCCTGGCCCACCCTCGTGACCACCTTCACCTACGGCGTGCAGTG
CTTCAGCCGCTACCCCGACCACATGAAGCAGCACGACTTCTTCAAGTCCGCCATGCCCGAAGGCTACGTCCAGGA
GCGCACCATCTTCTTCAAGGACGACGGCAACTACAAGACCCGCGCCGAGGTGAAGTTCGAGGGCGACACCCTGG
TGAACCGCATCGAGCTGAAGGGCATCGACTTCAAGGAGGACGGCAACATCCTGGGGCACAAGCTGGAGTACAAC
TACAACAGCCACAACGTCTATATCATGGCCGACAAGCAGAAGAACGGCATCAAGGTGAACTTCAAGATCCGCCAC
AACATCGAGGACGGCAGCGTGCAGCTCGCCGACCACTACCAGCAGAACACCCCCATCGGCGACGGCCCCGTGCT
GCTGCCCGACAACCACTACCTGAGCACCCAGTCCGCCCTGAGCAAAGACCCCAACGAGAAGCGCGATCACATGGT
CCTGCTGGAGTTCGTGACCGCCGCCGGGATCACTCTCGGCATGGACGAGCTGTACAAGTAA

(B)

NCU04120 start

GCCGGGATGGGCTCCAGGGCATCTTTAGTTTTAGTCTCATTTTAGCGAGTGTGTTACAGTTAGGTAGGGAGGGAC
CCCGCCCCGCCTCCCTCCACTCCATGCTTCGCAATCGGCGGCCCAGCTGCTCATTTAAGGAACGTCGAACTAGGAG
AACGGGGACTTGGACCTACCTGGTAGGTAGCCAACGGGTCTCGTTCGTTTCTACTGGGGG

CaM-RIP-FP-1

ACCTCCATATCTACCACTTCCAAACCAGAACACCTTCGAAATCCTCCTTCGAACACATCCAACTATCTCACACGCTC
GCTCTCCCCAGACCCTCTATCCACCCCTTAATACTATATCAAGATGGTATGCTCATTCCTTATCTCGGTGCCTCCCG
GTCGAATCTGTTTGAGCGCAACAAGAACCCCGCGGGTTAGCTCGAGGGGCTGCGGCCGGGCTGCGAACATACGA
TGATGGCTGGAAAGGAGACGGGTGACTGACAAGGCTATCAACAACAGGCGGACTCCCTTACTGAAGAGCAGGTC
TCTGAGTTCAAGGAGGCCTTCTCCCTTTTTGTAAGTTGTTTTTCTTGCGCCGAGCTTCCTTGTCGCCTATGCTCAATC
CCCTGTGTCGCCGTTTGGCGCAAATCGTGCGAGCCTGATGACTGACCCGACACAACGTGACACAGGACAAGGAC

CaM-RIP-FP-2

GGTGATGGTTAGTCTTCCGAAACCCTACCCCCCCAGATATCCGAATTCATCCACCACCAAGTTAGCGGCAAGCGC
CTTGGATCATAGTAGTTGCGACGCACCCAACGCTTCTCACCGCCCGCCCCTGAACCGAGTTGCGATGTGAATACG
AGCCCTACCGTAATGCACGCATACTGAACAGCAGCTAGGCCAAATCACCACCAAGGAGCTCGGTACCGTCATGCG
CTCGTTGGGCCAGAACCCCTCCGAGTCTGAGCTTCAGGACATGATCAACGAGGTCGATGCCGACAACAACGGCAC
CATTGACTTCCCTGGTATGATATAAACATTTCGGACTATGGACCTGCCAGCTCGCCGCTGACAATAGCCTATAGAG
TTCCTTACCATGATGGCCAGAAAGATGAAGGATACCGACTCCGAGGAGGAGATCCGTGAGGCCTTCAAGGTGTT
CGATCGCGACAACAACGGCTTCATCTCCGCTGCCGAGCTCCGTCACGTCATGACCTCCATCGGCGAGAAGCTCAC
TGATGACGAGGTTGATGAGATGATCCGTGAGGCCGACCAGGACGGCGATGGGCGTATCGACTGTACGTCTTCAA
TTCATGCGACTCAGCCTGGGTATAGCTTACTAACACCTTGTTTCCAAACAGACAACGAGTTCGTCCAGCTCATGAT
GCAGAAGTAAACGGCTTTCTCCTATATTCCAACTCTACACGAAGACAGGTTTTAGCGTTCTCTTTGAATACCACTAT

CaM-RIP- RP

TAGTTGATATGCCTCCATTCGGATGTGAAGGGATCGCTTTGTTTCCCACGCTTGGTATGTTATGCAAGGATCACCT
GTGTTCTCGTGGTTGCGCGTTATGCTGGACTGTTACCTCTCCTCCTGCCTCAAACCACCGAGTTCGGGAAGCAATG
GGGTGAAGTTGACATGGATTGACGCTAGCACCTCAAGTTTCTCTCCGTTTGACTTTGTGTCCGTGGCGGTTCGTCT
CCAAAGCAGTTATCAATCAAATCTTACTCCGCCTTTGCTAGTGAGGAGCCATTACCCACGGTGTTGTCTCCCAAGT
GGAAGCTGTACCACATGAGCAAAGGAGCACTTCCGTCCGGAGGTTCAGATGAAACCCTACTGTTTGCTACATAAA
CTTTTCAAATGCACAGCTGCTGAGTTCACGTCATCAGGGACCACCAGCAAGACCGGAGACCTGTCAACGAGTGGG
GATGACCTGCAGGATGATTGTGGCAGTGTTGCCTAGCGACATCAACCATCAAGCCCAGGCCGAATATGTGGATAT
CATCAGCCCTATAGGGATTTCCATATCGTACACATCCGTACGGCACAGCATCTAGAAAATCAACTCATCTCCCGAT
CACCGTTGATGTATGGAGGATCAGGTCATTGTCGGTCAGTGATGGCTGTAGGTTGCGCTGAGGCTGTTTGCTGCT
TGTGATGCCCTCGTCAATTTCATCAGTATTGTGACCATAGATGAACCGCATGTTCCCCAAAACTGAAGCTCGATGA
TACAGTATTCGCAC

NCU04120 end

Figure 4.1: Sequence of the *cmd* gene (NCU04120) and the primers used for generation and confirmation of the P_{tcu-1}::*cmd*::5xGly::V5::*gfp* construct. (A) Primers used for the ectopic construct of the *cmd* gene. The P_{tcu-1} (blue) followed by the sequence of the *cmd* gene (black) gene fused with 5X glycine (orange), V5 tag (pink) and *gfp* (green). (B) Primers used for the endogenous *cmd* gene. The sequence of the ~2187 bp fragment of the NCU04120 locus containing the *cmd* gene is shown. The start (ATG) and stop (TAG) codons are indicated and highlighted in green and red, respectively. The introns between the start and stop codons are highlighted in black. All primer sequences are highlighted and arrow head indicates the 5'→3' direction.

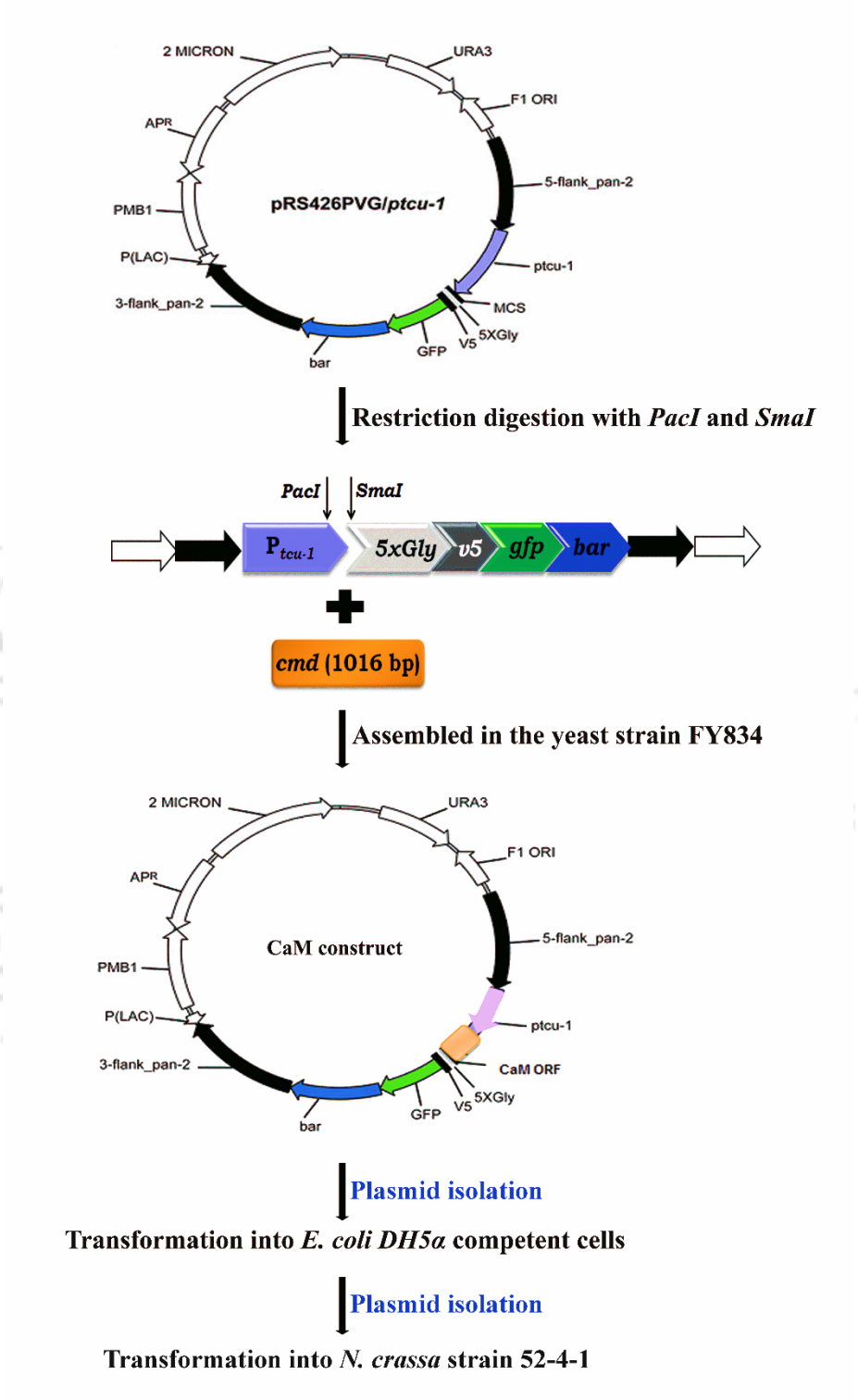

Figure 4.2: Schematics of generation and transformation of the P_{tcu-1}::*cmd*:: *5xGly*:: *V5*::*gfp* construct. The 1016 bp fragment of the *cmd* gene was cloned into the *Pac*I and *Sma*I sites of pRS426PVG plasmid vector (Ouyang *et al.* 2015) and transformed into the *N. crassa* strain 52-4-1 (Table 2.1).

4.2.2 Generation of the *cmd*^{RIP} mutant strains

The plasmid construct P_{tcu-1}*::cmd::5xGly::V5::gfp* was transformed into the *N. crassa* strain 51-IV-8a (Δ*rid-1::nat*; Δ*mus-51::hph; mat a*; Table 2.1) by electroporation (described in materials and methods) and the initial heterokaryotic transformants were selected on Vogel's sorbose agar medium (with VM containing 0.5% L-proline in lieu of NH_4NO_3) supplemented with basta (400 µg/ml) and pantothenate (0.01 mg/ml). Integration of the P_{tcu-1}*::cmd::5xGly::V5::gfp* construct at the *pan-2* locus in the LG VI of the transformed strains was PCR verified using primers P_{tcu}-CaM-RIP-FP-3 and GFP-RV (Table 4.1). PCRs were performed using custom oligonucleotide primers (IDT, USA), Phusion High-Fidelity PCR Kit (Thermo Scientific, USA) according to the manufacturer's protocol. The initial heterokaryotic transformants designated as 26-35-IV-8 of genotype [(Δ*rid-1::nat*; Δ*mus-51::hph mat a*) + (Δ*pan-2::bar::*P_{tcu-1}*::cmd::5xGly::V5::gfp; mat a*)], crossed with the wild-type; *mat A* strain. Crosses were harvested after about 20-25 days, ascospores were germinated by heat shock (described in materials and methods) and five homokaryotic strains of genotype Δ*rid-1::nat*; Δ*pan-2::bar::*P_{tcu-1}*::cmd::V5::gfp; mat a* (850, 851, 852, 853 and 854; Table 2.1) were isolated. The homokaryotic strains were isolated based on their resistance to basta (400 µg/ml) to verify the presence of the *bar* selectable marker, and also screened for nourseothricin (50 µg/ml) for the *nat* selectable marker on the Vogel's sorbose agar medium supplemented with pantothenate (0.01 mg/ml). These homokaryotic strains contained the *cmd* gene under the P_{tcu-1} in the *pan-2* locus, and its expression is regulated by the addition of BCS (induction) and $CuSO_4$ (repression). The 850 and 853 strains were crossed with the wild-type; *mat A* strain (Table 4.2) and isolated Δ*pan-2::bar::*P_{tcu-1}*::cmd::v5::gfp; mat A* (2, 4, 12, 13, 15, 16, 17, 24, 28, 30, 31, 34 and 41; Table 2.1) as well as Δ*pan-2::bar::*P_{tcu-1}*::cmd*^{RIP}*::V5::gfp; mat A* (RIP-26 and RIP-38; Table 2.1) progenies; and further used for generation of other *cmd*^{RIP} mutants and for meiotic silencing assay. Furthermore, I isolated the strains RIP-35 and RIP-50 (Table 2.1; Table 4.2) from the cross of the strains 24 with 850; strains RIP-3, RIP-6 and RIP-9 (Table 2.1; Table 4.2) from the cross of the strains RIP-26 with 850; and the strain RIP-55 from the cross of the strains RIP-38 with 853 (Table 2.1; Table 4.2) based on their initial slow growth phenotype (data not shown). Thus, I screened a total of 208 progenies from these crosses and isolated eight strains (Table 4.3) based on their initial slow growth phenotype (data not shown). All these eight strains contain the *cmd* gene in the endogenous locus

in the LG V and its tagged ectopy copy at the *pan-2* locus in the LG VI. A 1241 bp fragment of the *cmd* endogenous allele was PCR amplified using primer pairs CaM-RIP-FP-1 and CaM-RIP-RP and a 1272 bp fragment of the tagged *cmd* construct in *pan-2* locus was PCR amplified using primer pairs P_{tcu}-CaM-RIP-FP-3 and GFP-RV from the eight strains; PCR purified products were sequenced for confirmation of *cmd*^{RIP} mutant (SciGenom Labs, Cochin, India and Eurofins Genomics India Pvt. Ltd. Bangalore, India), using the same pairs of primers used for the PCR amplification and the common primer CaM-RIP-FP-2 for sequencing of middle region of both endogenous and the ectopic copies of the *cmd* gene (Figure 4.1; Figure 4.3; Table 4.1). The sequences of the eight *cmd*^{RIP} mutant alleles were aligned with the wild-type *cmd* gene sequence to identify the mutations and deposited in GenBank with accession numbers KX009461-71 (Table 4.3; Laxmi and Tamuli 2016). Analysis of the sequence revealed that the *cmd*^{RIP} mutants contained both conventional (G:C to A:T) as well as non-conventional RIP-induced mutations in the *cmd* allele (Figure 4.4; Figure 4.5; Table 4.3; Kim and Nelson 2005). However, only one mutant, the Δ*pan-2::bar::*P_{tcu-1}*::cmd*^{RIP}*::V5::gfp; mat A* (RIP-26) contained nonsynonymous substitutions in both the endogenous and ectopic *cmd* gene (Laxmi and Tamuli 2016). The Δ*pan-2::bar::*P_{tcu-1}*::cmd*^{RIP}*::V5::gfp; mat A* (RIP-26) mutant strain contained D57Y (GAT–TAT codon change) and Q148H (CAG–CAC codon change) mutations in the endogenous copy and M1W (ATG–TGG codon change) and E8K (GAG–AAG codon change) mutations in the ectopic copy of the *cmd* (Figure 4.6). Therefore, the Δ*pan-2::bar::*P_{tcu-1}*::cmd*^{RIP}*::V5::gfp; mat A* (RIP-26) mutant strain has been used for further studies. In addition, I found that the CaM::V5::GFP fusion protein was expressed in the *N. crassa* strains (Figure 4.7; Laxmi and Tamuli 2016).

Table 4.2: Crosses to generate the P_{tcu-1}*::cmd::V5::gfp; mat A* and *cmd*^{RIP} mutant strains

Sl. no.	Cross	Strains
1.	Δ*rid-1::nat*; Δ*pan-2::bar::*P_{tcu-1}*::cmd::V5::gfp; mat a* (850) X Wild-type; *mat A*	Δ*pan-2::bar::*P_{tcu-1}*::cmd::V5::gfp; mat A* (4)
		Δ*pan-2::bar::*P_{tcu-1}*::cmd::V5::gfp; mat A* (13)
		Δ*pan-2::bar::*P_{tcu-1}*::cmd::V5::gfp; mat A* (15)
		Δ*pan-2::bar::*P_{tcu-1}*::cmd::V5::gfp; mat A* (24)
		Δ*pan-2::bar::*P_{tcu-1}*::cmd*^{RIP}*::V5::gfp; mat A* (RIP-26)
		Δ*pan-2::bar::*P_{tcu-1}*::cmd::V5::gfp; mat A* (30)
		Δ*pan-2::bar::*P_{tcu-1}*::cmd::V5::gfp; mat A* (31)
		Δ*pan-2::bar::*P_{tcu-1}*::cmd::V5::gfp; mat A* (34)
2.	Δ*rid-1::nat*; Δ*pan-2::bar::*P_{tcu-1}*::cmd::V5::gfp; mat a* (853) X Wild-type; *mat A*	Δ*pan-2::bar::*P_{tcu-1}*::cmd::V5::gfp; mat A* (2)
		Δ*pan-2::bar::*P_{tcu-1}*::cmd::V5::gfp; mat A* (12)
		Δ*pan-2::bar::*P_{tcu-1}*::cmd::V5::gfp; mat A* (16)
		Δ*pan-2::bar::*P_{tcu-1}*::cmd::V5::gfp; mat A* (17)
		Δ*pan-2::bar::*P_{tcu-1}*::cmd::V5::gfp; mat A* (28)

		Δ*pan-2::bar::*P$_{tcu-1}$*::cmd*^{RIP}*::V5::gfp; mat A* (RIP-38)
		Δ*pan-2::bar::*P$_{tcu-1}$*::cmd::V5::gfp; mat A* (41)
3	Δ*rid-1::nat*; Δ*pan-2::bar::*P$_{tcu-1}$*::cmd::V5::gfp; mat a* (850) X Δ*pan-2::bar::*P$_{tcu-1}$*::cmd*^{RIP}*::V5::gfp; mat A* (26)	Δ*pan-2::bar::*P$_{tcu-1}$*::cmd*^{RIP}*::V5::gfp; mat A* (RIP-3)
		Δ*rid-1::nat*; Δ*pan-2::bar::*P$_{tcu-1}$*::cmd*^{RIP}*::V5::gfp; mat a* (RIP-6)
		Δ*pan-2::bar::*P$_{tcu-1}$*::cmd*^{RIP}*::V5::gfp; mat A* (RIP-9)
4.	Δ*rid-1::nat*; Δ*pan-2::bar::*P$_{tcu-1}$*::cmd::V5::gfp; mat a* (853) X Δ*pan-2::bar::*P$_{tcu-1}$*::cmd*^{RIP}*::V5::gfp; mat A* (38)	Δ*pan-2::bar::*P$_{tcu-1}$*::cmd*^{RIP}*::V5::gfp; mat A* (RIP-55)
5.	Δ*rid-1::nat*; Δ*pan-2::bar::*P$_{tcu-1}$*::cmd::V5::gfp; mat a* (850) X Δ*pan-2::bar::*P$_{tcu-1}$*::cmd*^{RIP}*::V5::gfp; mat A* (24)	Δ*rid-1::nat*; Δ*pan-2::bar::*P$_{tcu-1}$*::cmd*^{RIP}*::V5::gfp; mat a* (RIP-35)
		Δ*rid-1::nat*; Δ*pan-2::bar::*P$_{tcu-1}$*::cmd*^{RIP}*::V5::gfp; mat a* (RIP-50)

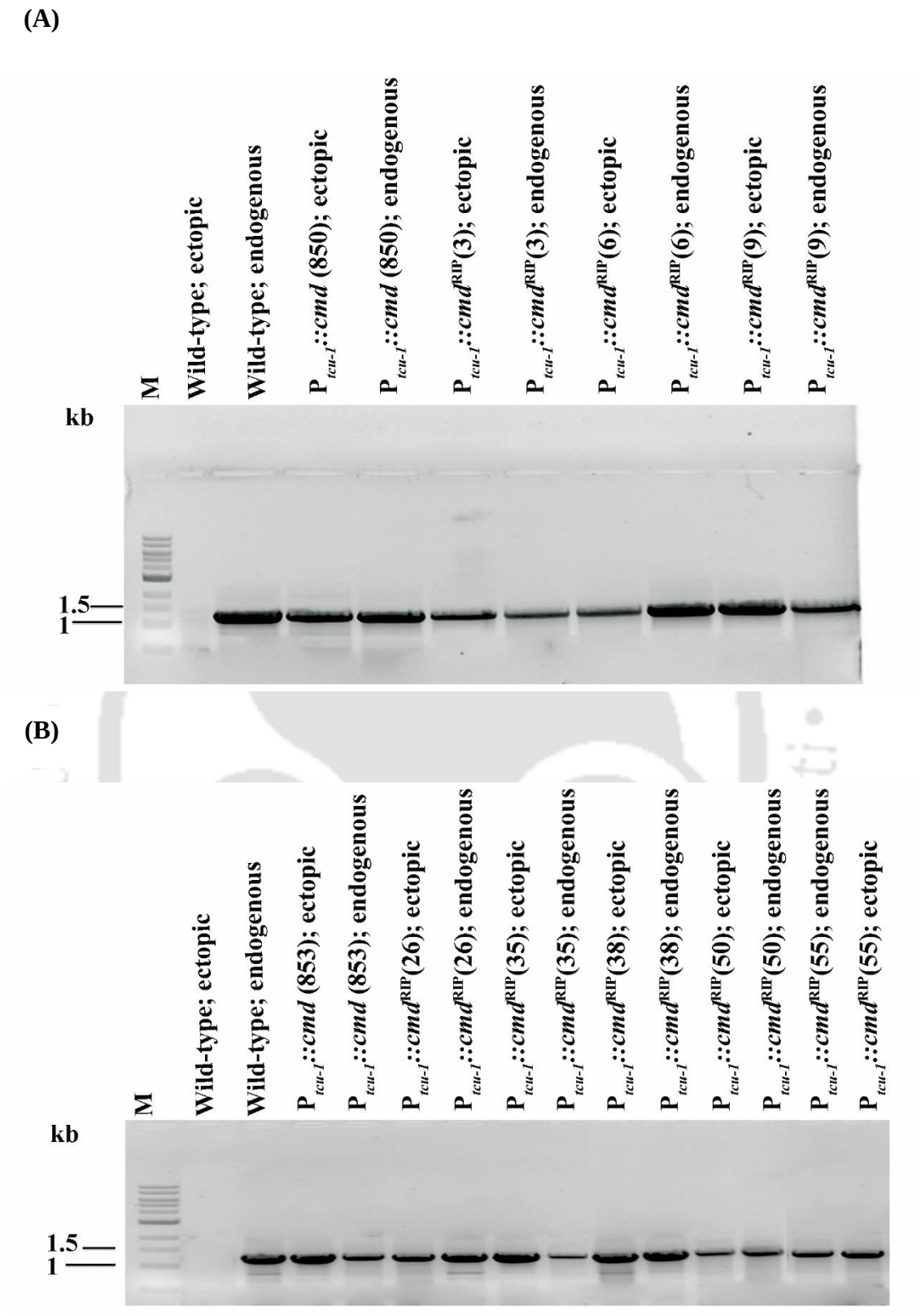

Figure 4.3: PCR amplification of the *cmd* gene from the *cmd*^{RIP} mutants. PCR amplification of both endogenous (1241 bp) and ectopic (1272 bp) copies of 8 RIP mutant alleles of *cmd* gene.

Table 4.3[a]: Sequence analysis of *cmd*^{RIP} mutant alleles

Sl. no.	*cmd*^{RIP} mutant strain	*cmd* allele	GenBank accession number (if any)	Total number of nucleotides mutated	Altered amino acids
1.	Δ*pan-2::bar::*P$_{tcu-1}$*::cmd*^{RIP}*::V5::gfp ; mat A* (RIP-3)	*cmd* (endogenous)	-	None	None
		P$_{tcu-1}$*:: cmd*^{RIP}*::V5:: gfp* (ectopic)	KX009461	100	M1W, A2G, S4P, E8K, Q9R, K14R, S18P, F20L, K22R, D25E, I28F, V36A, M37L, G41A, N43T, E46K, E48D, V56A, D59N, T63P, I64F
2.	Δ*rid-1::nat*; Δ*pan-2::bar::*P$_{tcu-1}$*::cmd*^{RIP}*::V5::gfp ; mat a* (RIP-6)	*cmd* (endogenous)	-	None	None
		P$_{tcu-1}$*:: cmd*^{RIP}*::V5:: gfp* (ectopic)	KX009462	83	M1W, A2G, S4P, E8K, S11P, E12K, K14R, S18P, F20L, M37L, N43T, E46K, E48D, L49F, D59N, N61T, I64F, P67L

3.	Δ*pan-2::bar::*P*tcu-1::cmd*RIP*::V5::gfp; mat A* (RIP-9)	*cmd*RIP (endogenous)	KX009469	1	None
		P*tcu-1*:: *cmd*RIP*::V5:: gfp* (ectopic)	KX009463	98	M1W, A2G, E8N, Q9R, E12D, K14R, S18P, D25E, K31R, V36A, S39P, E46K, E48K, E55K, V56A, D59N, N61T, T63P
4.	Δ*pan-2::bar::*P*tcu-1::cmd*RIP*::V5::gfp ; mat A* (RIP-26)	*cmd*RIP (endogenous)	KX009470	2	D57Y, Q148H
		P*tcu-1*:: *cmd*RIP*::V5:: gfp* (ectopic)	KX009464	11	M1W, E8K
5.	Δ*rid-1::nat*; Δ*pan-2::bar::*P*tcu-1::cmd*RIP*::V5::gfp ; mat a* (RIP-35)	*cmd* (endogenous)	-	None	None
		P*tcu-1*:: *cmd*RIP*::V5:: gfp* (ectopic)	KX009465	97	M1W, A2G, S4P, E8K, E12D, K14R, S18P, D25E, I28F, T29P, T30P, K31R, L33F, T35P, M37L, L40W, N43T, E46K, E48D, M52L, N54T, I64F, P67L
6.		*cmd* (endogenous)	-	None	None

	Δ*pan-2::bar::*P$_{tcu-1}$*::cmd*^{RIP}*::V5::gfp ; mat A* (RIP-38)	P$_{tcu-1}$*:: cmd*^{RIP}*::V5:: gfp* (ectopic)	KX009466	81	M1W, A2G, E8K, E12N, K14R, S18P, V36F, L40W, N43T, E48D, V56A,D59N, N61T, P67L, L70F
7.	Δ*rid-1::nat*; Δ*pan-2::bar::*P$_{tcu-1}$*:: cmd*^{RIP}*::V5::gfp; mat a* (RIP-50)	*cmd* (endogenous)	-	None	None
		P$_{tcu-1}$*:: cmd*^{RIP}*::V5:: gfp* (ectopic)	KX009467	121	M1W, A2G, D3N, E8K, E12N, K14R, S18P, K22R, D25E, I28F, T30P, E32D, L33F, M37W, R38P, N43T, E46K, E48N, L49F, D57N, D59N, N61T, T63P
8.	Δ*pan-2::bar::*P$_{tcu-1}$*::cmd*^{RIP}*::V5::gfp ; mat A* (RIP-55)	*cmd*^{RIP} (endogenous)	KX009471	1	None
		P$_{tcu-1}$*:: cmd*^{RIP}*::V5:: gfp* (ectopic)	KX009468	72	M1R, A2G, E8K, E12N, K14R, S18P, K31R, M37L, E46N, D57N, D59N

[a]Adapted from Laxmi and Tamuli 2016

```
                    *        20         *        40         *        60
cmd         : ATGGTATGCTCATTCCTTATCTCGGTGCCTCCCGGTCGAATCTGTTTGAGCGCAACAAGA :   60
RIP-3-ED    : ATGGTATGCTCATTCCTTATCTCGGTGCCTCCCGGTCGAATCTGTTTGAGCGCAACAAGA :   60
RIP-6-ED    : ATGGTATGCTCATTCCTTATCTCGGTGCCTCCCGGTCGAATCTGTTTGAGCGCAACAAGA :   60
RIP-9-ED    : ATGGTATGCTCATTCCTTATCTCGGTGCCTCCCGGTCGAATCTGTTTGAGCGCAACAAGA :   60
RIP-26-ED   : ATGGTATGCTCATTCCTTATCTCGGTGCCTCCCGGTCGAATCTGTTTGAGCGCAACAAGA :   60
RIP-35-ED   : ATGGTATGCTCATTCCTTATCTCGGTGCCTCCCGGTCGAATCTGTTTGAGCGCAACAAGA :   60
RIP-38-ED   : ATGGTATGCTCATTCCTTATCTCGGTGCCTCCCGGTCGAATCTGTTTGAGCGCAACAAGA :   60
RIP-50-ED   : ATGGTATGCTCATTCCTTATCTCGGTGCCTCCCGGTCGAATCTGTTTGAGCGCAACAAGA :   60
RIP-55-ED   : ATGGTATGCTCATTCCTTATCTCGGTGCCTCCCGGTCGAATCTGTTTGAGCGCAACAAGA :   60

                    *        80         *       100         *       120
cmd         : ACCCCGCGGGTTAGCTCGAGGGGCTGCGGCCGGGCTGCGAACATACGATGATGGCTGGAA :  120
RIP-3-ED    : ACCCCGCGGGTTAGCTCGAGGGGCTGCGGCCGGGCTGCGAACATACGATGATGGCTGGAA :  120
RIP-6-ED    : ACCCCGCGGGTTAGCTCGAGGGGCTGCGGCCGGGCTGCGAACATACGATGATGGCTGGAA :  120
RIP-9-ED    : ACCCCGCGGGTTAGCTCGAGGGGCTGCGGCCGGGCTGCGAACATACGATGATGGCTGGAA :  120
RIP-26-ED   : ACCCCGCGGGTTAGCTCGAGGGGCTGCGGCCGGGCTGCGAACATACGATGATGGCTGGAA :  120
RIP-35-ED   : ACCCCGCGGGTTAGCTCGAGGGGCTGCGGCCGGGCTGCGAACATACGATGATGGCTGGAA :  120
RIP-38-ED   : ACCCCGCGGGTTAGCTCGAGGGGCTGCGGCCGGGCTGCGAACATACGATGATGGCTGGAA :  120
RIP-50-ED   : ACCCCGCGGGTTAGCTCGAGGGGCTGCGGCCGGGCTGCGAACATACGATGATGGCTGGAA :  120
RIP-55-ED   : ACCCCGCGGGTTAGCTCGAGGGGCTGCGGCCGGGCTGCGAACATACGATGATGGCTGGAA :  120

                    *       140         *       160         *       180
cmd         : AGGAGACGGGTGACTGACAAGGCTATCAACAACAGGCGGACTCCCTTACTGAAGAGCAGG :  180
RIP-3-ED    : AGGAGACGGGTGACTGACAAGGCTATCAACAACAGGCGGACTCCCTTACTGAAGAGCAGG :  180
RIP-6-ED    : AGGAGACGGGTGACTGACAAGGCTATCAACAACAGGCGGACTCCCTTACTGAAGAGCAGG :  180
RIP-9-ED    : AGGAGACGGGTGACTGACAAGGCTATCAACAACAGGCGGACTCCCTTACTGAAGAGCAGG :  180
RIP-26-ED   : AGGAGACGGGTGACTGACAAGGCTATCAACAACAGGCGGACTCCCTTACTGAAGAGCAGG :  180
RIP-35-ED   : AGGAGACGGGTGACTGACAAGGCTATCAACAACAGGCGGACTCCCTTACTGAAGAGCAGG :  180
RIP-38-ED   : AGGAGACGGGTGACTGACAAGGCTATCAACAACAGGCGGACTCCCTTACTGAAGAGCAGG :  180
RIP-50-ED   : AGGAGACGGGTGACTGACAAGGCTATCAACAACAGGCGGACTCCCTTACTGAAGAGCAGG :  180
RIP-55-ED   : AGGAGACGGGTGACTGACAAGGCTATCAACAACAGGCGGACTCCCTTACTGAAGAGCAGG :  180

                    *       200         *       220         *       240
cmd         : TCTCTGAGTTCAAGGAGGCCTTCTCCCTTTTTGTAAGTTGTTTTTCTTGCGCCGAGCTTC :  240
RIP-3-ED    : TCTCTGAGTTCAAGGAGGCCTTCTCCCTTTTTGTAAGTTGTTTTTCTTGCGCCGAGCTTC :  240
RIP-6-ED    : TCTCTGAGTTCAAGGAGGCCTTCTCCCTTTTTGTAAGTTGTTTTTCTTGCGCCGAGCTTC :  240
RIP-9-ED    : TCTCTGAGTTCAAGGAGGCCTTCTCCCTTTTTGTAAGTTGTTTTTCTTGCGCCGAGCTTC :  240
RIP-26-ED   : TCTCTGAGTTCAAGGAGGCCTTCTCCCTTTTTGTAAGTTGTTTTTCTTGCGCCGAGCTTC :  240
RIP-35-ED   : TCTCTGAGTTCAAGGAGGCCTTCTCCCTTTTTGTAAGTTGTTTTTCTTGCGCCGAGCTTC :  240
RIP-38-ED   : TCTCTGAGTTCAAGGAGGCCTTCTCCCTTTTTGTAAGTTGTTTTTCTTGCGCCGAGCTTC :  240
RIP-50-ED   : TCTCTGAGTTCAAGGAGGCCTTCTCCCTTTTTGTAAGTTGTTTTTCTTGCGCCGAGCTTC :  240
RIP-55-ED   : TCTCTGAGTTCAAGGAGGCCTTCTCCCTTTTTGTAAGTTGTTTTTCTTGCGCCGAGCTTC :  240

                    *       260         *       280         *       300
cmd         : CTTGTCGCCTATGCTCAATCCCCTGTGTCGCCGTTTGGCGCAAATCGTGCGAGCCTGATG :  300
RIP-3-ED    : CTTGTCGCCTATGCTCAATCCCCTGTGTCGCCGTTTGGCGCAAATCGTGCGAGCCTGATG :  300
RIP-6-ED    : CTTGTCGCCTATGCTCAATCCCCTGTGTCGCCGTTTGGCGCAAATCGTGCGAGCCTGATG :  300
RIP-9-ED    : CTTGTCGCCTATGCTCAATCCCCTGTGTCGCCGTTTGGCGCAAATCGTGCGAGCGTGATG :  300
RIP-26-ED   : CTTGTCGCCTATGCTCAATCCCCTGTGTCGCCGTTTGGCGCAAATCGTGCGAGCCTGATG :  300
RIP-35-ED   : CTTGTCGCCTATGCTCAATCCCCTGTGTCGCCGTTTGGCGCAAATCGTGCGAGCCTGATG :  300
RIP-38-ED   : CTTGTCGCCTATGCTCAATCCCCTGTGTCGCCGTTTGGCGCAAATCGTGCGAGCCTGATG :  300
RIP-50-ED   : CTTGTCGCCTATGCTCAATCCCCTGTGTCGCCGTTTGGCGCAAATCGTGCGAGCCTGATG :  300
RIP-55-ED   : CTTGTCGCCTATGCTCAATCCCCTGTGTCGCCGTTTGGCGCAAATCGTGCGAGCATGATG :  300
```

```
                    *       320         *       340         *       360
cmd         : ACTGACCCGACACAACGTGACACAGGACAAGGACGGTGATGGTTAGTCTTCCGAAACCCT :  360
RIP-3-ED    : ACTGACCCGACACAACGTGACACAGGACAAGGACGGTGATGGTTAGTCTTCCGAAACCCT :  360
RIP-6-ED    : ACTGACCCGACACAACGTGACACAGGACAAGGACGGTGATGGTTAGTCTTCCGAAACCCT :  360
RIP-9-ED    : ACTGACCCGACACAACGTGACACAGGACAAGGACGGTGATGGTTAGTCTTCCGAAACCCT :  360
RIP-26-ED   : ACTGACCCGACACAACGTGACACAGGACAAGGACGGTGATGGTTAGTCTTCCGAAACCCT :  360
RIP-35-ED   : ACTGACCCGACACAACGTGACACAGGACAAGGACGGTGATGGTTAGTCTTCCGAAACCCT :  360
RIP-38-ED   : ACTGACCCGACACAACGTGACACAGGACAAGGACGGTGATGGTTAGTCTTCCGAAACCCT :  360
RIP-50-ED   : ACTGACCCGACACAACGTGACACAGGACAAGGACGGTGATGGTTAGTCTTCCGAAACCCT :  360
RIP-55-ED   : ACTGACCCGACACAACGTGACACAGGACAAGGACGGTGATGGTTAGTCTTCCGAAACCCT :  360

                    *       380         *       400         *       420
cmd         : ACCCCCCCCAGATATCCGAATTCATCCACCACCAAGTTAGCGGCAAGCGCCTTGGATCATA :  420
RIP-3-ED    : ACCCCCCCCAGATATCCGAATTCATCCACCACCAAGTTAGCGGCAAGCGCCTTGGATCATA :  420
RIP-6-ED    : ACCCCCCCCAGATATCCGAATTCATCCACCACCAAGTTAGCGGCAAGCGCCTTGGATCATA :  420
RIP-9-ED    : ACCCCCCCCAGATATCCGAATTCATCCACCACCAAGTTAGCGGCAAGCGCCTTGGATCATA :  420
RIP-26-ED   : ACCCCCCCCAGATATCCGAATTCATCCACCACCAAGTTAGCGGCAAGCGCCTTGGATCATA :  420
RIP-35-ED   : ACCCCCCCCAGATATCCGAATTCATCCACCACCAAGTTAGCGGCAAGCGCCTTGGATCATA :  420
RIP-38-ED   : ACCCCCCCCAGATATCCGAATTCATCCACCACCAAGTTAGCGGCAAGCGCCTTGGATCATA :  420
RIP-50-ED   : ACCCCCCCCAGATATCCGAATTCATCCACCACCAAGTTAGCGGCAAGCGCCTTGGATCATA :  420
RIP-55-ED   : ACCCCCCCCAGATATCCGAATTCATCCACCACCAAGTTAGCGGCAAGCGCCTTGGATCATA :  420

                    *       440         *       460         *       480
cmd         : GTAGTTGCGACGCACCCAACGCTTCTCACCGCCCGCCCCTGAACCGAGTTGCGATGTGAA :  480
RIP-3-ED    : GTAGTTGCGACGCACCCAACGCTTCTCACCGCCCGCCCCTGAACCGAGTTGCGATGTGAA :  480
RIP-6-ED    : GTAGTTGCGACGCACCCAACGCTTCTCACCGCCCGCCCCTGAACCGAGTTGCGATGTGAA :  480
RIP-9-ED    : GTAGTTGCGACGCACCCAACGCTTCTCACCGCCCGCCCCTGAACCGAGTTGCGATGTGAA :  480
RIP-26-ED   : GTAGTTGCGACGCACCCAACGCTTCTCACCGCCCGCCCCTGAACCGAGTTGCGATGTGAA :  480
RIP-35-ED   : GTAGTTGCGACGCACCCAACGCTTCTCACCGCCCGCCCCTGAACCGAGTTGCGATGTGAA :  480
RIP-38-ED   : GTAGTTGCGACGCACCCAACGCTTCTCACCGCCCGCCCCTGAACCGAGTTGCGATGTGAA :  480
RIP-50-ED   : GTAGTTGCGACGCACCCAACGCTTCTCACCGCCCGCCCCTGAACCGAGTTGCGATGTGAA :  480
RIP-55-ED   : GTAGTTGCGACGCACCCAACGCTTCTCACCGCCCGCCCCTGAACCGAGTTGCGATGTGAA :  480

                    *       500         *       520         *       540
cmd         : TACGAGCCCTACCGTAATGCACGCATACTGAACAGCAGCTAGGCCAAATCACCACCAAGG :  540
RIP-3-ED    : TACGAGCCCTACCGTAATGCACGCATACTGAACAGCAGCTAGGCCAAATCACCACCAAGG :  540
RIP-6-ED    : TACGAGCCCTACCGTAATGCACGCATACTGAACAGCAGCTAGGCCAAATCACCACCAAGG :  540
RIP-9-ED    : TACGAGCCCTACCGTAATGCACGCATACTGAACAGCAGCTAGGCCAAATCACCACCAAGG :  540
RIP-26-ED   : TACGAGCCCTACCGTAATGCACGCATACTGAACAGCAGCTAGGCCAAATCACCACCAAGG :  540
RIP-35-ED   : TACGAGCCCTACCGTAATGCACGCATACTGAACAGCAGCTAGGCCAAATCACCACCAAGG :  540
RIP-38-ED   : TACGAGCCCTACCGTAATGCACGCATACTGAACAGCAGCTAGGCCAAATCACCACCAAGG :  540
RIP-50-ED   : TACGAGCCCTACCGTAATGCACGCATACTGAACAGCAGCTAGGCCAAATCACCACCAAGG :  540
RIP-55-ED   : TACGAGCCCTACCGTAATGCACGCATACTGAACAGCAGCTAGGCCAAATCACCACCAAGG :  540

                    *       560         *       580         *       600
cmd         : AGCTCGGTACCGTCATGCGCTCGTTGGGCCAGAACCCCTCCGAGTCTGAGCTTCAGGACA :  600
RIP-3-ED    : AGCTCGGTACCGTCATGCGCTCGTTGGGCCAGAACCCCTCCGAGTCTGAGCTTCAGGACA :  600
RIP-6-ED    : AGCTCGGTACCGTCATGCGCTCGTTGGGCCAGAACCCCTCCGAGTCTGAGCTTCAGGACA :  600
RIP-9-ED    : AGCTCGGTACCGTCATGCGCTCGTTGGGCCAGAACCCCTCCGAGTCTGAGCTTCAGGACA :  600
RIP-26-ED   : AGCTCGGTACCGTCATGCGCTCGTTGGGCCAGAACCCCTCCGAGTCTGAGCTTCAGGACA :  600
RIP-35-ED   : AGCTCGGTACCGTCATGCGCTCGTTGGGCCAGAACCCCTCCGAGTCTGAGCTTCAGGACA :  600
RIP-38-ED   : AGCTCGGTACCGTCATGCGCTCGTTGGGCCAGAACCCCTCCGAGTCTGAGCTTCAGGACA :  600
RIP-50-ED   : AGCTCGGTACCGTCATGCGCTCGTTGGGCCAGAACCCCTCCGAGTCTGAGCTTCAGGACA :  600
RIP-55-ED   : AGCTCGGTACCGTCATGCGCTCGTTGGGCCAGAACCCCTCCGAGTCTGAGCTTCAGGACA :  600
```

```
                    *       620         *       640         *       660
cmd         : TGATCAACGAGGTCGATGCCGACAACAACGGCACCATTGACTTCCCTGGTATGATATAAA :  660
RIP-3-ED    : TGATCAACGAGGTCGATGCCGACAACAACGGCACCATTGACTTCCCTGGTATGATATAAA :  660
RIP-6-ED    : TGATCAACGAGGTCGATGCCGACAACAACGGCACCATTGACTTCCCTGGTATGATATAAA :  660
RIP-9-ED    : TGATCAACGAGGTCGATGCCGACAACAACGGCACCATTGACTTCCCTGGTATGATATAAA :  660
RIP-26-ED   : TGATCAACGAGGTCTATGCCGACAACAACGGCACCATTGACTTCCCTGGTATGATATAAA :  660
RIP-35-ED   : TGATCAACGAGGTCGATGCCGACAACAACGGCACCATTGACTTCCCTGGTATGATATAAA :  660
RIP-38-ED   : TGATCAACGAGGTCGATGCCGACAACAACGGCACCATTGACTTCCCTGGTATGATATAAA :  660
RIP-50-ED   : TGATCAACGAGGTCGATGCCGACAACAACGGCACCATTGACTTCCCTGGTATGATATAAA :  660
RIP-55-ED   : TGATCAACGAGGTCGATGCCGACAACAACGGCACCATTGACTTCCCTGGTATGATATAAA :  660

                    *       680         *       700         *       720
cmd         : CATTTCGGACTATGGACCTGCCAGCTCGCCGCTGACAATAGCCTATAGAGTTCCTTACCA :  720
RIP-3-ED    : CATTTCGGACTATGGACCTGCCAGCTCGCCGCTGACAATAGCCTATAGAGTTCCTTACCA :  720
RIP-6-ED    : CATTTCGGACTATGGACCTGCCAGCTCGCCGCTGACAATAGCCTATAGAGTTCCTTACCA :  720
RIP-9-ED    : CATTTCGGACTATGGACCTGCCAGCTCGCCGCTGACAATAGCCTATAGAGTTCCTTACCA :  720
RIP-26-ED   : CATTTCGGACTATGGACCTGCCAGCTCGCCGCTGACAATAGCCTATAGAGTTCCTTACCA :  720
RIP-35-ED   : CATTTCGGACTATGGACCTGCCAGCTCGCCGCTGACAATAGCCTATAGAGTTCCTTACCA :  720
RIP-38-ED   : CATTTCGGACTATGGACCTGCCAGCTCGCCGCTGACAATAGCCTATAGAGTTCCTTACCA :  720
RIP-50-ED   : CATTTCGGACTATGGACCTGCCAGCTCGCCGCTGACAATAGCCTATAGAGTTCCTTACCA :  720
RIP-55-ED   : CATTTCGGACTATGGACCTGCCAGCTCGCCGCTGACAATAGCCTATAGAGTTCCTTACCA :  720

                    *       740         *       760         *       780
cmd         : TGATGGCCAGAAAGATGAAGGATACCGACTCCGAGGAGGAGATCCGTGAGGCCTTCAAGG :  780
RIP-3-ED    : TGATGGCCAGAAAGATGAAGGATACCGACTCCGAGGAGGAGATCCGTGAGGCCTTCAAGG :  780
RIP-6-ED    : TGATGGCCAGAAAGATGAAGGATACCGACTCCGAGGAGGAGATCCGTGAGGCCTTCAAGG :  780
RIP-9-ED    : TGATGGCCAGAAAGATGAAGGATACCGACTCCGAGGAGGAGATCCGTGAGGCCTTCAAGG :  780
RIP-26-ED   : TGATGGCCAGAAAGATGAAGGATACCGACTCCGAGGAGGAGATCCGTGAGGCCTTCAAGG :  780
RIP-35-ED   : TGATGGCCAGAAAGATGAAGGATACCGACTCCGAGGAGGAGATCCGTGAGGCCTTCAAGG :  780
RIP-38-ED   : TGATGGCCAGAAAGATGAAGGATACCGACTCCGAGGAGGAGATCCGTGAGGCCTTCAAGG :  780
RIP-50-ED   : TGATGGCCAGAAAGATGAAGGATACCGACTCCGAGGAGGAGATCCGTGAGGCCTTCAAGG :  780
RIP-55-ED   : TGATGGCCAGAAAGATGAAGGATACCGACTCCGAGGAGGAGATCCGTGAGGCCTTCAAGG :  780

                    *       800         *       820         *       840
cmd         : TGTTCGATCGCGACAACAACGGCTTCATCTCCGCTGCCGAGCTCCGTCACGTCATGACCT :  840
RIP-3-ED    : TGTTCGATCGCGACAACAACGGCTTCATCTCCGCTGCCGAGCTCCGTCACGTCATGACCT :  840
RIP-6-ED    : TGTTCGATCGCGACAACAACGGCTTCATCTCCGCTGCCGAGCTCCGTCACGTCATGACCT :  840
RIP-9-ED    : TGTTCGATCGCGACAACAACGGCTTCATCTCCGCTGCCGAGCTCCGTCACGTCATGACCT :  840
RIP-26-ED   : TGTTCGATCGCGACAACAACGGCTTCATCTCCGCTGCCGAGCTCCGTCACGTCATGACCT :  840
RIP-35-ED   : TGTTCGATCGCGACAACAACGGCTTCATCTCCGCTGCCGAGCTCCGTCACGTCATGACCT :  840
RIP-38-ED   : TGTTCGATCGCGACAACAACGGCTTCATCTCCGCTGCCGAGCTCCGTCACGTCATGACCT :  840
RIP-50-ED   : TGTTCGATCGCGACAACAACGGCTTCATCTCCGCTGCCGAGCTCCGTCACGTCATGACCT :  840
RIP-55-ED   : TGTTCGATCGCGACAACAACGGCTTCATCTCCGCTGCCGAGCTCCGTCACGTCATGACCT :  840

                    *       860         *       880         *       900
cmd         : CCATCGGCGAGAAGCTCACTGATGACGAGGTTGATGAGATGATCCGTGAGGCCGACCAGG :  900
RIP-3-ED    : CCATCGGCGAGAAGCTCACTGATGACGAGGTTGATGAGATGATCCGTGAGGCCGACCAGG :  900
RIP-6-ED    : CCATCGGCGAGAAGCTCACTGATGACGAGGTTGATGAGATGATCCGTGAGGCCGACCAGG :  900
RIP-9-ED    : CCATCGGCGAGAAGCTCACTGATGACGAGGTTGATGAGATGATCCGTGAGGCCGACCAGG :  900
RIP-26-ED   : CCATCGGCGAGAAGCTCACTGATGACGAGGTTGATGAGATGATCCGTGAGGCCGACCAGG :  900
RIP-35-ED   : CCATCGGCGAGAAGCTCACTGATGACGAGGTTGATGAGATGATCCGTGAGGCCGACCAGG :  900
RIP-38-ED   : CCATCGGCGAGAAGCTCACTGATGACGAGGTTGATGAGATGATCCGTGAGGCCGACCAGG :  900
RIP-50-ED   : CCATCGGCGAGAAGCTCACTGATGACGAGGTTGATGAGATGATCCGTGAGGCCGACCAGG :  900
RIP-55-ED   : CCATCGGCGAGAAGCTCACTGATGACGAGGTTGATGAGATGATCCGTGAGGCCGACCAGG :  900
```

```
                    *       920         *       940         *       960
cmd         : ACGGCGATGGGCGTATCGACTGTACGTCTTCAATTCATGCGACTCAGCCTGGGTATAGCT :  960
RIP-3-ED    : ACGGCGATGGGCGTATCGACTGTACGTCTTCAATTCATGCGACTCAGCCTGGGTATAGCT :  960
RIP-6-ED    : ACGGCGATGGGCGTATCGACTGTACGTCTTCAATTCATGCGACTCAGCCTGGGTATAGCT :  960
RIP-9-ED    : ACGGCGATGGGCGTATCGACTGTACGTCTTCAATTCATGCGACTCAGCCTGGGTATAGCT :  960
RIP-26-ED   : ACGGCGATGGGCGTATCGACTGTACGTCTTCAATTCATGCGACTCAGCCTGGGTATAGCT :  960
RIP-35-ED   : ACGGCGATGGGCGTATCGACTGTACGTCTTCAATTCATGCGACTCAGCCTGGGTATAGCT :  960
RIP-38-ED   : ACGGCGATGGGCGTATCGACTGTACGTCTTCAATTCATGCGACTCAGCCTGGGTATAGCT :  960
RIP-50-ED   : ACGGCGATGGGCGTATCGACTGTACGTCTTCAATTCATGCGACTCAGCCTGGGTATAGCT :  960
RIP-55-ED   : ACGGCGATGGGCGTATCGACTGTACGTCTTCAATTCATGCGACTCAGCCTGGGTATAGCT :  960

                    *       980         *      1000         *
cmd         : TACTAACACCTTGTTTCCAAACAGACAACGAGTTCGTCCAGCTCATGATGCAGAAGTAA : 1019
RIP-3-ED    : TACTAACACCTTGTTTCCAAACAGACAACGAGTTCGTCCAGCTCATGATGCAGAAGTAA : 1019
RIP-6-ED    : TACTAACACCTTGTTTCCAAACAGACAACGAGTTCGTCCAGCTCATGATGCAGAAGTAA : 1019
RIP-9-ED    : TACTAACACCTTGTTTCCAAACAGACAACGAGTTCGTCCAGCTCATGATGCAGAAGTAA : 1019
RIP-26-ED   : TACTAACACCTTGTTTCCAAACAGACAACGAGTTCGTCCAGCTCATGATGCACAAGTAA : 1019
RIP-35-ED   : TACTAACACCTTGTTTCCAAACAGACAACGAGTTCGTCCAGCTCATGATGCAGAAGTAA : 1019
RIP-38-ED   : TACTAACACCTTGTTTCCAAACAGACAACGAGTTCGTCCAGCTCATGATGCAGAAGTAA : 1019
RIP-50-ED   : TACTAACACCTTGTTTCCAAACAGACAACGAGTTCGTCCAGCTCATGATGCAGAAGTAA : 1019
RIP-55-ED   : TACTAACACCTTGTTTCCAAACAGACAACGAGTTCGTCCAGCTCATGATGCAGAAGTAA : 1019
```

Figure 4.4: Nucleotide sequence analysis of the endogenous *cmd*^{RIP} mutant alleles. Mismatched nucleotide sequences were highlighted with red. The endogenous *cmd*^{RIP} alleles of RIP-9, RIP-26 and RIP-55 (Δ*pan-2::bar::*P$_{tcu-1}$*::cmd*^{RIP}*::V5::gfp; mat A*) of *cmd*^{RIP} mutants strains contain both conventional (G:C to A:T) as well as non-conventional mutations .

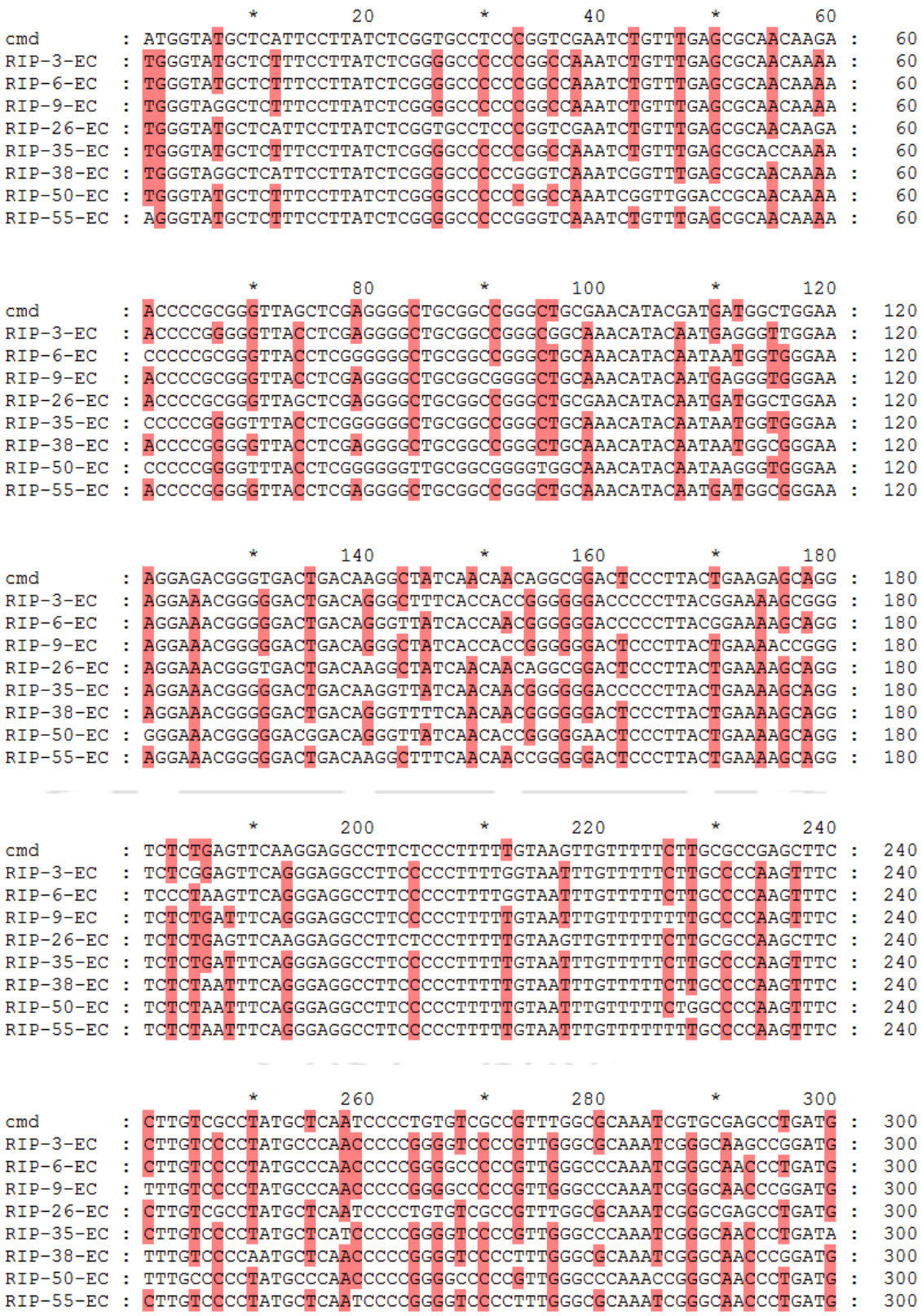

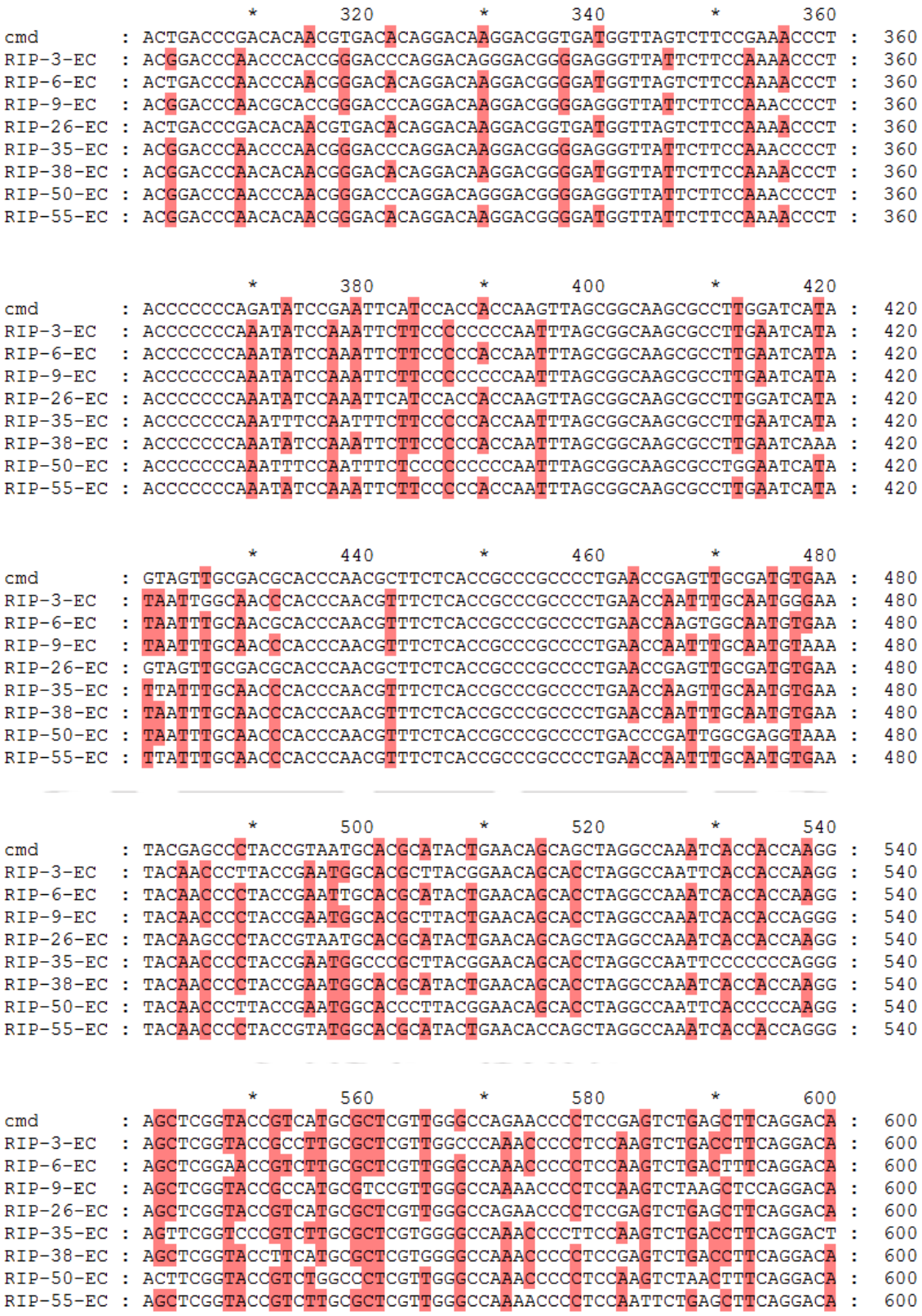

```
                    *       620         *       640         *       660
cmd         : TGATCAACGAGGTCGATGCCGACAACAACGGCACCATTGACTTCCCTGGTATGATATAAA :  660
RIP-3-EC    : TGATCAACGAGGCCGATGCCAACAACAACGGCCCCTTTGACTTCCCGGGTATGATATAAA :  660
RIP-6-EC    : TGATCAACGAGGTCGATGCCAACAACACCGGCACCTTTGACTTCCTTGGTAGGATATAAA :  660
RIP-9-EC    : TGATCAACAAGGCCGATGCCAACAACACCGGCCCCATTGACTTCCCGGGTATAATATAAA :  660
RIP-26-EC   : TGATCAACGAGGTCGATGCCGACAACAACGGCACCATTGACTTCCCTGGTATGATATAAA :  660
RIP-35-EC   : TGATCACCGAGGTCGATGCCGACAACAACGGCACCTTTGACTTCCTGGGTATGATATAAA :  660
RIP-38-EC   : TGATCAACGAGGCCGATGCCAACAACACCGGCACCATTGACTTCCTGGGTATGATATAAA :  660
RIP-50-EC   : TGATCAACGAGGTCAATGCCAACAACACCGGCCCCATTGACTTCCCTGGAAGAATATAAA :  660
RIP-55-EC   : TGATCAACGAGGTCAATGCCAACAACAACGGCACCATTGACTTCCCTGGTATGATATAAA :  660

                    *       680         *       700         *       720
cmd         : CATTTCGGACTATGGACCTGCCAGCTCGCCGCTGACAATAGCCTATAGAGTTCCTTACCA :  720
RIP-3-EC    : CTTTCCGGATAATGGACCTGCCAGCTCGCCGCTGACAATAGCCTATAGAGTTCCTTACCA :  720
RIP-6-EC    : CATTTCGGACTATGGACCTGCCAGCTCGCCGCTGACAATAGCCTATAGAGTTCCTTACCA :  720
RIP-9-EC    : CATTTCGAACTATGGACCTGCCAGCTCGCCGCTGACAATAGCCTATAGAGTTCCTTACCA :  720
RIP-26-EC   : CATTTCGGACTATGGACCTGCCAGCTCGCCGCTGACAATAGCCTATAGAGTTCCTTACCA :  720
RIP-35-EC   : CTTTTCGGACTATGGACCTGCCAGCTCGCCGCTGACAATAGCCTATAGAGTTCCTTACCA :  720
RIP-38-EC   : CTTTTCGGACTATGGACCTGCCAGCTCGCCGCTGACAATAGCCTATAGAGTTCTTTACCA :  720
RIP-50-EC   : CTTTTCGGACTATGGACCTGCCAGCTCGCCGCTGACAATAGCCTATAGAGTTCCTTACCA :  720
RIP-55-EC   : CATTTCGGACTATGGACCTGCCAGCTCGCCGCTGACAATAGCCTATAGAGTTCCTTACCA :  720

                    *       740         *       760         *       780
cmd         : TGATGGCCAGAAAGATGAAGGATACCGACTCCGAGGAGGAGATCCGTGAGGCCTTCAAGG :  780
RIP-3-EC    : TGATGGCCAGAAAGATGAAGGATACCGACTCCGAGGAGGAGATCCGTGAGGCCTTCAAGG :  780
RIP-6-EC    : TGATGGCCAGAAAGATGAAGGATACCGACTCCGAGGAGGAGATCCGTGAGGCCTTCAAGG :  780
RIP-9-EC    : TGATGGCCAGAAAGATGAAGGATACCGACTCCGAGGAGGAGATCCGTGAGGCCTTCAAGG :  780
RIP-26-EC   : TGATGGCCAGAAAGATGAAGGATACCGACTCCGAGGAGGAGATCCGTGAGGCCTTCAAGG :  780
RIP-35-EC   : TGATGGCCAGAAAGATGAAGGATACCGACTCCGAGGAGGAGATCCGTGAGGCCTTCAAGG :  780
RIP-38-EC   : TGATGGCCAGAAAGATGAAGGATACCGACTCCGAGGAGGAGATCCGTGAGGCCTTCAAGG :  780
RIP-50-EC   : TGATGGCCAGAAAGATGAAGGATACCGACTCCGAGGAGGAGATCCGTGAGGCCTTCAAGG :  780
RIP-55-EC   : TGATGGCCAGAAAGATGAAGGATACCGACTCCGAGGAGGAGATCCGTGAGGCCTTCAAGG :  780

                    *       800         *       820         *       840
cmd         : TGTTCGATCGCGACAACAACGGCTTCATCTCCGCTGCCGAGCTCCGTCACGTCATGACCT :  840
RIP-3-EC    : TGTTCGATCGCGACAACAACGGCTTCATCTCCGCTGCCGAGCTCCGTCACGTCATGACCT :  840
RIP-6-EC    : TGTTCGATCGCGACAACAACGGCTTCATCTCCGCTGCCGAGCTCCGTCACGTCATGACCT :  840
RIP-9-EC    : TGTTCGATCGCGACAACAACGGCTTCATCTCCGCTGCCGAGCTCCGTCACGTCATGACCT :  840
RIP-26-EC   : TGTTCGATCGCGACAACAACGGCTTCATCTCCGCTGCCGAGCTCCGTCACGTCATGACCT :  840
RIP-35-EC   : TGTTCGATCGCGACAACAACGGCTTCATCTCCGCTGCCGAGCTCCGTCACGTCATGACCT :  840
RIP-38-EC   : TGTTCGATCGCGACAACAACGGCTTCATCTCCGCTGCCGAGCTCCGTCACGTCATGACCT :  840
RIP-50-EC   : TGTTCGATCGCGACAACAACGGCTTCATCTCCGCTGCCGAGCTCCGTCACGTCATGACCT :  840
RIP-55-EC   : TGTTCGATCGCGACAACAACGGCTTCATCTCCGCTGCCGAGCTCCGTCACGTCATGACCT :  840

                    *       860         *       880         *       900
cmd         : CCATCGGCGAGAAGCTCACTGATGACGAGGTTGATGAGATGATCCGTGAGGCCGACCAGG :  900
RIP-3-EC    : CCATCGGCGAGAAGCTCACTGATGACGAGGTTGATGAGATGATCCGTGAGGCCGACCAGG :  900
RIP-6-EC    : CCATCGGCGAGAAGCTCACTGATGACGAGGTTGATGAGATGATCCGTGAGGCCGACCAGG :  900
RIP-9-EC    : CCATCGGCGAGAAGCTCACTGATGACGAGGTTGATGAGATGATCCGTGAGGCCGACCAGG :  900
RIP-26-EC   : CCATCGGCGAGAAGCTCACTGATGACGAGGTTGATGAGATGATCCGTGAGGCCGACCAGG :  900
RIP-35-EC   : CCATCGGCGAGAAGCTCACTGATGACGAGGTTGATGAGATGATCCGTGAGGCCGACCAGG :  900
RIP-38-EC   : CCATCGGCGAGAAGCTCACTGATGACGAGGTTGATGAGATGATCCGTGAGGCCGACCAGG :  900
RIP-50-EC   : CCATCGGCGAGAAGCTCACTGATGACGAGGTTGATGAGATGATCCGTGAGGCCGACCAGG :  900
RIP-55-EC   : CCATCGGCGAGAAGCTCACTGATGACGAGGTTGATGAGATGATCCGTGAGGCCGACCAGG :  900
```

```
                    *       920         *       940         *       960
cmd        : ACGGCGATGGGCGTATCGACTGTACGTCTTCAATTCATGCGACTCAGCCTGGGTATAGCT :  960
RIP-3-EC   : ACGGCGATGGGCGTATCGACTGTACGTCTTCAATTCATGCGACTCAGCCTGGGTATAGCT :  960
RIP-6-EC   : ACGGCGATGGGCGTATCGACTGTACGTCTTCAATTCATGCGACTCAGCCTGGGTATAGCT :  960
RIP-9-EC   : ACGGCGATGGGCGTATCGACTGTACGTCTTCAATTCATGCGACTCAGCCTGGGTATAGCT :  960
RIP-26-EC  : ACGGCGATGGGCGTATCGACTGTACGTCTTCAATTCATGCGACTCAGCCTGGGTATAGCT :  960
RIP-35-EC  : ACGGCGATGGGCGTATCGACTGTACGTCTTCAATTCATGCGACTCAGCCTGGGTATAGCT :  960
RIP-38-EC  : ACGGCGATGGGCGTATCGACTGTACGTCTTCAATTCATGCGACTCAGCCTGGGTATAGCT :  960
RIP-50-EC  : ACGGCGATGGGCGTATCGACTGTACGTCTTCAATTCATGCGACTCAGCCTGGGTATAGCT :  960
RIP-55-EC  : ACGGCGATGGGCGTATCGACTGTACGTCTTCAATTCATGCGACTCAGCCTGGGTATAGCT :  960

                    *       980         *      1000         *
cmd        : TACTAACACCTTGTTTCCAAACAGACAACGAGTTCGTCCAGCTCATGATGCAGAAGTAA : 1019
RIP-3-EC   : TACTAACACCTTGTTTCCAAACAGACAACGAGTTCGTCCAGCTCATGATGCAGAAGTAA : 1019
RIP-6-EC   : TACTAACACCTTGTTTCCAAACAGACAACGAGTTCGTCCAGCTCATGATGCAGAAGTAA : 1019
RIP-9-EC   : TACTAACACCTTGTTTCCAAACAGACAACGAGTTCGTCCAGCTCATGATGCAGAAGTAA : 1019
RIP-26-EC  : TACTAACACCTTGTTTCCAAACAGACAACGAGTTCGTCCAGCTCATGATGCAGAAGTAA : 1019
RIP-35-EC  : TACTAACACCTTGTTTCCAAACAGACAACGAGTTCGTCCAGCTCATGATGCAGAAGTAA : 1019
RIP-38-EC  : TACTAACACCTTGTTTCCAAACAGACAACGAGTTCGTCCAGCTCATGATGCAGAAGTAA : 1019
RIP-50-EC  : TACTAACACCTTGTTTCCAAACAGACAACGAGTTCGTCCAGCTCATGATGCAGAAGTAA : 1019
RIP-55-EC  : TACTAACACCTTGTTTCCAAACAGACAACGAGTTCGTCCAGCTCATGATGCAGAAGTAA : 1019
```

Figure 4.5: Nucleotide sequence analysis of the ectopic *cmd*^{RIP} mutant alleles. Mismatched nucleotide sequences were highlighted with red. The ectopic *cmd*^{RIP} alleles of RIP-3, RIP-9, RIP-26, RIP-38 and RIP-55 (Δ*pan-2::bar::*P$_{tcu-1}$*::cmd*^{RIP}*::V5::gfp; mat A*) and RIP-6, RIP-35 and RIP-50 (Δ*rid-1::nat*; Δ*pan-2::bar::*P$_{tcu-1}$*::cmd*^{RIP}*::V5::gfp; mat a*) of *cmd*^{RIP} mutants strains contain numerous conventional (G:C to A:T) as well as non-conventional mutations.

(A)

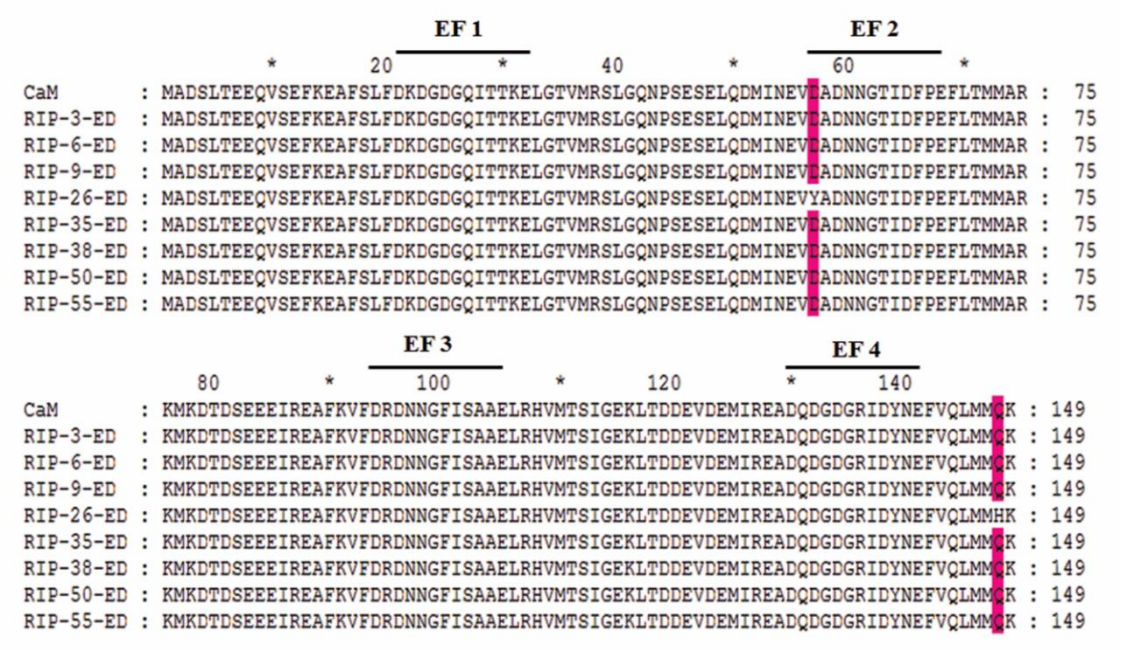

(B)

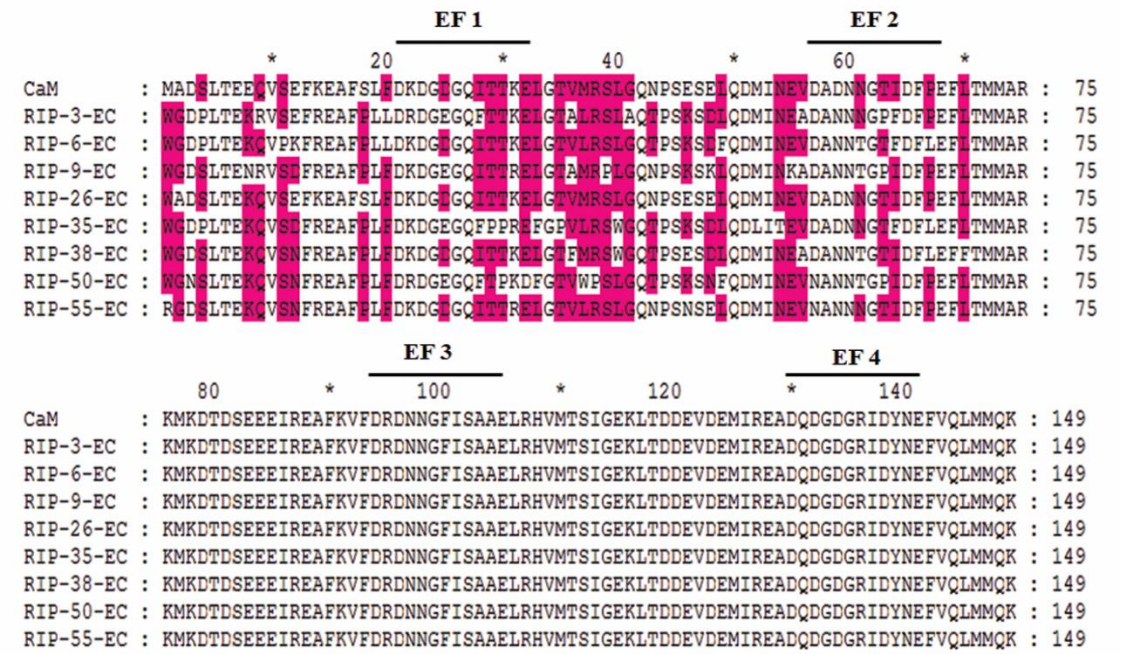

Figure 4.6: Alignment of the CaM protein sequence of the wild-type and *cmd*^{RIP} mutant alleles. Alignment of the amino acid sequences of the (A) endogenous *cmd*^{RIP} mutant alleles and (B) ectopic *cmd* ^{RIP} mutant alleles. Mismatched amino acid sequences were highlighted with pink. There are several mutations in the ectopic copy of the *cmd*^{RIP}

alleles, which encode truncated CaM protein. Only the *cmd*^{RIP} mutant strain Δ*pan-2::bar::*P$_{tcu-1}$*::cmd*^{RIP}*::V5::gfp; mat A* (RIP-26) contains two nonsynonymous mutations in endogenous allele. There are four EF-hand domain, indicated by solid line above the sequence, present in the CaM protein. In endogenous allele of *cmd*^{RIP} mutant strain, RIP-26, aspartic acid at position 57 is mutated to tyrosine (within EF-hand domain 2) and glutamine at position 148 is mutated to histidine whereas methionine at position 1 is mutated to tryptophan and glutamic acid at position 8 is mutated to lysine in the ectopic copy.

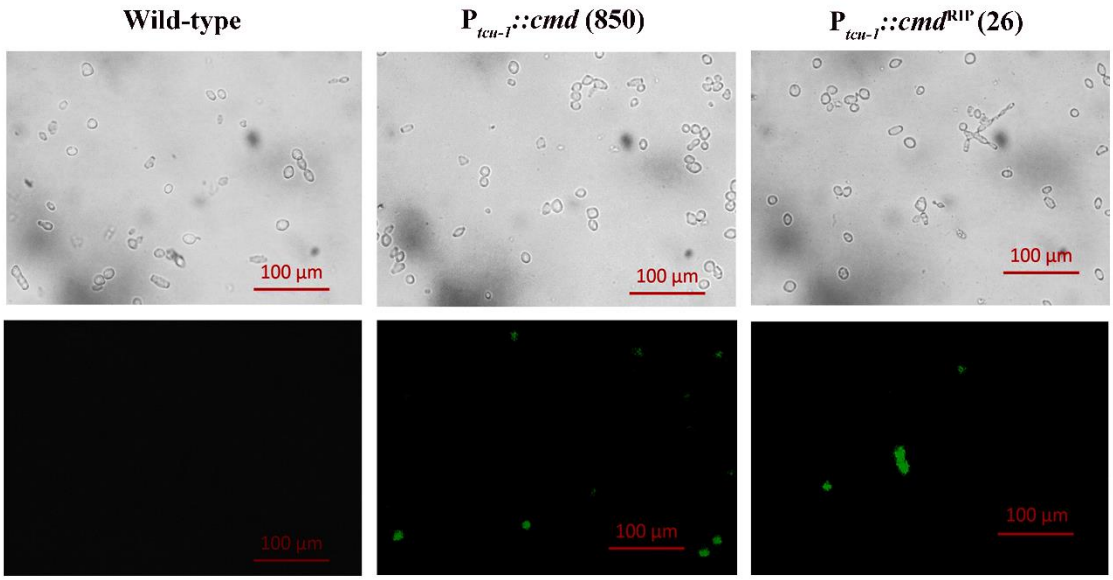

Figure 4.7: Expression of the CaM::V5::GFP protein under the P$_{tcu-1}$ in *N. crassa* strains. The wild-type, Δ*rid-1::nat*; Δ*pan-2::bar::*P$_{tcu-1}$*::cmd::V5::gfp; mat a* (850) and Δ*pan-2::bar::*P$_{tcu-1}$*::cmd*^{RIP}*::V5::gfp; mat A* (RIP-26) strains were grown in 13 x 100 mm glass tubes containing Vogel's glucose agar medium supplemented with pantothenate (0.01 mg/ml) and BCS (250 µM), and grown for 3 days at 30°C in the dark followed by 4 days under constant light at room temperature. Conidia were harvested by using sterile water and analyzed by using a Trinocular inverted microscope (AxioVertA1FL, Carl Zeiss, Göttingen, Germany) with a 450–490 nm excitation filter and 515 nm emission filter and photographed with a CCD camera (ProgRess C5, JENOPTIK AG, Jena, Germany). Scale bar 100 µm (Adapted from Laxmi and Tamuli 2016).

4.2.3 The *cmd*^{RIP} (26) mutant shows a defect in vegetative growth, aerial hyphae development and carotenoid accumulation

I studied the vegetative growth, aerial hyphae development and carotenoid accumulation of *cmd*^{RIP} (26) strain (as described in materials and methods). The Δ*pan-2::bar::*P$_{tcu-1}$*::cmd*^{RIP}*::V5::gfp; mat A* (RIP-26) mutant strains showed an abnormal colony morphology with matty-growth (Figure 4.8). Moreover, the Δ*pan-2::bar::*P$_{tcu-1}$*::cmd*^{RIP}*::V5::gfp; mat A* (RIP-26) mutant strain exhibited slow growth phenotype (Figure 4.9, Table 4.4) and produced very short aerial hyphae (Figure 4.10). In addition, carotenoid accumulation in this mutant was reduced by four fold as compared to wild-type and the parental strain Δ*rid-1::nat*; Δ*pan-2::bar::*P$_{tcu-1}$*::cmd::V5::gfp; mat a* (850), (Figure 4.11, Table 4.5). Furthermore, crosses involving the Δ*pan-2::bar::*P$_{tcu-1}$*::cmd*^{RIP}*::V5::gfp; mat A* (RIP-26) and the Δ*pan-2::bar::*P$_{tcu-1}$*::cmd*^{RIP}*::V5::gfp; mat a* (RIP-35) mutant showed a reduction in normal black ascospores and a significant increase in white ascospores (Figure 4.12).

(A)

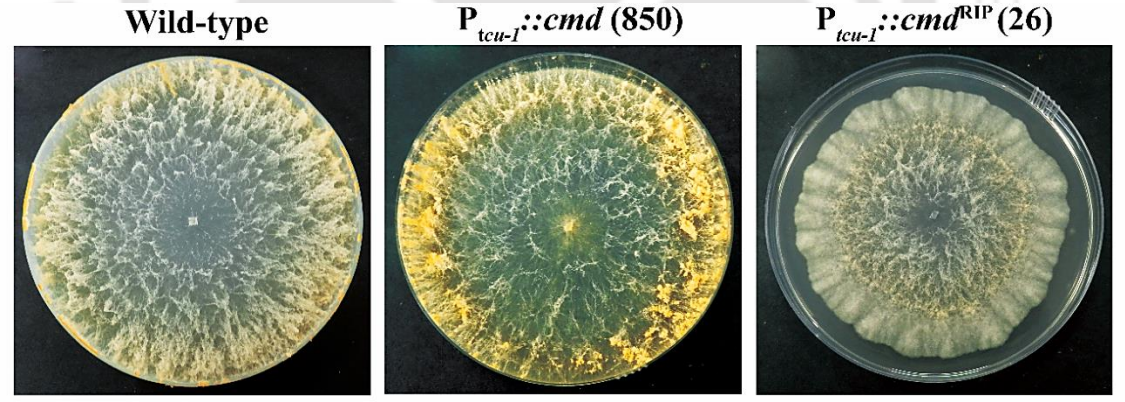

(B)

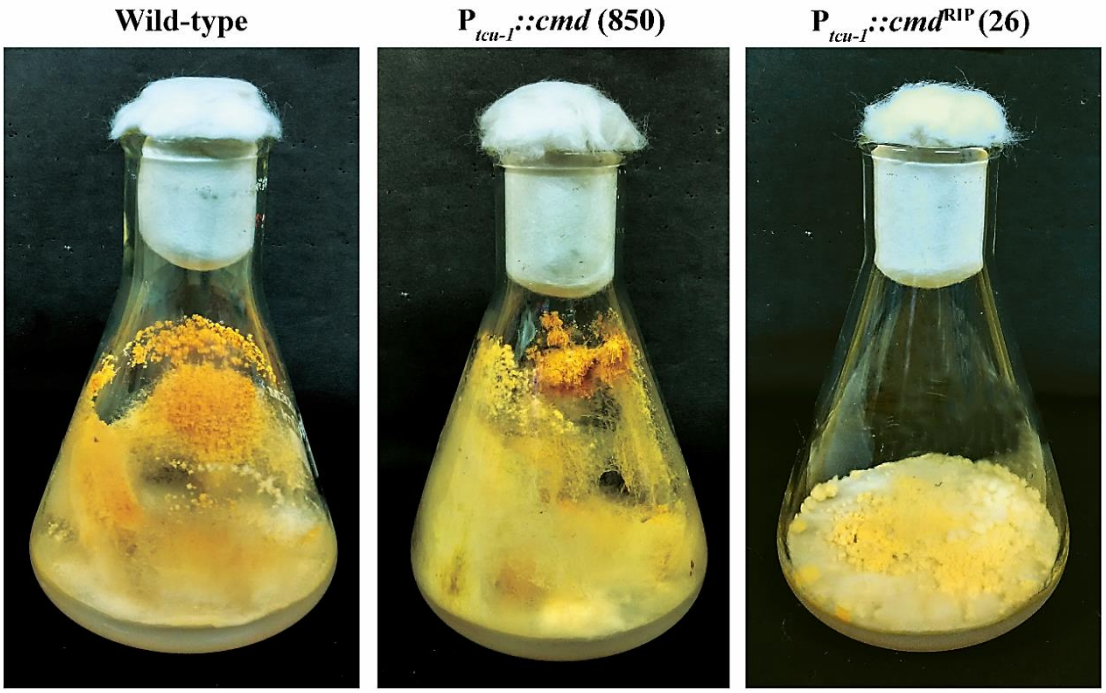

(C)

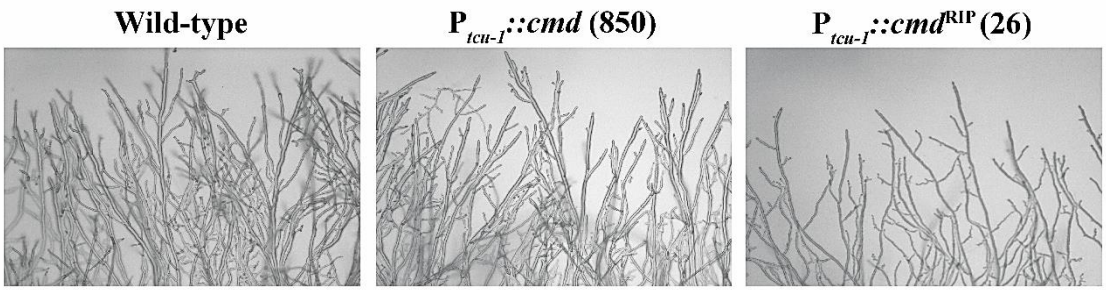

Figure 4.8: Morphology of the *cmd*^{RIP} (26) mutant. (A) Colony morphology. Wild - type, Δ*rid-1::nat*; Δ*pan-2::bar::*P$_{tcu-1}$*::cmd::V5::gfp; mat a* (850) and Δ*pan-2::bar::*P$_{tcu-1}$*::cmd*^{RIP}*::V5::gfp; mat A* (RIP-26) strains were cultured on Vogel's glucose agar plates supplemented with pantothenate (0.01 mg/ml) and BCS (250 µM). Strains were grown for two days at 30°C in dark and one day in constant light at room temperature and photographed. (B) Growth in flask. The wild-type, Δ*rid-1::nat*; Δ*pan-2::bar::*P$_{tcu-1}$*::cmd::V5::gfp; mat a* (850) and Δ*pan-2::bar::*P$_{tcu-1}$*::cmd*^{RIP}*::V5::gfp; mat A* (RIP-26) strains were grown on Vogel's glucose agar plates supplemented with pantothenate (0.01 mg/ml) and BCS (250 µM) for three days at 30°C in dark, followed by four days under

constant light at room temperature and photographed. (C) Hyphal morphology. Wild-type, Δ*rid-1::nat*; Δ*pan-2::bar::*P$_{tcu-1}$*::cmd::V5::gfp; mat a* (850) and Δ*pan-2::bar::*P$_{tcu-1}$*::cmd*^{RIP}*::V5::gfp; mat A* (RIP-26) strains were grown for 16 h on a thin layer of Vogel's glucose agar medium on glass slide, and observed under microscope at 20X magnification (Adapted from Laxmi and Tamuli 2016).

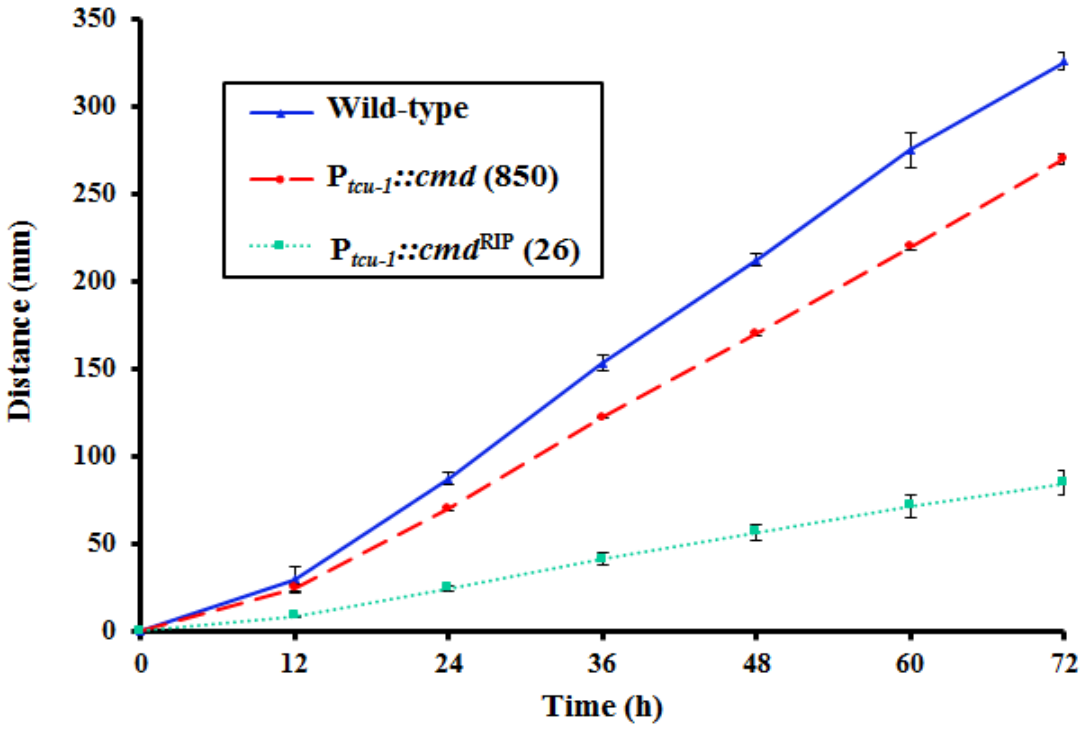

Figure 4.9: The *cmd*^{RIP} (26) mutant showed a slow growth rate. The *N. crassa* strains were grown in race tubes containing Vogel's glucose agar medium supplemented with pantothenate (0.01 mg/ml) and BCS (250 µM) and incubated at 30°C for 72 h. Each data point represents the mean of at least three independent experiments (Adapted from Laxmi and Tamuli 2016).

Table 4.4: Apical growth study of *cmd*^{RIP} (26) mutant strain

Sl. no.	Strain	Growth rate (cm h^{-1})
1.	Wild-type	0.37 ± 0.21
2.	P$_{tcu-1}$*::cmd* (850)	0.32 ± 0.02
3.	P$_{tcu-1}$*::cmd*^{RIP} (26)	0.10 ± 0.07

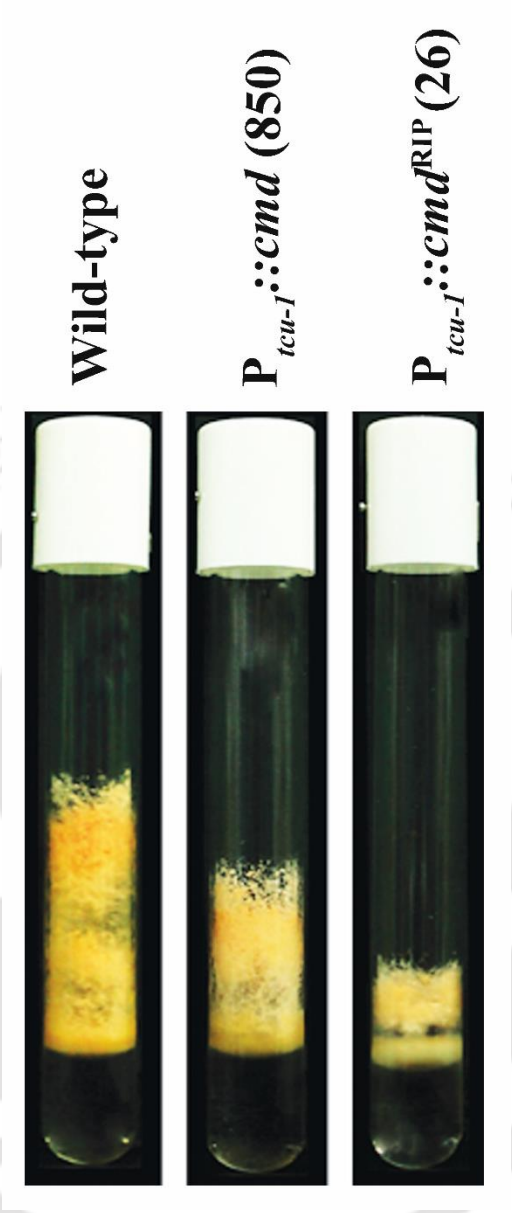

Figure 4.10: Aerial hyphae growth of *cmd*^{RIP} (26) mutant. Wild-type, Δ*rid-1::nat*; Δ*pan-2::bar::*P$_{tcu-1}$*::cmd::V5::gfp* (850) and Δ*pan-2::bar::*P$_{tcu-1}$*::cmd*^{RIP}*::V5::gfp; mat A* (RIP-26) strains were grown on VGM supplemented with pantothenate (0.01 mg/ml) and BCS (250 μM). Cultures were grown for three days at 30°C in dark and four days in constant light at room temperature and photographed (Adapted from Laxmi and Tamuli 2016).

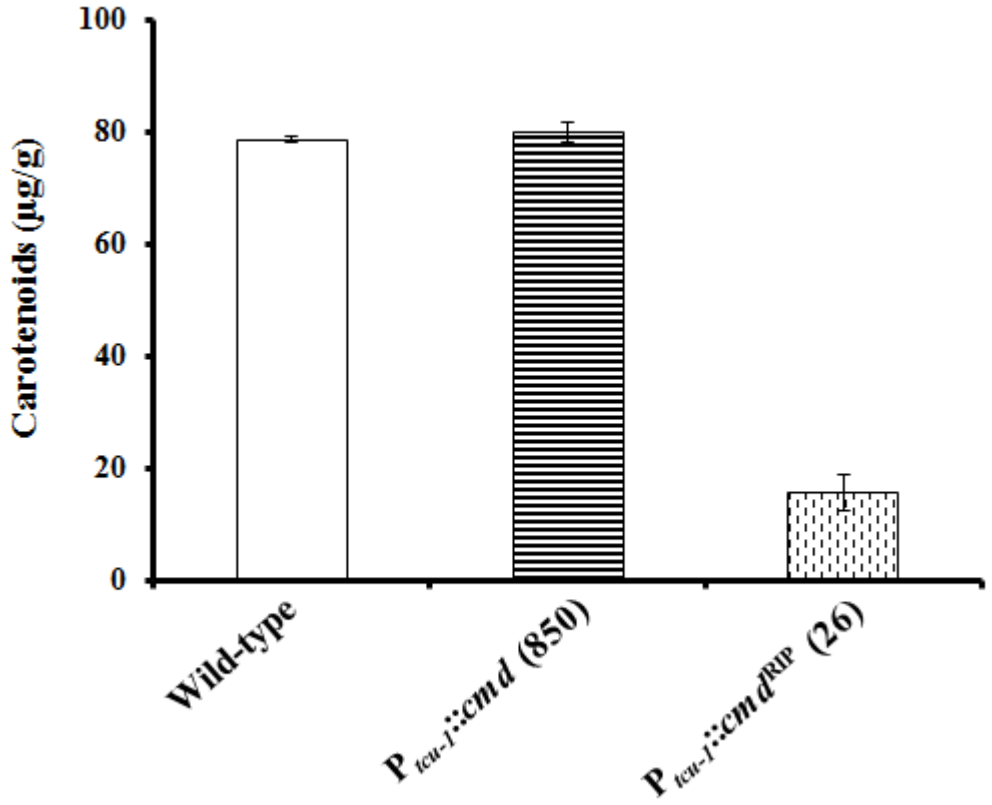

Figure 4.11: Carotenoids accumulation in the *cmd*^{RIP} (26) mutant. Carotenoid content of wild-type, Δ*rid-1::nat*; Δ*pan-2::bar::*P$_{tcu-1}$*::cmd::V5::gfp; mat a* (850) and Δ*pan-2::bar::*P$_{tcu-1}$*::cmd*^{RIP}*::V5::gfp; mat A* (RIP-26) strains. Carotenoids were extracted and estimated in µg carotenoids per g of dry weight. Error bars show the standard errors calculated from the data for three independent experiments (Adapted from Laxmi and Tamuli 2016).

Table 4.5: Carotenoids accumulation of *cmd*^{RIP} (26) muatnt strain at 30°C

Sl. no.	Strain	Carotenoid (µg/g dry mycelial powder)
1.	Wild-type	78.66 ± 0.471
2.	P$_{tcu-1}$*::cmd* (850)	80.00 ± 1.632
3.	P$_{tcu-1}$*::cmd*^{RIP} (26)	15.66 ± 3.299

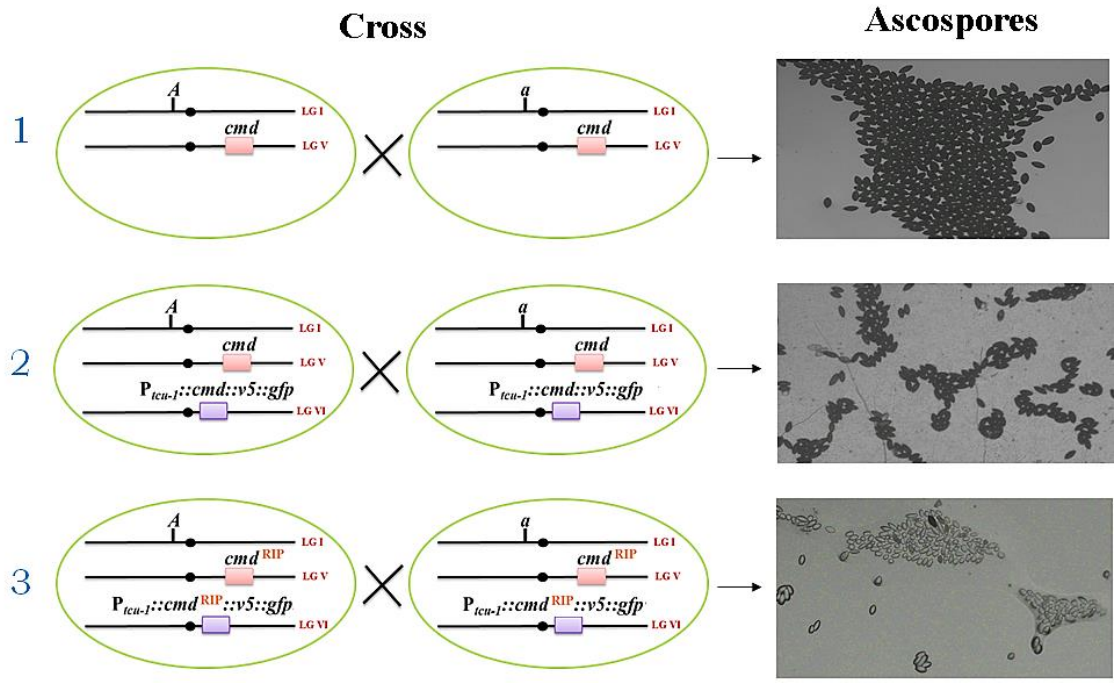

Figure 4.12: Fertility defect in cross homozygous of *cmd*^{RIP} mutant strains. Type 1 involves homozygous cross of wild-type *cmd* gene of opposite mating type. Type 2 is a homozygous cross of P_{tcu-1}*::cmd::V5::gfp* strains of opposite mating type. Type 3 involves cross of Δ*pan-2::bar::*P_{tcu-1}*::cmd*^{RIP}*::V5::gfp; mat A* (RIP-26) strain with Δ*pan-2::bar::*P_{tcu-1}*::cmd*^{RIP}*::V5::gfp; mat a* (RIP-35) of opposite mating type. For each type of cross, representative images for ejected ascospores on the lid of the petri dish examined under microscope are shown.

4.2.4 The *cmd*^{RIP} (26) mutant showed a severe defect in ultraviolet survival

Earlier it was reported that CaM and its binding proteins plays an important role in DNA repair and DNA synthesis in CHO and human cell lines (Charp 1987; Mirzayans *et al.* 1995). Therefore, I assayed UV-sensitivity of the Δ*pan-2::bar::*P_{tcu-1}*::cmd*^{RIP}*::V5::gfp; mat A* (RIP-26) mutant qualitatively and quantitatively to evaluate the role of CaM in UV survival (as described in materials and methods). The results of the spot test (Figure 4.13 A) and the UV dose-response curves (Figure 4.13 B) revealed severe sensitivity of the Δ*pan-2::bar::*P_{tcu-1}*::cmd*^{RIP}*::V5::gfp; mat A* (RIP-26) mutant to UV-irradiation. The UV sensitivity of the Δ*pan-2::bar::*P_{tcu-1}*::cmd*^{RIP}*::V5::gfp; mat A* (RIP-26) mutant was

like the *upr-1* mutant, suggesting that CaM has a major role in UV-induced DNA damage repair process similar to the translesion DNA polymerase REV-3 encoded by the *upr-1* gene (Sakai *et al.* 2002, 2003).

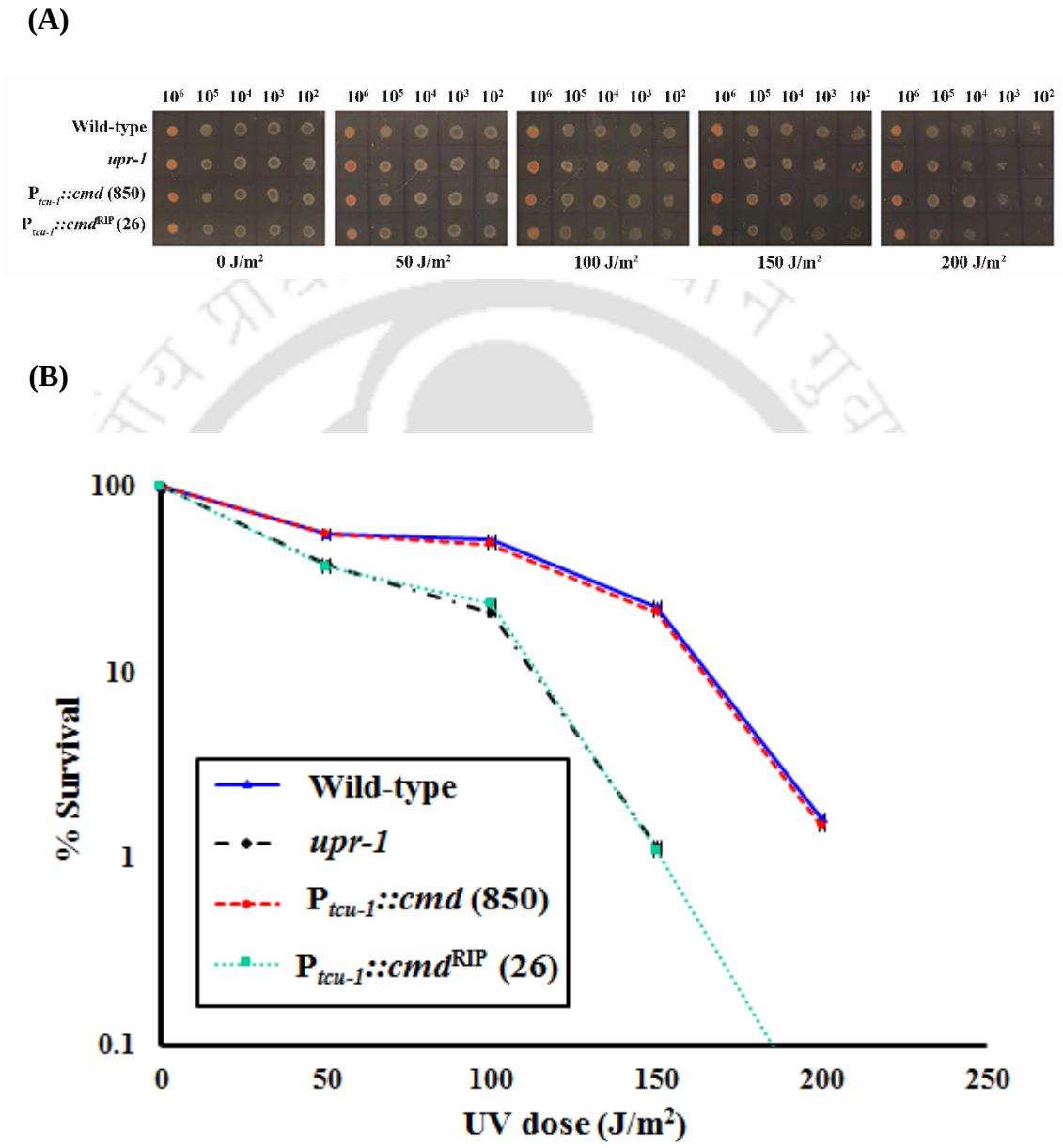

Figure 4.13: UV survival assay of the *cmd*^{RIP} (26) mutant. (A) Qualitative analysis of UV sensitivity. Approximately 10^5, 10^4, 10^3, 10^2 and 10^1 conidia were spotted from left to right on Vogel's sorbose agar medium plates and irradiated with the indicated UV doses. The *upr-1* strain was used as a reference strain to compare the relative UV sensitivity of the Δ*pan-2::bar::*P_{tcu-1}*::cmd*^{RIP}*::V5::gfp; mat A* (RIP-26) mutant. (B) Quantitative assay. Dose-response curves of the wild-type, Δ*rid-1::nat*; Δ*pan-*

2::bar::P_{tcu-1}*::cmd::V5::gfp; mat a* (850), Δ*pan-2::bar::*P_{tcu-1}*::cmd*^{RIP}*::V5::gfp; mat A* (RIP-26) and the *upr-1* strain on exposure to UV irradiations. Each data point represents the mean of at least three independent experiments (Adapted from Laxmi and Tamuli 2016).

4.2.5 CaM in *N. crassa* is required during meiosis for full fertility

Since *cmd* is an essential gene, I performed crosses involving strains engineered for inducing meiotic silencing of *cmd* to understand its role in sexual development (as described in materials and methods). The engineered Δ*pan-2::bar::*P_{tcu-1}*::cmd::V5::gfp* strains, possesses an endogeneous *cmd* gene in the LG V and an ectopic copy of the *cmd* gene (P_{tcu-1}*::cmd::V5::gfp*) tagged with V5 and GFP under the P_{tcu-1} in the *pan-2* locus in the LG VI (Figure 4.14). Silencing by an ectopic transgene is potentially a quick and easy tool for investigating the role of genes in meiosis and ascospores development, including genes for which a knockout construct would be lethal in vegetative phase of *N. crassa* (Shiu *et al.* 2001). The cross of the Δ*pan-2::bar::*P_{tcu-1}*::cmd::V5::gfp* strain with the wild-type was barren phenotype (Figure 4.14; Table 4.6) whereas cross homozygous for Δ*pan-2::bar::*P_{tcu-1}*::cmd::V5::gfp* showed fertile phenotype (Figure 4.14; Table 4.6). In addition, the cross of the Δ*pan-2::bar::*P_{tcu-1}*::cmd::V5::gfp* strain with the Δ*Sad-1* (suppressor of ascus dominance-1) mutant strain, the semi-dominant suppressor of meiotic silencing, was fully fertile (Figure 4.14; Table 4.6). The semidominant mutant, Δ*Sad-1* was shown to be deficient in meiotic silencing (Shiu *et al.* 2001). Moreover, microscopic analysis of perithecia from these crosses showed that they produced less number of asci as compared to the control crosses involving wild-type strain (Figure 4.14; Laxmi and Tamuli 2016). These results indicated meiotic silencing of *cmd* in the heterozygous crosses, when a copy of the *cmd* gene remains unpaired; and therefore, suggesting the requirement of CaM during meiosis for full fertility.

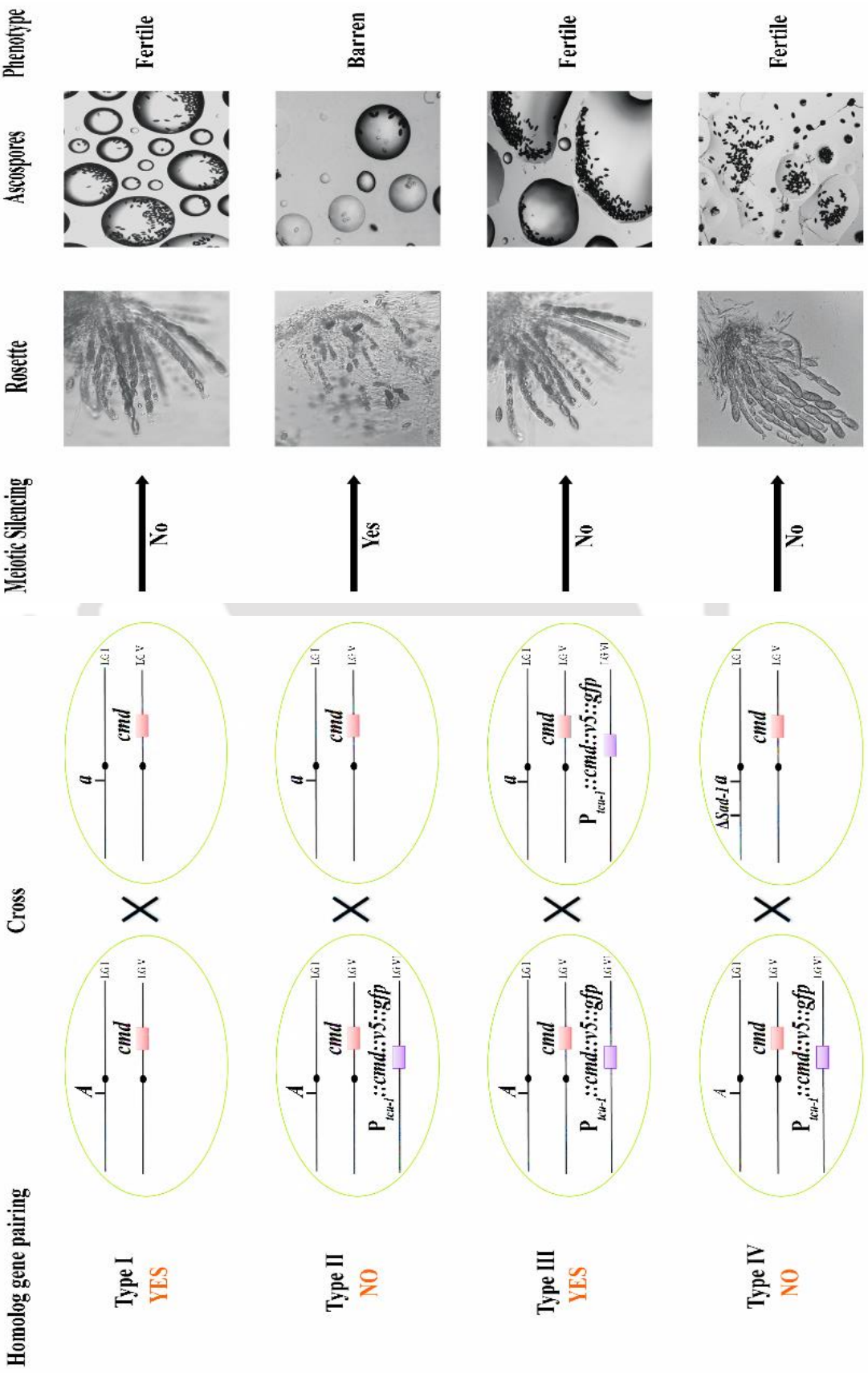

Figure 4.14: Meiotic silencing assay of the *cmd* gene. Type 1 involves homozygous cross of *cmd* strains, containing the wild-type *cmd* gene, of opposite mating type. Type 2 involves cross of $P_{tcu\text{-}1}$*::cmd::V5::gfp* strain with the wild-type of opposite mating type. Type 3 is a homozygous cross of $P_{tcu\text{-}1}$*::cmd::V5::gfp* strains of opposite mating type. Type 4 involves cross of $P_{tcu\text{-}1}$*::cmd::V5::gfp* strain with Δ*Sad-1* of opposite mating type. Phenotype of the Type 2 cross was barren due to meiotic silencing of *cmd* (the ectopic *cmd* copy, $P_{tcu\text{-}1}$*::cmd::V5::gfp*, was unpaired). However, meiotic silencing was not occurred in both Type 3 (all copies of the *cmd* were paired in the homozygous cross) and Type 4 (due to presence of the semi-dominant suppressor of meiotic silencing allele; Δ*Sad-1*) crosses; and therefore, these crosses were fully fertile. For each type of cross, representative images for a rosette of maturing asci and ejected ascospores on the lid of the petri dish examined under microscope are shown (Adapted from Laxmi and Tamuli 2016).

Table 4.6: Phenotypes of crosses involving strains inducing meiotic silencing of the *cmd* gene

Sl. no.	Cross	Meiotic Silencing (Yes/No)	Phenotype
1.	Wild-type; *mat A* X Wild-type; *mat a*	No	Fertile
2.	Δ*Sad-1::hph; mat A* X Δ*Sad-1::hph; mat a*	No	Sterile
3.	Δ*Sad-1::hph; mat A* X Wild-type; *mat a*	No	Fertile
4.	Δ*Sad-1::hph; mat a* X Wild-type; *mat A*	No	Fertile
5.	Δ*rid-1::nat*; Δ*pan-2::bar::*$P_{tcu\text{-}1}$*::cmd::V5::gfp; mat a* (850) X Wild-type; *mat A*	Yes	Barren
6.	Δ*rid-1::nat*; Δ*pan-2::bar::*$P_{tcu\text{-}1}$*::cmd::V5::gfp; mat a* (850) X Δ*Sad-1::hph; mat A*	No	Fertile

7.	Δ*pan-2::bar::*P$_{tcu-1}$*::cmd::v5::gfp; mat A* (4) X Wild-type; *mat a*	Yes	Barren
8.	Δ*pan-2::bar::*P$_{tcu-1}$*::cmd::v5::gfp; mat A* (4) X Δ*Sad-1::hph; mat a*	No	Fertile
9.	Δ*rid-1::nat*; Δ*pan-2::bar::*P$_{tcu-1}$*::cmd::V5::gfp; mat a* (850) X Δ*pan-2::bar::*P$_{tcu-1}$*::cmd::v5::gfp; mat A* (4)	No	Fertile
10.	Δ*pan-2::bar::*P$_{tcu-1}$*::cmd::v5::gfp; mat A* (13) X Wild-type; *mat a*	Yes	Barren
11.	Δ*pan-2::bar::*P$_{tcu-1}$*::cmd::v5::gfp; mat A* (13) X Δ*Sad-1::hph; mat a*	No	Fertile
12.	Δ*rid-1::nat*; Δ*pan-2::bar::*P$_{tcu-1}$*::cmd::V5::gfp; mat a* (850) X Δ*pan-2::bar::*P$_{tcu-1}$*::cmd::v5::gfp; mat A* (13)	No	Fertile
13.	Δ*pan-2::bar::*P$_{tcu-1}$*::cmd::v5::gfp; mat A* (15) X Wild-type; *mat a*	Yes	Barren
14.	Δ*pan-2::bar::*P$_{tcu-1}$*::cmd::v5::gfp; mat A* (15) X Δ*Sad-1::hph; mat a*	No	Fertile
15.	Δ*rid-1::nat*; Δ*pan-2::bar::*P$_{tcu-1}$*::cmd::V5::gfp; mat a* (850) X Δ*pan-2::bar::*P$_{tcu-1}$*::cmd::v5::gfp; mat A* (15)	No	Fertile
16.	Δ*pan-2::bar::*P$_{tcu-1}$*::cmd::v5::gfp; mat A* (24) X Wild-type; *mat a*	Yes	Barren
17.	Δ*pan-2::bar::*P$_{tcu-1}$*::cmd::v5::gfp; mat A* (24) X Δ*Sad-1::hph; mat a*	No	Fertile
18.	Δ*rid-1::nat*; Δ*pan-2::bar::*P$_{tcu-1}$*::cmd::V5::gfp; mat a* (850) X Δ*pan-2::bar::*P$_{tcu-1}$*::cmd::v5::gfp; mat A* (24)	No	Fertile
19.	Δ*pan-2::bar::*P$_{tcu-1}$*::cmd::v5::gfp; mat A* (30) X Wild-type; *mat a*	Yes	Barren
20.	Δ*pan-2::bar::*P$_{tcu-1}$*::cmd::v5::gfp; mat A* (30) X Δ*Sad-1::hph; mat a*	No	Fertile

21.	Δ*rid-1::nat*; Δ*pan-2::bar::*P$_{tcu-1}$*::cmd::V5::gfp; mat a* (850) X Δ*pan-2::bar::*P$_{tcu-1}$*::cmd::v5::gfp; mat A* (30)	No	Fertile
22.	Δ*pan-2::bar::*P$_{tcu-1}$*::cmd::v5::gfp; mat A* (31) X Wild-type; *mat a*	Yes	Barren
23.	Δ*pan-2::bar::*P$_{tcu-1}$*::cmd::v5::gfp; mat A* (31) X Δ*Sad-1::hph; mat a*	No	Fertile
24.	Δ*rid-1::nat*; Δ*pan-2::bar::*P$_{tcu-1}$*::cmd::V5::gfp; mat a* (850) X Δ*pan-2::bar::*P$_{tcu-1}$*::cmd::v5::gfp; mat A* (31)	No	Fertile
25.	Δ*rid-1::nat*; Δ*pan-2::bar::*P$_{tcu-1}$*::cmd::V5::gfp; mat a* (851) X Wild-type; *mat A*	Yes	Barren
26.	Δ*rid-1::nat*; Δ*pan-2::bar::*P$_{tcu-1}$*::cmd::V5::gfp; mat a* (851) X Δ*Sad-1::hph; mat A*	No	Fertile
27.	Δ*rid-1::nat*; Δ*pan-2::bar::*P$_{tcu-1}$*::cmd::V5::gfp; mat a* (851) X Δ*pan-2::bar::*P$_{tcu-1}$*::cmd::v5::gfp; mat A* (24)	No	Fertile
28.	Δ*rid-1::nat*; Δ*pan-2::bar::*P$_{tcu-1}$*::cmd::V5::gfp; mat a* (852) X Wild-type; *mat A*	Yes	Barren
29.	Δ*rid-1::nat*; Δ*pan-2::bar::*P$_{tcu-1}$*::cmd::V5::gfp; mat a* (852) X Δ*Sad-1::hph; mat A*	No	Fertile
30.	Δ*rid-1::nat*; Δ*pan-2::bar::*P$_{tcu-1}$*::cmd::V5::gfp; mat a* (852) X Δ*pan-2::bar::*P$_{tcu-1}$*::cmd::v5::gfp; mat A* (24)	No	Fertile
31.	Δ*rid-1::nat*; Δ*pan-2::bar::*P$_{tcu-1}$*::cmd::V5::gfp; mat a* (853) X Wild-type; *mat A*	Yes	Barren
32.	Δ*rid-1::nat*; Δ*pan-2::bar::*P$_{tcu-1}$*::cmd::V5::gfp; mat a* (853) X Δ*Sad-1::hph; mat A*	No	Fertile
33.	Δ*rid-1::nat*; Δ*pan-2::bar::*P$_{tcu-1}$*::cmd::V5::gfp; mat a* (853) X Δ*pan-2::bar::*P$_{tcu-1}$*::cmd::v5::gfp; mat A* (24)	No	Fertile

34.	Δ*pan-2::bar::*P$_{tcu-1}$*::cmd::v5::gfp; mat A* (2) X Wild-type; *mat a*	Yes	Barren
35.	Δ*pan-2::bar::*P$_{tcu-1}$*::cmd::v5::gfp; mat A* (2) X Δ*Sad-1::hph; mat a*	No	Fertile
36.	Δ*rid-1::nat*; Δ*pan-2::bar::*P$_{tcu-1}$*::cmd::V5::gfp; mat a* (853) X Δ*pan-2::bar::*P$_{tcu-1}$*::cmd::v5::gfp; mat A* (2)	No	Fertile
37.	Δ*pan-2::bar::*P$_{tcu-1}$*::cmd::v5::gfp; mat A* (12) X Wild-type; *mat a*	Yes	Barren
38.	Δ*pan-2::bar::*P$_{tcu-1}$*::cmd::v5::gfp; mat A* (12) X Δ*Sad-1::hph; mat a*	No	Fertile
39.	Δ*rid-1::nat*; Δ*pan-2::bar::*P$_{tcu-1}$*::cmd::V5::gfp; mat a* (853) X Δ*pan-2::bar::*P$_{tcu-1}$*::cmd::v5::gfp; mat A* (12)	No	Fertile
40.	Δ*pan-2::bar::*P$_{tcu-1}$*::cmd::v5::gfp; mat A* (16) X Wild-type; *mat a*	Yes	Barren
41.	Δ*pan-2::bar::*P$_{tcu-1}$*::cmd::v5::gfp; mat A* (16) X Δ*Sad-1::hph; mat a*	No	Fertile
42.	Δ*rid-1::nat*; Δ*pan-2::bar::*P$_{tcu-1}$*::cmd::V5::gfp; mat a* (853) X Δ*pan-2::bar::*P$_{tcu-1}$*::cmd::v5::gfp; mat A* (16)	No	Fertile
43.	Δ*pan-2::bar::*P$_{tcu-1}$*::cmd::v5::gfp; mat A* (17) X Wild-type; *mat a*	Yes	Barren
44.	Δ*pan-2::bar::*P$_{tcu-1}$*::cmd::v5::gfp; mat A* (17) X Δ*Sad-1::hph; mat a*	No	Fertile
45.	Δ*rid-1::nat*; Δ*pan-2::bar::*P$_{tcu-1}$*::cmd::V5::gfp; mat a* (853) X Δ*pan-2::bar::*P$_{tcu-1}$*::cmd::v5::gfp; mat A* (17)	No	Fertile
46.	Δ*pan-2::bar::*P$_{tcu-1}$*::cmd::v5::gfp; mat A* (28) X Wild-type; *mat a*	Yes	Barren
47.	Δ*pan-2::bar::*P$_{tcu-1}$*::cmd::v5::gfp; mat A* (28) X Δ*Sad-1::hph; mat a*	No	Fertile

48.	Δ*rid-1::nat*; Δ*pan-2::bar::*P$_{tcu-1}$*::cmd::V5::gfp; mat a* (853) X Δ*pan-2::bar::*P$_{tcu-1}$*::cmd::v5::gfp; mat A* (28)	No	Fertile
49.	Δ*pan-2::bar::*P$_{tcu-1}$*::cmd::v5::gfp; mat A* (41) X Wild-type; *mat a*	Yes	Barren
50.	Δ*pan-2::bar::*P$_{tcu-1}$*::cmd::v5::gfp; mat A* (41) X Δ*Sad-1::hph; mat a*	No	Fertile
51.	Δ*rid-1::nat*; Δ*pan-2::bar::*P$_{tcu-1}$*::cmd::V5::gfp; mat a* (853) X Δ*pan-2::bar::*P$_{tcu-1}$*::cmd::v5::gfp; mat A* (41)	No	Fertile
52.	Δ*rid-1::nat*; Δ*pan-2::bar::*P$_{tcu-1}$*::cmd::V5::gfp; mat a* (854) X Wild-type; *mat A*	Yes	Barren
53.	Δ*rid-1::nat*; Δ*pan-2::bar::*P$_{tcu-1}$*::cmd::V5::gfp; mat a* (854) X Δ*Sad-1::hph; mat A*	No	Fertile
54.	Δ*rid-1::nat*; Δ*pan-2::bar::*P$_{tcu-1}$*::cmd::V5::gfp; mat a* (854) X Δ*pan-2::bar::*P$_{tcu-1}$*::cmd::v5::gfp; mat A* (24)	No	Fertile

4.3 Discussion

I generated *N. crassa cmd*^{RIP} mutant strains to disrupt the *cmd* gene and identification of its critical amino acid residues using RIP mechanism. *N. crassa* is one of only four fungal species in which RIP has been demonstrated. The other three fugal species are *Podospora anserina*, *M. grisea* and *Leptosphaeria maculans*. RIP occurs in the haploid nuclei of the premeiotic dikaryon that forms during a sexual cross and causes multiple G : C to A : T mutations and methylation of remaining cytosine residues within the duplicated DNA sequences that are > 500 bp and share > 80% similarity (Cambareri *et al.* 1989; Selker 1990). The RIP associated cytosine methylation can also spread into the adjacent flanking regions (Selker *et al.* 1993; Irelan and Selker 1997). I isolated eight *cmd* RIP mutants containing both conventional (G:C to A:T) as well as unconventional mutations (Figure 4.4-4.5; Table 4.3), but I could not isolate a single progeny with in-frame stop codon in the *cmd* ORF, which further supports that the *cmd* gene is essential in *N. crassa*. Therefore, nuclei harboring a disrupted *cmd* gene could only be maintained in a heterokaryon form. The non-conventional RIP-induced mutations in the CaM could be due to the essential requirement of the sole *cmd* gene like the essential gene *poi-2* (*p*lenty *o*f *i*t) that also play a role during the vegetative growth and sexual development in *N. crassa* (Kim and Nelson 2005). Among the eight RIP-induced mutants, only one mutant, the *Δpan-2::bar::*P$_{tcu-1}$*::cmd*^{RIP}*::V5::gfp; mat A* (RIP-26) contained mutations in both the endogenous (D57Y and Q148H) and ectopic (M1W and E8K) copy of *cmd* gene and showed a defect in colony morphology, reduce growth rate, aerial hyphae and carotenoid accumulation (Figure 4.6; Figure 4.8-4.11). In addition, the *Δpan-2::bar::*P$_{tcu-1}$*::cmd*^{RIP}*::V5::gfp; mat A* (RIP-26) mutant was severely sensitive to the UV irradiation like the *upr-1* mutant, demonstrating role of CaM protein in DNA damage repair process in *N. crassa* (Figure 4.13). The *N. crassa* REV homolog genes, *upr-1* (*ncrev3*), *mus-42* (*ncrev1*) and *mus-26* (*ncrev7*) play an important role in DNA repair and UV mutagenesis through the bypass of (6-4) photoproducts (Sakai *et al.* 2002, 2003). Similar to *upr-1*, expression of *ncrev1* and *ncrev7* was found to be UV-inducible (Sakai *et al.* 2002, 2003). Previously it was reported that, CaM mediates DNA repair by modulating the initial step of excision repair of UV-damaged DNA (Charp 1987) and H2AX phosphorylation in response to low-dose radiation exposure of RAW 264.7 macrophages (Smallwood *et al.* 2009).

Next I also tested the requirement of the *cmd* gene during meiosis by performing crosses involving strains to induce meiotic silencing of *cmd*. If any gene essential during meiosis is inserted ectopically into a wild-type or innocuously-marked strain and the resulting strain is crossed to wild-type, this heterozygous cross should be barren (Shiu *et al.* 2001; Shiu and Metzenberg 2002). I found that the crosses involving an unpaired copy of the *cmd* gene showed a barren phenotype and this phenotype was suppressed both in the crosses homozygous for strains with *cmd* ectopic copy and in the heterozygous cross with Δ*Sad-1* mutant (Figure 4.14; Table 4.6). Thus it indicates that, in these crosses, meiotic silencing of *cmd* gene was responsible for the barren phenotype, suggesting that the product of *cmd* is essential during meiosis for full fertility in *N. crassa*. Meiotic silencing is a post-transcriptional gene silencing mechanism in *N. crassa*, where a gene not paired with a homolog in prophase I of meiosis generates a signal that transiently silences all sequences homologous to it by cleavage of the target mRNA (Shiu *et al.* 2001; Shiu and Metzenberg 2002). Some of the previously tested genes for meiotic silencing were ones coding for the globally important proteins, ascospore maturation l (*asm-1*; Aramayo *et al.* 1996; Shiu *et al.* 2001) β-tubulin (*Bml*), actin (*act*), histones H3 and H4-1 (hH3hH4-1+), plasma membrane ATPase (*pma-1*), RecA/RAD51 homolog meiotic-3 (*mei-3*; Shiu *et al.* 2001), Ca^{2+}/CaM-dependent kinase-2 (*camk-2*; Kumar and Tamuli 2014). Therefore, this study showed role of CaM in vegetative growth, carotenoid accumulation, a severe reduction in viability upon UV irradiation and a fertility defect in *N. crassa*.

A part of this chapter was published in Archives of Microbiology (Laxmi and Tamuli 2016).

In the next Chapter, site-directed mutational analysis of the Ca^{2+}/CaMK-2, a target of the CaM protein, have been discussed.

Chapter 5

Site-directed mutational analysis of calcium/calmodulin-dependent kinase-2 and expression studies of selected calcium signaling genes

5.1 Introduction

In the previous Chapter, I isolated a *N. crassa* CaM mutant using RIP mechanism and studied its phenotypes. The *cmd*^{RIP} mutant showed a defect in growth, reduced aerial hyphae, decreased carotenoid accumulation, a severe reduction in viability upon UV irradiation and a fertility defect. Moreover, meiotic silencing of the *cmd* gene resulted in a barren phenotype. In this chapter, I performed site directed mutational analysis of Ca^{2+}/CaMK-2, a target of the CaM protein, to identify its critical amino acid residues. In a previous study, the CaMK-2 was shown essential for full fertility in *N. crassa* (Kumar and Tamuli 2014). In addition, I studied expression of *cmd, trm-9* and *nca-2* gene in selected Ca^{2+}-signaling single and double knockout mutant strains using real-time PCR.

CaM is a well-studied prototypical example of the EF-hand family of Ca^{2+} sensing protein. Changes in intracellular Ca^{2+} concentration regulate CaM in three distinct ways (Chin and Means 2000). First, at the cellular level, by directing its subcellular distribution. Second, at the molecular level, by promoting different modes of association with many target proteins. Third, by directing a variety of conformational states in the CaM that result in target-specific activation. The CaM-dependent regulation of protein kinases illustrates the potential mechanisms by which Ca^{2+}-sensing proteins can recognize and generate affinity and specificity for effectors in a Ca^{2+}-dependent manner (Chin and Means 2000). In addition, the total intracellular concentration of the CaM in cell appears to be significantly below the total concentration of its targets, making it a limiting factor in their regulation (Persechini and Stemmer 2002), and by itself, binding of CaM with Ca^{2+} binding kinetics (kd of ~10 µM) would make it a relatively poor Ca^{2+} sensor in a cellular context where global Ca^{2+} concentrations tend to peak around 1 µM (Persechini and Stemmer 2002; Swulius and Waxham 2008).

CaM interacts with various proteins and enzymes including the Ca^{2+}/CaMKs (Figure 5.1), members of the CaM-kinase family are all classified as Ser/Thr kinases whose substrate P-sites (the targeted site of phosphorylation) all contain either a Ser or a Thr (Swulius and Waxham 2008). Kinase refers to a large category of enzymes that catalyze the transfer of phosphate from the gamma position of ATP to the hydroxyl group of Ser, Thr or Tyr within protein substrates (Swulius and Waxham 2008). It was first reported by Burnett and Kennedy, as the phosphorylation of the protein casein by a partially purified protein sample (Burnett and Kennedy 1954). The Ca^{2+}/CaMK II contains a conserved N-terminal catalytic domain and a C-terminal regulatory domain

containing overlapping autoinhibitory and Ca^{2+}/CaM binding domains, including *N. crassa* Ca^{2+}/CaMK-2 (Swulius and Waxham 2008; Tamuli *et al.* 2011; Kumar and Tamuli 2014). The autoinhibitory segment is positioned in the active site, sterically blocking access to its substrates. Binding of Ca^{2+}/CaM displaces the autoinhibitory segment by wrapping around kinase, resulting in its activation (Hoffman *et al.* 2011). The Ca^{2+}/CaMK II can then lock itself into activated states by autophosphorylation on a conserved threonine (Thr 286) in the autoinhibitory segment that increases its affinity for CaM to about 1000-fold, which markedly reduces the dissociation rate of bound Ca^{2+}/CaM (Meyer *et al.* 1992). There are four Ca^{2+}/CaMKs were identified in *N. crassa*, of which CAMK-1 and CAMK-2 were shown essential for full fertility (Kumar and Tamuli 2014). The *N. crassa* Ca^{2+}/CaMK-2 possess 11 conserved kinase domains, one putative CaM binding domain and nine putative phosphorylation sites (Figure 5.2A; Tamuli *et al.* 2011; Kumar and Tamuli 2014). Previously, it was found that crosses homozygous for Δ*camk-2::hph* mutants were barren and the *camk-2* has an important role during meiosis for full fertility in *N. crassa* (Deka *et al.* 2011; Tamuli *et al.* 2011; Kumar and Tamuli 2014). However, due to essential requirement, detailed cellular roles of the *N. crassa* CaM and its interactions with target proteins including Ca^{2+}/CaMK-2 have remained elusive. To identify important amino acid residues of the *camk-2*, I performed site-directed mutational analysis.

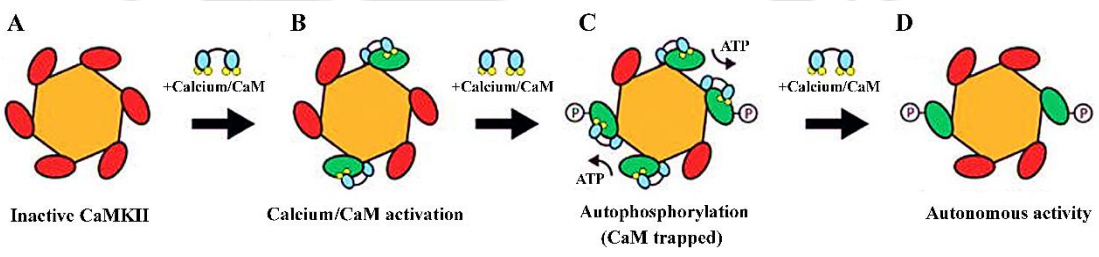

Figure 5.1: Diagram depicting the sequence of events leading to the activation and autophosphorylation of CaMKII. (A) CaMKII initially resides in an inactive state due to autoinhibition. (B) As Ca^{2+} levels rise CaM becomes saturated with the ion and binds individual subunits of the holoenzyme, thus inducing Ca^{2+}/CaM-dependent activity. (C) If adjacent subunits within a holoenzyme are activated by Ca^{2+}/CaM then

autophosphorylation at Thr^{286} may occur between them, which leads to CaM-Trapping. (D) When Ca^{2+}/CaM dissociates from CaMKII the subunits phosphorylated at Thr^{286} remain autonomously active beyond the duration of the Ca^{2+} signal that caused its activation (Adapted from Swulius and Waxham 2008).

(A)

(B)

CaM kinase I (bovine brain) L24907	300	NFA KSKWKQAFNRTAV VRH
CaM kinase II (rat α/β/δ) A30355	296	FNA RRKLKGAILTTML ATR
CaM kinse II (rat γ) A31908	297	FNA RRKLKGAILTTML VSR
CaM kinse II (*D. melanogaster*) JU0270	297	FNA RRKLKGAILTTML ATR

(C)

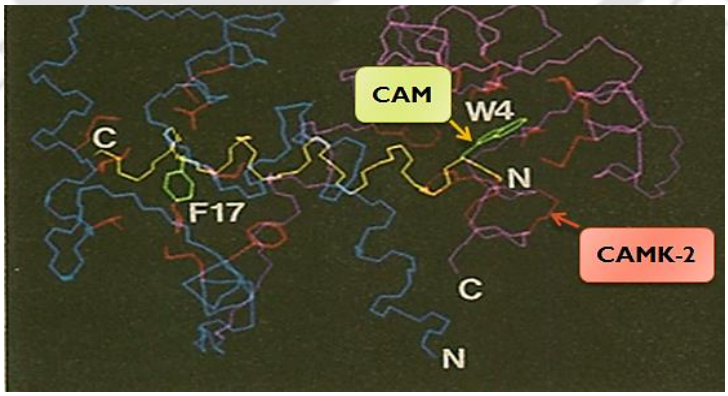

(D)

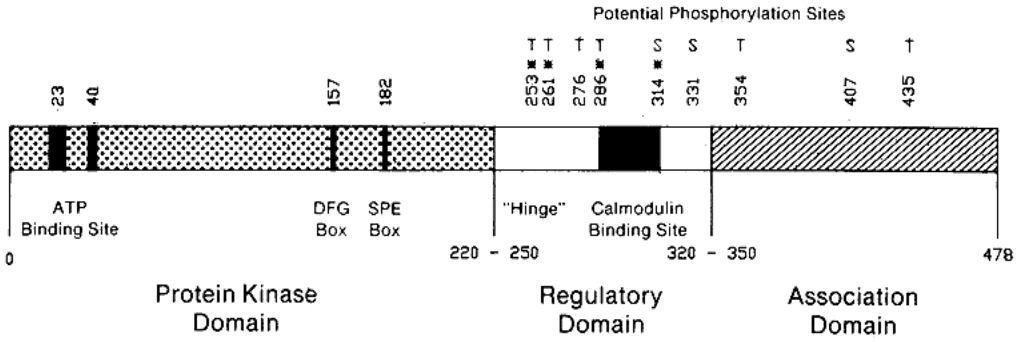

Figure 5.2: Sequence analysis of the Ca^{2+}/CaM protein. (A) Domain organization of the Ca^{2+}/CaMKs. Ca^{2+}/ CaMKs contain an N-terminal kinase domain (red), followed by an autoinhibitory (yellow) and overlapping CaM-binding domain (blue), (Adapted from Tamuli *et al.* 2011). (B) CaM binding motif. The 13 residue consensus motif with three flanking residues on each side. The accession number is given after the name and species. The interacting amino acid residues are indicated by solid arrows above the alignment (Adapted from Rhoads and Friedberg 1997). (C) Stereo view of the restrained minimized mean structure of the CaM illustrating the interaction of Trp4 and Phe17 of the peptide (shown in green) with hydrophobic side chains of the carboxyl- and amino-terminal domains of CaM (shown in red), respectively. The backbone atoms of the amino- and carboxyl-terminal domains are shown in blue and purple, respectively, while the backbone atoms of the peptide are shown in yellow. The residues shown are 6 to 146 of CaM and 3 to 21 of M13; the amino and carboxyl termini of both CaM and M13 are disordered (Adapted from Ikura *et al.* 1992). (D) Model of domain structure of CaM-K-α of rat brain. Potential serine (S) and threonine (T) sites for phosphorylation are noted; those with the greatest site homology are marked with an asterisk (Adapted from Lin *et al.* 1987).

In addition, I performed expression analysis of CaM and some of its predicted interacting partners through real-time PCR. I predicted the cmd (Figure 5.3), trm-9 (Figure 5.4) and nca-2 (Figure 5.5) interacting partners using the string software (http://string-db.org). The STRING database (Search Tool for the Retrieval of Interacting

Genes/Proteins) provide a critical assessment and integration of protein-protein interactions, including direct (physical) as well as indirect (functional) associations. This database not only include experimental data, but also used computational information to predict protein interactions network (Mering *et al.* 2007; Jensen *et al.* 2009; Szklarczyk *et al.* 2011, 2015; Franceschini *et al.* 2013).

CaM and its target proteins can bind to different target enzymes and proteins, including Ca^{2+}-transport ATPase, Ca^{2+}/H^{+} exchanger, Ca^{2+}-permeable channel, MLCK and other CaM-dependent protein kinases, phosphatase. Most highly characterized effectors are directly or indirectly involved in protein phosphorylation. In addition, CaM also regulates the activities of the plasma membrane Ca^{2+}-pump, various ion channels, the ryanodine receptor and isoforms of the inositol (1,4,5)-trisphosphate receptor directly or indirectly via a CaMK (James *et al.* 1995; Jurado *et al.* 1999; Chin and Means 2000; Haiech *et al.* 2011). CaM is able to exert two opposing effects on P/Q-type calcium channels, first promoting then inhibiting channel opening (DeMaria *et al.* 2001). Both apo CaM and Ca^{2+}-CaM modulate skeletal muscle Ca^{2+} release channel (RYR1), but the functional consequences of the binding of these two forms of CaM to RYR1 are completely different: apo CaM is a channel activator, whereas Ca^{2+}-CaM is a channel inhibitor. Binding sites for calcium-free CaM and Ca^{2+}-bound CaM are overlapping and, when Ca^{2+} binds to CaM, the CaM molecule shifts to a more N-terminal location on the ryanodine receptor converting it from an activator to an inhibitor of the channel, suggesting the possibility that CaM regulates ryanodine receptor activity by regulating subunit-subunit interactions (Rodney *et al.* 2001). In addition, interaction of NCA-2, a Ca^{2+}-ATPase with CaM in *N. crassa* further supported by the using software STRING (Figure 5.5). In chapter 3, I describe that the *N. crassa* homologues of *cmd, trm-9* and *nca-2* genes play a role in growth, Ca^{2+} sensitivity, UV survival and in acquisition of thermotolerance induced by heat shock temperature. In addition to these genes, some other Ca^{2+}-signaling genes also showed similar functions in *N. crassa* (Table 5.1). I performed real-time PCR analysis to determine the fold change in expression level of *cmd, trm-9, nca-2* and some selected Ca^{2+}-signaling genes to show genetic interactions among them.

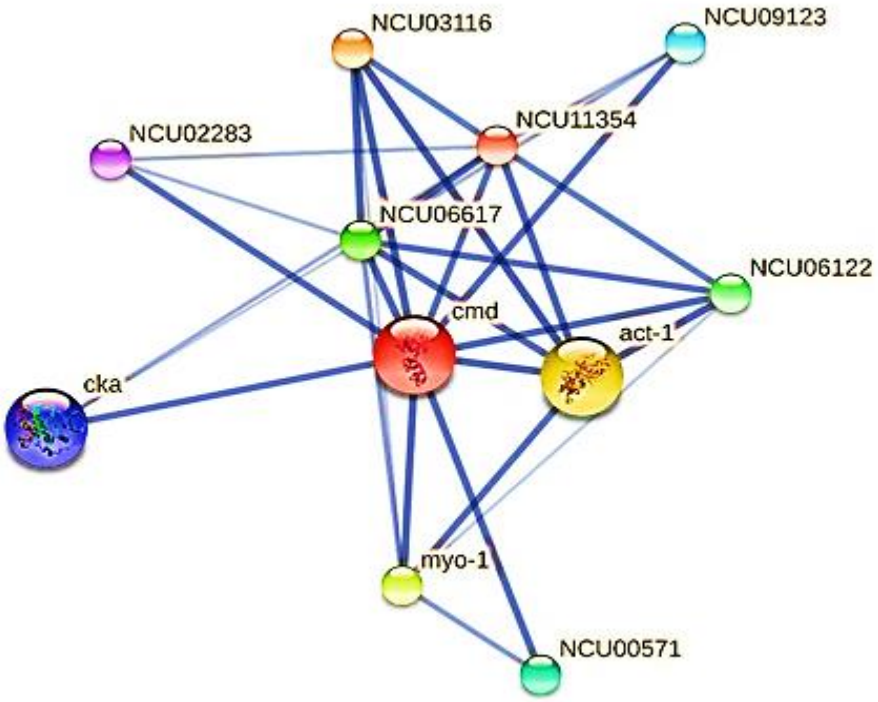

Figure 5.3: Schematic representation of STRING network view of cmd or CaM protein of *N. crassa*. The edges represent protein-protein associations. Associations are meant to be specific and meaningful, i.e. proteins jointly contribute to a shared function, which does not necessarily mean they are physically binding each other. Small nodes represent protein of unknown 3D structure and large nodes represent some 3D structure is known or predicted. The interaction of the cmd protein with NCU03116 (putative uncharacterized protein), act-1 (actin), myo-1 (myosin-1), NCU06617 (myosin regulatory light chain cdc-4), NCU06122 (putative uncharacterized protein), NCU00571 (putative uncharacterized protein), NCU09123 (Ca^{2+}/CaMK), cka (casein kinase II subunit alpha that phosphorylates the FRQ clock protein and regulates the circadian clock), NCU02283 (Ca^{2+}/CaMK) and NCU11354 (putative uncharacterized protein).

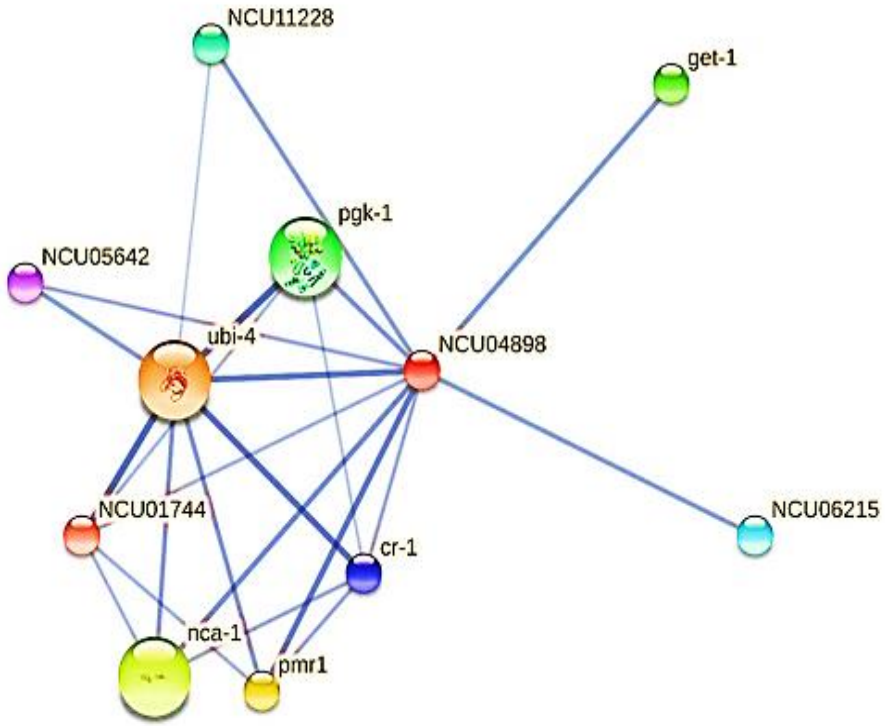

Figure 5.4: Schematic representation of STRING network view of trm-9 protein of *N. crassa*. The edges represent protein-protein associations. Associations are meant to be specific and meaningful, i.e. proteins jointly contribute to a shared function, which does not necessarily mean they are physically binding each other. Small nodes represent protein of unknown 3D structure and large nodes represent some 3D structure is known or predicted. The interaction of the trm-9 protein with ubi-4 (ubiquitin), pmr1 (calcium-transporting ATPase type 2C member 1), nca-1 (calcium-transporting ATPase sarcoplasmic/endoplasmic reticulum type), get-1 (protein get-1), pgk-1 (phosphoglycerate kinase), NCU11228 (putative uncharacterized protein), NCU06215 (putative uncharacterized protein), cr-1 (adenylate cyclase), NCU05642 (putative uncharacterized protein) and NCU01744 (glutamate synthase).

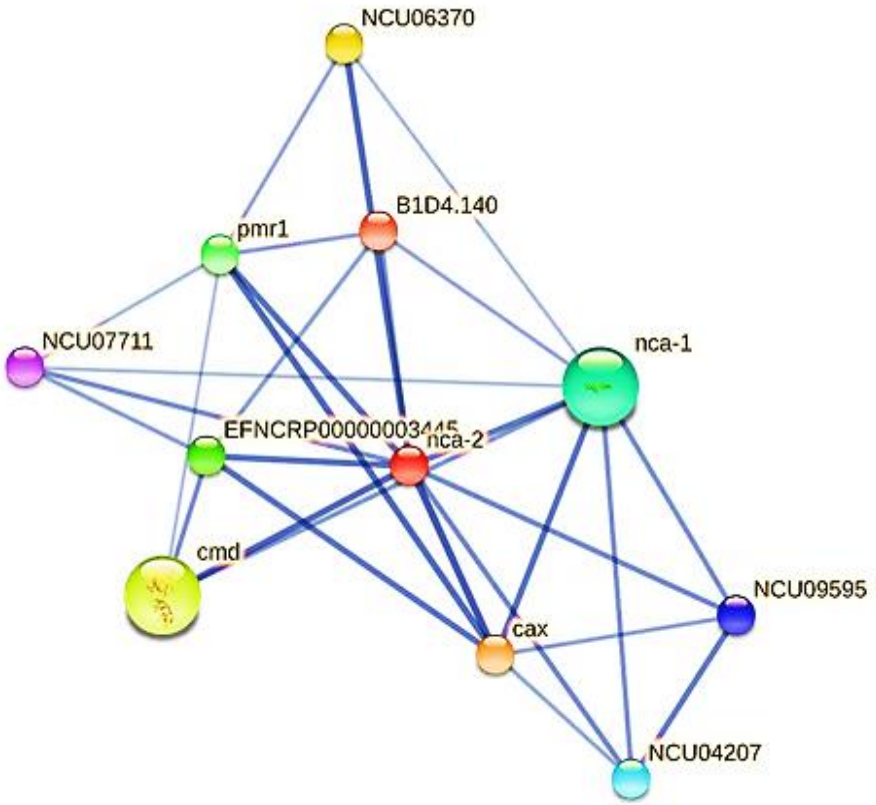

Figure 5.5: Schematic representation of STRING network view of nca-2 protein of *N. crassa*. The edges represent protein-protein associations. Associations are meant to be specific and meaningful, i.e. proteins jointly contribute to a shared function, which does not necessarily mean they are physically binding each other. Small nodes represent protein of unknown 3D structure and large nodes represent some 3D structure is known or predicted. The interaction of the nca-2 protein with *cax* (putative uncharacterized protein), NCU06370 (putative uncharacterized protein), cmd, EFNCRP00000003445 (calcineurin subunit B), pmr1 (calcium-transporting ATPase type 2C member 1), nca-1 (calcium-transporting ATPase sarcoplasmic/endoplasmic reticulum type), NCU04207 (predicted protein), NCU09595 (putative uncharacterized protein), NCU07711 (putative uncharacterized protein) and B1D4.140 (putative uncharacterized protein).

Table 5.1: Functions of some of the important Ca^{2+}-signaling genes in *N. crassa*

Sl. no.	NCU No.	Name	Type of protein	Function
1.	04898	*trm-9*	Ca^{2+}-ATPase	Growth, carotenoid accumulation, Ca^{2+} stress tolerance, UV survival and thermotolerance
2.	04736	*nca-2*	Ca^{2+}-ATPase	Growth, carotenoid accumulation, Ca^{2+} stress tolerance, UV survival, thermotolerance, regulation of ROS level and circadian regulated conidiation
3.	06366	*cpe-1*	Ca^{2+}/H^{+} exchanger	Regulation of cytosolic Ca^{2+} ion, carotenoid accumulation, oxidative stress tolerance and thermotolerance
4.	06703	*mid-1*	Ca^{2+}-permeable channel	UV survival, regulation of ROS level and circadian regulated conidiation
5.	06245	*plc1*	Phospholipase C	Regulation of cytosolic Ca^{2+} ion, carotenoid accumulation, oxidative stress tolerance and thermotolerance
6.	06650	*splA2*	Phospholipase	Regulation of cytosolic Ca^{2+} ion, carotenoid accumulation, oxidative stress tolerance and thermotolerance
7.	04379	*ncs-1*	Ca^{2+} and/or CaM binding	Growth, carotenoid accumulation, Ca^{2+} stress tolerance , UV survival,

				regulation of ROS level and circadian regulated conidiation
8.	09123.2	*camk-1*	Ca^{2+} and/or CaM binding	Growth, thermotolerance, oxidative stress tolerance and fertility
9.	02283.2	*camk-2*	Ca^{2+} and/or CaM binding	Growth, thermotolerance, oxidative stress tolerance and fertility
10.	06177.2	*camk-3*	Ca^{2+} and/or CaM binding	Thermotolerance, oxidative stress tolerance
11.	09212.2	*camk-4*	Ca^{2+} and/or CaM binding	Thermotolerance, oxidative stress tolerance

5.2 Results

5.2.1 Site-directed mutational analysis of the Ca^{2+}/CaMK-2

Site-directed mutational analysis of Ca^{2+}/CaMK-2 was performed to identify its important amino acid residues. In the rat Ca^{2+}/CaM kinase II, autophosphorylation of threonine 286, the adjacent phosphorylation site to the CaM-binding domain (Figure 5.2D; Lin *et al.* 1987), was found essential for the kinase to become autonomous (Schworer *et al.* 1988; Hanson *et al.* 1989). Furthermore, phosphorylation at threonine 286 was followed by the phosphorylation at serine 279 in the rat Ca^{2+}/CaM kinase II (Miller *et al.* 1988; Hanson *et al.* 1989). But, the *N. crassa camk-2* does not contain conserved phosphorylation sites corresponding to the threonine 286 and serine 279 (Lin *et al.* 1987; Miller *et al.* 1988; Hanson *et al.* 1989) as well as a conserved CaM binding domain (Rhoads and Friedberg 1997).

I had performed site-directed mutational analysis of the Ca^{2+}/CaMK-2 using the pRK-2 (P_{T7}*::camk-2::bar*) construct (Figures 5.6, Figures 5.7; Kumar and Tamuli 2014). In the Ca^{2+}/CaMK-2, I targeted two putative phosphorylation sites threonine 267 and serine 247 that are adjacent to the CaM-binding domain and contain the $^{R}_{K}XX^{T}_{S}$ consensus sequence (Kim *et al.* 1998), and leucine 309 in the CaM binding domain for site-directed mutations (Figure 5.8). I replaced threonine 267 and serine 247 with alanine, and leucine 309 with aspartic acid. For the site-directed mutations, I used the mutagenic primer pairs S247A-2283-F and S247A-2283-R, F-T267A-2283 and R-

T267A-2283, and F-L309D-2283 and R-L309D-2283 (Figure 5.9; Table 5.2) for the S247A, T267A and L309D mutations, respectively, and the procedure essentially as described in described in materials and methods. The plasmid constructs pVL-2, pVL-3 and pVL-4 containing the *camk-2*^{S247A}, *camk-2*^{T267A} and *camk-2*^{L309D} mutations, respectively, were isolated and confirmed by sequencing using the primer Seq-NCU02283F (Figure 5.10; Figure 5.11; Figure 5.12; Figure 5.13; SciGenom Labs, Cochin, India, and Eurofins Genomics India Pvt Ltd., Bangalore, India). The GenBank accession numbers for the *camk-2*^{S247A}, *camk-2*^{T267A} and *camk-2*^{L309D} mutant alleles are KX021884, KX021885 and KX021886, respectively (Laxmi and Tamuli 2016).

Table 5.2: Primers used for site-directed mutational analysis

Sl. no.	Primer	Sequence (5'→ 3')
1.	[a]S247A-2283-F	GGCGCGGCGTC**GCG**GACAACGCC
2.	[a]S247A-2283-R	GGCGTTGTCCG**CGA**CGCCGCGCC
3.	[a]F-T267A-2283	GCCAAGCGCATG**GCC**GCCCACGAGG
4.	[a]R-T267A-2283	CCTCGTGGGCGG**CCA**TGCGCTTGGC
5.	[a]F-L309D-2283	AACTTTAATGCGAGAAGGACG**GAT**CATGCGG CTATCGATACAGTA
6.	[a]R-L309D-2283	TACTGTATCGATAGCCGCATG**ATC**CGTCCTTC TCGCATTAAAGTT
7.	3NCU2283F	GCAGCCGTGTCGATACAAAG
8.	4NCU2283R	GTCAATGGTCAAGCACCTGC
9.	16NCU02283F-HI	AGTACGAGATCGACGGAGGA
10.	5HPHR	ATCCACTTAACGTTACTGAAATC
11.	Seq-NCU02283F	CGTCGACATCTGGGCCTTGG
12.	Seq-NCU02283R	CACGCCGTCAGATCCATCGC

[a] The target codon in the mutagenic primers is shown bold, and the nucleotides changed are underlined

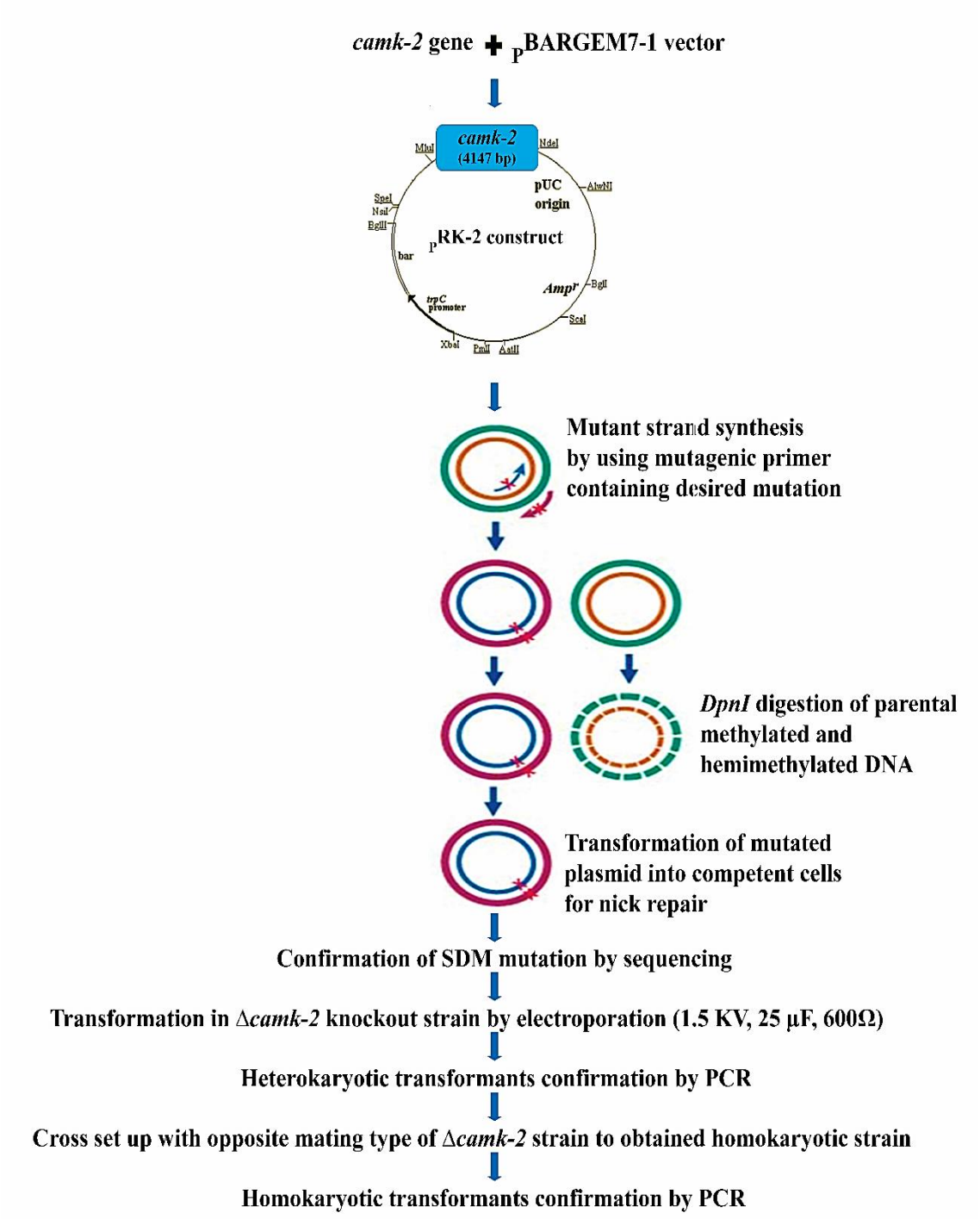

Figure 5.6: Schematic representation site-directed mutation of *camk-2*. Procedure for site-directed mutation of *camk-2* gene by using pRK-2 construct, and transformation into the Δ*camk-2::hph* mutant knockout strain.

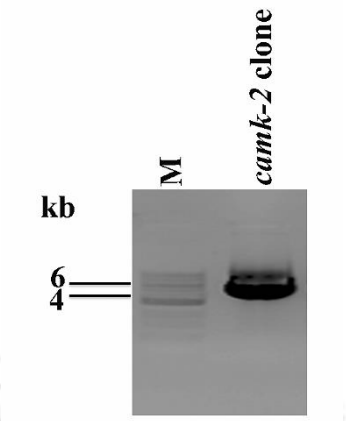

Figure 5.7: Clone reconfirmation of pRK-2 constructs. Cloning of the ~4157 bp fragment carrying *camk-2* genes into the *SmaI* site of the pBARGEM7-1 plasmid vector that contains *bar* selectable marker, *lacZα* for β-galactosidase and *amp* for bacterial selection (Kumar and Tamuli 2014).

(A)

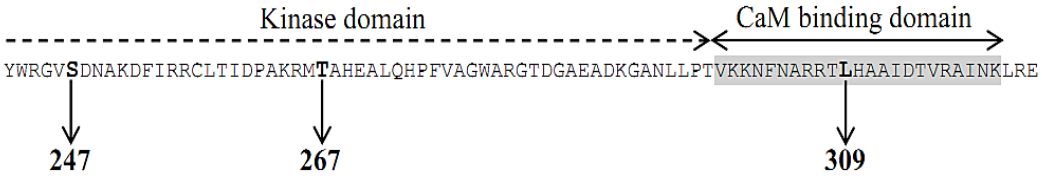

(B)

```
ATGAGTGCCGCCAACGGTCGACAACCCGAAGTGCAGCCGTGTCGATACAAAGTTGGCAAG
 M  S  A  A  N  G  R  Q  P  E  V  Q  P  C  R  Y  K  V  G  K
ACTTTGGGCGCCGGTTCATACTCGGTCGTTAAGGAATGCGTACACATAGACACCGGTCGC
 T  L  G  A  G  S  Y  S  V  V  K  E  C  V  H  I  D  T  G  R
TACTATGCGGCCAAGGTGATCAACAAGCGCCTGATGGCCGGCCGGGAACACATGGTTCGC
 Y  Y  A  A  K  V  I  N  K  R  L  M  A  G  R  E  H  M  V  R
AATGAAATCGCCGTGCTCAAGAAGGTGTCCATGGGCCACCAGAACATCCTGACCCTGGTC
 N  E  I  A  V  L  K  K  V  S  M  G  H  Q  N  I  L  T  L  V
GACTACTTCGAGACCATGAACAACCTCTACCTCGTCACTGACCTCGCCCTCGGCGGCGAG
 D  Y  F  E  T  M  N  N  L  Y  L  V  T  D  L  A  L  G  G  E
CTCTTCGATCGCATCTGTCGCAAAGGCTCTTACTACGAATCCGACGCCGCCGACCTCATC
 L  F  D  R  I  C  R  K  G  S  Y  Y  E  S  D  A  A  D  L  I
CGCGCCACCCTGTCCGCCGTCGCCTACCTGCATGACCACGGCATCGTCCACCGCGACCTC
 R  A  T  L  S  A  V  A  Y  L  H  D  H  G  I  V  H  R  D  L
AAGCCCGAGAACCTCCTTTTCCGTACGCCCGAGGACAATGCCGACTTGCTGATCGCCGAC
 K  P  E  N  L  L  F  R  T  P  E  D  N  A  D  L  L  I  A  D
TTTGGTCTTAGCCGGATCATGGATGAGGAGCAATTCCATGTCCTAACCACCACCTGCGGC
 F  G  L  S  R  I  M  D  E  E  Q  F  H  V  L  T  T  T  C  G
ACACCCGGCTACATGGCCCCAGAGATCTTCAAAAAGACCGGCCACGGCAAACCCGTCGAC
 T  P  G  Y  M  A  P  E  I  F  K  K  T  G  H  G  K  P  V  D
ATCTGGGCCTTGGGAGTAATCACTTACTTTCTGCTGTGCGGCTACACCCCCTTCGACCGC
 I  W  A  L  G  V  I  T  Y  F  L  L  C  G  Y  T  P  F  D  R
GACTCGGACTTTGAGGAGATGCAGGCCATCCTCAATGCCGATTACTCCTTCACCCCACTC
 D  S  D  F  E  E  M  Q  A  I  L  N  A  D  Y  S  F  T  P  L

                    TCG to GCG; S247A
                    ↑
GAGTACTGGCGCGGCGTCTCGGACAACGCCAAGGACTTTATTCGCAGGTGCTTGACCATT
 E  Y  W  R  G  V  S  D  N  A  K  D  F  I  R  R  C  L  T  I
                    ACC to GCC; T267A
                    ↑
GACCCGGCCAAGCGCATGACCGCCCACGAGGCGCTGCAGCACCCCTTCGTTGCTGGCTGG
 D  P  A  K  R  M  T  A  H  E  A  L  Q  H  P  F  V  A  G  W
GCCCGCGGAACCGATGGTGCGGAGGCCGATAAGGGCGCTAACCTGCTGCCGACCGTCAAG
 A  R  G  T  D  G  A  E  A  D  K  G  A  N  L  L  P  T  V  K

                          CTG to GAT; L309D
                          ┌─┐
AAGAACTTTAATGCGAGAAGGACGCTGCATGCGGCTATCGATACAGTACGTGCTATTAAC
 K  N  F  N  A  R  R  T  L  H  A  A  I  D  T  V  R  A  I  N
AAGCTGCGTGAGGGCCAGTTCATGAACGGCGGGAGGAGCCGTGAGCCCGCGAAGAAAGCG
 K  L  R  E  G  Q  F  M  N  G  G  R  S  R  E  P  A  K  K  A
GCAGCGGGTGCGGGTGCGGTGCCCCCAGCGGCAGGAGGTGGAGGAGGAGGCCCAGGAGTG
 A  A  G  A  G  A  V  P  P  A  A  G  G  G  G  G  P  G  V
GATGACGGATTGGCGGTAGCGCTCGGCCCAACGCTCGGGAAGGAGGCAAGCATGGTGTCA
 D  D  G  L  A  V  A  L  G  P  T  L  G  K  E  A  S  M  V  S
ACGGCGAGCAGCAATGTCACCAAGGACAGCGGCTACGCAACACAGCCGGAAGGGGAGGGA
 T  A  S  S  N  V  T  K  D  S  G  Y  A  T  Q  P  E  G  E  G
GGCTCTAGGGACGGAGACGATGTTCTTATGAAGGATGCGTCGGTGCCAGCGCCAACATCA
 G  S  R  D  G  D  D  V  L  M  K  D  A  S  V  P  A  P  T  S
TCATCGCCAGCGCCGGTGCATGGGAACACACAGAATGCACAGCATGCGGGAGTGCCGAGT
 S  S  P  A  P  V  H  G  N  T  Q  N  A  Q  H  A  G  V  P  S
ATCCTACGGCCGGGCAGTATCGAGAATAAGGTTGTCGAGACTGGTAAAGGCTTGTGGAAT
 I  L  R  P  G  S  I  E  N  K  V  V  E  T  G  K  G  L  W  N
GGGACTAGTGTTAAGCGATGA
 G  T  S  V  K  R  -
```

Figure 5.8: Sequences selected for site-directed mutations. (A) Schematic representation of partial amino acid sequence of the CAMK-2 protein of *N. crassa*. The dash line and solid line represent the kinase domain and CaM-binding region, respectively. The position of the amino acid residues targeted for site-directed are indicated with arrows (Adapted from Laxmi and Tamuli 2016). (B) Translated sequence of *N. crassa* homologue of CaMK-2 including its nucleotide sequence. Translate tool available from the ExPASy bioinformatics resource portal

(http://web.expasy.org/translate/) was used to translate the nucleotide sequence to a protein sequence. Yellow and blue shaded regions are putative phosphorylation sites containing the $^{R}_{K}XX^{T}_{S}$ consensus (Kim *et al.* 1998) and CaM binding domain respectively (Rhoads and Friedberg 1997) respectively. The codons targeted for site-directed mutations (bold letter), are also shown. The start (ATG) and stop (TAG) codons are highlighted in green and red colors, respectively.

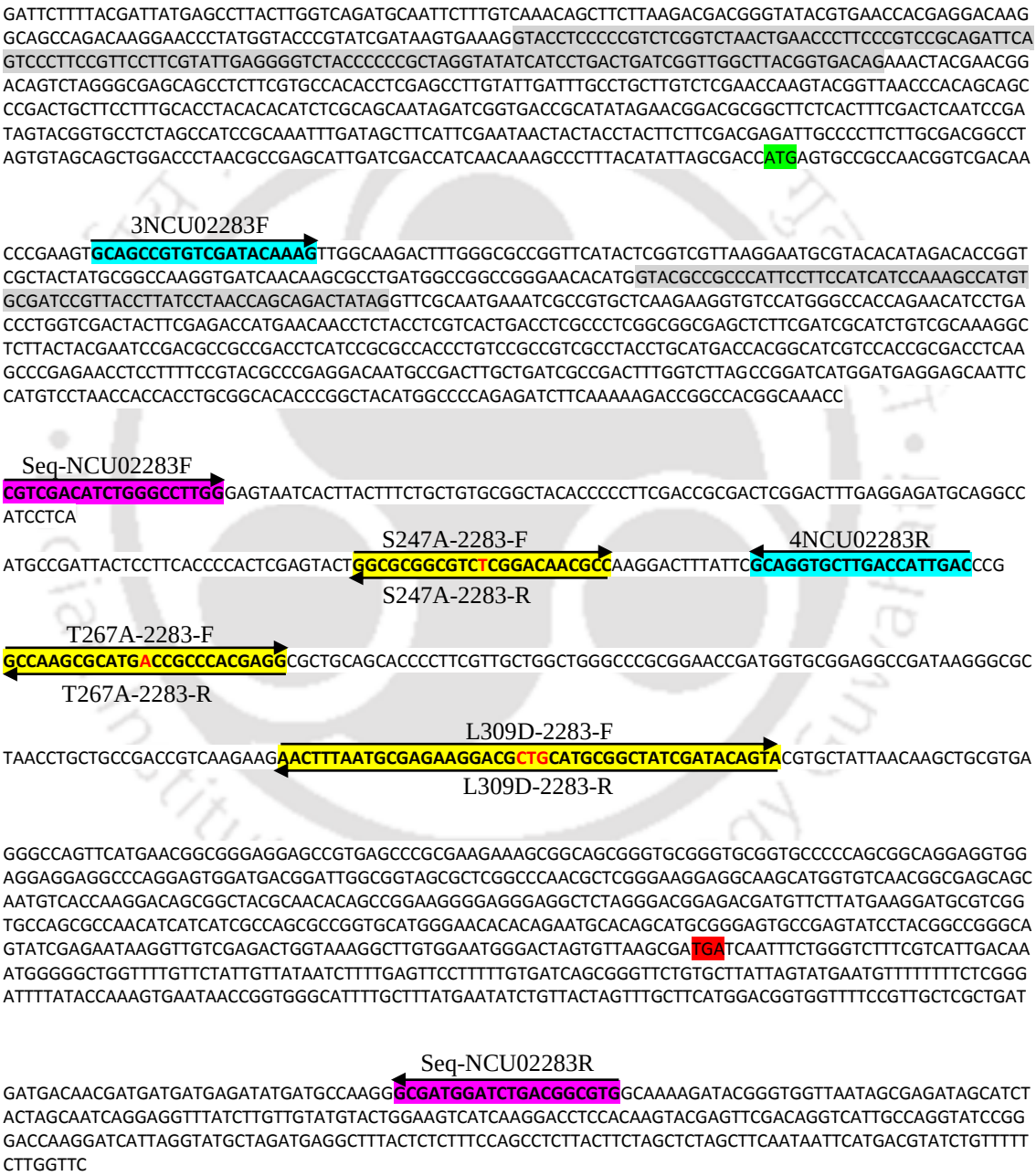

Figure 5.9: Primers locations of the *camk-2* gene for site-directed mutation. The

sequence of the ~2628 bp fragment carrying the *camk-2* ORF is shown. The mutagenic primers are highlighted in yellow color and arrow head indicates the 5'→3' direction. Primers used for confirmation of the *camk-2* clone and sequencing are highlighted in light blue and pink colors, respectively and arrow head indicates the 5'→3' direction. The start (ATG) and stop (TAG) codons are highlighted in green and red colors, respectively. The exons between the start and stop codons are highlighted in gray color.

(A)

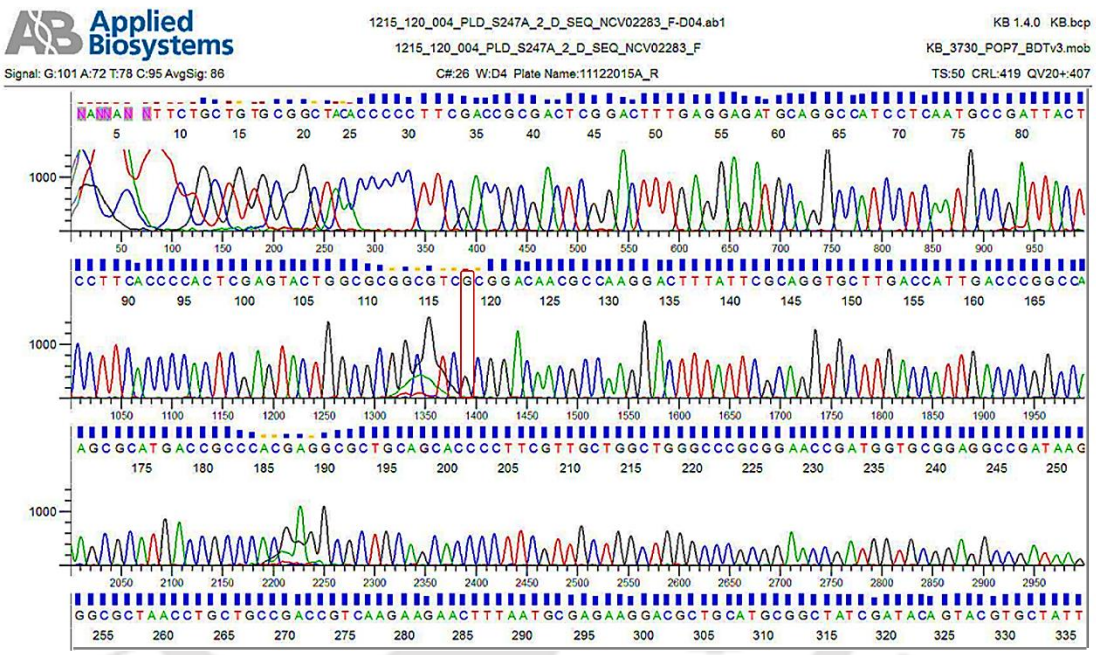

(B)

```
camk-2            CCCCTTCGACCGCGACTCGGACTTTGAGGAGATGCAGGCCATCCTCAATGCCGATTACTC
camk-2_S247A      CCCCTTCGACCGCGACTCGGACTTTGAGGAGATGCAGGCCATCCTCAATGCCGATTACTC
                  ************************************************************

camk-2            CTTCACCCCACTCGAGTACTGGCGCGGCGTCTCGGACAACGCCAAGGACTTTATTCGCAG
camk-2_S247A      CTTCACCCCACTCGAGTACTGGCGCGGCGTCGCGGACAACGCCAAGGACTTTATTCGCAG
                  ***************************** ****************************

camk-2            GTGCTTGACCATTGACCCGGCCAAGCGCATGACCGCCCACGAGGCGCTGCAGCACCCCTT
camk-2_S247A      GTGCTTGACCATTGACCCGGCCAAGCGCATGACCGCCCACGAGGCGCTGCAGCACCCCTT
                  ************************************************************

camk-2            CGTTGCTGGCTGGGCCCGCGGAACCGATGGTGCGGAGGCCGATAAGGGCGCTAACCTGCT
camk-2_S247A      CGTTGCTGGCTGGGCCCGCGGAACCGATGGTGCGGAGGCCGATAAGGGCGCTAACCTGCT
                  ************************************************************

camk-2            GCCGACCGTCAAGAAGAACTTTAATGCGAGAAGGACGCTGCATGCGGCTATCGATACAGT
camk-2_S247A      GCCGACCGTCAAGAAGAACTTTAATGCGAGAAGGACGCTGCATGCGGCTATCGATACAGT
                  ************************************************************
```

(C)

```
camk-2            MSAANGRQPEVQPCRYKVGKTLGAGSYSVVKECVHIDTGRYYAAKVINKRLMAGREHMVR
camk-2_S247A      MSAANGRQPEVQPCRYKVGKTLGAGSYSVVKECVHIDTGRYYAAKVINKRLMAGREHMVR
                  ************************************************************

camk-2            NEIAVLKKVSMGHQNILTLVDYFETMNNLYLVTDLALGGELFDRICRKGSYYESDAADLI
camk-2_S247A      NEIAVLKKVSMGHQNILTLVDYFETMNNLYLVTDLALGGELFDRICRKGSYYESDAADLI
                  ************************************************************

camk-2            RATLSAVAYLHDHGIVHRDLKPENLLFRTPEDNADLLIADFGLSRIMDEEQFHVLTTTCG
camk-2_S247A      RATLSAVAYLHDHGIVHRDLKPENLLFRTPEDNADLLIADFGLSRIMDEEQFHVLTTTCG
                  ************************************************************

camk-2            TPGYMAPEIFKKTGHGKPVDIWALGVITYFLLCGYTPFDRDSDFEEMQAILNADYSFTPL
camk-2_S247A      TPGYMAPEIFKKTGHGKPVDIWALGVITYFLLCGYTPFDRDSDFEEMQAILNADYSFTPL
                  ************************************************************

camk-2            EYWRGVSDNAKDFIRRCLTIDPAKRMTAHEALQHPFVAGWARGTDGAEADKGANLLPTVK
camk-2_S247A      EYWRGVADNAKDFIRRCLTIDPAKRMTAHEALQHPFVAGWARGTDGAEADKGANLLPTVK
                  ******:*****************************************************

camk-2            KNFNARRTLHAAIDTVRAINKLREGQFMNGGRSREPAKKAAAGAGAVPPAAGGGGGGPGV
camk-2_S247A      KNFNARRTLHAAIDTVRAINKLREGQFMNGGRSREPAKKAAAGAGAVPPAAGGGGGGPGV
                  ************************************************************

camk-2            DDGLAVALGPTLGKEASMVSTASSNVTKDSGYATQPEGEGGSRDGDDVLMKDASVPAPTS
camk-2_S247A      DDGLAVALGPTLGKEASMVSTASSNVTKDSGYATQPEGEGGSRDGDDVLMKDASVPAPTS
                  ************************************************************

camk-2            SSPAPVHGNTQNAQHAGVPSILRPGSIENKVVETGKGLWNGTSVKR
camk-2_S247A      SSPAPVHGNTQNAQHAGVPSILRPGSIENKVVETGKGLWNGTSVKR
                  **********************************************
```

Figure 5.10: Confirmation of the S247A mutation in the pVL-2 construct. (A) Chromatogram profile of the *camk-2*^{S247A} mutant allele generated by partial sequencing of the pVL-2 construct. The T→G point mutation changes the codon TCG to GCG, which changes serine to alanine in the CAMK-2 protein. The position of point mutation is shown using an unfilled box in the chromatogram in the corresponding sequence. (B) Partial sequence of the pVL-2 construct was aligned with the sequence of *camk-2* wild-type allele using the ClustalW. Asterisks below the alignment indicate the identical nucleotide. Absence of asterisk below the unmatched nucleotide (indicated with a pink shade) in the alignment, confirmed the mutation (the triplet codon TCG to GCG) that changes the amino acid residue serine to alanine at position 247 (S247A) of the CaMK-2 protein. (C) Alignment of the protein sequence of the CaMK-2^{S247A}. The partial sequence of the pVL-2 was translated using the translate tool of ExPASy and aligned with the sequence of CaMK-2 using the ClustalW to verify the amino acid changed. Asterisks below the alignment indicate the identical residues and the S247A mutation is indicated with a gray shade. The GenBank with accession number for the *camk-2*^{S247A} mutant allele is KX021884.

(A)

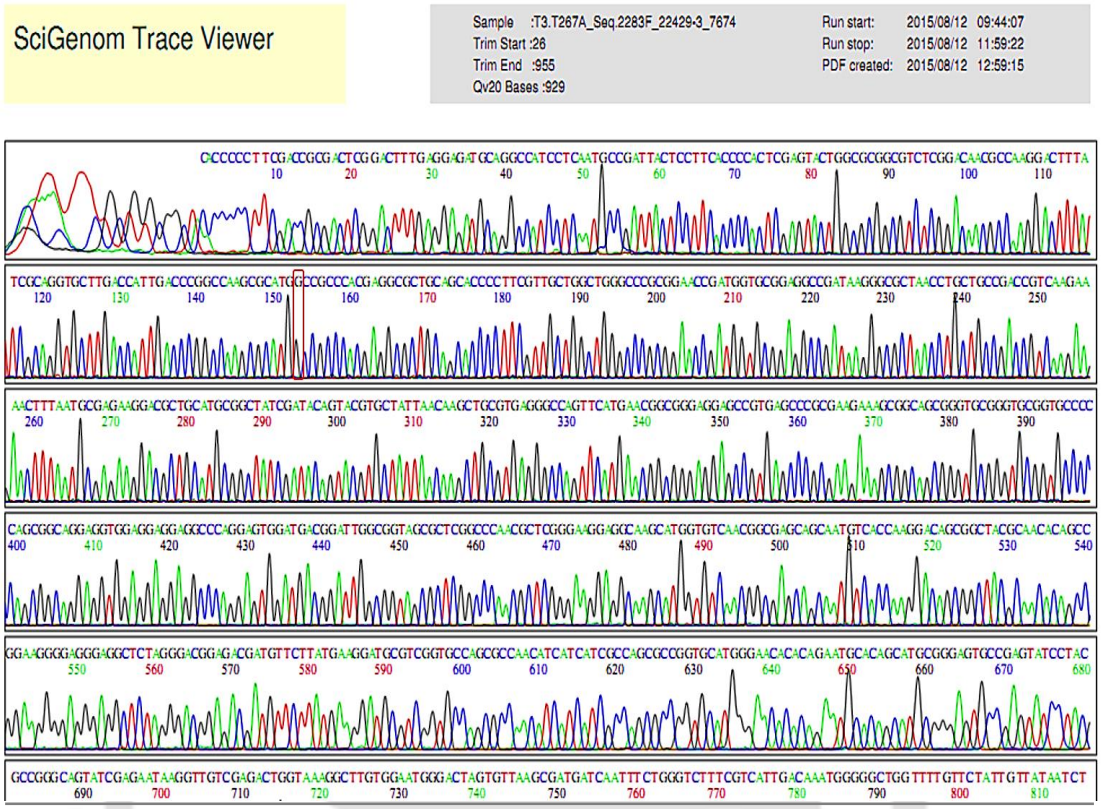

(B)

```
camk-2          CTTCACCCCACTCGAGTACTGGCGCGGCGTCTCGGACAACGCCAAGGACTTTATTCGCAG
camk-2_T267A    CTTCACCCCACTCGAGTACTGGCGCGGCGTCTCGGACAACGCCAAGGACTTTATTCGCAG
                ************************************************************

camk-2          GTGCTTGACCATTGACCCGGCCAAGCGCATGACCGCCCACGAGGCGCTGCAGCACCCCTT
camk-2_T267A    GTGCTTGACCATTGACCCGGCCAAGCGCATGGCCGCCCACGAGGCGCTGCAGCACCCCTT
                *********************************.**************************

camk-2          CGTTGCTGGCTGGGCCCGCGGAACCGATGGTGCGGAGGCCGATAAGGGCGCTAACCTGCT
camk-2_T267A    CGTTGCTGGCTGGGCCCGCGGAACCGATGGTGCGGAGGCCGATAAGGGCGCTAACCTGCT
                ************************************************************

camk-2          GCCGACCGTCAAGAAGAACTTTAATGCGAGAAGGACGCTGCATGCGGCTATCGATACAGT
camk-2_T267A    GCCGACCGTCAAGAAGAACTTTAATGCGAGAAGGACGCTGCATGCGGCTATCGATACAGT
                ************************************************************

camk-2          ACGTGCTATTAACAAGCTGCGTGAGGGCCAGTTCATGAACGGCGGGAGGAGCCGTGAGCC
camk-2_T267A    ACGTGCTATTAACAAGCTGCGTGAGGGCCAGTTCATGAACGGCGGGAGGAGCCGTGAGCC
                ************************************************************
```

(C)

```
camk-2            MSAANGRQPEVQPCRYKVGKTLGAGSYSVVKECVHIDTGRYYAAKVINKRLMAGREHMVR
camk-2_T267A      MSAANGRQPEVQPCRYKVGKTLGAGSYSVVKECVHIDTGRYYAAKVINKRLMAGREHMVR
                  ************************************************************

camk-2            NEIAVLKKVSMGHQNILTLVDYFETMNNLYLVTDLALGGELFDRICRKGSYYESDAADLI
camk-2_T267A      NEIAVLKKVSMGHQNILTLVDYFETMNNLYLVTDLALGGELFDRICRKGSYYESDAADLI
                  ************************************************************

camk-2            RATLSAVAYLHDHGIVHRDLKPENLLFRTPEDNADLLIADFGLSRIMDEEQFHVLTTTCG
camk-2_T267A      RATLSAVAYLHDHGIVHRDLKPENLLFRTPEDNADLLIADFGLSRIMDEEQFHVLTTTCG
                  ************************************************************

camk-2            TPGYMAPEIFKKTGHGKPVDIWALGVITYFLLCGYTPFDRDSDFEEMQAILNADYSFTPL
camk-2_T267A      TPGYMAPEIFKKTGHGKPVDIWALGVITYFLLCGYTPFDRDSDFEEMQAILNADYSFTPL
                  ************************************************************

camk-2            EYWRGVSDNAKDFIRRCLTIDPAKRMTAHEALQHPFVAGWARGTDGAEADKGANLLPTVK
camk-2_T267A      EYWRGVSDNAKDFIRRCLTIDPAKRMAAHEALQHPFVAGWARGTDGAEADKGANLLPTVK
                  ************************:***********************************

camk-2            KNFNARRTLHAAIDTVRAINKLREGQFMNGGRSREPAKKAAAGAGAVPPAAGGGGGGPGV
camk-2_T267A      KNFNARRTLHAAIDTVRAINKLREGQFMNGGRSREPAKKAAAGAGAVPPAAGGGGGGPGV
                  ************************************************************

camk-2            DDGLAVALGPTLGKEASMVSTASSNVTKDSGYATQPEGEGGSRDGDDVLMKDASVPAPTS
camk-2_T267A      DDGLAVALGPTLGKEASMVSTASSNVTKDSGYATQPEGEGGSRDGDDVLMKDASVPAPTS
                  ************************************************************

camk-2            SSPAPVHGNTQNAQHAGVPSILRPGSIENKVVETGKGLWNGTSVKR
camk-2_T267A      SSPAPVHGNTQNAQHAGVPSILRPGSIENKVVETGKGLWNGTSVKR
                  ***********************************************
```

Figure 5.11: Confirmation of the T267A mutation in the pVL-3 construct. (A) Chromatogram profile of the *camk-2*^{T267A} mutant allele generated by partial sequencing of the pVL-3 construct. The A→G point mutation changes the codon ACC to GCC, which changes threonine to alanine in the CAMK-2 protein. The position of point mutation is shown using an unfilled box in the chromatogram in the corresponding sequence. (B) Partial sequence of the pVL-3 construct was aligned with the sequence of *camk-2* wild-type allele using the ClustalW. Asterisks below the alignment indicate the identical nucleotide. Absence of asterisk below the unmatched nucleotide (indicated with a pink shade) in the alignment, confirmed the mutation (the triplet codon ACC to GCC) that changes the amino acid residue threonine to alanine at position 247 (T267A) of the CaMK-2 protein. (C) Alignment of the protein sequence of the CaMK-2^{T267A}. The partial sequence of the pVL-3 was translated using the translate tool of ExPASy and aligned with the sequence of CaMK-2 using the ClustalW to verify the amino acid changed. Asterisks below the alignment indicate the identical residues and the T267A mutation is indicated with a gray shade. The GenBank accession number for the *camk-2*^{T267A} mutant allele is KX021885.

(A)

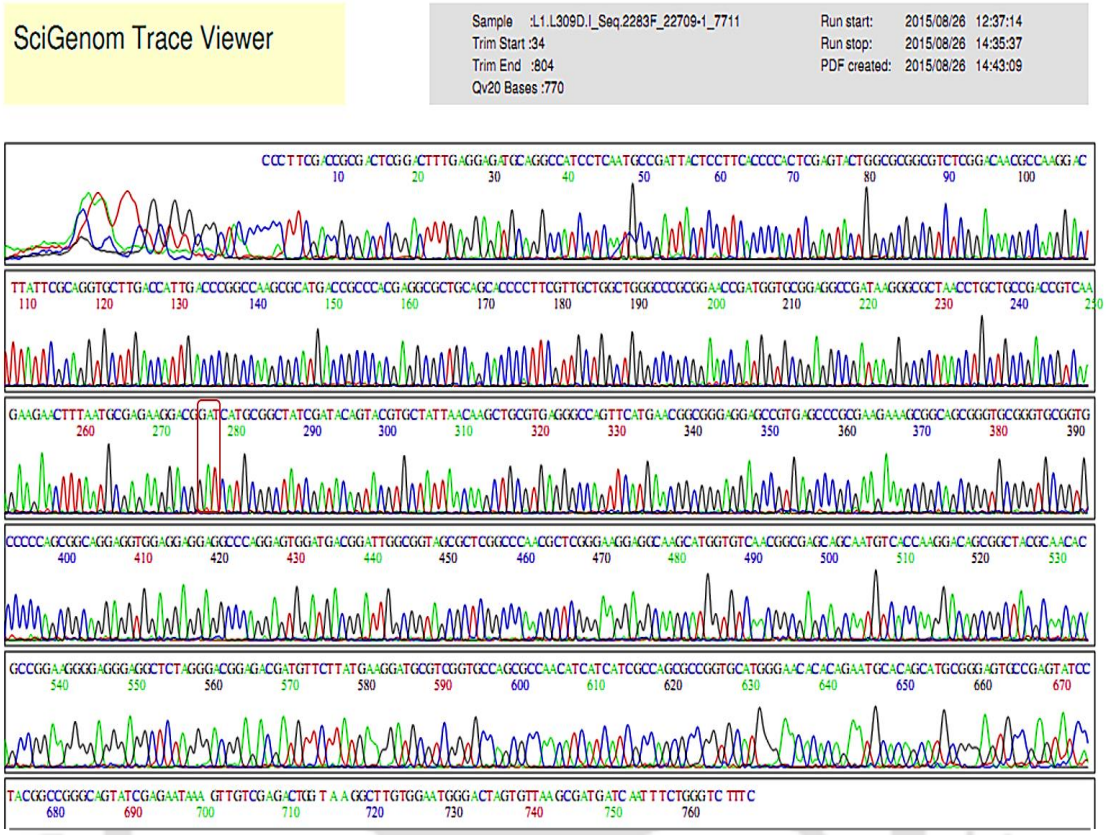

(B)

```
camk-2          GTGCTTGACCATTGACCCGGCCAAGCGCATGACCGCCCACGAGGCGCTGCAGCACCCCTT
camk-2_L309D    GTGCTTGACCATTGACCCGGCCAAGCGCATGACCGCCCACGAGGCGCTGCAGCACCCCTT
                ************************************************************

camk-2          CGTTGCTGGCTGGGCCCGCGGAACCGATGGTGCGGAGGCCGATAAGGGCGCTAACCTGCT
camk-2_L309D    CGTTGCTGGCTGGGCCCGCGGAACCGATGGTGCGGAGGCCGATAAGGGCGCTAACCTGCT
                ************************************************************

camk-2          GCCGACCGTCAAGAAGAACTTTAATGCGAGAAGGACGCTGCATGCGGCTATCGATACAGT
camk-2_L309D    GCCGACCGTCAAGAAGAACTTTAATGCGAGAAGGACGGATCATGCGGCTATCGATACAGT
                ************************************ : ********************

camk-2          ACGTGCTATTAACAAGCTGCGTGAGGGCCAGTTCATGAACGGCGGGAGGAGCCGTGAGCC
camk-2_L309D    ACGTGCTATTAACAAGCTGCGTGAGGGCCAGTTCATGAACGGCGGGAGGAGCCGTGAGCC
                ************************************************************

camk-2          CGCGAAGAAAGCGGCAGCGGGTGCGGGTGCGGTGCCCCCAGCGGCAGGAGGTGGAGGAGG
camk-2_L309D    CGCGAAGAAAGCGGCAGCGGGTGCGGGTGCGGTGCCCCCAGCGGCAGGAGGTGGAGGAGG
                ************************************************************
```

(C)

```
camk-2            MSAANGRQPEVQPCRYKVGKTLGAGSYSVVKECVHIDTGRYYAAKVINKRLMAGREHMVR
camk-2_L309D      MSAANGRQPEVQPCRYKVGKTLGAGSYSVVKECVHIDTGRYYAAKVINKRLMAGREHMVR
                  ************************************************************

camk-2            NEIAVLKKVSMGHQNILTLVDYFETMNNLYLVTDLALGGELFDRICRKGSYYESDAADLI
camk-2_L309D      NEIAVLKKVSMGHQNILTLVDYFETMNNLYLVTDLALGGELFDRICRKGSYYESDAADLI
                  ************************************************************

camk-2            RATLSAVAYLHDHGIVHRDLKPENLLFRTPEDNADLLIADFGLSRIMDEEQFHVLTTTCG
camk-2_L309D      RATLSAVAYLHDHGIVHRDLKPENLLFRTPEDNADLLIADFGLSRIMDEEQFHVLTTTCG
                  ************************************************************

camk-2            TPGYMAPEIFKKTGHGKPVDIWALGVITYFLLCGYTPFDRDSDFEEMQAILNADYSFTPL
camk-2_L309D      TPGYMAPEIFKKTGHGKPVDIWALGVITYFLLCGYTPFDRDSDFEEMQAILNADYSFTPL
                  ************************************************************

camk-2            EYWRGVSDNAKDFIRRCLTIDPAKRMTAHEALQHPFVAGWARGTDGAEADKGANLLPTVK
camk-2_L309D      EYWRGVSDNAKDFIRRCLTIDPAKRMTAHEALQHPFVAGWARGTDGAEADKGANLLPTVK
                  ************************************************************

camk-2            KNFNARRTLHAAIDTVRAINKLREGQFMNGGRSREPAKKAAAGAGAVPPAAGGGGGGPGV
camk-2_L309D      KNFNARRTDHAAIDTVRAINKLREGQFMNGGRSREPAKKAAAGAGAVPPAAGGGGGGPGV
                  ******** ***************************************************

camk-2            DDGLAVALGPTLGKEASMVSTASSNVTKDSGYATQPEGEGGSRDGDDVLMKDASVPAPTS
camk-2_L309D      DDGLAVALGPTLGKEASMVSTASSNVTKDSGYATQPEGEGGSRDGDDVLMKDASVPAPTS
                  ************************************************************

camk-2            SSPAPVHGNTQNAQHAGVPSILRPGSIENKVVETGKGLWNGTSVKR
camk-2_L309D      SSPAPVHGNTQNAQHAGVPSILRPGSIENKVVETGKGLWNGTSVKR
                  **********************************************
```

Figure 5.12: Confirmation of the mutation in the pVL-4 construct.

(A) Chromatogram profile of the *camk-2*^{L309D} mutant allele generated by partial sequencing of the pVL-4 construct. The CTG→GAT triple point mutations change the codon CTG to GAT, which changes leucine to aspartic acid in the CAMK-2 protein. The position of point mutation is shown using an unfilled box in the chromatogram in the corresponding sequence. (B) Partial sequence of the pVL-4 construct was aligned with the sequence of *camk-2* wild-type allele using the ClustalW. Asterisks below the alignment indicate the identical nucleotide. Absence of asterisk below the unmatched nucleotide (indicated with a pink shade) in the alignment, confirmed the mutation (the triplet codon CTG to GAT) that changes the amino acid residue leucine to aspartic acid at position 309 (L309D) of the CaMK-2 protein. (C) Alignment of the protein sequence of the CaMK-2^{L309}. The partial sequence of the pVL-4 was translated using the translate tool of ExPASy and aligned with the sequence of CaMK-2 using the ClustalW to verify the amino acid changed. Asterisks below the alignment indicate the identical residues and the L309D mutation is indicated with a gray shade. The GenBank accession number for the *camk-2*^{L309D} mutant allele is KX021886.

5.2.2 Transformation of pRK-2, pVL-2, pVL-3 and pVL-4 constructs into the Δ*camk-2::hph* strain and confirmation of transformants

The pRK-2 (Kumar and Tamuli 2014), pVL-2, pVL-3 and pVL-4 plasmids were transformed into the Δ*camk-2::hph; mat A* recipient strain by electroporation (described in materials and methods) and initial heterokaryotic transformants (HT) were selected on Vogel's sorbose agar plate containing basta (400 µg/ml). I isolated four HT strains (HT-C6, HT-S29, HT-T23, HT-L1; Table 2.1) that were verified by PCR using primer pairs 3NCU02283F and 4NCU02283R (Figure 5.13A; Table 5.2). To generate homokaryotic strains, I crossed HT-C6, HT-S29, HT-T23 and HT-L1 strains of genotype [(Δ*camk-2::hph; mat A*) + (*camk-2::bar; mat A*)], [(Δ*camk-2::hph; mat A*) + (*camk-2*^{S247A}*::bar; mat A*)], [(Δ*camk-2::hph; mat A*) + (*camk-2*^{T267A}*::bar; mat A*)] and [(Δ*camk-2::hph; mat A*) + (*camk-2*^{L309D}*::bar; mat A*)], (Table 2.1) with the Δ*camk-2::hph; mat a* strain and isolate 12 homokaryotic progenies (HOP; Table 2.1). Strain HOP-102, HOP-116, HOP-119 and HOP-120 of genotype Δ*camk-2::hph; camk-2::bar* (Table 2.1) are homokaryotic strains for the *camk-2* construct (transformed with the pRK-2 construct), strain HOP-17 and HOP-51 of genotype Δ*camk-2::hph; camk-2*^{S247A}*::bar* (Table 2.1) are homokaryotic strains for the *camk-2*^{S247A} mutant allele (transformed with the pVL-2 construct), strain HOP-12 and HOP-19 of genotype Δ*camk-2::hph; camk-2*^{T267A}*::bar* (Table 2.1) are homokaryotic strains for the *camk-2*^{T267A} mutant allele (transformed with the pVL-3 construct), and strain HOP-4, HOP-34, HOP-36 and HOP-37 of genotype Δ*camk-2::hph; camk-2*^{L309D}*::bar* (Table 2.1) are homokaryotic strains of *camk-2*^{L309D} mutant allele (transformed with the pVL-4 construct). Moreover, PCR was performed for verification of the *camk-2* alleles (Figure 5.13A) and the Δ*camk-2::hph* allele (Figure 5.13B) using the primer pairs 3NCU02283F and 4NCU02283R (Table 5.2), and 16NCU02283F-HI and 5HPHR (Table 5.2), respectively, in the homokaryotic strains.

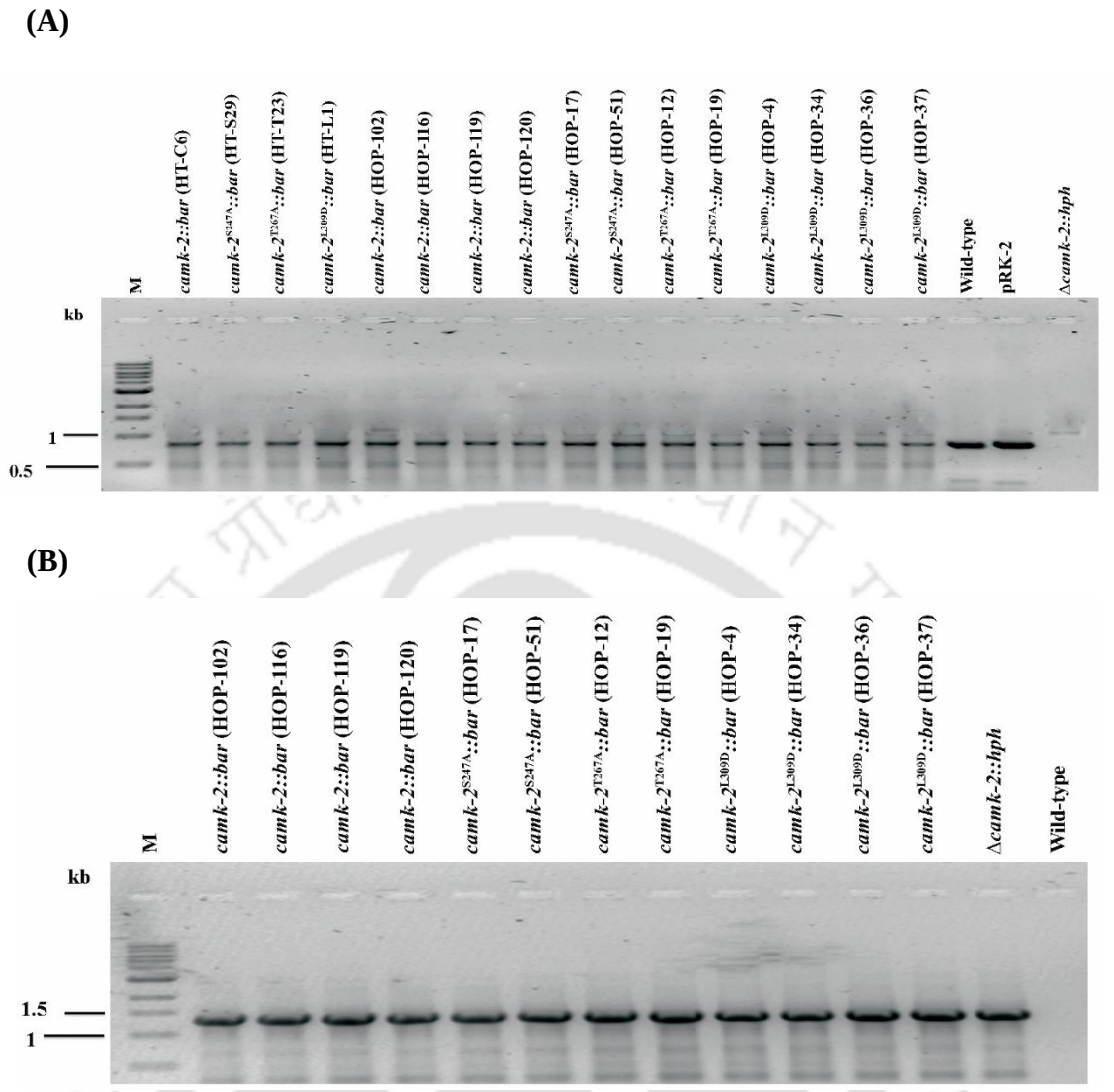

Figure 5.13: Confirmation of *camk-2*, *camk-2*^{S247A}, *camk-2*^{T267A} and *camk-2*^{L309D} transformants strains by PCR. (A) Verification of the presence of part of *camk-2* ORF in the HT and HOP of c*amk-2*, c*amk-2*^{S247A}, *camk-2*^{T267A} and *camk-2*^{L309D} constructs. The PCR products of size 824 bp, obtained using primer pairs 3NCU02283F and 4NCU02283R (Table 5.2), indicated presence of the *camk-2* gene. Wild-type and pRK-2 construct were used as positive control, however, no PCR product is obtained from the Δ*camk-2::hph* knockout mutant strain. (B) Verification of *hph* cassette in HOP of c*amk-2*, c*amk-2*^{S247A}, *camk-2*^{T267A} and *camk-2*^{L309D} constructs. The *hph* cassette was verified using the forward primers 16NCU02283F-HI specific for the upstream of the 5' flank of the *camk-2* along with the common reverse primer 5HPHR that is specific for the *hph* cassette (Table 5.2). Amplification of PCR product of size 1.466 kb, verified presence of the Δ*camk-2::hph* knockout alleles in HOP. No amplification was observed in wild-type control.

5.2.3 Site-directed mutational analysis of the Ca^{2+}/CaMK-2 revealed two important residues serine 247 and threonine 267

I generated *N. crassa* strains with S247A and T267A mutations in the putative phosphorylation sites in the catalytic domain, and L309D mutation in the CaM binding domain of the CaMK-2 protein. The homozygous crosses of the *camk-2*^{S247A} and the *camk-2*^{T267A} mutants, or the crosses involving these mutants with the Δ*camk-2* mutant showed an intermediate phenotype (Figure 5.14; Table 5.3; Laxmi and Tamuli 2016), whcih suggest an essential requirement of the serine 247 and threonine 267 phosphorylation sites for full fertility in *N. crassa*. However, the crosses homozygous for the *camk-2*^{L309D} mutant or its crosses with the Δ*camk-2* mutant were fertile (Figure 5.14; Table 5.3; Laxmi and Tamuli 2016), therefore, the leucine 309 is dispensable for full fertility in *N. crassa*.

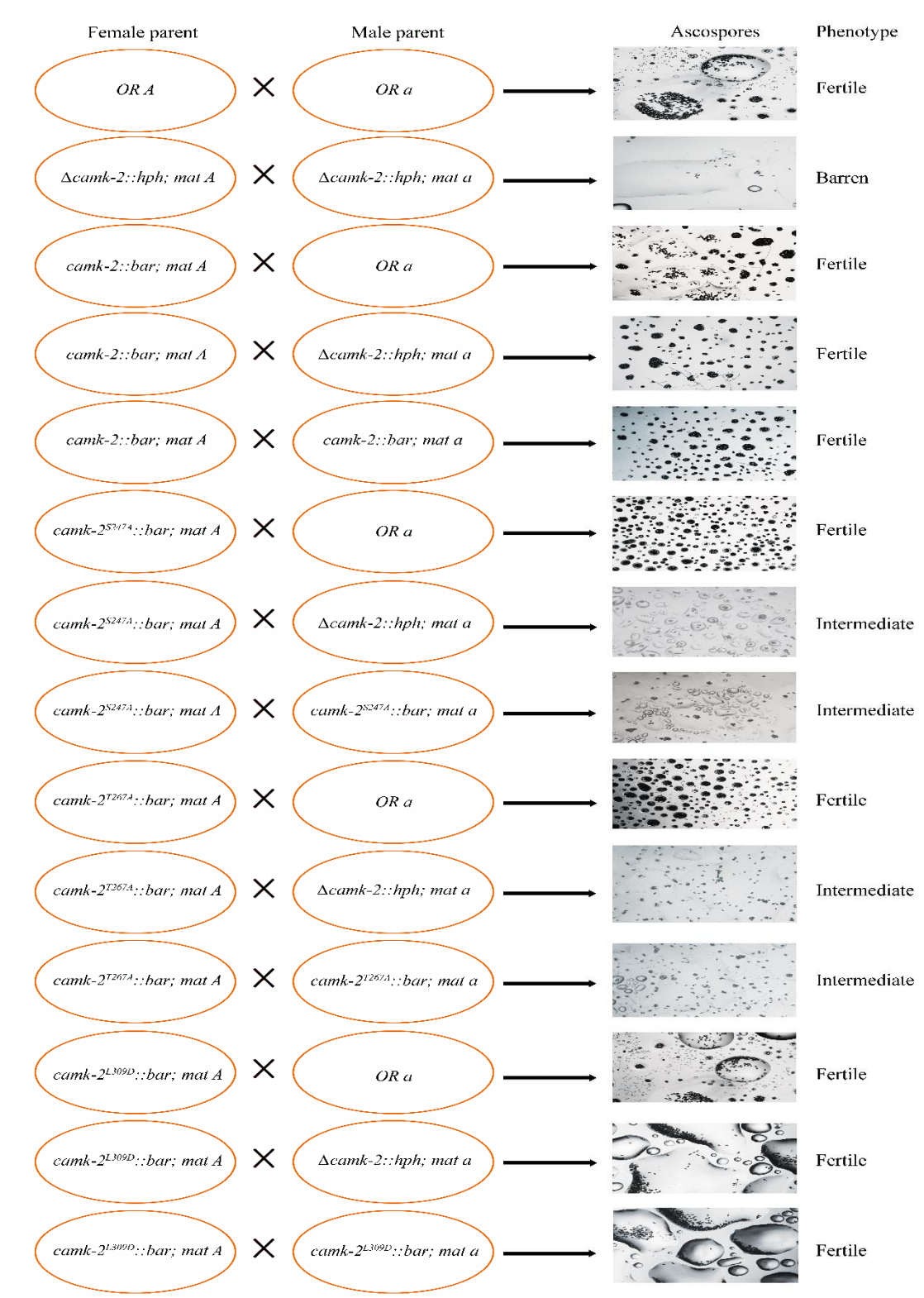

Figure 5.14: Phenotype of crosses involving the *N. crassa camk-2*, *camk-2*^{S247A}, *camk-2*^{T267A} and the *camk-2*^{L309D} mutant strains. The representative images of ejected ascospores on the lid of the petri dish examined under microscope are shown for each type of the cross.

Table 5.3[a]: Phenotype of crosses involving the *camk-2* mutant alleles

Sl. no.	Female parent	Male Parent	Phenotype
1.	Wild-type; *mat A*	Wild-type; *mat a*	Fertile
2.	Δ*camk-2::hph; mat A*	Δ*camk-2::hph; mat a*	Barren
3.	Δ*camk-2::hph; camk-2::bar; mat a* (HOP-102)	Wild-type; *mat A*	Fertile
4.	Δ*camk-2::hph; camk-2::bar; mat a* (HOP-119)	Wild-type; *mat A*	Fertile
5.	Δ*camk-2::hph; camk-2::bar; mat A* (HOP-116)	Wild-type; *mat a*	Fertile
6.	Δ*camk-2::hph; camk-2::bar; mat A* (HOP-120)	Wild-type; *mat a*	Fertile
7.	Wild-type; *mat A*	Δ*camk-2::hph; camk-2::bar; mat a* (HOP-102)	Fertile
8.	Wild-type; *mat A*	Δ*camk-2::hph; camk-2::bar; mat a* (HOP-119)	Fertile
9.	Wild-type; *mat a*	Δ*camk-2::hph; camk-2::bar; mat A* (HOP-116)	Fertile
10.	Wild-type; *mat a*	Δ*camk-2::hph; camk-2::bar; mat A* (HOP-120)	Fertile
11.	Δ*camk-2::hph; camk-2::bar; mat a* (HOP-102)	Δ*camk-2::hph; mat A*	Fertile
12.	Δ*camk-2::hph; camk-2::bar; mat a* (HOP-119)	Δ*camk-2::hph; mat A*	Fertile
13.	Δ*camk-2::hph; camk-2::bar; mat A* (HOP-116)	Δ*camk-2::hph; mat a*	Fertile
14.	Δ*camk-2::hph; camk-2::bar; mat A* (HOP-120)	Δ*camk-2::hph; mat a*	Fertile
15.	Δ*camk-2::hph; mat A*	Δ*camk-2::hph; camk-2::bar; mat a* (HOP-102)	Fertile

16.	Δ*camk-2::hph; mat A*	Δ*camk-2::hph; camk-2::bar; mat a* (HOP-119)	Fertile
17.	Δ*camk-2::hph; mat a*	Δ*camk-2::hph; camk-2::bar; mat A* (HOP-116)	Fertile
18.	Δ*camk-2::hph; mat a*	Δ*camk-2::hph; camk-2::bar; mat A* (HOP-120)	Fertile
19.	Δ*camk-2::hph; camk-2::bar; mat A* (HOP-120)	Δ*camk-2::hph; camk-2::bar; mat a* (HOP-102)	Fertile
20.	Δ*camk-2::hph; camk-2::bar; mat a* (HOP-102)	Δ*camk-2::hph; camk-2::bar; mat A* (HOP-116)	Fertile
21.	Δ*camk-2::hph; camk-2::bar; mat a* (HOP-119)	Δ*camk-2::hph; camk-2::bar; mat A* (HOP-120)	Fertile
22.	Δ*camk-2::hph; camk-2::bar; mat a* (HOP-102)	Δ*camk-2::hph; camk-2::bar; mat A* (HOP-120)	Fertile
23.	Δ*camk-2::hph; camk-2*^{S247A}*::bar; mat A* (HOP-17)	Wild-type; *mat a*	Fertile
24.	Δ*camk-2::hph; camk-2*^{S247A}*::bar; mat a* (HOP-51)	Wild-type; *mat A*	Fertile
25.	Wild-type; *mat a*	Δ*camk-2::hph; camk-2*^{S247A}*::bar; mat A* (HOP-17)	Fertile
26.	Wild-type; *mat A*	Δ*camk-2::hph; camk-2*^{S247A}*::bar; mat a* (HOP-51)	Fertile
27.	Δ*camk-2::hph; camk-2*^{S247A}*::bar; mat A* (HOP-17)	Δ*camk-2::hph; mat a*	Intermediate
28.	Δ*camk-2::hph; camk-2*^{S247A}*::bar; mat a* (HOP-51)	Δ*camk-2::hph; mat A*	Intermediate

29.	Δ*camk-2::hph; mat a* (HOP-17)	Δ*camk-2::hph; camk-2*^{S247A}*::bar; mat A* (HOP-17)	Intermediate
30.	Δ*camk-2::hph; mat A* (HOP-51)	Δ*camk-2::hph; camk-2*^{S247A}*::bar; mat a* (HOP-51)	Intermediate
31.	Δ*camk-2::hph; camk-2*^{S247A}*::bar; mat A* (HOP-17)	Δ*camk-2::hph; camk-2*^{S247A}*::bar; mat a* (HOP-51)	Intermediate
32.	Δ*camk-2::hph; camk-2*^{S247A}*::bar; mat a* (HOP-51)	Δ*camk-2::hph; camk-2*^{S247A}*::bar; mat A* (HOP-17)	Intermediate
33.	Δ*camk-2::hph; camk-2*^{T267A}*::bar; mat a* (HOP-12)	Wild-type; *mat A*	Fertile
34.	Δ*camk-2::hph; camk-2*^{T267A}*::bar; mat A* (HOP-19)	Wild-type; *mat a*	Fertile
35.	Wild-type; *mat A*	Δ*camk-2::hph; camk-2*^{T267A}*::bar; mat a* (HOP-12)	Fertile
36.	Wild-type; *mat a*	Δ*camk-2::hph; camk-2*^{T267A}*::bar; mat A* (HOP-19)	Fertile
37.	Δ*camk-2::hph; camk-2*^{T267A}*::bar; mat a* (HOP-12)	Δ*camk-2::hph; mat A*	Intermediate
38.	Δ*camk-2::hph; camk-2*^{T267A}*::bar; mat A* (HOP-19)	Δ*camk-2::hph; mat a*	Intermediate
39.	Δ*camk-2::hph; mat A*	Δ*camk-2::hph; camk-2*^{T267A}*::bar; mat a* (HOP-12)	Intermediate

40.	Δ*camk-2::hph; mat a*	Δ*camk-2::hph; camk-2*^{T267A}*::bar; mat A* (HOP-19)	Intermediate
41.	Δ*camk-2::hph; camk-2*^{T267A}*::bar; mat a* (HOP-12)	Δ*camk-2::hph; camk-2*^{T267A}*::bar; mat A* (HOP-19)	Intermediate
42.	Δ*camk-2::hph; camk-2*^{T267A}*::bar; mat A* (HOP-19)	Δ*camk-2::hph; camk-2*^{T267A}*::bar; mat a* (HOP-12)	Intermediate
43.	Δ*camk-2::hph; camk-2*^{L309D}*::bar; mat A* (HOP-4)	Wild-type; *mat a*	Fertile
44.	Δ*camk-2::hph; camk-2*^{L309D}*::bar; mat A* (HOP-37)	Wild-type; *mat a*	Fertile
45.	Δ*camk-2::hph; camk-2*^{L309D}*::bar; mat a* (HOP-34)	Wild-type; *mat A*	Fertile
46.	Δ*camk-2::hph; camk-2*^{L309D}*::bar; mat a* (HOP-36)	Wild-type; *mat A*	Fertile
47.	Wild-type; *mat a*	Δ*camk-2::hph; camk-2*^{L309D}*::bar; mat A* (HOP-4)	Fertile
48.	Wild-type; *mat a*	Δ*camk-2::hph; camk-2*^{L309D}*::bar; mat A* (HOP-37)	Fertile
49.	Wild-type; *mat A*	Δ*camk-2::hph; camk-2*^{L309D}*::bar; mat a* (HOP-34)	Fertile
50.	Wild-type; *mat A*	Δ*camk-2::hph; camk-2*^{L309D}*::bar; mat a* (HOP-36)	Fertile

51.	Δ*camk-2::hph; camk-2*^{L309D}*::bar; mat A* (HOP-4)	Δ*camk-2::hph; mat a*	Fertile
52.	Δ*camk-2::hph; camk-2*^{L309D}*::bar; mat A* (HOP-37)	Δ*camk-2::hph; mat a*	Fertile
53.	Δ*camk-2::hph; camk-2*^{L309D}*::bar; mat a* (HOP-34)	Δ*camk-2::hph; mat A*	Fertile
54.	Δ*camk-2::hph; camk-2*^{L309D}*::bar; mat a* (HOP-36)	Δ*camk-2::hph; mat A*	Fertile
55.	Δ*camk-2::hph; mat a*	Δ*camk-2::hph; camk-2*^{L309D}*::bar; mat A* (HOP-4)	Fertile
56.	Δ*camk-2::hph; mat a*	Δ*camk-2::hph; camk-2*^{L309D}*::bar; mat A* (HOP-37)	Fertile
57.	Δ*camk-2::hph; mat A*	Δ*camk-2::hph; camk-2*^{L309D}*::bar; mat a* (HOP-34)	Fertile
58.	Δ*camk-2::hph; mat A*	Δ*camk-2::hph; camk-2*^{L309D}*::bar; mat a* (HOP-36)	Fertile
59.	Δ*camk-2::hph; camk-2*^{L309D}*::bar; mat A* (HOP-4)	Δ*camk-2::hph; camk-2*^{L309D}*::bar; mat a* (HOP-34)	Fertile
60.	Δ*camk-2::hph; camk-2*^{L309D}*::bar; mat A* (HOP-37)	Δ*camk-2::hph; camk-2*^{L309D}*::bar; mat a* (HOP-34)	Fertile
61.	Δ*camk-2::hph; camk-2*^{L309D}*::bar; mat A* (HOP-37)	Δ*camk-2::hph; camk-2*^{L309D}*::bar; mat a* (HOP-36)	Fertile

62.	Δ*camk-2::hph; camk-2*^{L309D}*::bar; mat A* (HOP-4)	Δ*camk-2::hph; camk-2*^{L309D}*::bar; mat a* (HOP-36)	Fertile

[a]Adapted from Laxmi and Tamuli 2016

5.2.4 Expression studies of the *cmd*, *trm-9* and *nca-2* gene in selected Ca^{2+}-signaling knockout mutant strains

I performed expression analysis of the *cmd*, *trm-9* and *nca-2* gene (Table 5.4) in other Ca^{2+}-signaling gene knockout mutant strains. Fold changes in expression was calculated by $2^{-\Delta\Delta C}{}_T$ method, using wild-type and β-tubulin as calibrator and endogenous control respectively (as desribed I materials and methods). I found that fold change expression of the *cmd* gene was high in the Δ*splA2* and Δ*ncs-1* knockout mutants (Figure 5.15A; Appendix Table 1). Additionally, in the Δ*splA2*, Δ*cpe-1* and Δ*ncs-1* knockout mutants, fold change expression of *trm-9* gene was high (Figure 5.15B; Appendix Table 1), whereas, fold change expression of *nca-2* gene was high in the Δ*camk-2*, Δ*cpe-1* and Δ*ncs-1* knockout mutants (Figure 5.15C; Appendix Table 1).

Table 5.4: Primers used for real-time PCR analysis

Sl. no.	Primer	Target Gene	Sequence (5'→ 3')
1.	RT-NCU04054-F	β-tubulin	TTGAGGACCAGATGCGCAAC
2.	RT-NCU04054-R		TTGAAGAGCTCCTGGATGGC
3.	RT-NCU04379-F	*ncs-1*	CAGTTCTTCCCCTTTGGCGA
4.	RT-NCU04379-R		CGAGCTTGTCCTCCATCTTG
5.	RT-NCU04898-F	*trm-9*	CCTCTCTACCTCCACGCCTA
6.	RT-NCU04898-R		CCAAACAAAGGTCCATTCCT
7.	RT-NCU06245-F	*plc1*	GCACGGGTACACGCTAACTA
8.	RT-NCU06245-R		TCGAGACTGACGATCAGAGG
9.	RT-NCU04736-F	*nca-2*	GAGATGACTCCTCTCCAGTC
10.	RT-NCU04736-R		GGAGTGTGCTGTGATTTGGG
11.	RT-NCU06650-R	s*plA2*	AAACCATCCAGCAGACGACG
12.	RT-NCU06650-R		CATGACGATTGCAAGCAGGC

13.	RT-NCU06177-F	*camk-3*	CTTTGCCCGAGGAACAATGC
14.	RT-NCU06177-R		GGAGACTCCAAAGTCGACGA
15.	RT-NCU06703-F	*mid-1*	GCTCGCGGATCGATGAGTTT
16.	RT-NCU06703-R		ATTGAACCCCTTCTGGCCAG
17.	RT-NCU09212-F	*camk-4*	TAGTGAGGATCTCTCCAGGC
18.	RT-NCU09212-R		ATCACCTGGCTGCTTGGGTT
19.	RT-NCU02283-F	*camk-2*	GCAGCCGTGTCGATACAAAG
20.	RT-NCU02283-R		ACCTTCTTGAGCACGGCGAT
21.	RT-NCU04120-F	*cmd*	GTGAGGCCTTCAAGGTGTTC
22.	RT-NCU04120-R		CGTCATCAGTGAGCTTCTCG
23.	RT-NCU06366-F	*cpe-1*	CCGCTGTCTTGCTCATCATC
24.	RT-NCU06366-R		GATCAGAGTGAGGCGATGAC
25.	RT-NCU09123-F	*camk-1*	CGCCAACATGCTTAATCGCC
26.	RT-NCU09123-R		GAACCATCTGTTCGTTGCCC

(A)

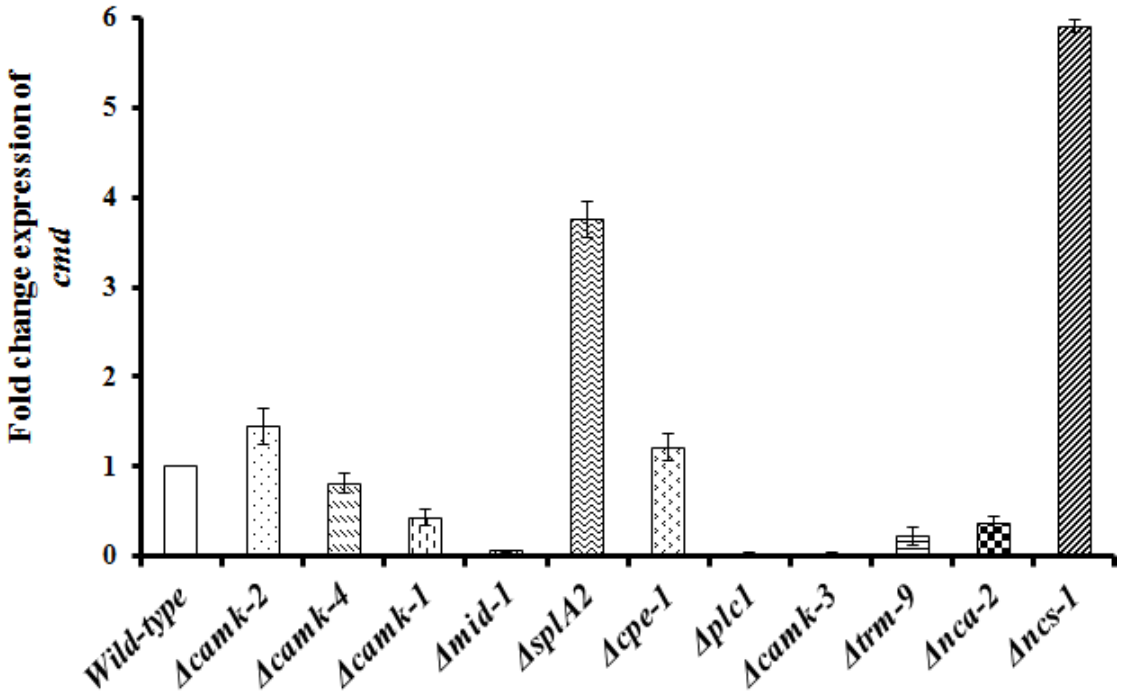

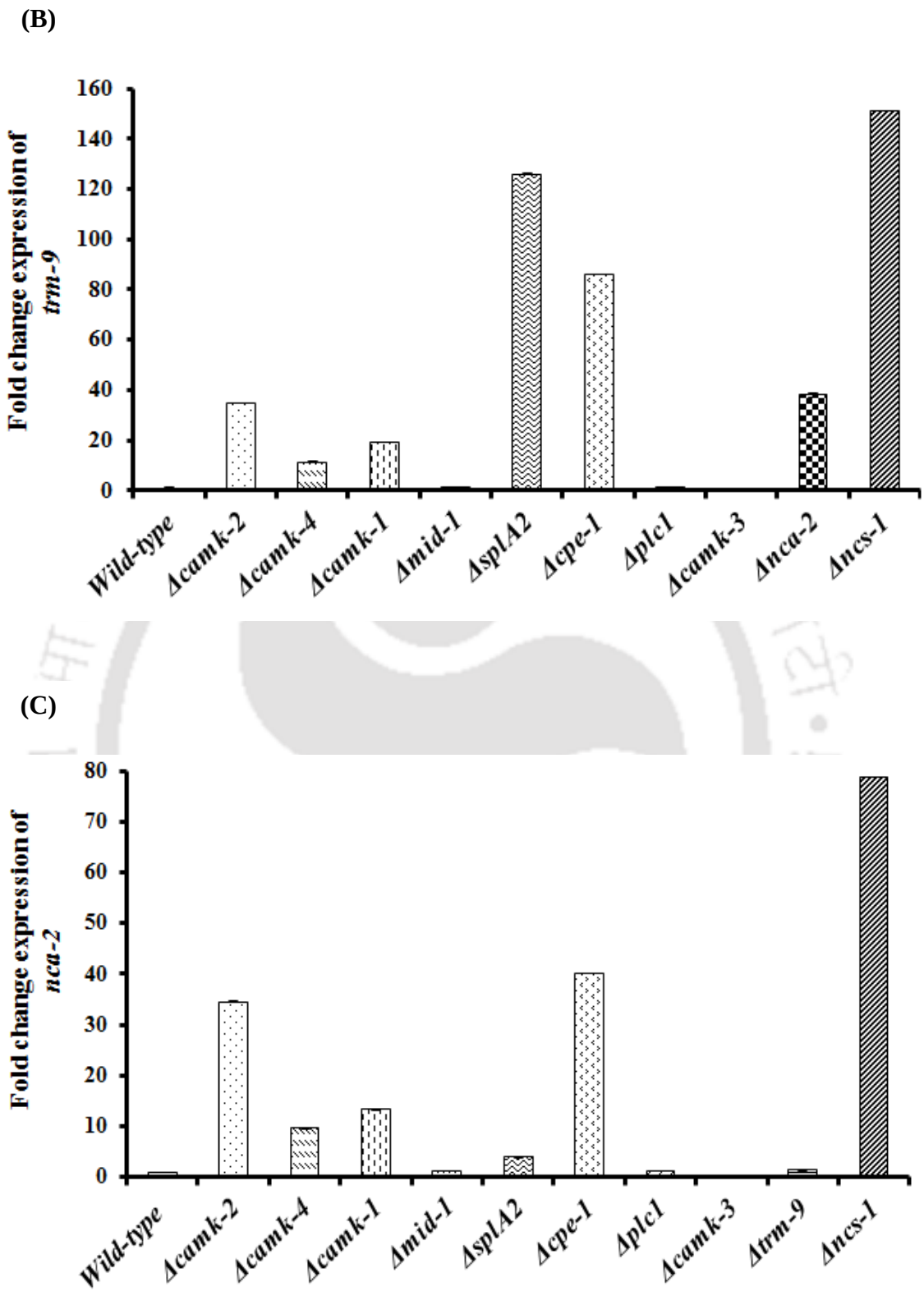

Figure 5.15: Fold change in expression of (A) *cmd*, (B) *trm-9* and (C) *nca-2* genes in selected Ca^{2+}-signaling knockout mutants. Real-time PCR was performed with the

RNA of wild-type and knockout mutants. Fold change was calculated by $2^{-\Delta\Delta C_T}$, using wild-type and β-tubulin as calibrator and endogenous control respectively (Livak and Schmittgen 2001). Standard errors calculated from the data for two independent experiments are shown using error bars.

5.2.5 Expression studies of selected Ca^{2+}-signaling genes in the Δ*trm-9* and Δ*nca-2* knockout mutants

I also studied the fold change expression of various important Ca^{2+}-signaling genes in the Δ*trm-9* and Δ*nca-2* knockout mutants. Interestingly, fold change expression of the *nca-2* genes was high in the Δ*trm-9* mutant (Figure 5.16A; Appendix Table 2), as well as fold change expression of the *trm-9* gene was high in the Δ*nca-2* mutant background (Figure 5.16B; Appendix Table 2).

(A)

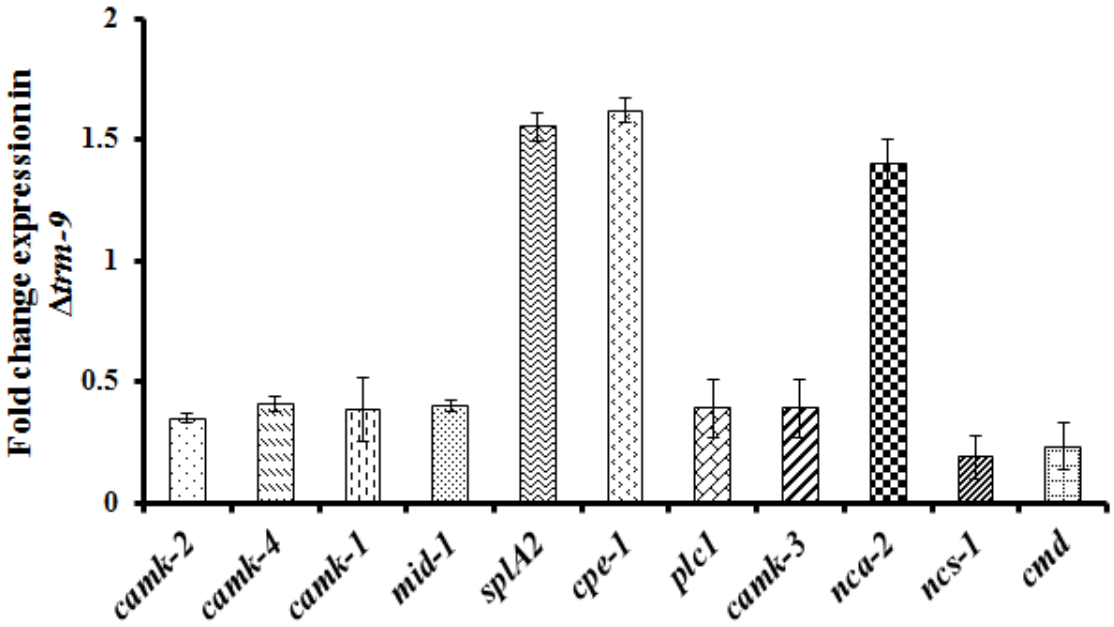

(B)

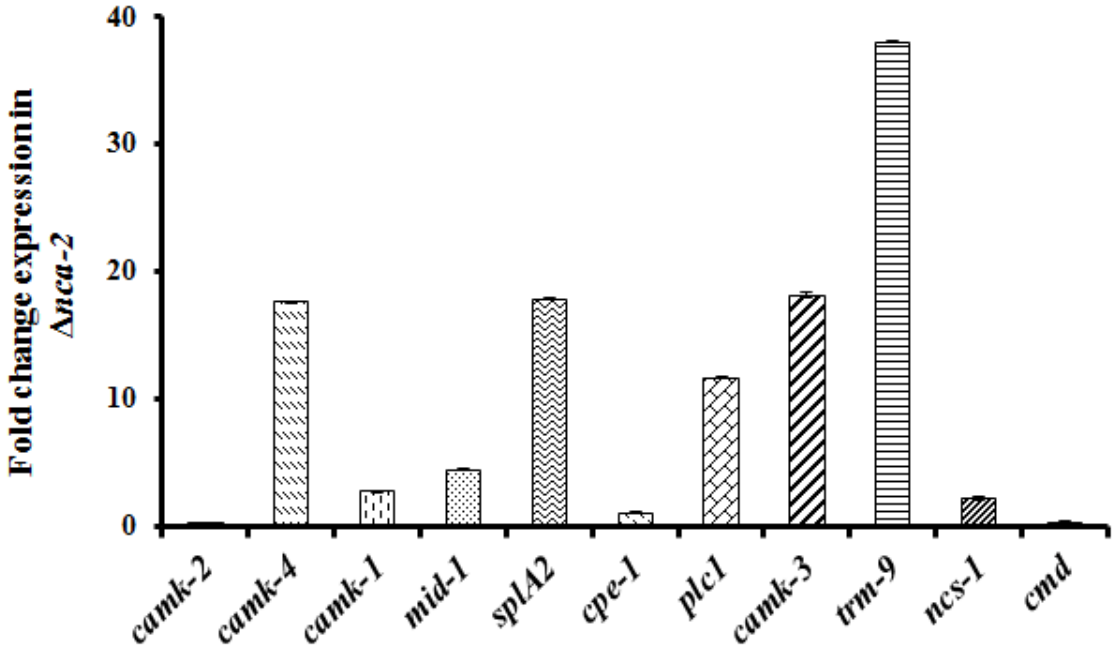

Figure 5.16: Fold change profile of selected Ca^{2+}-signaling genes in (A) Δ*trm-9* and (B) Δ*nca-2* knockout mutants. Real-time PCR was performed for various targeted genes with RNA isolated from the Δ*trm-9* and Δ*nca-2* mutants. Fold change was calculated by $2^{-\Delta\Delta Ct}$, using wild-type and β-tubulin as calibrator and endogenous control respectively (Livak and Schmittgen 2001). Standard errors calculated from the data for two independent experiments are shown using error bars.

5.2.6 Expression studies of *cmd*, *trm-9* and *nca-2* gene in double mutant strains

Next, I analyzed expression levels of the *cmd*, *trm-9* and *nca-2* genes in double knockout mutants Δ*camk-2*Δ*camk-3*, Δ*camk-2*Δ*camk-1* and Δ*trm-9*Δ*nca-2*, to evaluate the effect of double mutations in the expression of these genes, which showed that, fold change expression of the *cmd* gene was low in all three double mutants, but *cmd* expression was lowest in Δ*trm-9*Δ*nca-2* (Figure 5.17A; Appendix Table 3). In addition, fold change expression level of the *trm-9* gene was high in the Δ*camk-2*Δ*camk*-3 double mutant (Figure 5.17B; Appendix Table 3), whereas fold change expression of the *nca-2* gene was high in the Δ*camk-1*Δ*camk*-2 double mutant (Figure 5.17C; Appendix Table 3).

(A)

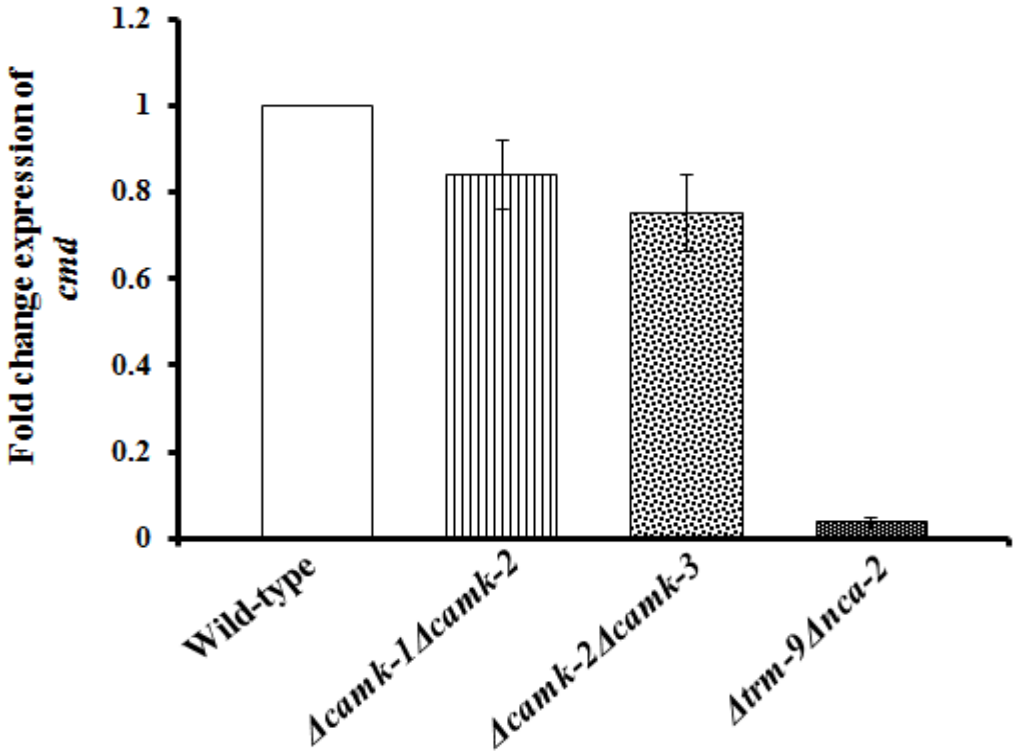

(B)

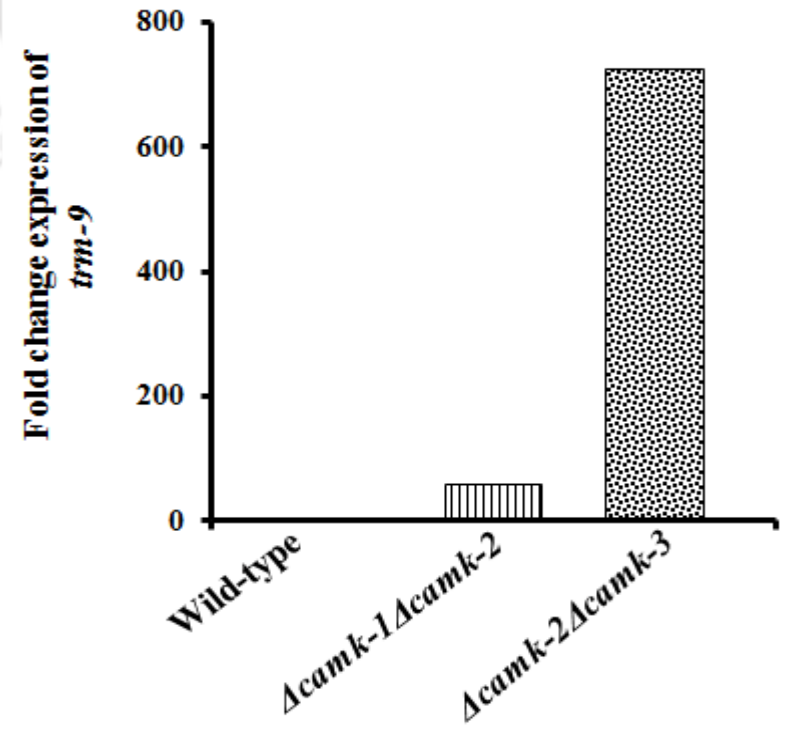

(C)

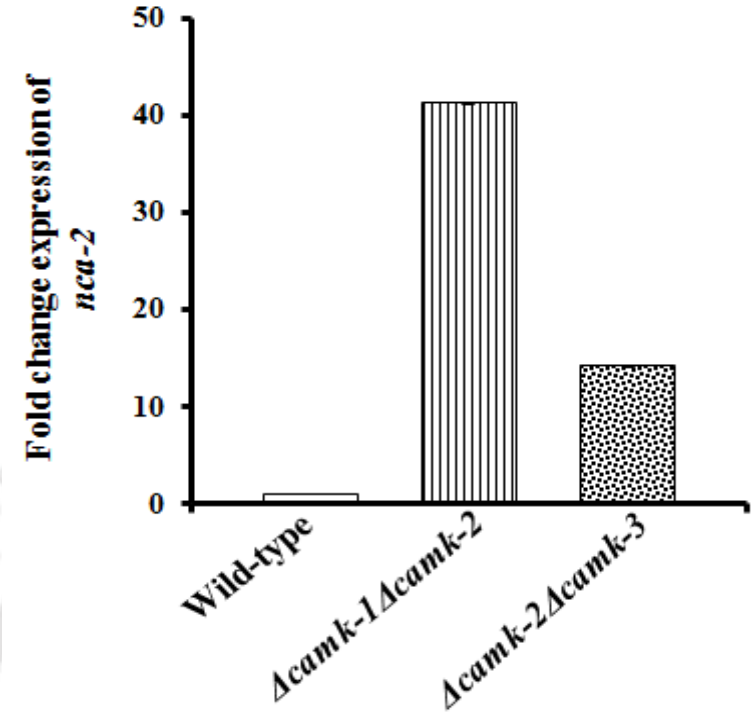

Figure 5.17: Fold change in expression profile of (A) *cmd*, (B) *trm-9* and (C) *nca-2* gene in the double knockout mutant strains. Real-time PCR was performed with the RNA isolated from the wild-type and double mutant strains. Fold change was calculated by $2^{-\Delta\Delta C_T}$, using wild-type and β-tubulin as calibrator and endogenous control respectively (Livak and Schmittgen 2001). Standard errors calculated from the data for two independent experiments are shown using error bars.

5.2.7 Expression profile of selected genes in wild-type, Δ*trm-9*, Δ*nca-2* and Δ*trm-9*Δ*nca-2* strains in response to Ca^{2+} and UV stress

In Chapter 3, I described that the *N. crassa* homologues of the *cmd*, *trm-9* and *nca-2* genes play a role in growth, Ca^{2+} sensitivity, UV survival, and in acquisition of thermotolerance induced by heat shock temperature. I studied expression profiles of some of the imporatnt Ca^{2+}-signaling genes in response to Ca^{2+} and UV stress in the knockout background of Δ*trm-9*, Δ*nca-2* and Δ*trm-9*Δ*nca-2* strains (Figure 5.18; Appendix Table 4). I studied the expressions profile of the *ncs-1*, *nca-2*, *mid-1*, *cpe-1*,

crz1, *trm-9* and *cmd* genes in response to Ca^{2+} stress by real-time PCR by using the gene specific primers (Table 5.2). The *ncs-1* and *trm-9* genes encode neuronal calcium sensor and Ca^{2+}-ATPase protein, respectively, in *N. crassa* (Deka *et al.* 2011; Tamuli *et al.* 2011; Laxmi and Tamuli 2015). The *ncs-1* knockout mutant shows slow growth, increased sensitivity to Ca^{2+} and UV irradiation (Deka *et al.* 2011). The *N. crassa* Δ*trm-9* mutant displayed a slow growth phenotype, reduced dry weight, while the Δ*trm-9*Δ*nca-2* double mutant showed a severe growth defect and an increased sensitivity to $CaCl_2$ (Laxmi and Tamuli 2015). In addition, the *N. crassa* strain lacking the *nca-2 gene*, which encode Ca^{2+}-ATPase and a homologue of the PMCA, grew slowly in normal medium and was unable to grow in high concentrations of Ca^{2+} tolerated by the wild-type (Bowman *et al.* 2011). Furthermore, the Ca^{2+}-permeable channel protein, MID-1, a homologue of the mating-induced death (MID1) protein of *S. cerevisiae*, plays a role in regulation of ion transport via Ca^{2+} homeostasis (Lew *et al.* 2008). Another important gene, *crz-1* encodes the *N. crassa* homologue of the zinc finger transcription factor, CRZ-1. In response to high level of cytosolic free Ca^{2+} ($[Ca^{2+}]_c$), cytoplasmically localized CRZ-1 is dephosphorylated by CNA, a Ca^{2+}-dependent phosphatase, and results in nuclear translocation of dephosphorylated CRZ-1. In yeast, the nuclear localized CRZ-1 then activates the expression of genes possessing the 5'-GNGGC(G/T)CA-3' consensus sequence for the calcineurin-dependent response elements (CDREs) in their promoters (Matheos *et al.* 1997; Stathopoulos and Cyert 1997; Serrano *et al.* 2002).

Strains were grown in the VGM that contains 0.68 mM Ca^{2+} as control, and in the VGM supplemented with 0.2 M $CaCl_2$ was used to evaluate the Ca^{2+} stress response. Fold change in expression of the genes in the control VGM medium and in the VGM medium supplemented with 0.2 M $CaCl_2$ were compared. Fold change expression profile of these genes in response to Ca^{2+} stress showed the complex genetic interactions between genes (Figure 5.18; Appendix Table 4). The major outcome of this experiment was that the expression level of the *cmd* gene was low in wild-type, Δ*trm-9* and Δ*nca-2* strain, but its fold change in expression was higher in the Δ*trm-9*Δ*nca-2* double mutant during Ca^{2+} stress (Figure 5.18D; Appendix Table 4).

(A)

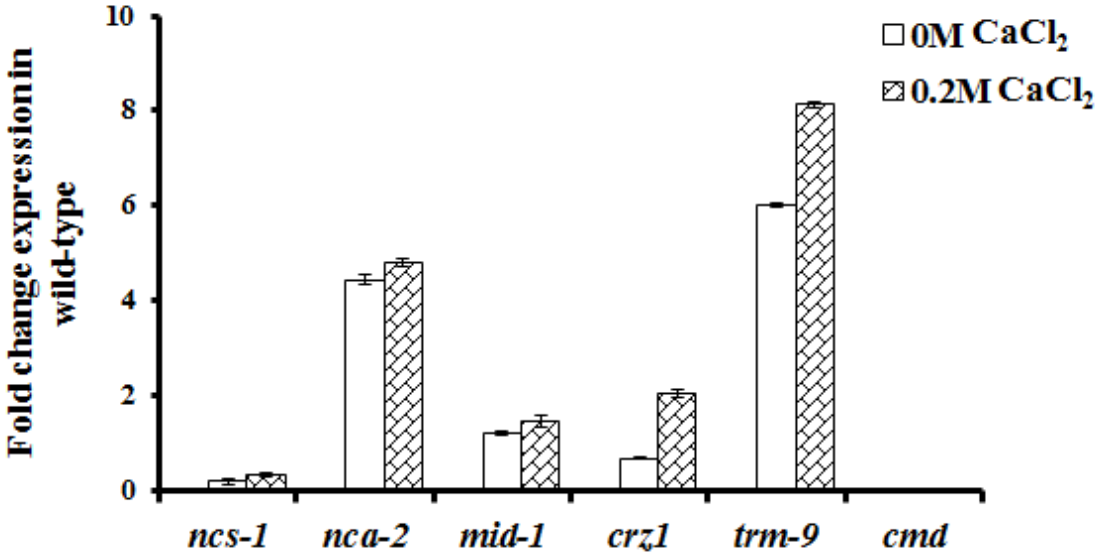

(B)

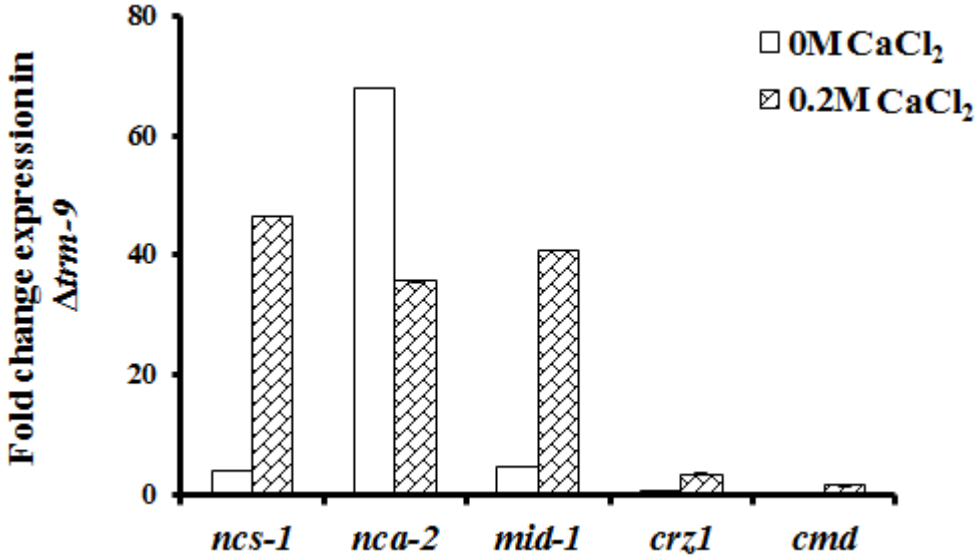

(C)

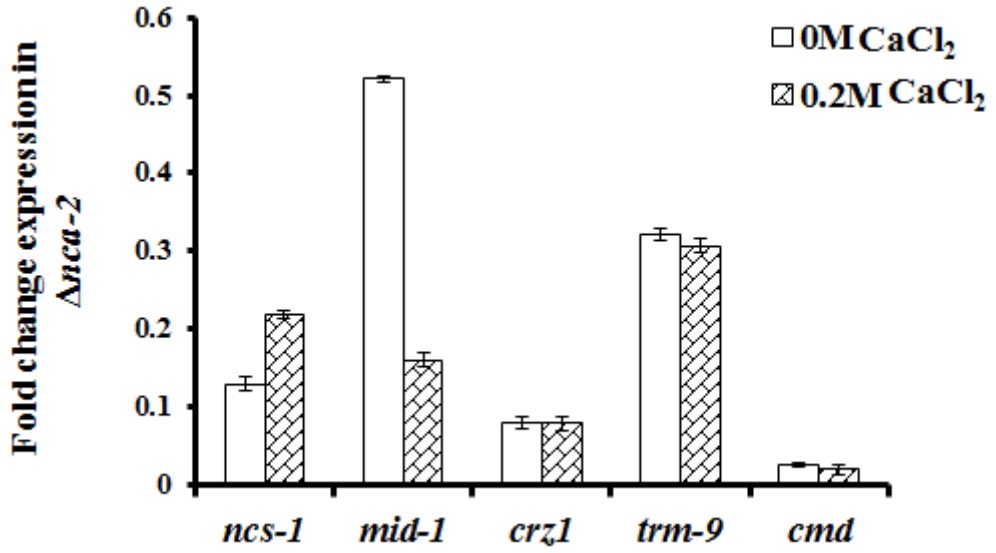

(D)

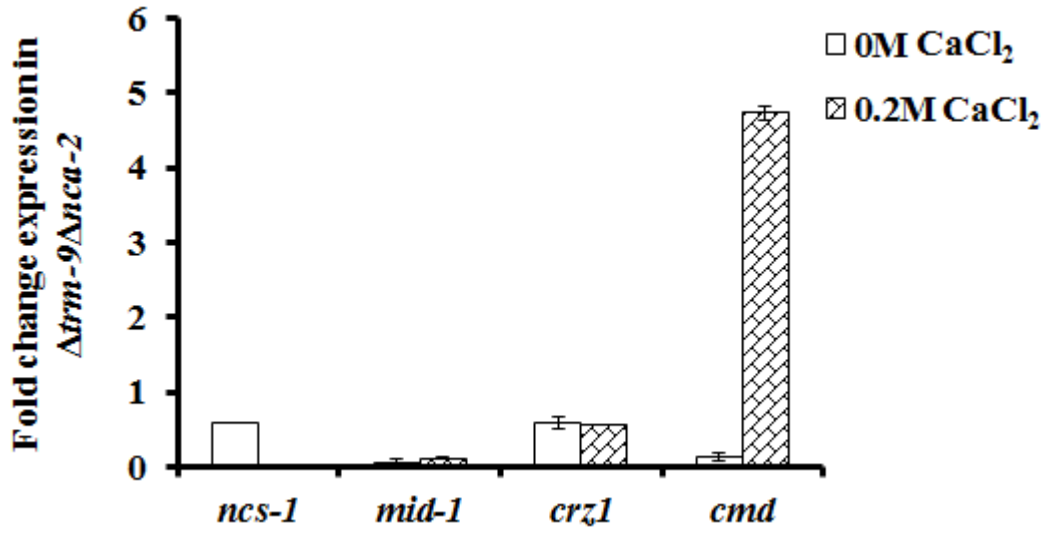

Figure 5.18: Fold change in expression profile of selected Ca^{2+}-signaling genes in (A) wild-type (B) Δ*trm-9* and (C) Δ*nca-2* (C) Δ*trm-9*Δ*nca-2* strains in response to Ca^{2+} stress. Strains were cultured for 16 h at 30°C and transferred in VGM lacking $CaCl_2$ and in VGM medium supplemented with 0.2 M $CaCl_2$ for 30 minutes for growth. Real-

time PCR was performed with the RNA of wild-type and double mutant strains. Fold change was calculated by $2^{-\Delta\Delta C_T}$ method using expression of each gene in normal VGM (contains 0.68 mM $CaCl_2$) and β-tubulin as calibrator and endogenous control respectively (Livak and Schmittgen 2001). Standard errors calculated from the data for two independent experiments are shown using error bars.

In addition, I also performed the expression analysis of the *cmd* and *upr-1* genes in exposure to UV irradiation in the knockout background of Δ*trm-9*, Δ*nca-2* and Δ*trm-9*Δ*nca-2* strains (Figure 5.19; Appendix Table 5). In chapter 4, I discussed that *N. crassa* CaM protein could be involved in UV-induced DNA damage repair process like the *upr-1* gene that plays a major role in UV-induced DNA repair and mutagenesis through the bypass of (6-4) photoproducts (Sakai *et al.* 2002, 2003; Tamuli *et al.* 2006). The *upr-1* mutant is 3 to 4 times less viable than the wild-type on exposure to UV irradiation. The *upr-1* gene is inducible by UV, and its transcript appeared within 15 min after UV irradiation, attained its maximum 30 min after UV irradiation, and then decreased gradually in the wild-type, suggesting that the *upr-1* gene product functions at an early stage of the response to UV irradiation (Sakai *et al.* 2002, 2003). Similar to the Ca^{2+} stress, the fold change expression of the *cmd* gene was high in the Δ*trm-9*Δ*nca-2* double mutant relative to the parental and wild-type strain in response to the UV dose up to 150 J/m^2. In addition, the expression level of the *cmd* gene was higher relative to the *upr-1* gene expression in different doses of UV energy in the Δ*trm-9*Δ*nca-2* double mutant strain (Figure 5.19D; Appendix Table 5). Thus, the expression analysis supports a role of the *cmd* gene in UV survival of *N. crassa*.

(A)

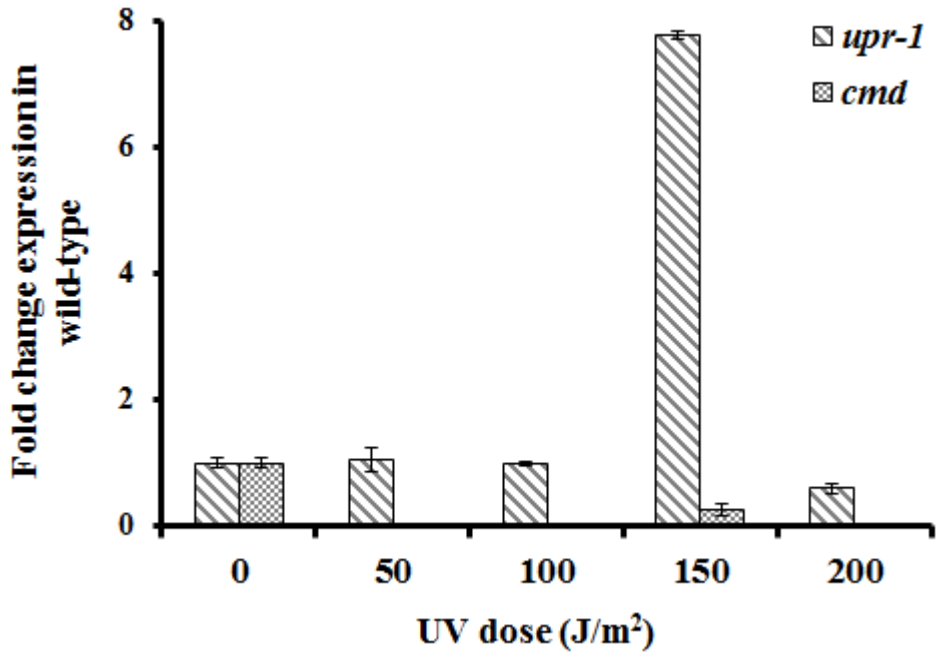

(B)

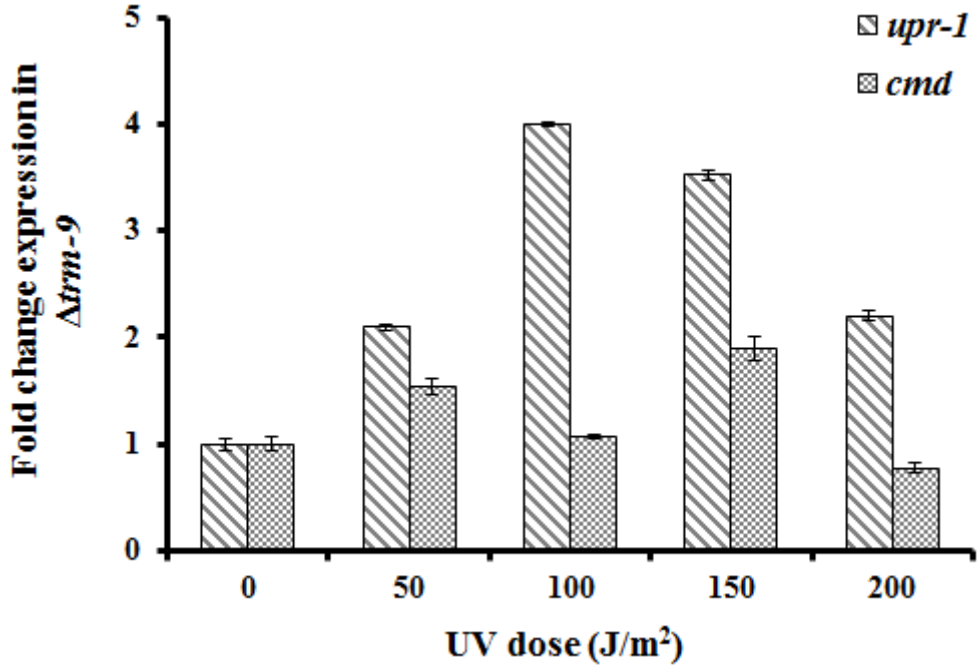

(C)

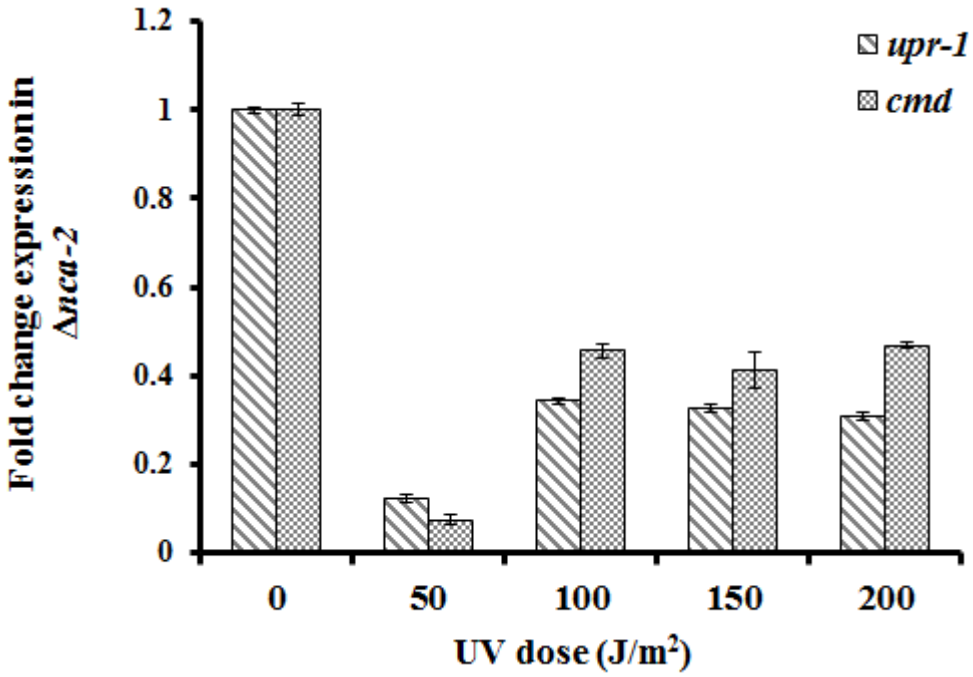

(D)

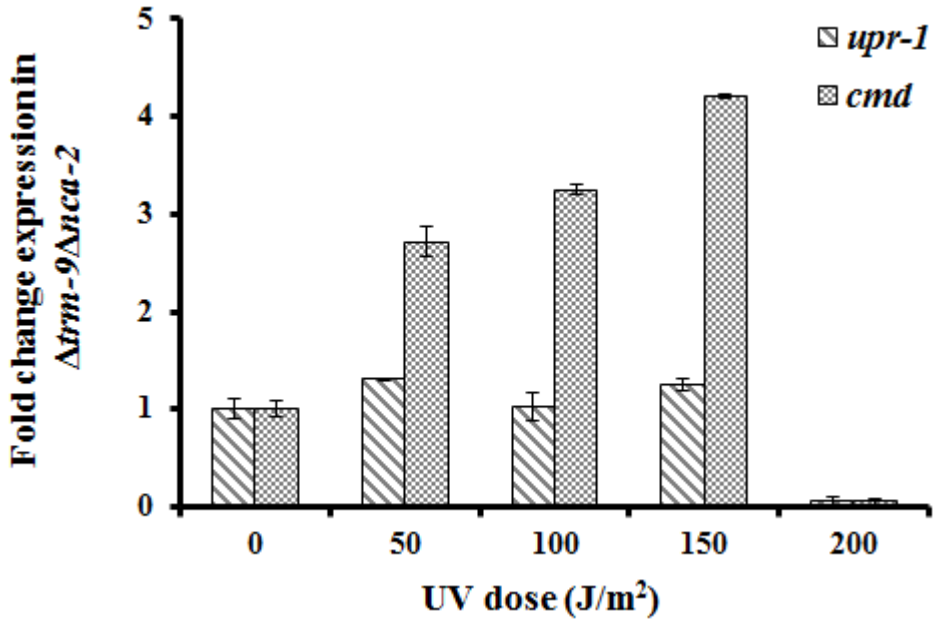

Figure 5.19: Fold change in expression profile of *upr-1* and *cmd* gene in (A) wild-type, (B) Δ*trm-9*, (C) Δ*nca-2* and (D) Δ*trm-9*Δ*nca-2* strains in response to UV stress.

Strains were cultured for 16 h at 30°C and irradiated with different UV light at a different dose (0 J/m^2, 50 J/m^2, 100 J/m^2, 150 J/m^2, 200 J/m^2) in fresh VGM and further cultured for 30 minutes. Real-time PCR was performed with the RNA of wild-type and double mutant strains. Fold change was calculated by $2^{-\Delta\Delta C_T}$ method using expression of the *upr-1* and the *cmd* gene in 0 J/m^2 and β-tubulin as calibrator and endogenous control respectively (Livak and Schmittgen 2001). Standard errors calculated from the data for two independent experiments are shown using error bars.

5.3 Discussion

In this study, I had performed site-directed mutational analysis of Ca^{2+}/CaMK-2 to identify the key amino acid residues for fertility. Members of the CaM-kinase family are all classified as Ser/Thr kinases (Swulius and Waxham 2008). The Ca^{2+}/CaMK-2 of *N. crassa* possesses nine potential serine/threonine autophosphorylation sites (Deka *et al.* 2011; Kumar and Tamuli 2014). In the *N. crassa* Ca^{2+}/CaMK-2, the threonine 267 and serine 247 are the potential autophosphorylation sites adjacent to the CaM-binding domain and contain the $^{R}_{K}XX^{T}_{S}$ consensus sequence (Figure 5.8; Kim *et al.* 1998). I replaced these two putative autophosphorylation sites of the *N. crassa* Ca^{2+}/CaMK-2 with non-phosphorylable alanine and examined its effects on fertility. The *camk-2*^{S247A} and the *camk-2*^{T267A} mutants in homozygous cross, or in a cross with a Δ*camk-2* mutant, displayed an intermediate phenotype, suggesting that these mutant alleles act in a recessive manner, and phosphorylation of serine 247 and threonine 267 play a role in full fertility in *N. crassa* (Figure 5.14; Table 5.3).

The homologues of the Ca^{2+}/CaMK-2 in other organisms were also studied previously. It was found that in the rat Ca^{2+}/CaM kinase II, threonine 286, which is adjacent to the CaM-binding domain (Lin *et al.* 1987), autophosphorylation is indispensable for transition to an autonomous kinase (Schworer *et al.* 1988; Hanson *et al.* 1989). The initial phosphorylation at threonine 286 is followed by the phosphorylation at serine 279 in the rat Ca^{2+}/CaM kinase II (Miller *et al.* 1988; Hanson *et al.* 1989). Moreover, in the absence of autophosphorylation, such as in the T286L mutant, removal of Ca^{2+}/CaM results in a rapid deactivation of the kinase in COS cells (Hanson *et al.* 1989; Hanson and Schulman 1992). In *N. crassa*, there is no conserved phosphorylation sites of threonine at 286 and serine at 279 position. The autoinhibitory and CaM-binding

domains overlap slightly and binding of Ca^{2+}/CaM regulates functioning of the autoinhibitory domain (Swulius and Waxham 2008).

I also studied the effect of the L309D mutation, located in the CaM-binding domain, of the Ca^{2+}/CaMK-2 in *N. crassa*. The CaM-binding sequences of the Ca^{2+}/CaM kinases usually contain basic and hydrophobic amino acid residues, but lack acidic amino acid residues (Colbran and Soderling 1990; Cruzalegui *et al.* 1992; Ikura *et al.* 1992; Rhoads and Friedberg 1997; Tokumitsu *et al.* 2000). In the rat Ca^{2+}/CaMK kinase, mutations of three consecutive residues, valine, lysine, and leucine to triple aspartic acid in the CaM-binding domain reduced the binding ability of Ca^{2+}-CaM, probably because of an intermolecular electrostatic repulsion (Tokumitsu *et al.* 1997, 2000). I found that the crosses homozygous and heterozygous for the *camk-2*^{L309D} were fertile, indicating that leucine at position 309 might be non-essential for CaMK-2 and CaM interaction and dispensable full fertility of *N. crassa* (Figure 5.14; Table 5.3).

In addition, expression analysis of the *cmd, trm-9, nca-2* and others selected genes indicates the complex genetic interactions between Ca^{2+}-signaling genes (Figure 5.15-5.17; Appendix Table 1-3), which was supported by the STRING analysis of cmd (Figure 5.3), trm-9 (Figure 5.4) and nca-2 (Figure 5.5). Fold change expression profile of the *cmd, ncs-1, trm-9, nca-2, mid-1* and *crz-1* gene in response to Ca^{2+} stress showed a difference in the expression pattern in wild-type, Δ*trm-9,* Δ*nca-2* and Δ*trm-9*Δ*nca-2* strain (Figure 5.18; Appendix Table 4). Moreover, fold change expression of the *cmd* gene was high in Δ*trm-9*Δ*nca-2* double mutant background as compared to parental and wild-type strain in response to UV energy till 150 J/m^2. In addition, expression level of the *cmd* gene was higher than the *upr-1* gene expression in different doses of UV irradiation in the Δ*trm-9*Δ*nca-2* double mutant background (Figure 5.19D). Thus, the expression analysis provided additional evidences in support of expression of the *cmd,* like the *upr-1* gene in response to UV survival. CPDs and (6-4) photoproducts at 5'-CC-3' and 5'-TC-3' sites, are the major types of DNA damage produced by UV irradiation in both yeast and human DNA and cause cytotoxic, mutagenic and carcinogenic effects (Sancar 1994; Shimura *et al.* 1999; Yu *et al.* 2001). UV-induced mutations occur primarily by 3' C to T transitions. Genetic studies reveal a role for yeast Pol η in the error-free bypass of CPDs and (6-4) photoproducts formed at CC and TC sites (Yu *et al.* 2001). There is no TC (6-4) photolyase activity in *N. crassa* (Shimura *et al.* 1999), which was found first in *Drosophila melanogaster* (Todo *et al.* 1993). The (6-4) photoproducts are removed by the dark repair systems in *N. crassa*. When the replication

machinery encounters (6-4) photoproducts during replication, the error-prone DNA polymerase ζ (pol ζ) and other DNA translesion synthesis (TLS) polymerase (s) might bypass these lesions efficiently in the wild-type, but not in the *upr-1* mutant due to its partial photoreactivation defect (PPD). The PPD phenotype of the *upr-1* mutant is due to lack of efficient bypass of (6-4) photoproducts, which suggest that *upr*-1 gene product functions in damage-induced mutagenesis as an error-prone DNA polymerase in *N. crassa* (Sakai *et al.* 2002, 2003). CaM also plays a central role in mediating macrophage radioresistance, where increases in CaM abundance in response to a single dose of ionizing radiation enhances DNA repair pathways involving the histone variant γH2AX by changing the balance between phosphatase and kinase. CaM dependent response pathways synergize with repair pathways activated directly by DNA damage to increase levels of histone H2AX phosphorylation. The ability of CaM dependent pathways to promote histone H2AX phosphorylation, which in turn mediates the recruitment of DNA repair proteins to sites of damage, enhances macrophage survival upon cellular irradiation. Thus, the relative amount of CaM and target proteins is likely to contribute to an integrated cellular response to radiation exposure (Charp 1987; Smallwood *et al.* 2009).

Thus, this Chapter described an essential role of the serine 247 and the threonine 267 of the Ca^{2+}/CaMK-2 for full fertility, an important role of the CaM in UV survival, and a complex interaction between Ca^{2+}-signaling genes in *N. crassa*.

A part of this chapter was published in Archives of Microbiology (Laxmi and Tamuli 2016) and presented in "National Symposium on Biophysics and Golden Jubilee Meeting of Indian Biophysical Society, 2015" held at Jamia Millia Islamia, New Delhi, India.

Additional data

Appendix Table 1: Fold change in expression of *cmd*, *trm-9* and *nca-2* gene in selected knockout mutant strains

Sl. no.	Strain	Name	Regulation (Up/ Down)		
			cmd	***trm-9***	***nca-2***
1.	ΔNCU02283	*camk-2*	Up (1.442 ± 0.20)	Up (34.655 ± 0.20)	Up (34.487 ± 0.20)
2.	ΔNCU09212	*camk-4*	Down (0.814 ± 0.11)	Up (11.321 ± 0.11)	Up (9.626 ± 0.11)
3.	ΔNCU09123	*camk-1*	Down (0.429 ± 0.09)	Up (19.306 ± 0.09)	Up (13.259 ± 0.09)
4.	ΔNCU06177	*camk-3*	Down (0.019 ± 0.02)	Down (0.421 ± 0.06)	Down (0.318 ± 0.06)
5.	ΔNCU06650	*splA2*	Up (3.760 ± 0.20)	Up (125.975 ± 0.20)	Up (3.912 ± 0.20)
6.	ΔNCU04379	*ncs-1*	Up (5.909 ± 0.07)	Up (151.062 ± 0.97)	Up (78.684 ± 0.07)
7.	ΔNCU06245	*plc1*	Down (0.033± 0.002)	Up (1.483 ± 0.002)	Up (1.264 ± 0.002)
8.	ΔNCU06703	*mid-1*	Down (0.057 ± 0.01)	Up (1.166 ± 0.01)	Up (1.199 ± 0.01)
9.	ΔNCU06366	*cpe-1*	Up (1.216 ± 0.15)	Up (85.865 ± 0.15)	Up (40.05 ± 0.04)
10.	ΔNCU04736	*nca-2*	Down (0.363 ± 0.09)	Up (38.001 ± 0.09)	-
11.	ΔNCU04898	*trm-9*	Down (0.232 ± 0.10)	-	Up (1.399 ± 0.10)

Appendix Table 2: Fold change in expression of selected Ca^{2+}-signaling genes in Δ*trm-9* and Δ*nca-2* knockout mutant strains

Sl. no.	Gene	Name	Regulation (Up/ Down)	
			Δ*trm-9*	**Δ*nca-2***
1.	NCU02283	*camk-2*	Down (0.348 ± 0.02)	Down (0.348 ± 0.03)
2.	NCU09212	*camk-4*	Down (0.405 ± 0.03)	Up (17.618 ± 0.03)
3.	NCU09123	*camk-1*	Down (0.385 ± 0.13)	Up (2.739 ± 0.009)
4.	NCU06177	*camk-3*	Down (0.389 ± 0.12)	Up (18.163 ± 0.22)
5.	NCU06650	*splA2*	Up (1.511 ± 0.06)	Up (17.864 ± 0.09)
6.	NCU04379	*ncs-1*	Down (0.189 ± 0.09)	Up (2.245 ± 0.10)
7.	NCU06245	*plc1*	Down (0.389 ± 0.12)	Up (11.704 ± 0.09)
8.	NCU06703	*mid-1*	Down (0.399 ± 0.01)	Up (4.456 ± 0.07)
9.	NCU06366	*cpe-1*	Up (1.621 ± 0.05)	Up (1.108 ± 0.06)
10.	NCU04736	*nca-2*	Up (1.399 ± 0.10)	-
11.	NCU04898	*trm-9*	-	Up (38.001 ± 0.04)
12.	NCU04120	*cmd*	Down (0.232 ± 0.10)	Down (0.363 ± 0.09)

Appendix Table 3: Fold change in expression of *cmd*, *trm-9* and *nca-2* gene in double mutant strains

Sl. no.	Strain	Name	Regulation (Up/ Down)		
			cmd	***trm-9***	***nca-2***
1.	ΔNCU09123ΔNCU02283	Δ*camk-1*Δ*camk-2*	Down (0.840 ± 0.08)	Up (57.083 ± 0.08)	Up (41.240 ± 0.08)
2.	ΔNCU02283ΔNCU06177	Δ*camk-2*Δ*camk-3*	Down (0.751 ± 0.09)	Up (726.087 ± 0.09)	Up (14.182 ± 0.09)
3.	ΔNCU04898ΔNCU04736	Δ*trm-9*Δ*nca-2*	Down (0.036 ± 0.01)	-	-

Appendix Table 4: Fold change in expression of selected genes in response to Ca^{2+} stress

Sl. no.	Gene	Name	Regulation (Up/ Down)							
			Wild-type		**Δ*trm-9***		**Δ*nca-2***		**Δ*trm-9*Δ*nca-2***	
			0M	**0.2M**	**0M**	**0.2M**	**0M**	**0.2M**	**0M**	**0.2M**
1.	NCU04379	*ncs-1*	Down (0.208 ± 0.06)	Down (0.335 ± 0.03)	Up (3.972 ± 0.01)	Up (46.59 ± 0.03	Down (0.130 ± 0.008)	Down (0.218 ± 0.005)	Down (0.586 ± 0.01)	Down (0.0008 ± 0)
2.	NCU04736	*nca-2*	Up (4.447 ± 0.09)	Up (4.809 ± 0.1)	Up (67.88 ± 0.023)	Up (35.604 ± 0.03				
3.	NCU06703	*mid-1*	Up (1.199 ± 0.04)	Up (1.454 ± 0.12)	Up (4.475 ± 0.04)	Up (40.78 ± 0.009	Down (0.520 ± 0.004)	Down (0.160 ± 0.009)	Down (0.054 ± 0.04)	Down (0.110 ± 0.009)
4.	NCU06366	*cpe-1*	Down (0.200 ± 0.06)	Down (0.483 ± 0.07)	Down (0.322 ± 0.01)	Up (1.374 ± 0.07	Down (0.262 ± 0.006)	Down (0.259 ± 0.007)	Up (1.449 ± 0.1)	Up (1.698 ± 0.07)
5.	NCU07952	*crz-1*	Down (0.694 ± 0.009)	Up (2.060 ± 0.09)	Down (0.429 ± 0.08)	Up (3.377 ± 0.09	Down (0.080 ± 0.008)	Down (0.080 ± 0.009)	Down (0.581 ± 0.08)	Down (0.561± 0.001)
6.	NCU04898	*trm-9*	Up (6.00 ± 0.05)	Up (8.134 ± 0.06)			Down (0.321 ± 0.007)	Down (0.306 ± 0.009)		
7.	NCU04120	*cmd*	Down (0.007 ± 0.001)	Down (0.007± 0.002)	Down (0.036 ± 0.03)	Up (1.404 ± 0.06	Down (0.026 ± 0.003)	Down (0.020 ± 0.006)	Down (0.137 ± 0.06)	Up (4.730 ± 0.09)

Appendix Table 5: Fold change in expression of selected genes in strains in response to UV stress

Sl. no.	Strain	Regulation (Up/ Down)									
		upr-1					***cmd***				
		UV dose (J/m^2)					**UV dose (J/m^2)**				
		0	**50**	**100**	**150**	**200**	**0**	**50**	**100**	**150**	**200**
1.	Wild-type	1 ± 0.08	Up (1.040 ± 0.19)	Down (0.989 ± 0.04)	Up (7.786 ± 0.065)	Down (0.598 ± 0.08)	1 ± 0.07	Down (0.004 ± 0.002)	Down (0.004 ± 0.001)	Down 0.258 ± 0.09	Down (0.003 ± 0.001)
2.	Δ*trm-9*	1 ± 0.058	Up (2.095 ± 0.027)	Up (4.002 ± 0.018)	Up (3.525 ± 0.047)	Up (2.199 ± 0.05)	1 ± 0.067	Up (1.536 ± 0.082)	Up (1.074 ± 0.023)	Up (1.896 ± 0.12)	Down (0.776 ± 0.04)
3.	Δ*nca-2*	1 ± 0.008	Down (0.123 ± 0.009)	Down (0.342 ± 0.008)	Down (0.327 ± 0.009)	Down (0.308 ± 0.008)	1 ± 0.014	Down (0.075 ± 0.011)	Down (0.456 ± 0.015)	Down (0.411 ± 0.04)	Down (0.469 ± 0.007)
4.	Δ*trm-9*Δ*nca-2*	1 ± 0.098	Up (1.305 ± 0.016)	Up (1.020 ± 0.14)	Up (1.247 ± 0.056)	Down (0.051 ± 0.045)	1 ± 0.079	Up (2.715 ± 0.15)	Up (3.251 ± 0.047)	Up (4.204 ± 0.021)	Down (0.051 ± 0.021)

Conclusion and Future perspectives

In this work, I studied the functions of CaM and some of its target proteins. *N. crassa* has a single CaM, which is essential for survival. Therefore, I used CaM antagonists TFP and CPZ to investigate the cellular role of CaM in *N. crassa*, I used TFP and CPZ, CaM antagonists. In addition, I generated *cmd*^{RIP} mutants that showed defect in vegetative and sexual development in *N. crassa*. Moreover, meiotic silencing of *cmd* gene resulted in barren phenotype. I also studied cellular role of *trm-9, nca-2* and *camk-2* genes in *N. crassa.*

I have shown that CaM antagonists TFP and CPZ inhibit vegetative growth and sexual development in *N. crassa.* In addition, I generated Δ*trm-9*Δ*nca-2* double mutant and analysis of the mutant phenotypes revealed that the *trm-9* and the *nca-2* genes synthetically regulate apical and aerial hyphae growth, conidia development, carotenoid accumulation, Ca^{2+} and heat stress tolerance in *N. crassa*.

I also generated *cmd*^{RIP} mutants, containing both conventional as well as unconventional RIP mutations, using RIP. Out of eight RIP-induced mutants isolated, only one mutant, the Δ*pan-2::bar::*P$_{tcu-1}$*::cmd*^{RIP}*::V5::gfp; mat A* (RIP-26) contained mutations in both the endogenous and ectopic copies of the *cmd* gene, and therefore, this mutant was used for further studies. The Δ*pan-2::bar::*P$_{tcu-1}$*::cmd*^{RIP}*::V5::gfp; mat A* (RIP-26) mutant showed a defect in vegetative growth, carotenoid accumulation, UV survival, and sexual development. Additionally, meiotic silencing studies revealed that the product of the *cmd* gene during meiosis is essential for full fertility in *N. crassa*.

In addition, I performed site-directed mutational analysis of the Ca^{2+}/CaMK-2, a target of the CaM, to identify its critical amino acid residues. I changed two potential autophosphorylation sites threonine 267 and serine 247 to alanine (T267A and S247A) in the region adjacent to the CaM-binding domain, and leucine 309 to aspartic acid (L309D) in the CaM binding domain of the Ca^{2+}/CaMK-2 protein. I studied the *N. crassa camk-2*^{S247A}, *camk-2*^{T267A}, and *camk-2*^{L209D} mutant strains and found that the serine 247 and threonine 267 phosphorylation sites are essential for full fertility in *N. crassa*. In addition, expression profiles of the *cmd, trm-9, nca-2* and other Ca^{2+}-signaling genes suggested for a complex interaction of these genes.

Therefore, in this study showed the role of CaM and its target proteins in vegetative as well as sexual development in *N. crassa*. Future work using yeast-two hybrid system and its localization studies in response to various stress conditions in *N. crassa* will enable us to determine the molecular targets of CaM. In addition, structural analysis

using various biophysical techniques such as X-ray crystallography, NMR, etc. will be helpful to understand the structure-function relationship of CaM.

References

Ahn I. P., Kim S., Choi W. B., Lee Y. H., 2003a Calcium restores prepenetration morphogenesis abolished by polyamines in *Colletotrichum gloeosporioides* infecting red pepper. FEMS Microbiology Letters 227: 237–241.

Ahn I. P., Uhm K. H., Kim S., Lee Y. H., 2003b Signaling pathways involved in preinfection development of *Colletotrichum gloeosporioides*, *C. coccodes*, and *C. dematium* pathogenic on red pepper. Physiological and Molecular Plant Pathology 63: 281–289.

Ahn I. P., Suh S. C., 2007a Calcium/calmodulin-dependent signaling for prepenetration development in *Cochliobolus miyabeanus* infecting rice. Journal of General Plant Pathology 73: 113–120.

Ahn I. P., Suh S. C., 2007b Calcium restores prepenetration morphogenesis abolished by Methylglyoxal-Bis-Guanyl Hydrazone in *Cochliobolus miyabeanus* infecting rice. Phytopathology 97: 331–337.

Alexander W. G., Raju N. B., Xiao H., Hammond T. M., Perdue T. D., Metzenberg R. L., Pukkila P. J., Shiu P. K., 2008 DCL-1 colocalizes with other components of the MSUD machinery and is required for silencing. Fungal Genetics and Biology 45: 719–727.

Altschul S. F., Gish W., Miller W., Myers E. W., Lipman D. J., 1990 Basic Local Alignment Search Tool. Journal of Molecular Biology 215: 403–410.

Altschul S. F., Madden T. L., Schäffer A. A., Zhang J., Zhang Z., Miller W., Lipman D. J., 1997 Gapped BLAST and PSI-BLAST: a new generation of protein database search programs. Nucleic Acids Research 25: 3389–3402.

Altschul S. F., Wootton J. C., Gertz E. M., Agarwala R., Morgulis A., Schäffer A. A., Yu Y., 2005 Protein database searches using compositionally adjusted substitution matrices. FEBS Journal 272: 5101–5109.

Anraku Y., Ohya Y., Iida H., 1991 Cell cycle control by calcium and calmodulin in *Saccharomyces cerevisiae*. Biochimica et Biophysica Acta 1093: 169–177.

Aramayo R., Metzenberg R. L., 1996 Meiotic transvection in fungi. Cell 86: 103–113.

Aramayo R., Peleg Y., Addison R., Metzenberg R., 1996 Asm-1^{+}, a *Neurospora crassa* gene related to transcriptional regulators of fungal development. Genetics 144: 991–1003.

Babu Y. S., Bugg C. E., Cook W. J., 1988 Structure of calmodulin refined at 2.2 Å resolution. Journal of Molecular Biology 204: 191–204.

Barbas C. F., Burton D. R., Scott J. K., Silverman G. J., 2007 Quantitation of DNA and RNA. Cold Spring Harbor Protocols 2007: pdb.ip47.

Beadle G. W., and Tatum E. L., 1941 Genetic control of biochemical reactions in Neurospora. Proc. Natl. Acad. Sci. U.S.A 27: 499–506.

Benito B., Garciadeblás B., Rodríguez-Navarro A., 2000 Molecular cloning of the calcium and sodium ATPases in *Neurospora crassa*. Molecular Microbiology 35: 1079–1088.

Berridge M. J., Bootman M. D., Peter L., 1998 Calcium – a life and death signal. Nature 395: 645–648.

Berridge M. J., Lipp P., Bootman M. D., 2000 The versatility and universality of calcium signalling. Nature reviews. Molecular cell biology 1: 11–21.

Bistoni F., Vecchiarelli A., Cenci E., Puccetti P., Marconi P., Cassone A., 1986 Evidence for macrophage-mediated protection against lethal *Candida albicans* infection. Infection and Immunity 51: 668–674.

Blankenship J. R., Wormley F. L., Boyce M. K., Schell W. A., Filler S. G., Perfect J. R., Heitman J., 2003 Calcineurin is essential for *Candida albicans* survival in serum and virulence. Eukaryotic Cell 2: 422–430.

Bootman M. D., Collins T. J., Peppiatt C. M., Prothero L. S., Mackenzie L., Smet P. De, Travers M., Tovey S. C., Jeong T., Berridge M. J., Ciccolini F., Lipp P., 2001 Calcium signalling — an overview. Cell & Developmental Biology 12: 3–10.

Borkovich K. A., Alex L. A., Yarden O., Freitag M., Turner G. E., Read N. D., Seiler S., Bell-Pedersen D., Paietta J., Plesofsky N., Plamann M., Goodrich-Tanrikulu M., Schulte U., Mannhaupt G., Nargang F. E., Radford A., Selitrennikoff C., Galagan J. E., Dunlap J. C., Loros J. J., Catcheside D., Inoue H., Aramayo R., Polymenis M., Selker E. U., Sachs M. S., Marzluf G. A., Paulsen I., Davis R., Ebbole D. J., Zelter A., Kalkman E. R., O'Rourke R., Bowring F., Yeadon J., Ishii C., Suzuki K., Sakai W., Pratt R., 2004 Lessons from the genome sequence of *Neurospora crassa*: tracing the path from genomic blueprint to multicellular organism. Microbiology and molecular biology reviews : Microbiology and Molecular Biology Reviews 68: 1–108.

Bowman B. J., Draskovic M., Freitag M., Bowman E. J., 2009 Structure and distribution of organelles and cellular location of calcium transporters in *Neurospora crassa*. Eukaryotic Cell 8: 1845–1855.

Bowman B. J., Abreu S., Margolles-Clark E., Draskovic M., Bowman E. J., 2011 Role of four calcium transport proteins, encoded by *nca-1*, *nca-2*, *nca-3*, and *cax*, in maintaining intracellular calcium levels in *Neurospora crassa*. Eukaryotic Cell 10: 654–661.

Brockerhoff S. E., Davis T. N., 1992 Calmodulin concentrates at regions of cell growth in *Saccharomyces cerevisiae*. The Journal of Cell biology 118: 619–629.

Brockerhoff S. E., Stevens R. C., Davis T. N., 1994 The unconventional myosin, Myo2p, is a calmodulin target at sites of cell growth in *Saccharomyces cerevisiae*. Journal of Cell Biology 124: 315–323.

Buchan A. D. B., Kelly V. A., Kinsman O. S., Gooday G. W., Gow N. A. R., 1993 Effect of trifluoperazine on growth, morphogenesis and pathogenicity of *Candida albicans*. Journal of Medical and Veterinary Mycology 31: 427–433.

Burnett G., Kennedy E. P., 1954 The enzymatic phosphorylation of proteins. The Journal of Biological Chemistry 211: 969–980.

Cadet J., Sage E., Douki T., 2005 Ultraviolet radiation-mediated damage to cellular DNA. Mutation Research 571: 3–17.

Cambareri E. B., Jensen B. C., Schabtach E., Selker E. U., 1989 Repeat-induced G-C to A-T mutations in Neurospora. Science 244: 1571–1575.

Carugo O., Kristina D., Rizzi M., 1993 Comparison of the co-ordinative behaviour of calcium(II) and magnesium(II) from crystallographic data. J. Chem. Soc. Dalton Trans 14: 2127–2135.

Catalanotto C., Azzalin G., Macino G., Cogoni C., 2002 Involvement of small RNAs and role of the *qde* genes in the gene silencing pathway in Neurospora. Genes & Development: 790–795.

Catalanotto C., Pallotta M., ReFalo P., Sachs M. S., Vayssie L., Macino G., Cogoni C., 2004 Redundancy of the two dicer genes in transgene-induced posttranscriptional gene silencing in *Neurospora crassa*. Molecular and Cellular biology 24: 2536–2545.

Catalanotto C., Nolan T., Cogoni C., 2006 Homology effects in *Neurospora crassa*. FEMS Microbiology Letters 254: 182–189.

Chang S. S., Zhang Z., Liu Y., 2012 RNA interference pathways in fungi: mechanisms and functions. Annual review of Microbiology 66: 305–323.

Charp P. A., 1987 DNA repair in human cells: methods for the determination of calmodulin involvement. Methods in Enzymology 139: 715–730.

Chen S., Song Y., Cao J., Wang G., Wei H., Xu X., Lu L., 2010 Localization and function of calmodulin in live-cells of *Aspergillus nidulans*. Fungal Genetics and Biology 47: 268–278.

Cheung W. Y., 1970 Cyclic 3',5'-nucleotide phosphodiesterase. Demonstration of an activator. Biochemical and Biophysical Research Communications 38: 533–538.

Chin D., Means A. R., 2000 Calmodulin: A prototypical calcium sensor. Trends in Cell Biology 10: 322–328.

Clapham D. E., 2007 Calcium Signaling. Cell 131: 1047–1058.

Cogoni C., Irelan J. T., Schumacher M., Schmidhauser T. J., Selker E. U., Macino G., 1996 Transgene silencing of the *al-1* gene in vegetative cells of Neurospora is mediated by a cytoplasmic effector and does not depend on DNA-DNA interactions or DNA methylation. The EMBO journal 15: 3153–3163.

Cogoni C., Macino G., 1997 Isolation of quelling-defective (*qde*) mutants impaired in posttranscriptional transgene-induced gene silencing in *Neurospora crassa*. Proceedings of the National Academy of Sciences 94: 10233–10238.

Cogoni C., Macino G., 1999a Gene silencing in *Neurospora crassa* requires a protein homologous to RNA-dependent RNA polymerase. Nature 399: 166–169.

Cogoni C., Macino G., 1999b Posttranscriptional gene silencing in Neurospora by a RecQ DNA helicase. Science 286: 2342–2344.

Colbran R. J., Soderling R., 1990 Calcium/calmodulin- independent auto-phosphorylation sites of calcium/calmodulin-dependent autophosphorylation protein kinase II. The Journal of Biological Chemistry 265: 11213–11219.

Colot H. V., Park G., Turner G. E., Ringelberg C., Crew C. M., Litvinkova L., Weiss R. L., Borkovich K. A., Dunlap J. C., 2006 A high-throughput gene knockout procedure for Neurospora reveals functions for multiple transcription factors. PNAS 103: 10352–10357.

Cook W. J., Walter L. J., Walter M. R., 1994 Drug binding by calmodulin: crystal structure of a calmodulin-trifluoperazine complex. Biochemistry 33: 15259–15265.

Cox J. A., Ferraz C., Demaille J. G., Perez R. O., Tuinen D. Van, Marme D., 1982 Calmodulin from *Neurospora crassa*. General properties and conformational changes. Journal of Biological Chemistry 257: 10694–10700.

Cronin S. R., Khoury A., Ferry D. K., Hampton R. Y., 2000 Regulation of HMG-CoA reductase degradation requires the P-type ATPase Cod1p/Spf1p. Journal of Cell Biology 148: 915–924.

Cruz M. C., Fox D. S., Heitman J., 2001 Calcineurin is required for hyphal elongation during mating and haploid fruiting in *Cryptococcus neoformans*. EMBO Journal 20: 1020–1032.

Cruzalegui F. H., Kapiloff M. S., Morfin J. P., Kemp B. E., Rosenfeld M. G., Means A. R., 1992 Regulation of intrasteric inhibition of the multifunctional calcium/calmodulin-dependent protein kinase. Proceedings of the National Academy of Sciences 89: 12127–12131.

Cyert M. S., 2001 Genetic analysis of calmodulin and its targets in *Saccharomyces cerevisiae*. Annual review of genetics 35: 647–672.

Datta A., 1992 What makes *Candida albicans* pathogenic? Current Science 62: 400–403.

Davies S. A, Terhzaz S., 2009 Organellar calcium signalling mechanisms in Drosophila epithelial function. The Journal of Experimental Biology 212: 387–400.

Davis R. H., de Serres F. J., 1970 Genetic and microbiological research techniques for *Neurospora crassa*. Methods in enzymology 17: 79–143.

Davis T. N., Urdea M. S., Masiarz F. R., Thorner J., 1986 Isolation of the yeast calmodulin gene: Calmodulin is an essential protein. Cell 47: 423–431.

Davis T. N., Thorner J., 1989 Vertebrate and yeast calmodulin, despite significant sequence divergence, are functionally interchangeable. Proceedings of the National Academy of Sciences of the United States of America 86: 7909–7913.

Deka R., Kumar R., Tamuli R., 2011 *Neurospora crassa* homologue of Neuronal Calcium Sensor-1 has a role in growth, calcium stress tolerance, and ultraviolet survival. Genetica 139: 885–894.

Deka R., Tamuli R., 2013 *Neurospora crassa ncs-1, mid-1* and *nca-2* double-mutant phenotypes suggest diverse interaction among three Ca^{2+}-regulating gene products. Journal of Genetics 92: 559–563.

DeMaria C. D., Soong T. W., Alseikhan B. A., Alvania R. S., Yue D. T., 2001 Calmodulin bifurcates the local Ca^{2+} signal that modulates P/Q-type Ca^{2+} channels. Nature 411: 484–489.

Díaz-Sánchez V., Estrada A. F., Trautmann D., Limón M. C., Al-Babili S., Avalos J., 2011 Analysis of *al-2* mutations in Neurospora. PLoS ONE 6: e21948.

Ding X., Yu Q., Zhang B., Xu N., Jia C., Dong Y., Chen Y., Xing L., Li M., 2014 The type II Ca^{2+}/calmodulin-dependent protein kinases are involved in the regulation of cell wall integrity and oxidative stress response in *Candida albicans*. Biochemical and Biophysical Research Communications 446: 1073–1078.

Dumesic P. A., Madhani H. D., 2014 Recognizing the enemy within: Licensing RNA-guided genome defense. Trends in Biochemical Sciences 39: 25–34.

Felsenstein J., 1985 Confidence limits on phylogenies: an approach using the bootstrap. Evolution 39: 783–791.

Flory M. R., Morphew M., Joseph J. D., Means A. R., Davis T. N., 2002 Pcp1p, an Spc110p-related calmodulin target at the centrosome of the fission yeast *Schizosaccharomyces pombe*. Cell growth and differentiation 13: 47–58.

Foss H. M., Selker E. U., 1991 Efficient DNA pairing in a Neurospora mutant defective in chromosome pairing. Molecular and General Genetics 231: 49–52.

Fox D. S., Cruz M. C., Sia R. A. L., Ke H., Cox G. M., Cardenas M. E., Heitman J., 2001 Calcineurin regulatory subunit is essential for virulence and mediates interactions with FKBP12-FK506 in *Cryptococcus neoformans*. Molecular Microbiology 39: 835–849.

Franceschini A., Szklarczyk D., Frankild S., Kuhn M., Simonovic M., Roth A., Lin J., Minguez P., Bork P., Mering C. V., Jensen L. J., 2013 STRING v9.1: Protein-protein interaction networks, with increased coverage and integration. Nucleic Acids Research 41: D808–D815.

Freitag M., Williams R. L., Kothe G. O., Selker E. U., 2002 A cytosine methyltransferase homologue is essential for repeat-induced point mutation in *Neurospora crassa*. PNAS 99: 8802-8807

Galagan J. E., Calvo S. E., Borkovich K. A., Selker E. U., Read N. D., Jaffe D., FitzHugh W., Ma L. J., Smirnov S., Purcell S., Rehman B., Elkins T., Engels R., Wang S., Nielsen C. B., Butler J., Endrizzi M., Qui D., Ianakiev P., Bell-Pedersen D., Nelson M. A., Werner-Washburne M., Selitrennikoff C. P., Kinsey J. A., Braun E. L., Zelter A., Schulte U., Kothe G. O., Jedd G., Mewes W., Staben C., Marcotte E., Greenberg D., Roy A., Foley K., Naylor J., Stange-Thomann N., Barrett R., Gnerre S., Kamal M., Kamvysselis M., Mauceli E., Bielke C., Rudd S., Frishman D., Krystofova S., Rasmussen C., Metzenberg R. L., Perkins D. D., Kroken S., Cogoni C., Macino G., Catcheside D., Li W., Pratt R. J., Osmani S. A., DeSouza C. P. C., Glass L., Orbach M. J., Berglund J. A., Voelker R., Yarden O., Plamann M., Seiler S., Dunlap J.,

Radford A., Aramayo R., Natvig D. O., Alex L. A., Mannhaupt G., Ebbole D. J., Freitag M., Paulsen I., Sachs M. S., Lander E. S., Nusbaum C., Birren B., 2003 The genome sequence of the filamentous fungus *Neurospora crassa*. Nature 422: 859–868.

Galagan J. E., Selker E. U., 2004 RIP: The evolutionary cost of genome defense. Trends in Genetics 20: 417–423.

Geiser J. R., Tuinen D. V., Brockerhoff S. E., Neff M. M., Davis T. N., 1991 Can calmodulin function without binding calcium? Cell 65: 949–959.

Geiser J. R., Sundberg H. A., Chang B. H., Muller E. G. D., Davis T. N., 1993 The essential mitotic target of calmodulin is the 110-kilodalton component of the spindle pole body in *Saccharomyces cerevisiae*. Molecular and Cellular Biology 13: 7913–7924.

Giacomello M., Mario A. De, Scarlatti C., Primerano S., Carafoli E., 2013 Plasma membrane calcium ATPases and related disorders. The International Journal of Biochemistry & Cell Biology 45: 753–762.

Gifford J. L., Walsh M. P., Vogel H. J., 2007 Structures and metal - ion - binding properties of the Ca^{2+} -binding helix – loop – helix EF-hand motifs. The Biochemical Journal 405: 199–221.

Haiech J., Audran E., Fève M., Ranjeva R., Kilhoffer M. C., 2011 Revisiting intracellular calcium signaling semantics. Biochimie 93: 2029–2037.

Hait W. N., Lee G. L., 1985 Characteristics of the cytotoxic effects of the phenothiazine class of calmodulin antagonists. Biochemical Pharmacology 34: 3973–3978.

Hammond T. M., Spollen W. G., Decker L. M., Blake S. M., Springer G. K., Shiu P. K., 2013 Identification of small RNAs associated with meiotic silencing by unpaired DNA. Genetics 194: 279–284.

Hanson P. I., Kapiloff M. S., Lou L., Rosenfeld M. C., Schulman H., 1989 Expression of a multifunctional Ca^{2+}/Calmodulin-dependent protein kinase and mutational analysis of its autoregulation. Neuron 3: 59–70.

Hanson P. I., Schulman H., 1992 Inhibitory autophosphorylation of multifunctional Ca^{2+}/calmodulin-dependent protein kinase analyzed by site-directed mutagenesis. The Journal of Biological Chemistry 267: 17216–17224.

Harding R. W., Huang P. C., Mitchell H. K., 1969 Photochemical studies of the carotenoid biosynthetic pathway in *Neurospora crassa*. Archives of Biochemistry and Biophysics 129: 696–707.

Harding R. W., Turner R. V, 1981 Photoregulation of the carotenoid biosynthetic pathway in albino and white collar mutants of *Neurospora crassa*. Plant Physiology 68: 745–749.

Higuchi S., Tamura J., Giri P. R., Polli J. W., Kincaid R. L., 1991 Calmodulin-dependent protein phosphatase from *Neurospora crassa*. Molecular cloning and expression of recombinant catalytic subunit. The Journal of Biological Chemistry 266: 18104–18112.

Hoffman L., Stein R. A., Colbran R. J., Mchaourab H. S., 2011 Conformational changes underlying calcium/calmodulin-dependent protein kinase II activation. The EMBO Journal 30: 1251–1262.

Hoshino T., Mizutani A., Sasaki T., Hidaka H., Yamane T., 1994 Purification and partial amino acid sequence of calmodulin from *Fusarium oxysporum*. The Journal of General and Applied Microbiology 40: 43–51.

Hubbard M., Bradley M., Sullivan P., Shepherd M., Forrester I., 1982 Evidence for the occurrence of calmodulin in the yeasts *Candidas albicans* and *Saccharomyces cerevisiae*. FEBS letters 137: 85–88.

Iida H., Ohya Y., Anraku Y., 1995 Calmodulin-dependent protein kinase II and calmodulin are required for induced thermotolerance in *Saccharomyces cerevisiae*. Current Genetics 27: 190–193.

Ikura M., Clore G. M., Gronenborn A. M., Zhu G., Klee C. B., Bax A., 1992 Solution structure of a calmodulin-target peptide complex by multidimensional NMR. Science 256: 632–638.

Irelan J. T., Hagemann A. T., Selker E. U., 1994 High frequency repeat-induced point mutation (RIP) is not associated with efficient recombination. Genetics 138: 1093–1103.

Irelan J. T., Selker E. U., 1997 Cytosine methylation associated with repeat-induced point mutation causes epigenetic gene silencing in *Neurospora crassa*. Genetics 146: 509–523.

Jackson S. L., Heath I. B., 1993 Roles of calcium ions in hyphal tip growth. Microbiological Reviews 57: 367–382.

Jaiswal J. K., 2001 Calcium – how and why? Indian Academy of Sciences 26: 357–363.

James P., Vorherr T., Carafoli E., 1995 Calmodulin-binding domains: just two faced or multifaceted? Trends in biochemical sciences 20: 38–42.

Jensen L. J., Kuhn M., Stark M., Chaffron S., Creevey C., Muller J., Doerks T., Julien P., Roth A., Simonovic M., Bork P., Mering C. V., 2009 STRING 8 - A global view on proteins and their functional interactions in 630 organisms. Nucleic Acids Research 37: D412–D416.

Jurado L. A., Chockalingam P. S., Jarrett H. W., 1999 Apocalmodulin. Physiological Reviews 79: 661–682.

Kakiuchi and Yamazaki, 1970 Calcium dependent phosphodiesterase activity and its activating factor (PAF) from brain. Biochemical and Biophysical Research Communications 41: 1104–1110.

Kapoor M., Sreenivasan G. M., Goel N., Lewis J., 1990 Development of thermotolerance in *Neurospora crassa* by heat shock and other stresses eliciting peroxidase induction. Journal of Bacteriology 172: 2798–2801.

Kelly W. G., Aramayo R., 2007 Meiotic silencing and the epigenetics of sex. Chromosome Research 15: 633–651.

Kim Y., Li D., Kolattukudy P. E., 1998 Induction of Ca^{2+}-calmodulin signaling by hard-surface contact primes *Colletotrichum gloeosporioides* conidia to germinate and form appressoria. Journal of Bacteriology 180: 5144–5150.

Kim H., Nelson M. A., 2005 Molecular and functional analyses of *poi-2*, a novel gene highly expressed in sexual and perithecial tissues of *Neurospora crassa*. Eukaryotic Cell 4: 900–910.

Kim H., Wright S. J., Park G., Ouyang S., Krystofova S., Borkovich K. A., 2012 Roles for receptors, pheromones, G proteins,and mating type genes during sexual reproduction in *Neurospora crassa*. Genetics 190: 1389–1404.

Korripally P., Tiwari A., Haritha A., Kiranmayi P., Bhanoori M., 2010 Characterization of Ctr family genes and the elucidation of their role in the life cycle of *Neurospora crassa*. Fungal Genetics and Biology 47: 237–245.

Kraus P. R., Heitman J., 2003 Coping with stress: calmodulin and calcineurin in model and pathogenic fungi. Biochemical and Biophysical Research Communications 311: 1151–1157.

Kraus P. R., Fox D. S., Cox G. M., Heitman J., 2003 The *Cryptococcus neoformans* MAP kinase Mpk1 regulates cell integrity in response to antifungal drugs and loss of calcineurin function. Molecular Microbiology 48: 1377–1387.

Kraus P. R., Nichols C. B., Heitman J., 2005 Calcium- and calcineurin-independent roles for calmodulin in *Cryptococcus neoformans* morphogenesis and high-temperature growth. Eukaryotic Cell 4: 1079–1087.

Kulkarni R. K., Nickerson K. W., 1981 Nutritional control of dimorphism in *Ceratocystis ulmi*. Experimental Mycology 5: 148–154.

Kumar R., Tamuli R., 2014 Calcium/calmodulin-dependent kinases are involved in growth, thermotolerance, oxidative stress survival, and fertility in *Neurospora crassa*. Archives of Microbiology 196: 295–305.

Lamb T. M., Vickery J., Bell-Pedersen D., 2013 Regulation of gene expression in *Neurospora crassa* with a copper responsive promoter. G3: Genes| Genomes| Genetics 3: 2273–2280.

Laxmi V., Tamuli R., 2015 The *Neurospora crassa cmd*, *trm-9*, and *nca-2* genes play a role in growth, development, and survival in stress conditions. Genomics and Applied Biology 6: 1–8.

Laxmi V., Tamuli R., 2016 The calmodulin gene in *Neurospora crassa* is required for normal vegetative growth, ultraviolet survival, and sexual development. Archives of Microbiology: 1–12.

Lee S. C., Lee Y. H., 1998 Calcium/calmodulin-dependent signaling for appressorium formation in the plant pathogenic fungus *Magnaporthe grisea*. Molecules and Cells 8: 698–704.

Lee D. W., Pratt R. J., McLaughlin M., Aramayo R., 2003 An Argonaute-like protein is required for meiotic silencing. Genetics 164: 821–828.

Lee D. W., Seong K. Y., Pratt R. J., Baker K., Aramayo R., 2004 Properties of unpaired DNA required for efficient silencing in *Neurospora crassa*. Genetics 167: 131–150.

Lee D. W., Millimaki R., Aramayo R., 2010 QIP, a component of the vegetative RNA silencing pathway, is essential for meiosis and suppresses meiotic silencing in *Neurospora crassa*. Genetics 186: 127–133.

Levin R. M., Weiss B., 1976 Mechanism by which psychotropic drugs inhibit adenosine cyclic 3',5'-monophosphate phosphodiesterase of brain. Molecular pharmacology 12: 581–589.

Levin R. M., Weiss B., 1977 Binding of trifluoperazine to the calcium-dependent activator of cyclic nucleotide phosphodiesterase. Molecular pharmacology 13: 690–697.

Lew R. R., Abbas Z., Anderca M. I., Free S. J., 2008 Phenotype of a mechanosensitive channel mutant, *mid-1*, in a filamentous fungus, *Neurospora crassa*. Eukaryotic Cell 7: 647–655.

Li L., Chang S. S., Liu Y., 2010 RNA interference pathways in filamentous fungi. Cellular and Molecular Life Sciences 67: 3849–3863.

Lin C. R., Kapiloff M. S., Durgerian S., Tatemoto K., Russo A. F., Hanson P., Schulman H., Rosenfeld M. G., 1987 Molecular cloning of a brain- specific calcium/ calmodulin-dependent protein kinase. Proceedings of the National Academy of Sciences of the United States of America 84: 5962–5966.

Lindegren C. C., 1936 A six-point map of the sex-chromosome of *Neurospora crassa*. Journal of Genetics 32: 243–256.

Liu Z. M., Kolattukudy P. E., 1999 Early expression of the calmodulin gene, which precedes appressorium formation in *Magnaporthe grisea*, is inhibited by self-inhibitors and requires surface attachment. Journal of Bacteriology 181: 3571–3577.

Livak K. J., Schmittgen T. D., 2001 Analysis of relative gene expression data using real-time quantitative PCR and the $2^{-\Delta\Delta C}{}_{T}$ method. Methods 25: 402–408.

Lu K. P., Rasmussen C. D., May G. S., Means A. R., 1992 Cooperative regulation of cell proliferation by calcium and calmodulin in *Aspergillus nidulans*. Molecular Endocrinology 6: 365–374.

Lu K. P., Osmani S. A., Osmani A. H., Means A. R., 1993 Essential roles for calcium and calmodulin in G2/M progression in *Aspergillus nidulans*. The Journal of cell biology 121: 621–630.

Luan Y., Matsuura I., Yazawa M., Nakamura T., Yagi K., 1987 Yeast calmodulin: structural and functional differences compared with vertebrate calmodulin. Journal of Biochemistry 102: 1531–1537.

Luque E. M., Gutiérrez G., Navarro-Sampedro L., Olmedo M., Rodríguez-Romero J., Ruger-Herreros C., Tagua V. G., Corrochano L. M., 2012 A relationship between carotenoid accumulation and the distribution of species of the fungus Neurospora in spain. PLoS ONE **7**: e33658.

Ma Z. B., Zhao J. X., Wang L. A., Zheng X. B., 2009 Cloning, prokaryotic expression and bioactivity of the calmodulin gene of *Magnaporthe grisea*. FEMS Microbiology Letters 300: 107–114.

Marchler-Bauer A., Bryant S. H., 2004 CD-Search: Protein domain annotations on the fly. Nucleic Acids Research 32: W327–W331.

Marchler-Bauer A., Anderson J. B., Chitsaz F., Derbyshire M. K., Deweese-Scott C., Fong J. H., Geer L. Y., Geer R. C., Gonzales N. R., Gwadz M., He S., Hurwitz D. I., Jackson J. D., Ke Z., Lanczycki C. J., Liebert C. A., Liu C., Lu F., Lu S., Marchler G. H., Mullokandov M., Song J. S., Tasneem A., Thanki N., Yamashita R. A., Zhang D., Zhang N., Bryant S. H., 2009 CDD: Specific functional annotation with the Conserved Domain Database. Nucleic Acids Research 37: D205–D210.

Margolin B. S., Freitag M., Selker E. U., 2000 Improved plasmids for gene targeting at the his-3 locus of *Neurospora crassa* by electroporation: correction. Fungal Genet. Newsl 47: 112.

Martínez-Luis S., Pérez-Vásquez A., Mata R., 2007 Natural products with calmodulin inhibitor properties. Phytochemistry 68: 1882–1903.

Mata R., Figueroa M., González-Andrade M., Rivera-Chávez J. A., Madariaga-Mazón A., Valle P. D., 2014 Calmodulin inhibitors from natural sources: An update. Journal of Natural Products 78: 576–586.

Matheos D. P., Kingsbury T. J., Ahsan U. S., Cunningham K. W., 1997 Tcn1p/Crz1p, a calcineurin-dependent transcription factor that differentially regulates gene expression in *Saccharomyces cerevisiae*. Genes & Development 11: 3445–3458.

Matsuura I., Ishihara K., Nakai Y., Yazawa M., Toda H., Yagi K., 1991 A site-directed mutagenesis study of yeast calmodulin. Journal of biochemistry 109: 190–197.

Means A. R., Dedman J. R., 1980 Calmodulin-an intracellular calcium receptor. Nature 285: 73–77.

Melnick M. B., Melnick C., Lee M., Woodward D. O., 1993 Structure and sequence of the calmodulin gene from *Neurospora crassa*. 1171: 334–336.

Mering C. V., Jensen L. J., Kuhn M., Chaffron S., Doerks T., Krüger B., Snel B., Bork P., 2007 STRING 7-Recent developments in the integration and prediction of protein interactions. Nucleic Acids Research 35: D358–D362.

Meyer T., Hanson P. I., Stryer L., Schulman H., 1992 Calmodulin trapping by calcium-calmodulin-dependent protein kinase. Science 256: 1199–1202.

Miller S. G., Patton B. L., Kennedy M. B., 1988 Sequences of autophosphorylation sites in neuronal type II CaM kinase that control Ca^{2+}-independent activity. Neuron 1: 593–604.

Mirzayans R., Famulski K. S., Enns L., Fraser M., Paterson M. C., 1995 Characterization of the signal transduction pathway mediating gamma ray-induced inhibition of DNA synthesis in human cells: indirect evidence for involvement of calmodulin but not protein kinase C nor p53. Oncogene 11: 1597–1605.

Montagne C., 1843 Quatrième centurie de plantes cellulaires exotiques nouvelles: décades 1-6.

Mori T., Takai Y., Minakuchi R., Yu B., Nishizuka Y., 1980 Inhibitory action of chlorpromazine, dibucaine, and other phospholipid-interacting drugs on calcium-activated, phospholipid-dependent protein kinase. The Journal of Biological Chemistry 255: 8378–8380.

Moser M. J., Lee S. Y., Klevit R. E., Davis T. N., 1995 Ca^{2+} binding to calmodulin and its role in *Schizosaccharomyces pombe* as revealed by mutagenesis and NMR spectroscopy. The Journal of Biological Chemistry 270: 20643–20652.

Moser M. J., Flory M. R., Davis T. N., 1997 Calmodulin localizes to the spindle pole body of *Schizosaccharomyces pombe* and perform an essential function in chromosome segragation. Journal of Cell Science 110: 1805–1812.

Mulè G., Susca A., Stea G., Moretti A., 2004a Specific detection of the toxigenic species *Fusarium proliferatum* and *F. oxysporum* from asparagus plants using primers based on calmodulin gene sequences. FEMS Microbiology Letters 230: 235–240.

Mulè G., Susca A., Stea G., Moretti A., 2004b A species-specific PCR assay based on the calmodulin partial gene for identification of *Fusarium verticillioides*, *F. proliferatum* and *F. subglutinans*. European Journal of Plant Pathology 110: 495–502.

Muthukumar G., Nickerson K. W., 1984 Ca(II)-calmodulin regulation of fungal dimorphism in *Ceratocystis ulmi*. Journal of Bacteriology 159: 390–392.

Muthukumar G., Kulkarni R. K., Nickerson K. W., 1985 Calmodulin levels in the yeast and mycelial phasses of *Ceratocystis ulmi*. Journal of Bacteriology 162: 47–49.

Muthukumar G., Nickerson K. W., 1985 Ca(II)-calmodulin regulation of morphological commitment in *Ceratocystis ulmi*. FEMS Microbiology letters 27: 199–202.

Muthukumar G., Nickerson K. W., 1986 Calmodulin activity in yeast and mycelial phases of *Ceratocystis ulmi*. FEMS Microbiology Letters 37: 313–316.

Nagasowjanya T., Raj K. B., Reddy K. S., Kasbekar D. P., 2013 An apparent increase in meiotic silencing strength in crosses involving inbred *Neurospora crassa* strains. Fungal Genetics and Biology 56: 158–162.

Nakamura T., Fujita K., Eguchi Y., Yazawa M., 1984 Properties of calcium-dependent regulatory proteins from fungi and yeast. Journal of Biochemistry 95: 1551–1557.

Nakashima K., Ishida H., Nakatomi A., Yazawa M., 2012 Specific conformation and Ca^{2+}-binding mode of yeast calmodulin: insight into evolutionary development. The Journal of Biochemistry 152: 27–35.

Nakayashiki H., 2005 RNA silencing in fungi: Mechanisms and applications. FEBS Letters 579: 5950–5957.

Nicholas K. B., Nicholas H. B. J., Deerfield D. W., 1997 GeneDoc: analysis and visualization of genetic variation. Embnew. news 4.

Odom A, Muir S., Lim E., Toffaletti D. L., Perfect J., Heitman J., 1997 Calcineurin is required for virulence of *Cryptococcus neoformans*. The EMBO journal 16: 2576–2589.

Ohya Y., Uno I., Ishikawa T., Anraku Y., 1987 Purification and biochemical properties of calmodulin from *Saccharomyces cerevisiae*. European Journal of Biochemistry 168: 13–19.

Ohya Y., Anraku Y., 1989 A galactose-dependent *cmd1* mutant of *Saccharomyces cerevisiae*: involvement of calmodulin in nuclear division. Current genetics 15: 113–120.

Ohya Y., Botstein D., 1994a Structure-based systematic isolation of conditional-lethal mutations in the single yeast calmodulin gene. Genetics 138: 1041–1054.

Ohya Y., Botstein D., 1994b Diverse essential functions revealed by complementing yeast calmodulin mutants. Science 263: 963–966.

Osborn K. D., Zaidi A., Mandal A., Urbauer R. J. B., Johnson C. K., 2004 Single-molecule dynamics of the calcium-dependent activation of plasma-membrane Ca^{2+} -ATPase by calmodulin. Biophysical Journal 87: 1892–1899.

Ouyang S., Beecher C. N., Wang K., Larive C. K., Borkovich K. A., 2015 Metabolic impacts of using nitrogen and copper-regulated promoters to regulate gene expression in *Neurospora crassa*. G3: Genes| Genomes| Genetics 5: 1899–1908.

Pall M. L., Brunelli J. P., 1993 A series of six compact fungal transformation vectors containing polylinkers with multiple unique restriction sites. Fungal Genet Newsl 40: 59–62.

Pandit N. N., Russo V. E. A., 1992 Reversible inactivation of a foreign gene, *hph*, during the asexual cycle in *Neurospora crassa* transformants. Molecular and General Genetics 234: 412–422.

Paranjape V., Roy B. G., Datta A., 1990 Involvement of calcium, calmodulin and protein phosphorylation in morphogenesis of *Candida albicans*. Journal of General Microbiology 136: 2149–2154.

Parks L. W., Casey W. M., 1995 Physiological implications of sterol biosynthesis in yeast. Annual Reviews in Microbiology 49: 95–116.

Payen A. d., 1843 Extrait d'un rapport adressé aM. Le Maréchal Duc de Dalmatie, Ministre de la Guerre, Président du Conseil, sur une altération extraordinaire du pain de munition. Ann. Chim. Phys 3: 5–21.

Perez R. O., Tuinen D. V., Marmé D., Cox J. A., Turian G., 1981 Purification and identification of calmodulin from *Neurospora crassa*. FEBS letters 133: 205–208.

Perkins D. D., Margolin, B.S., Selker E.U., Haedo S.D., 1997 Occurrence of repeat induced point mutation in long segmental duplications of Neurospora. Genetics 147: 125–136.

Perkins D. D., Davis R. H., 2000 Neurospora at the millennium. Fungal Genetics and Biology 31: 153–167.

Persechini A., Stemmer P. M., 2002 Calmodulin is a limiting factor in the cell. Trends in cardiovascular medicine 12: 32–37.

Pickford A. S., Catalanotto C., Cogoni C., Macino G., 2002 Quelling in *Neurospora crassa*. Advances in Genetics 46: 277–303.

Prakash A., Sengupta S., Aparna K., Kasbekar D. P., 1999 The erg-3 (sterol Δ14, 15-reductase) gene of *Neurospora crassa*: generation of null mutants by repeat-induced point mutation and complementation by proteins chimeric for human lamin B receptor sequences. Microbiology 145: 1443–1451.

Pratt R. J., Lee D. W., Aramayo R., 2004 DNA methylation affects meiotic trans-sensing, not meiotic silencing, in Neurospora. Genetics 168: 1925–1935.

Quandt K., Frech K., Karas H., Wingender E., Werner T., 1995 MatInd and MatInspector: new fast and versatile tools for detection of consensus matches in nucleotide sequence data. Nucleic Acids Research 23: 4878–4884.

Raess B. U., Vincenzi F. F., 1980 Calmodulin activation of red blood cell (Ca^{2+} + Mg^{2+})-ATPase and its antagonism by phenothiazines. Molecular Pharmacology 18: 253–258.

Rainteau D., Wolf C., Bereziat G., Polonovski J., 1984 Binding of a spin-labelled chlorpromazine analogue to calmodulin. Biochemical Journal 221: 659–663.

Raju N. B., 1980 Meiosis and ascospore genesis in Neurospora. European Journal of Cell Biology 23: 208–223.

Raju N. B., 1992 Genetic control of the sexual cycle in Neurospora. Mycological Research 96: 241–262.

Rasmussen C. D., Means R. L., Lu K. P., May G. S., Means A. R., 1990 Characterization and expression of the unique calmodulin gene of *Aspergillus nidulans*. The Journal of Biological Chemistry 265: 13767–13775.

Rasmussen C. D., Lu K. P., Means R. L., Means A. R., 1992 Calmodulin and cell cycle control. Journal of Physiology-Paris 86: 83–88.

Reedy J. L., Filler S. G., Heitman J., 2010 Elucidating the *Candida albicans* calcineurin signaling cascade controlling stress response and virulence. Fungal Genetics and Biology 47: 107–116.

Reig J. A., Téllez-Iñón M. T., Flawiá M. M., Torres H. N., 1984 Activation of *Neurospora crassa* soluble adenylate cyclase by calmodulin. Biochemical Journal 221: 541–543.

Rhoads A. R., Friedberg F., 1997 Sequence motifs for calmodulin recognition. The FASEB journal 11: 331–340.

Robson G. D., Wiebe M. G., Trinci A. P. J., 1991 Involvement of Ca^{2+} in the regulation of hyphal extension and branching in *Fusarium graminearum* A 3/5. Experimental Mycology 15: 263–272.

Rodney G. G., Moore C. P., Williams B. Y., Zhang J. Z., Krol J., Pedersen S. E., Hamilton S. L., 2001 Calcium binding to calmodulin leads to an N-terminal shift in its binding site on the ryanodine receptor. The Journal of Biological Chemistry 276: 2069–2074.

Rodriguez-Amaya D. B., Kimura M., 2004 Harvest Plus Handbook for Carotenoid Analysis. Washington: International Food Policy Research Institute (IFPRI) 2.

Romano N., Macino G., 1992 Quelling: transient inactivation of gene expression in *Neurospora crassa* by transformation with homologous sequences. Molecular Microbiology 6: 3343–3353.

Roufogalis B. D., 1981 Phenothiazine antagonism of calmodulin: a structurally-nonspecific interaction. Biochemical and Biophysical Research Communications 98: 607–613.

Roufogalis B. D., 1985 Calmodulin antagonism. Calcium and cell physiology, Springer Berlin Heidelberg: 148–169.

Roy B. G., Datta A., 1987 A calmodulin inhibitor blocks morphogenesis in *Candida albicans*. FEMS Microbiology Letters 41: 327–329.

Ryan F. J., Beadle G. W., Tatum E. L., 1943 The tube method of measuring the growth rate of Neurospora. American Journal of Botany 30: 784–799.

Rzhetsky A., Nei M., 1992 Statistical properties of the ordinary least-squares, generalized least-squares, and minimum-evolution methods of phylogenetic inference. Journal of Molecular Evolution 35: 367–375.

Sabie F. T., Gadd G. M., 1989 Involvement of a Ca^{2+}-calmodulin interaction in the yeast-mycelial (Y-M) transition of *Candida albicans*. Mycopathologia 108: 47–54.

Sadakane Y., Nakashima H., 1996 Light-induced phase shifting of the circadian conidiation rhythm is inhibited by calmodulin antagonists in *Neurospora crassa*. Journal of Biological Rhythms 11: 234–240.

Sakai W., Ishii C., Inoue H., 2002 The *upr-1* gene encodes a catalytic subunit of the DNA polymerase ζ which is involved in damage-induced mutagenesis in *Neurospora crassa*. Molecular Genetics and Genomics 267: 401–408.

Sakai W., Wada Y., Naoi Y., Ishii C., Inoue H., 2003 Isolation and genetic characterization of the *Neurospora crassa REV1* and *REV7* homologs: evidence for involvement in damage-induced mutagenesis. DNA Repair 2: 337–346.

Saltarelli C. G., Gentile K. A., Mancuso S. C., 1975 Lethality of Candida strains as influenced by the host. Canadian Journal of Microbiology 21: 648–654.

Sambrook J., Russell D. W., 2001 Molecular cloning: a laboratory manual 3rd edition. Coldspring-Harbour Laboratory Press, UK.

Sancar A., 1994 Structure and function of DNA photolyase. Biochemistry 33: 2–9.

Sanders D., Pelloux J., Brownlee C., Harper J. F., 2002 Calcium at the crossroads of signaling. The Plant Cell 14: S401–S417.

Sanglard D., Ischer F., Marchetti O., Entenza J., Bille J., 2003 Calcineurin A of *Candida albicans*: involvement in antifungal tolerance, cell morphogenesis and virulence. Molecular Microbiology 48: 959–976.

Saporito S. M., Sypherd P. S., 1991 The isolation and characterization of a calmodulin-encoding gene (CMD1) from the dimorphic fungus *Candida albicans*. Gene 106: 43–49.

Sato T., Ueno Y., Watanabe T., Mikami T., Matsumoto T., 2004 Role of Ca^{2+}/calmodulin signaling pathway on morphological development of *Candida albicans*. Biological and Pharmaceutical Bulletin 27: 1281–1284.

Schworer C. M., Colbran R. J., Keefer J. R., Soderling T. R., 1988 Ca^{2+}/calmodulin-dependent protein kinase II. Identification of a regulatory autophosphorylation site adjacent to the inhibitory and calmodulin-binding domains. The Journal of Biological Chemistry 263: 13486–13489.

Selker E. U., 1990 Premeiotic instability of repeated sequences in *Neurospora crassa*. Annual Review of Genetics 24: 579–613.

Selker E. U., Fritz D. Y., Singer M. J., 1993 Dense nonsymmetrical DNA methylation resulting from repeat-induced point mutation in Neurospora. Science 262: 1724–1728.

Selker E. U., 1997 Epigenetic phenomena in filamentous fungi: useful paradigms or repeat-induced confusion? Trends in Genetics 13: 296–301.

Selker E. U., 1999 Gene Silencing: repeats that count. Cell 97: 157–160.

Selker E. U., Tountas N. A., Cross S. H., Margolin B. S., Murphy J. G., Bird A. P., Freitag M., 2003 The methylated component of the *Neurospora crassa* genome. Nature 422: 893–897.

Serrano R., Ruiz A., Bernal D., Chambers J. R., Ariño J., 2002 The transcriptional response to alkaline pH in *Saccharomyces cerevisiae*: evidence for calcium-mediated signalling. Molecular Microbiology 46: 1319–33.

Shear C. L., Dodge B. O., 1927 Life histories and heterothallism of the red bread-mold fungi of the Monilia sitophila group. US Government Printing Office 34: 1019–1042.

Shimura M., Ito Y., Ishii C., Yajima H., Linden H., Harashima T., Yasui A., Inoue H., 1999 Characterization of a *Neurospora crassa* photolyase-deficient mutant generated by repeat induced point mutation of the *phr* gene. Fungal Genetics and Biology 28: 12–20.

Shiu P. K., Raju N. B., Zickler D., Metzenberg R. L., 2001 Meiotic silencing by unpaired DNA. Cell 107: 905–916.

Shiu P. K., Metzenberg R. L., 2002 Meiotic silencing by unpaired DNA: properties, regulation and suppression. Genetics 161: 1483–1495.

Shiu P. K., Zickler D., Raju N. B., Ruprich-Robert G., Metzenberg R. L., 2006 SAD-2 is required for meiotic silencing by unpaired DNA and perinuclear localization of SAD-1 RNA-directed RNA polymerase. PNAS 103: 2243–2248.

Sinha R. P., Häder D. P., 2002 UV-induced DNA damage and repair: a review. Photochemical & Photobiological Sciences 1: 225–236.

Smallwood H. S., Lopez-Ferrer D., Eberlein P. E., Watson D. J., Squier T. C., 2009 Calmodulin mediates DNA repair pathways involving H2AX in response to low-dose radiation exposure of RAW 264.7 macrophages. Chemical Research in Toxicology 22: 460–470.

Springer M. L., 1993 Genetic control of fungal differentiation: The three sporulation pathways of *Neurospora crassa*. BioEssays 15: 365–374.

Staben C., Jensen B., Singer M., Pollock J., Schechtman M., Kinsey J., Selker E., 1989 Use of a bacterial hygromycin B resistance gene as a dominant selectable marker in *Neurospora crassa* transformation. Fungal Genet. Newsl 36: 79–81.

Starovasnik M. A., Davis T. N., Klevit R. E., 1993 Similarities and differences between yeast and vertebrate calmodulin: an examination of the calcium-binding and structural properties of calmodulin from the yeast *Saccharomyces cerevisiae*. Biochemistry 32: 3261–3270.

Stathopoulos A. M., Cyert M. S., 1997 Calcineurin acts through the CRZ1/TCN1-encoded transcription factor to regulate gene expression in yeast. Genes & Development 11: 3432–3444.

Stirling D. A., Welch K. A., Stark M. J., 1994 Interaction with calmodulin is required for the function of Spc110p, an essential component of the yeast spindle pole body. The EMBO Journal 13: 4329–4342.

Sun G. H., Hirata A., Ohya Y., Anraku Y., 1992 Mutations in yeast calmodulin cause defects in spindle pole body functions and nuclear integrity. The Journal of Cell Biology 119: 1625–1639.

Suresh K., Subramanyam C., 1997 A putative role for calmodulin in the activation of *Neurospora crassa* chitin synthase. FEMS Microbiology Letters 150: 95–100.

Suzuki S., Katagiri S., Nakashima H., 1996 Mutants with altered sensitivity to a calmodulin antagonist affect the circadian clock in *Neurospora crassa*. Genetics 143: 1175–1180.

Suzuki C., 2001 Immunochemical and mutational analyses of P-type ATPase Spf1p involved in the yeast secretory pathway. Bioscience, Biotechnology, and Biochemistry 65: 2405–2411.

Swain A. L., Amma E. L., 1989 The coordination polyhedron of Ca^{2+}, Cd^{2+} in parvalbumin. Inorganica Chimica Acta 163: 5–7.

Swulius M. T., Waxham M. N., 2008 Ca^{2+}/calmodulin-dependent protein kinases. Cellular and Molecular Life Sciences 65: 2637–2657.

Szklarczyk D., Franceschini A., Kuhn M., Simonovic M., Roth A., Minguez P., Doerks T., Stark M., Muller J., Bork P., Jensen L. J., Mering C. V., 2011 The STRING database in 2011: functional interaction networks of proteins, globally integrated and scored. Nucleic Acids Research 39: D561–D568.

Szklarczyk D., Franceschini A., Wyder S., Forslund K., Heller D., Huerta-Cepas J., Simonovic M., Roth A., Santos A., Tsafou K. P., Kuhn M., Bork P., Jensen L. J., Mering C. V., 2015 STRING v10: Protein-protein interaction networks, integrated over the tree of life. Nucleic Acids Research 43: D447–D452.

Takeda T., Yamamoto M., 1987 Analysis and in vivo disruption of the gene coding for calmodulin in *Schizosaccharomyces pombe*. Proceedings of the National Academy of Sciences of the United States of America 84: 3580–3584.

Tamuli R., Ravindran C., Kasbekar D. P., 2006 Translesion DNA polymerases Pol ζ, Pol η, Pol ι, Pol κ and Rev1 are not essential for repeat-induced point mutation in *Neurospora crassa*. Journal of Biosciences 31: 557–564.

Tamuli R., Kumar R., Deka R., 2011 Cellular roles of neuronal calcium sensor-1 and calcium/calmodulin-dependent kinases in fungi. Journal of Basic Microbiology 51: 120–128.

Tamuli R., Kumar R., Srivastava D. A., Deka R., 2013 Calcium signaling. In: Kasbekar DP, McCluskey K (ed) Neurospora: Genomics and Molecular Biology. Caister Academic Press, Norfolk, UK, pp 35-57.

Tamuli R., Deka R., Borkovich K. A., 2016 Calcineurin subunits A and B interact to regulate growth and asexual and sexual development in *Neurospora crassa*. PloS one 11: 1–17.

Tamura K., Peterson D., Peterson N., Stecher G., Nei M., Kumar S., 2011 MEGA5: Molecular evolutionary genetics analysis using maximum likelihood, evolutionary distance, and maximum parsimony methods. Molecular Biology and Evolution 28: 2731–2739.

Tellez-Inon M. T., Ulloa R. M., Glikin G. C., Torres H. N., 1985 Characterization of *Neurospora crassa* cyclic AMP phosphodiesterase activated by calmodulin. Biochemical journal 232: 425–430.

Thompson J. D., Gibson T. J., Plewniak F., Jeanmougin F., Higgins D. G., 1997 The CLUSTAL_X windows interface: flexible strategies for multiple sequence alignment aided by quality analysis tools. Nucleic Acids Research 25: 4876–4882.

Todo T., Takemori H., Ryo H., Ihara M., Matsunaga T., Nikaido O., Sato K., Nomura T., 1993 A new photoreactivating enzyme that specifically repairs ultraviolet light-induced (6-4) photoproducts. Nature 361: 371–374.

Tokumitsu H., Wayman G. A., Muramatsu M., Soderling T. R., 1997 Calcium/calmodulin-dependent protein kinase kinase: identification of regulatory domains. Biochemistry 36: 12823–12827.

Tokumitsu H., Muramatsu M., Ikura M., Kobayashi R., 2000 Regulatory mechanism of Ca^{2+}/calmodulin-dependent protein kinase kinase. The Journal of biological chemistry 275: 20090–20095.

Tuinen V. D., Ortega Perez R., Marme D., Turian G., 1984 Calcium, calmodulin-dependent protein phosphorylation in *Neurospora crassa*. FEBS letters 176: 317–320.

Ullmann A., Jacob F., Monod J., 1967 Characterization by in vitro complementation of a peptide corresponding to an operator-proximal segment of the β-galactosidase structural gene of *Escherichia coli*. Journal of Molecular Biology 24: 339–343.

Vandonselaar M., Hickie R. A., Quail J. W., Delbaere L. T., 1994 Trifluoperazine-induced conformational change in Ca^{2+}-calmodulin. Nature structural biology 1: 795–801.

Vershinin A., 1999 Biological functions of carotenoids-diversity and evolution. BioFactors 10: 99–104.

Vogel H. J., 1964 Distribution of lysine pathways among fungi: evolutionary implications. The American Naturalist 98: 435–446.

Wang G., Lu L., Zhang C. Y., Singapuri A., Yuan S., 2006 Calmodulin concentrates at the apex of growing hyphae and localizes to the spitzenkorper in *Aspergillus nidulans*. Protoplasma 228: 159–166.

Warwar V., Dickman M. B., 1996 Effects of calcium and calmodulin on spore germination and appressorium development in *Colletotrichum trifolii*. Applied and Environmental Microbiology 62: 74–79.

Warwar V., Oved S., Dickman M. B., 2000 Antisense expression of the calmodulin gene from *Colletotrichum trifolii* impairs prepenetration development. FEMS Microbiology Letters 191: 213–219.

Weiss B., Prozialeck W. C., Wallace T. L., 1982 Interaction of drugs with calmodulin: biochemical, pharmacological and clinical implications. Biochemical Pharmacology 31: 2217–2226.

Westergaard M., Mitchell H. K., 1947 Neurospora V. A synthetic medium favoring sexual reproduction. American Journal of Botany 34: 573–577.

Winston F., Dollard C., Ricupero-Hovasse S. L., 1995 Construction of a set of convenient *Saccharomyces cerevisiae* strains that are isogenic to S288C. Yeast 11: 53–55.

Wise B. C., Glass D. B., Chou C. H., Raynor R. L., Katoh N., Schatzman R. C., Turner R. S., Kibler R. F., Kuo J. F., 1982 Phospholipid-sensitive Ca^{2+}-dependent protein kinase from heart. II. Substrate specificity and inhibition by various agents. The Journal of biological chemistry 257: 8489–8495.

Xiao H., Alexander W. G., Hammond T. M., Boone E. C., Perdue T. D., Pukkila P. J., Shiu P. K., 2010 QIP, a protein that converts duplex siRNA into single strands, is required for meiotic silencing by unpaired DNA. Genetics 186: 119–126.

Yang Q., Borkovich K. A., 1999 Mutational activation of a Gαi causes uncontrolled proliferation of aerial hyphae and increased sensitivity to heat and oxidative stress in *Neurospora crassa*. Genetics 151: 107–117.

Yu S. L., Johnson R. E., Prakash S., Prakash L., 2001 Requirement of DNA polymerase η for error-free bypass of UV-induced CC and TC photoproducts. Molecular and Cellular Biology 21: 185-188.

Zalokar M., 1954 Studies on biosynthesis of carotenoids in *Neurospora crassa*. Archives of Biochemistry and Biophysics 50: 71–80.

Zelter A., Bencina M., Bowman B. J., Yarden O., Read N. D., 2004 A comparative genomic analysis of the calcium signaling machinery in *Neurospora crassa*, *Magnaporthe grisea*, and *Saccharomyces cerevisiae*. Fungal Genetics and Biology 41: 827–841.

Zhang M., Abrams C., Wang L., Gizzi A., He L., Lin R., Chen Y., Loll P. J., Pascal J. M., Zhang J. F., 2012 Structural basis for calmodulin as a dynamic calcium sensor. Structure 20: 911–923.

Zvelebil M. J., Thornton J. M., 1993 Peptide-protein interactions: an overview. Quarterly reviews of Biophysics 26: 333–363.

Publications

Conferences:

1. Laxmi V., Tamuli R. (2012). Cellular role of calmodulin in *Neurospora crassa.* Chromatin 2012, 4th Meeting of the Asian Forum of Chromosome and Chromatin Biology on 'Epigenetic Mechanisms in Development and Disease', Centre for Cellular and Molecular Biology, Hyderabad, India, November 22-24, 2012.

2. Laxmi V., Tamuli R. (2013). Function of calmodulin protein in *Neurospora crassa.* Yeast 2013, 8th International Conference on Yeast Biology, CSIR- Institute of Microbial Technology, Chandigarh, India, December 4-7, 2013.

3. Laxmi V., Tamuli R. (2014). Studies of calcium signaling pathway mediated by calmodulin and related proteins in *Neurospora crassa*. ICDBT_2014, International Conference on Disease Biology and Therapeutics-2014, Institute of Advanced Study in Science and Technology, Guwahati, India, December 3-5, 2014.

4. Laxmi V., Tamuli R. (2015). Expression studies of important calcium signaling genes in *Neurospora crassa.* IBS-2015, National Symposium on Biophysics and Golden Jubilee Meeting of Indian Biophysical Society, Jamia Millia Islamia, New Delhi 10025, India, February 14-17, 2015.

Publications:

1. Laxmi V., Tamuli R., 2015 The *Neurospora crassa cmd*, *trm-9*, and *nca-2* genes play a role in growth, development, and survival in stress conditions. Genomics and Applied Biology 6: 1–8.

2. Laxmi V., Tamuli R., 2016 The calmodulin gene in *Neurospora crassa* is required for normal vegetative growth, ultraviolet survival, and sexual development. Archives of Microbiology: 1–12.

Genomics and Applied Biology 2015, Vol. 6, No. 7, 1-8
http://gab.biopublisher.ca

Research Article **Open Access**

The *Neurospora crassa cmd*, *trm-9*, and *nca-2* Genes Play a Role in Growth, Development, and Survival in Stress conditions

Laxmi V., Tamuli R.

Department of Biosciences and Bioengineering, Indian Institute of Technology Guwahati, Guwahati 781 039, India
Corresponding author email: ranjantamuli@iitg.ernet.in

Genomics and Applied Biology, 2015, Vol.6, No.7 doi: 10.5376/gab.2015.06.0007
Received: 24 Apr., 2015
Accepted: 02 Aug., 2015
Published: 11 Sep., 2015

Preferred citation for this article:
Laxmi V. and Tamuli R., 2015, The *Neurospora crassa cmd*, *trm-9*, and *nca-2* Play a Role in Growth, Development, and Survival in Stress conditions, Genomics and Applied Biology, Vol.6, No.7, 1-8 (doi: 10.5376/gab.2015.06.0007)

Abstract The calmodulin protein antagonists, trifluoperazine (TFP) and chlorpromazine (CPZ) inhibit the growth, carotenoids accumulation and sexual development of *Neurospora crassa*. In addition, *N. crassa* strains lacking *trm-9*, a cation-ATPase, showed defect in growth. Moreover, strains lacking both *trm-9* and another Ca^{2+}-ATPase *nca-2*, exhibited a severe growth defect, an increased sensitivity to $CaCl_2$, and a reduction in acquisition of thermotolerance induced by heat shock temperature. Therefore, the *cmd*, *trm-9*, and *nca-2* play a role in growth, survival in calcium stress and induced heat shock temperature in *N. crassa*.

Keywords Calcium signaling; Ca^{2+}/cation ATPases; Calmodulin; *Neurospora crassa*; *nca-2*; thermotolerance

Introduction

Calcium (Ca^{2+}) signaling is involved in regulating numerous processes in eukaryotes ranging from fungi to mammals. The Ca^{2+}-signaling process is initiated primarily due to transient raise in concentration of cytosolic free Ca^{2+} ($[Ca^{2+}]_c$), which is recognized by Ca^{2+} sensor proteins. One of the versatile and evolutionary conserved Ca^{2+}-sensor proteins is calmodulin (CaM), which binds Ca^{2+} with high affinity and specificity. CaM plays an important role in modulating DNA repair, DNA synthesis, cell proliferation, cyclic nucleotide and glycogen metabolism, secretion, motility and Ca^{2+} transport (Means and Dedman 1980; Smallwood et al., 2009). CaM also plays an important role for the regulation of stress response pathways in pathogenic fungi *Candida albicans* and *Cryptococcus neoformans* (Kraus and Heitman, 2003). In the budding yeast *Saccharomyces cerevisiae*, CaM is required for mitotic progression and acquisition of induced thermotolerance (Iida et al., 1995). Similar to the *S. cerevisiae*, in the filamentous fungi *Aspergillus nidulans*, CaM is critical for the progression through the G2/M transition (Kahl and Means 2003).

The filamentous fungus *Neurospora crassa* has a unique calcium (Ca^{2+}) signaling machinery, CaM is encoded by NCU04120 that appears to be an essential gene for viability (Galagan et al., 2003; Borkovich et al., 2004; Tamuli et al., 2013). In *N. crassa*, unlike the vertebrate counterparts, only one CaM gene has been identified (Capelli et al., 1993; Cox et al., 1982; Perez et al., 1981; Galagan et al., 2003). In vertebrates, CaM protein is encoded by multiple genes, for example, six genes have been detected in zebra fish, three genes in human and rat, two genes in frog and two genes in chicken (Luan et al., 2007). Coding sequence of the CaM encoding gene NCU04120 contains six exons and five introns, and CaM possesses conserved EF-hand domains (Tamuli et al., 2013). In *N. crassa* CaM antagonists, trifluoperazine (TFP) and chlorpromazine (CPZ) caused shortening of period length of the conidiation rhythm and light induced phase shifting (Sadakane and Nakashima 1996; Suzuki et al., 1996). In addition, possible role of CaM in activation of chitin synthase enzyme in *N. crassa* was studied by examining the effects of TFP on protoplast regeneration (Suresh and Subramanyam, 1997).

One of the targets of CaM is the Ca^{2+}-ATPase, a Ca^{2+} pump that help in fine tuning of Ca^{2+} homeostasis in cells by pumping Ca^{2+} out of cells. Ca^{2+}-ATPases hydrolyze ATP to catalyze active Ca^{2+}-efflux across biological membranes, and maintain a steep Ca^{2+} gradient across the plasma membrane (Hao et al.,

1994). CaM stimulates plasma membrane Ca^{2+}-ATPase (PMCA) activity by binding to an autoinhibitory domain of PMCA. The CaM-binding domain is located near the C-terminus of PMCA (Osborn et al., 2004; Giacomello et al., 2013). Besides interacting with (Ca^{2+}+Mg^{2+}) -activated ATPase in isolated cardiac sarcoplasmic reticulum and RBC membrane, CaM also interacts with ciliary dynein ATPase of *Tetrahymena* (Blum et al., 1980; Kirchberger and Antonetz, 1982; Lopes et al., 1990). In plants, Ca^{2+}-activated CaM regulates different Ca^{2+}-ATPases (Peerseen et al., 1997; Harper et al., 1998; Hong et al., 1999; Chung et al., 2000; Malmström et al., 1997, 2000). In *N. crassa*, nine ATPases have been identified and they possess conserved cation transporter/ATPase domain in the proteins (Galagan et al., 2003; Borkovich et al., 2004; Tamuli et al., 2013). *N. crassa* ATPases are found distributed in different branches during a phylogenetic analysis, NCA1 in ERCA, NCA2 and NCA3 in PMCA, PMR1 in PMR1, and PH-7 in ENA branch (Haro et al., 1991; Benito et al., 2000). Lack of NCA-2 results in slow growth, Ca^{2+} sensitivity, female sterility, and accumulation of more Ca^{2+} than the wild-type; indicating that it functions in the plasma membrane to pump Ca^{2+} out of the cell (Bowman et al., 2011). NCA-2 is more similar to the PMC-type proteins of animal cell than the Pmc1p in *S. cerevisiae* that resides in the vacuole (Bowman et al., 2011). In addition, one of the cation-ATPases *trm-9*, which is encoded by the gene NCU04898, shows sequence homology to *spf1* gene of *S. cerevisiae.* SPF1 family ATPases genes are conserved from yeast to human; however, the functions of these ATPases remain unclear. SPF1 is not essential for cell viability and its substrate specificity is unknown and loss of SPF1 may perturb homeostasis of ions that affects modification and sorting of proteins in the secretory pathway of yeast (Cronin et al., 2000; Suzuki, 2001).

To investigate the cellular role of CaM in *N. crassa*, we used CaM antagonists, TFP and CPZ. Moreover, we studied two other genes *trm-9* and *nca-2* using their knockout mutants. We found that the *cmd*, *trm-9*, and *nca-2* genes play a role in growth, Ca^{2+} sensitivity, and in acquisition of thermotolerance induced by heat shock temperature in *N. crassa*.

Materials and Methods

Sequence analysis

BLAST (Altschul et al., 1990) analysis was performed using software tools available from NCBI (http://blast.ncbi.nlm.nih.gov/Blast.cgi) and the proteins were selected based on *E* value, % identities and gapes as described previously (Tamuli et al., 2011). The Conserved Domain Database (CCD) (Marchler-Bauer et al., 2009) database was used to identify conserved domains in the protein. The homologue protein sequences were aligned with ClustalX 1.83 (Thompson et al., 1997) and visualized using GeneDoc (Nicholas et al., 1997). Phylogenetic trees were constructed from the aligned sequences using the minimum-evolution method (Rzhetsky and Nei, 1992), 500 bootstrap replications as test of phylogeny (Felsenstein 1985) and the software MEGA5 (Tamura et al., 2011). Promoter region was analyzed by selecting ~2 kb sequences from upstream of Transcription Start Site and transferred to MatInspector in Genomatix software (http://www.genomatix. de/cgi-bin//matinspector_prof/mat_fam) to predict transcription factor binding sites (Quandt et al., 1995).

Strains, growth, crosses maintenance

N. crassa wild-type strains 74-OR23-1 *mat A* (FGSC 987), 74-OR8-1 *mat a* (FGSC 988), Ca^{2+} signaling mutant strain ΔNCU04898.2::*hph mat A* (FGSC 1304 0), and ΔNCU04736.2::*hph mat* A (FGSC 13071) were generated by the *Neurospora* genome project and obtained from the Fungal Genetics Stock Center (FGSC; University of Missouri, Kansas city, MO 64110) (Colot et al., 2006; McCluskey 2010). The ΔNCU04898.2::*hph* ΔNCU04736.2::*hph* double mutant was generated by crossing the individual single mutant strain, and presence of the knockout alleles

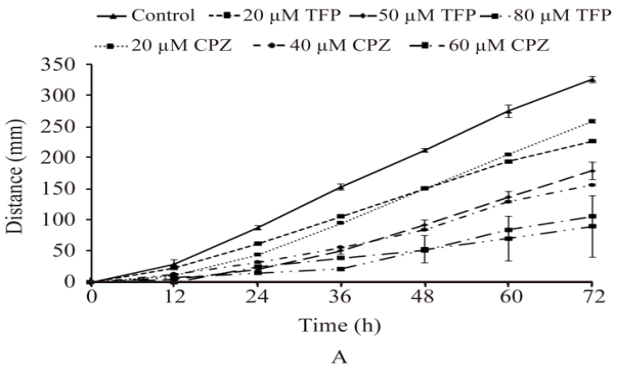

A

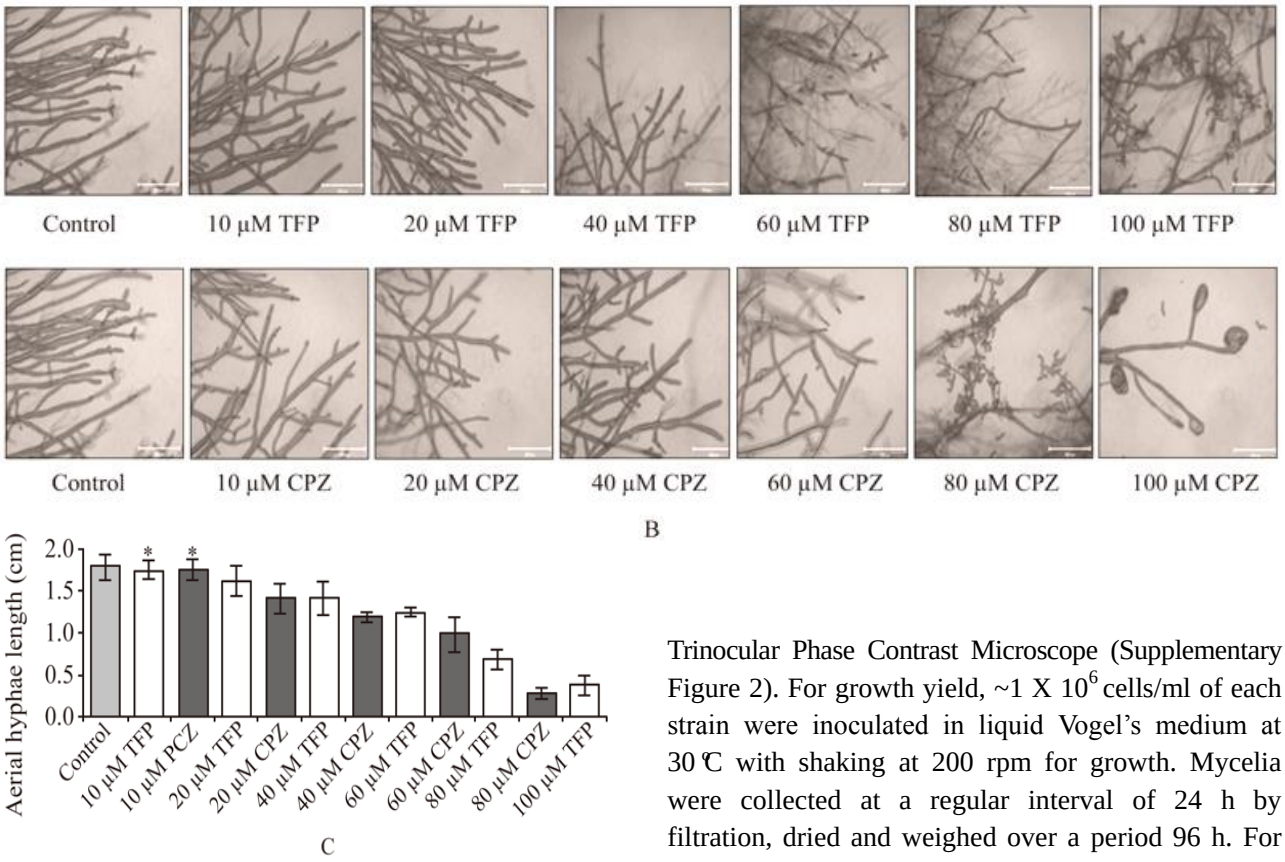

Figure 1 Effect of trifluoperazine (TFP) and chlorpromazine (CPZ) on growth of *N. crassa*. (A) Effect of TFP and CPZ at various concentrations on apical growth. (B) Abnormal hyphal morphology with increasing concentrations of TFP and CPZ. (C) Aerial hyphae length of cultures grown for 72 h in various concentrations of TFP and CPZ. Error bars indicate the standard errors calculated from the data for three independent experiments. Statistically significant values are indicated by asterisks, *P < 0.05

were verified using polymerase chain reactions (PCR) of the progeny strains (Supplementary Figure 1).

Growth, crossing, and maintenance of *Neurospora* strains were essentially as described by Davis and De Serres (1970). The apical growth was analyzed by using standard race tube assay and calculated as cm h^{-1} (Ryan et al., 1943, 1950). For aerial hyphae, ~1 X 10^6 cells/ml of each strain was grown in liquid Vogel's sucrose media (VSM) and incubated at 30°C for 48 h in dark followed by 24 h light illumination at room temperature and height of aerial hyphae was measured (Deka and Tamuli, 2013). Conidial count was done after 72 hours of growth; a sample of each strain was withdrawn and harvested using sterile water followed by conidial counting using a haemocytometer under a Trinocular Phase Contrast Microscope (Supplementary Figure 2). For growth yield, ~1 X 10^6 cells/ml of each strain were inoculated in liquid Vogel's medium at 30 ℃ with shaking at 200 rpm for growth. Mycelia were collected at a regular interval of 24 h by filtration, dried and weighed over a period 96 h. For analysis of hyphal morphology, strains were grown for 12 h on a thin layer of Vogel's agar on glass slide, and observed under microscope at 20X magnification. In addition, statistical significance was performed according to variance analysis (ANOVA, $P < 0.05$).

Assay for calcium sensitivity and thermotolerance

Assay for calcium sensitivity was done essentially as described previously (Deka et al., 2011). Briefly, conidia was placed in the centre of petri dishes containing Vogel's glucose (1.5%) media supplemented with 0.0 M, 0.2 M, 0.3 M, 0.4 M $CaCl_2$ incubated at 30 ℃ and colony diameter was measured every 3 h over a period of 24 h and growth rates were calculated as cm h^{-1}. For measuring thermotolerance, three days-old conidia were inoculated into liquid Vogel's Medium at a concentration of ~1 X 10^6 cells/ml and germinated for 2 h with shaking at 200 rpm at 30°C. These germlings were exposed to different heat treatment condition in two sets one set was held at 30°C for uninduced condition and the other set at 44°C for induced condition for 30 min, then one set of each were given a lethal heat shock at 52°C for 20 min. (Yang Qi and Borkovich, 1999; Kumar and Tamuli, 2014). After that these conidia were spread on sorbose agar (0.05 % fructose, 0.05 % glucose, 2% sorbose, 2 %

Bacto agar) plate and incubated at 30°C for 2 days. Percent survival was obtained by dividing the number of viable colonies on plates subjected to heat treatment by the number of viable colonies on plates held at 30°C (control) and multiplying by 100.

Carotenoid accumulation

To measure carotenoid accumulation, ~1 X 10^6 cells/ml of each *N. crassa* strains were inoculated into Vogel's sucrose (2%) medium supplemented with 0.2% Tween 80 used as a wetting agent to prevent conidiation (Zalokar, 1954) and kept for growth at 30°C for two days in dark, and at room temperature for one day under light. After that mycelia were filtered, lyophilized and powdered. Carotenoids were extracted from 50 mg lyophilized powder by using acetone and hexane. Total carotenoids content were calculated by measuring the maximum absorbance value at 470 nm and using formula: Total carotenoid content (µg/g) = [Total absorbance x Total volume of extract (ml) x 10^4]/ [Absorbance coefficient (2500) x Sample weight (g)] (Rodriguez-Amaya and Kimura 2004).

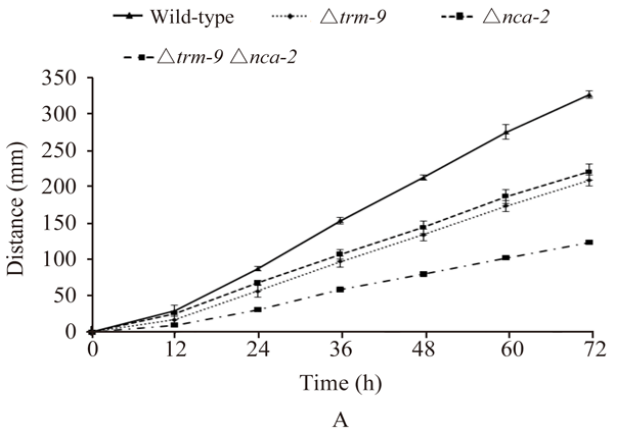

A

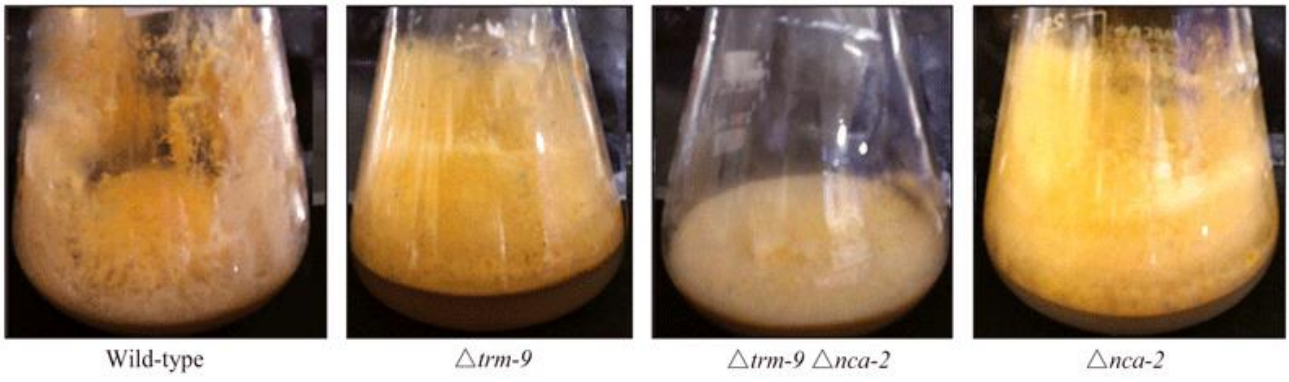

B

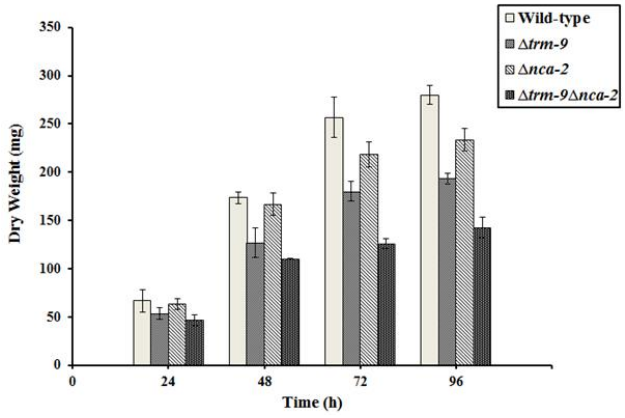

C

Figure 2 Growth phenotypes. (A) Rate of apical growth of the wild-type, Δ*trm-9*, Δ*nca-2*, and Δ*trm-9*Δ*nca-2* strains were measured using race tubes. Growth rate of Δ*trm-9*Δ*nca-2* double mutant strain was lesser as compared to parental single mutants and wild-type strain. (B) Colony morphology of wild-type, Δ*trm-9*, Δ*nca-2*, and Δ*trm-9*Δ*nca-2* double mutant strains. The Δ*trm-9*Δ*nca-2* double mutant strain showed matty-like growth and reduced pigmentation. (C) Dry weight of Δ*trm-9*, Δ*nca-2*, Δ*trm-9*Δ*nca-2* and wild-type strains. Dry weight yield of Δ*trm-9*Δ*nca-2* double mutant strain was less than parental single mutants and the wild-type

Results and Discussion

NCU04120, NCU04898, and NCU04736 genes encode CaM, TRM-9, and NCA-2, respectively, and contain conserved domains

The *N. crassa* calmodulin gene (*cmd*) NCU04120 encodes a highly conserved Ca^{2+} signaling protein CaM that possesses four conserved EF hand motifs (Supplementary Figure 3A). Similarly, the NCU04898 encodes a Ca^{2+}/cation ATPases annotated as TRM-9 (http://www.broadinstitute.org/annotation/genome/neur

ospora/MultiHome.html). The TRM-9 possesses one conserved E_1-E_2 ATPases domain, and one halo-acid dehalogenase like hydrolase domain (Supplementary Figure 3B). In addition, phylogenetic analysis revealed that CaM and TRM-9

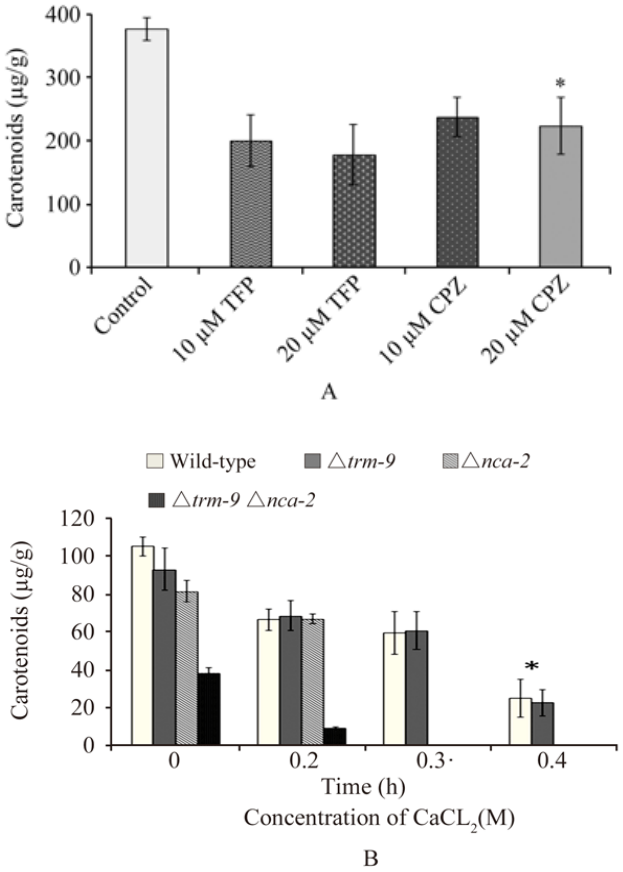

Figure 3 Analysis of carotenoids content. (A) Carotenoid content of wild-type strain in the presence of CaM antagonist TFP and CPZ. Standard errors calculated from the data for three independent experiments are shown using error bars. TFP act as negative regulator for carotenoid accumulation whereas CPZ act as positive regulator during carotenoid accumulation. (B) Carotenoids accumulation of wild-type, Δ*trm-9*, Δ*nca-2*, and Δ*trm-9*Δ*nca-2* double mutant strains during Ca^{2+}stress. Carotenoids extracted from these strains grown in Vogel's liquid medium without $CaCl_2$, supplemented with various concentrations of $CaCl_2$. Carotenoids were extracted and estimated in μg carotenoids per g of dry weight. Error bars show the standard errors calculated from the data for three independent experiments. Statistically significant values are indicated by asterisks, *P < 0.05

proteins are clustered with homologues from related (Supplementary Figure 4). Promoter analysis revealed important putative regulatory elements involved in transcription of *cmd* and *trm-9* gene by using MatInspector software (Supplementary Figure 5). The NCU04736 gene was previously shown to encode *nca-2* (Bowman et al., 2009; Bowman et al., 2011).

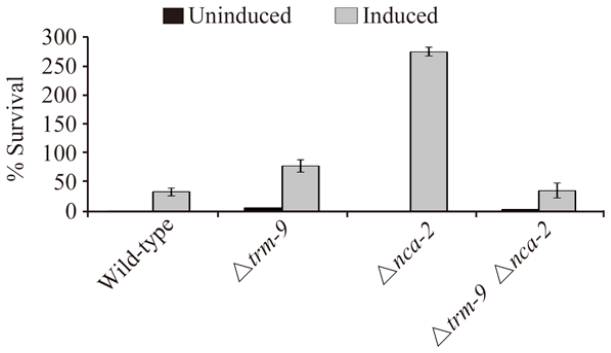

Figure 4 Thermotolerance measurement of wild-type, Δ*trm-9*, Δ*nca-2*, and Δ*trm-9*Δ*nca-2* double mutant strains in induced (44℃) and uninduced (30℃) conditions. Each data point represents the mean of three independent experiments

The *cmd*, *trm-9*, and *nca-2* genes are involved in growth

We used CaM antagonists, trifluoperazine (TFP) and chlorpromazine (CPZ) to study the effect of CaM inhibition on growth of wild-type strain of *N. crassa*. We found that both TFP and CPZ inhibit growth, a hyphal branching, and development of aerial hyphae in *N. crassa* (Figure 1). Moreover, addition of TFP (10, 20, 40, 60, 80, and 100 μM) or CPZ (20, 40, 60, 80, 100 μM) in the synthetic crossing medium (SCM) causes a defect in perithecia formation in *N. crassa* and results in a sterile phenotype (data not shown). In addition, the *cmd* transcript level was found to be decreased in the presence of TFP and CPZ as revealed by the real time PCR analysis (Supplementary Figure 6). These results suggest that CaM play a role in vegetative growth, hyphal development, and sexual development in *N. crassa*.

The Δ*trm-9* mutant displayed a slow growth phenotype (Figure 2A). However, the slow growth phenotype of the Δ*trm-9* mutant was not due to a defect in the ergosterol profile (Supplementary Figure 7) and the growth of the Δ*trm-9* mutant was not affected by addition of various amounts of $CaCl_2$, sucrose and NaCl in the medium indicating that the Δ*trm-9* mutant is insensitive to these stress conditions (data not shown). The growth defect was more severe in the Δ*trm-9*Δ*nca-2* double mutant that showed distinct

colony morphology with matty-like colony growth (Figure 2B). In addition, the dry weight of the strains followed the order wild-type>Δ*nca-2*> Δ*trm-9*> Δ*trm-9*Δ*nca-2* (Figure 2C). The Δ*trm-9*Δ*nca-2* double mutant also showed sensitivity to $CaCl_2$, reduced aerial hyphae development and ultraviolet (UV) survival (Supplementary Figure 8). Therefore, these results suggested that lack of both *trm-9* and *nca-2* result in impaired growth, hyphae development and conidial development in *N. crassa*.

Carotenoids accumulation

We also analyzed carotenoid accumulation in *N. crassa* in the presence of TFP and CPZ to investigate the role of CaM in carotenoid accumulation. The carotenoid profile of the wild-type strain in presence of the inhibitors followed the order wild-type > 10 μM CPZ > 20 μM CPZ >10 μM TFP > 20 μM TFP (Figure 3A). Therefore, these results indicate the CaM protein might modulate carotenoid accumulation in *N. crassa*. The difference of carotenoids accumulation in presence of TFP and CPZ might be due to the difference of mechanism of inhibition mediated by TFP and CPZ. Furthermore, carotenoids accumulation in the Δ*trm-9*Δ*nca-2* double mutant was lower than either of the parental single mutant strains, and reduced further on medium supplemented with high concentrations of $CaCl_2$ (Figure 3B). In addition, Δ*nca-2* mutant was unable to grow on medium supplemented with 0.3 M $CaCl_2$ or more (supplementray Figure 8A) and consequently, no carotenoids was accumulated; however, accumulation of carotenoids in the Δ*trm-9* was similar to the wild-type (Figure 3B). Therefore, these results suggest that *nca-2* plays a role in carotenoids biosynthesis.

Lack of both nca-2 and trm-9 affect in acquisition of induced thermotolerance

We studied the ability of the Δ*trm-9*Δ*nca-2* double mutant in acquisition of induced thermotolerance. The Δ*trm-9*Δ*nca-2* double mutants showed decreased survival in induced thermotolerance as compared to parental single mutants. The survival in induced heat shock temperature followed the order Δ*nca-2*> Δ*trm-9*>Δ*trm-9*Δ*nca-2*>wild-type (Figure 4). Therefore, lack of both *nca-2* and *trm-9* had a negative effect in acquisition of induced thermotolerance.

Conclusions

CaM and its target proteins mediate diverse cellular functions. The CaM antagonists TFP and CPZ affect growth, aerial hyphae development, carotenoids accumulation and sexual development in *N. crassa*. In addition, Δ*trm-9* mutant has a slow growth phenotype and less dry weight content. Moreover, the Δ*trm-9*Δ*nca-2* double mutant showed a severe growth defect, less carotenoid accumulation, reduced conidial count, an increased sensitivity to $CaCl_2$, and reduced viability in acquisition of thermotolerance induced by heat shock temperature. Thus, in this study, we have shown that *cmd*, *trm-9*, and *nca-2* genes play an important role in growth, pigmentation, and stress-tolerance in *N. crassa*.

Acknowledgements

The Fungal Genetic Stock Center (FGSC) generously waived charges for strains and race tube. The FGSC was supported by National Science Foundation grant BIR-9222772. We thank Upasana Sarma for performing some initial experiments. VL was supported by a Research Fellowship from the Ministry of Human Resource Development, Government of India. This work was supported partially by grants, including BT/PR3635/ BCE/8/ 892/2012, from the Department of Biotechnology, Government of India.

References

Altschul S.F., Gish W., Miller W., Myers E.W., et al., 1990, Basic local alignment search tool, J Mol Biol, 215:403-410
http://dx.doi.org/10.1016/S0022-2836(05)80360-2

Benito B., Garciadeblas B., et al., 2000, Molecular cloning of the calcium and sodium ATPases in *Neurospora crassa*, Mol. Microbiol, 35:1079-1088
http://dx.doi.org/10.1046/j.1365-2958.2000.01776.x

Blum J.J., Hayes A., Jamieson G.A. Jr., Vanaman T.C., 1980, Calmodulin confers calcium sensitivity on ciliary dynein ATPase, J Cell Bio, 87:386-397
http://dx.doi.org/10.1083/jcb.87.2.386

Borkovich K.A., Alex L.A., Yarden O., Freitag M., et al., 2004, Lessons from the genome sequence of *Neurospora crassa*: tracing the path from genomic blueprint to multicellular organism, Microbiol Mol Biol Rev, 68:1-108
http://dx.doi.org/10.1128/MMBR.68.1.1-108.2004

Bowman B.J., Draskovic M., Freitag M., Bowman E.J., 2009, Structure and distribution of organelles and cellular location of calcium transporters in *Neurospora crassa*, Eukaryot Cell, 8:1845-1855
http://dx.doi.org/10.1128/EC.00174-09

Bowman B.J., Abreu S., Margolles-Clark E., Draskovic M., et al., 2011, Role of four calcium transport proteins, encoded by *nca-1*, *nca-2*, *nca-3*, and *cax*, in maintaining intracellular calcium levels in *Neurospora crassa*, Eukaryot Cell, 10: 654-661
http://dx.doi.org/10.1128/EC.00239-10

Capelli N., Tuinen V.D., Perez O.R., Arrighi J.F., Turian G., 1993, Molecular cloning of a cDNA encoding CaM from *Neurospora crassa*, FEBS 321:63-68
http://dx.doi.org/10.1016/0014-5793(93)80622-2

Chung W.S., Lee S.H., Kim J.C., Heo W.D., Kim M.C., Park C.Y., Park H.C.,

Lim C.O., Kim W.B., Harper J.F., Cho M.J., 2000, Identification of a calmodulin-regulated soybean Ca^{2+} -ATPase (SCA1) that is located in the plasma membrane, Plant Cell, 12:1393-1407
http://dx.doi.org/10.1105/tpc.12.8.1393

Colot H.V., Park G., Turner G.E., Ringelberg C., Crew C.M., Litvinkova L., Weiss R.L., Borkovich K.A., Dunlap J.C., 2006, A high throughput gene knockout procedure for Neurospora reveals functions for multiple transcription factors, ProcNatlAcadSci USA 103:10352–10357
http://dx.doi.org/10.1073/pnas.0601456103

Cronin S.R., Khoury A., Ferry D.K., Hampton R.Y., 2000, Regulation of HMG-CoA reductase degradation requires the P-Type ATPase Cod1p/Spf1p, J Cell Bio 148: 915-924
http://dx.doi.org/10.1083/jcb.148.5.915

Cox J.A., Ferraz C., Demaille J.G., Perez R.O., Van Tuinen D., Marm é D., 1982, Calmodulin from *Neurosporacrassa*. General properties and conformational changes, J Biol Chem, 257:10694-10700

Davis R.H., De Serres F.J., 1970, Genetic and microbial research techniques for *Neurospora crassa*, Methods Enzymol, 17:79-143
http://dx.doi.org/10.1016/0076-6879(71)17168-6

Deka R., Kumar R., Tamuli R., 2011, *Neurospora crassa* homologue of neuronal calcium sensor-1 has a role in growth, calcium stress tolerance, and ultraviolet survival, Genetica 139:885-894
http://dx.doi.org/10.1007/s10709-011-9592-y

Deka R., Tamuli R., 2013, *Neurospora crassa ncs-1*, *mid-1* and *nca-2* double-mutantphenotypes suggest diverse interaction among three Ca^{2+}-regulating gene products, J Genet, 92:559-563
http://dx.doi.org/10.1007/s12041-013-0270-y

Felsenstein J., 1985, Confidence limits on phylogenies: an approach using the bootstrap, Evolution, 39:783-791
http://dx.doi.org/10.2307/2408678

Galagan J.E., Calvo S.E., Borkovich K.A., Selker E.U., et al., 2003, The genome sequence ofthe filamentous fungus *Neurospora crassa*, Nature 422:859–868
http://dx.doi.org/10.1038/nature01554

Giacomello M., De Mario A., Scarlatti C., Primerano S., Carafoli E., 2013, Plasma membrane calcium ATPases and related disorders, J Biochem and Cell Bio 45:753-762
http://dx.doi.org/10.1016/j.biocel.2012.09.016

Hao L., Rigaud J.L., Inesi G., 1994, Ca^{2+}/H^{+}countertransport and electrogenicity in proteoliposomes containing erythrocyte plasma membrane Ca- ATPase and exogenous lipids, J Bio Chem, 269:14268-14275

Haro R., Garciadeblas B., Rodr guez-Navarro A., 1991, A novel P-type ATPase from yeast involved in sodium transport, FEBS Lett, 291: 189-191
http://dx.doi.org/10.1016/0014-5793(91)81280-L

Harper J.F., Hong B., Hwang I., Guo H.Q., Stoddard R., Huang J.F., Palmgren M.G., Sze H., 1998, A novel calmodulin-regulated Ca^{2+}-ATPase (ACA2) from Arabidopsis with an N-terminal autoinhibitory domain, J Biol Chem, 273:1099-10106
http://dx.doi.org/10.1074/jbc.273.2.1099

Hong B., Ichida A., Wang Y., Gens J.S., Pickard B.G., Harper J.F., 1999, Identification of a calmodulin-regulated Ca^{2+}-ATPase in the endoplasmic reticulum, Plant Physio, 119:1165-1176
http://dx.doi.org/10.1104/pp.119.4.1165

Iida H., Ohya Y., Anraku Y., 1995, Calmodulin-dependent protein kinase II and calmodulin are required for induced thermotolerance in *Saccharomyces cerevisiae*, Curr Genet, 27:190-193
http://dx.doi.org/10.1007/BF00313434

Kahl C.R., Means A.R., 2003, Regulation of cell cycle progression by calcium/CaM-dependent pathways, Endocrine society, 24:719-736

Kirchberger A.M., Antonetz T., 1982, Calmodulin-mediated regulation of calcium transport and (Ca^{2+} + M^{2+})-activated ATPase activity in isolated cardiac sarcoplasmic reticulum, J Bio Chem, 257: 5685-5691

Kraus R.P., Heitman J., 2003, Coping with stress: CaM and calcineurin in model and pathogenic fungi, Biochem Biophy Res, 311:1151-1157
http://dx.doi.org/10.1016/S0006-291X(03)01528-6

Kumar R., Tamuli R., 2014, Calcium/calmodulin-dependent kinases are involved in growth, thermotolerance, oxidative stress survival, and fertility in *Neurospora crassa*, Archives of Microbio, 196: 295-305
http://dx.doi.org/10.1007/s00203-014-0966-2

Lopes M.C., Vale M.G., Carvalho A.P., 1990, Ca^{2+} -dependent binding of tamoxifen to calmodulin isolated from bovine brain, Cancer Res, 50:2753-2758

Luan J., Liu Z., Zhang S., Li H., Fan C., Li L., 2007, Characterization, evolution and expression of the calmodulin1 genes from the amphioxus *Branchiostomabelcheritsingtauense*, Acta Biochem Biophys Sin (Shanghai). 39:255-264
http://dx.doi.org/10.1111/j.1745-7270.2007.00277.x

Malmstrom S., Askerlund P., Palmgren M.G., 1997, A calmodulin-stimulated Ca^{2+} -ATPase from plant vacuolar membranes with a putative regulatory domain at its N-terminus, FEBS Letters, 400:324-328
http://dx.doi.org/10.1016/S0014-5793(96)01448-2

Malmstrom S., Akerlund H.E., Askerlund P., 2000, Regulatory role of the N terminus of the vacuolar calcium-ATPase in cauliflower, Plant Physiol, 122: 517-526
http://dx.doi.org/10.1104/pp.122.2.517

Marchler-Bauer A., Anderson J.B., Chitsaz F., Derbyshire M.K., et al., 2009, CDD: specific functional annotation with the Conserved Domain Database, Nucleic Acids Res 37 (Database issue):D205-D210
http://dx.doi.org/10.1093/nar/gkn845

McCluskey K., Wiest A., Plamann M., 2010, The Fungal Genetics Stock Center: a repository for 50 years of fungal genetics research, J Biosci, 35:119-126
http://dx.doi.org/10.1007/s12038-010-0014-6

Means R.A., Dedman R.J., 1980, CaM-an intracellular calcium receptor, Nature, 285:73-77
http://dx.doi.org/10.1038/285073a0

Nicholas K.B., Nicholas H.B., 1997, GeneDoc: a tool for editing and annotating multiple sequence alignments, Distributed by the author, http://www.psc.edu/biomed/genedoc

Osborn D.K., Zaidi A., Mandal A., Urbauer R.J., Johnson C.K., 2004, Single molecule dynamics of the calcium-dependent activation of plasma membrane Ca^{2+}-ATPase by calmodulin, Biophy J., 87: 1892-1899
http://dx.doi.org/10.1529/biophysj.103.039404

Peersen B.O., Madsen S.T., Falke J.J., 1997, Intermolecular tuning of calmodulin by target peptides and proteins: Differential effects on Ca^{2+} binding and implications for kinase activation, Protein Science, 6:794-807
http://dx.doi.org/10.1002/pro.5560060406

Perez O.R., Tuninen V.D., Marme D., Cox A.J., Turian G., 1981, Purification and identification of CaM from *Neurospora crassa*, FEBS 133:205-208
http://dx.doi.org/10.1016/0014-5793(81)80506-6

Quandt K., Frech K., Karas H., Wingender E., et al., 1995, MatInd and MatInspector: new fast and versatile tools for detection of consensus matches in nucleotide sequence data, Nucleic Acids Res, 23:4878-4884
http://dx.doi.org/10.1093/nar/23.23.4878

Rodriguez-Amaya D.B., Kimura M., 2004, Harvest Plus handbook for carotenoid analysis. Harvest Plus Technical Monograph 2, International Food Policy Research Institute (IFPRI) and International Center for Tropical Agriculture (CIAT), Washington, DC

Ryan F.J., Beadle G.W., Tatum E.L., 1943, the tube method of measuring the growth rate of *Neurospora*, Am J Bot, 30:784-799
http://dx.doi.org/10.2307/2437554

Ryan F.J., 1950, Selected method of *Neurospora* genetics, Method Med Res, 3:51-75

Rzhetsky A., Nei M., 1992, Statistical properties of the ordinary least-generalized least-squares, and minimum-evolution methods of phylogenetic inference, J Mol Evol, 35:367-375
http://dx.doi.org/10.1007/BF00161174

Sadakane Y., Nakashima H., 1996, Light-induced phase shifting of the circadian conidiation rhythm is inhibited by calmodulin antagonists in *Neurospora crassa*, J Biol Rhythms, 11:234-240
http://dx.doi.org/10.1177/074873049601100305

Smallwood S.H., Lopez F.D., Eberlein E.P., Watson J.D., and Squier C.T., 2009, Calmodulin mediates DNA repair pathways involving H2AX in response to low-dose radiation exposure of RAW 264.7 Macrophages, Chem Res Toxicol, 22:460-470
http://dx.doi.org/10.1021/tx800236r

Suresh K., Subramanyam C., 1997, A putative role for CaM in the activation of *Neurospora crassa* chitin synthase, FEMS Micro biol letters , 150:95-100
http://dx.doi.org/10.1111/j.1574-6968.1997.tb10355.x

Suzuki S., Katagiri S., Hideaki, 1996, Mutants with altered sensitivity to a CaM antagonist affect the circadian clock in *Neurospora crassa*, *Gen*ectics, 143:1175-1180

Suzuki C., 2001, Immunochemical and mutational analysis of P-type ATPase Spf1p involved in the yeast secretory pathway, Biosci Biotecnol Biochem, 65:2405-2411
http://dx.doi.org/10.1271/bbb.65.2405

Tamuli R., Kumar R., Deka R., 2011, Cellular roles of neuronal calcium sensor-1 and calcium/calmodulin-dependent kinases in fungi, J Basic Microbiol, 51:120-128
http://dx.doi.org/10.1002/jobm.201000184

Tamuli R., Kumar R., Srivastava D.A., Deka R., 2013, Calcium signaling. In: Kasbekar DP, McCluskey K (eds) Neurospora: genomics and molecular biology, Caister Academic Press, Norfolk, pp 35-57

Tamura K., Peterson D., Peterson N., Stecher G., et al., 2011, MEGA5: molecular evolutionary genetics analysis using maximum likelihood, evolutionary distance, and maximum parsimony methods, Mol Biol Evol, 28:2731-2739
http://dx.doi.org/10.1093/molbev/msr121

Thompson J.D., Gibson T.J., Plewniak F., Jeanmougin F., et al., 1997, The CLUSTAL_X windows interface: flexible strategies for multiple sequence alignment aided by quality analysis tools, Nucleic Acids Res, 25:4876-4882
http://dx.doi.org/10.1093/nar/25.24.4876

Yang Q., Borkovich K.A., 1999, Mutational activation of a Gαi causes uncontrolled proliferation of aerial hyphae and increased sensitivity to heat and oxidative stress in *Neurospora crassa*, Genetics, 151:107-117

Zalokar M., 1954, Studies on biosynthesis of carotenoids in *Neurospora crassa*, Arch Biochem Biophys, 50:71-80
http://dx.doi.org/10.1016/0003-9861(54)90010-7

Supplementary Materials

Supplementary Figure 1: PCR analysis for double mutant confirmation. The Δ*trm-9*Δ*nca-2* double mutants were verified by using the forward primers NCU04898-5F 5' GGTTAGTGAGCTTTGAGTCG 3' and NCU04736 -5F 5' TACACTGGTAATGGACCACG 3' specific for upstream of the open reading frame of genes *trm-9* and *nca-2*, respectively, and with the common reverse primer 5HPHR 5' ATCCACTTAACGTTACTGAAATC 3' that is specific for the *hph* cassette used to generate the knockout mutants (Colot et al., 2006; Deka et al., 2011). Amplification of PCR products of size ~1.2 and ~1.018 kb indicate the presence *trm-9* and *nca-2* knockout alleles respectively. The wild-type was used as negative controls for the knockout alleles (indicated in the parenthesis) using the allele specific primer pairs. PCR products were visualized in a 0.8% agarose gel with 1 kb DNA ladder.

Supplementary Figure 2: Conidial cell count of wild-type, Δ*trm-9*, Δ*nca-2*, and Δ*trm-9*Δ*nca-2* double mutant strains grown in Vogel's glucose medium. Conidia count of wild-type and mutant strains are plotted with relative counting with respect to wild-type. Error bars indicate the standard errors calculated from the data for three independent experiments. Conidial cell count of Δ*trm-9*Δ*nca-2* double mutant strain was less than the parental single knockout mutant strains and wild-type.

Supplementary Figure 3: Sequence alignment of *cmd* and *trm9* homologues. (A) Sequence alignment of the *Neurospora crassa* CaM homologues. (B) Sequence alignment of the *trm-9* homologues. Conserved amino acids are indicated in black (100%), dark gray (>80%) and light gray (>60%). The homologue sequences used for the sequence analysis are from *Ajellomyces capsulatus* (AC), *Ajellomyces dermatitidis SLH14081* (AD), *Aspergillus fumigatus* (AF), *Aspergillus nidulans* (AN), *Botryotinia fuckeliana B05.10* (BF), *Candida albicans* (CA), *Coccidioides immitis* (CI), *Cordyceps militaris CM01* (CM), *Coccidioides posadasii* (CP), *Dichotomomy cescejpii* (DC), *Esox lucius* (EL), *Grosmannia clavigera kw1407* (GC), *Glomerella graminicola* (GG),*Gibberella zeae PH-1* (GZ), *Homo sapiens* (HS), *Komagataella pastoris* (KP), *Magnaporthe grisea* (MG), *Neurospora crassa* (NC), *Neurospora tetrasperma* (NT), *Procambarus clarkii* (PC), *Phytophthora infestans T30-4* (PI), *Rhodomonas sp. CCMP768* (RS), *Saccharomyces cerevisiae* (SC), *Schistosoma mansoni* (SM), *Spathaspora passalidarum* (SP), *Trichoderma reesei* (TR), and *Talaromyces stipitatus ATCC 10500* (TS).

Supplementary Figure 4: Phylogenetic analysis of the (A) CaM and (B) TRM-9 proteins. Protein sequences are described using GenBank accession numbers, phylum is indicated at major clades, and bar indicates scale of genetic distances. The homologue sequences used for the sequence analysis are from *Ajellomyces capsulatus* (AC), *Ajellomyces dermatitidis SLH14081* (AD), *Aspergillus fumigatus* (AF), *Arthroderma gypseum* (AG), *Aspergillus kawachii* (AK), *Aspergillus nidulans* (AN), *Aspergillus oryzae* (AO), *Botryotinia fuckeliana B05.10* (BF), *Candida albicans* (CA), *Coccidioides immitis* (CI), *Cordyceps militaris CM01* (CM), *Coccidioides posadasii* (CP), *Dichotomomy cescejpii* (DC), *Drosophila melanogaster* (DM), *Exophiala dermatitidis* (ED), *Esox lucius* (EL), *Eurotium rubrum* (ER), *Emericella unguis* (EU), *Grosmannia clavigera kw1407* (GC), *Glomerella graminicola* (GG), *Gibberella zeae PH-1* (GZ), *Homo sapiens* (HS), *Komagataella pastoris* (KP), *Metarhizium anisopliae* (MA), *Magnaporthe grisea* (MG), *Neurospora crassa* (NC), *Neurospora tetrasperma* (NT), *Ogataeapara polymorpha* (OP), *Paracoccidioides brasiliensis* (PB), *Procambarus clarkii* (PC), *Puccinia graminis f. sp. Tritici* (PG), *Phytophthora infestans T30-4* (PI), *Penicillium rolfsii* (PR), *Pyrenophora tritici-repentis* (PT), *Rhodomonas sp. CCMP768* (RS), *Saccharomyces cerevisiae* (SC), *Saccharomyces cerevisiae RM11-1a* (SC RM11), *Saccharomyces cerevisiae* x *Saccharomyces kudriavzevii VIN7* (SCSK), *Sordaria macrospora* (SM), *Spathaspora passalidarum* (SP), *Scheffersomyce sstipitis* (SS), *Trichophyton equinum* (TE), *Trichoderma reesei* (TR), *Talaromyces stipitatus ATCC 10500* (TS), and *Verticillium albo-atrum* (VA).

Supplementary Figure 5: Promoter analysis of (A) *cmd* and (B) *trm-9* gene of *N. crassa*. Gray boxes showed the important regulatory sequences of gene and transcription start site (TSS) are indicated by using arrows.

Supplementary Figure 6: Expression studies of *cmd* gene in the presence of inhibitors. Fold change in expression was calculated by $2^{-\Delta\Delta Ct}$ method, using wild-type and β-tubulin as calibrator and endogenous control respectively. Standard errors calculated from the data for two independent experiments are shown using error bars.

Supplementary Figure 7: Ergosterol is present in the Δ*trm-9* mutant and Δ*trm-9*Δ*nca-2* double mutant strains. Profile of the sterols extracted from the wild-type, Δ*nca-2*, Δ*trm-9*, Δ*trm-9*Δ*nca-2*, and *erg-3* mutant strains were analysed by UV spectrophotometer.

Supplementary Figure 8: (A) Calcium sensitivity, (B) development of aerial hyphae, and (C) UV survival. (A) Ca^{2+}sensitivity analysis of wild-type, Δ*trm-9*, Δ*nca-2*, and Δ*trm-9*Δ*nca-2* double mutant strains. Colony diameter (cm h^{-1}) were measured at regular intervals and plotted against various concentrations of $CaCl_2$. Standard errors calculated from the data for three independent experiments are shown using error bars. (B) Aerial hyphae development of the wild-type, Δ*trm-9*, Δ*nca-2*, and Δ*trm-9*Δ*nca-2* double mutant strains on VSM agar media in test tube. The aerial hyphae growth of Δ*trm-9*Δ*nca-2* double mutant strain was less as compared to parental single mutants and wild-type strain. (C) UV survival. Spot-test analysis of wild-type, Δ*trm-9*, Δ*nca-2*, and Δ*trm-9*Δ*nca-2* double mutant and *upr-1* mutant strain grown on VG agar at 30°C for 48 h in dark then illuminated for 24 h. UV survival assay was done essentially as described previously (Deka et al., 2011).

Supplementary references:

Colot H.V., Park G., Turner G.E., Ringelberg C., Crew C.M., Litvinkova L., Weiss R.L., Borkovich K.A., Dunlap J.C., 2006, A high-throughput gene knockout procedure for *Neurospora* reveals functions for multiple transcription factors, Proc Natl Acad Sci U S A 103:10352-10357 http://dx.doi.org/10.1073/pnas.0601456103

Deka R., Kumar R., Tamuli R., 2011, *Neurospora crassa* homologue of Neuronal Calcium Sensor-1 has a role in growth, calcium stress tolerance, and ultraviolet survival, Genetica 139:885-894 http://dx.doi.org/10.1007/s10709-011-9592-y

Supplementary Figure 1

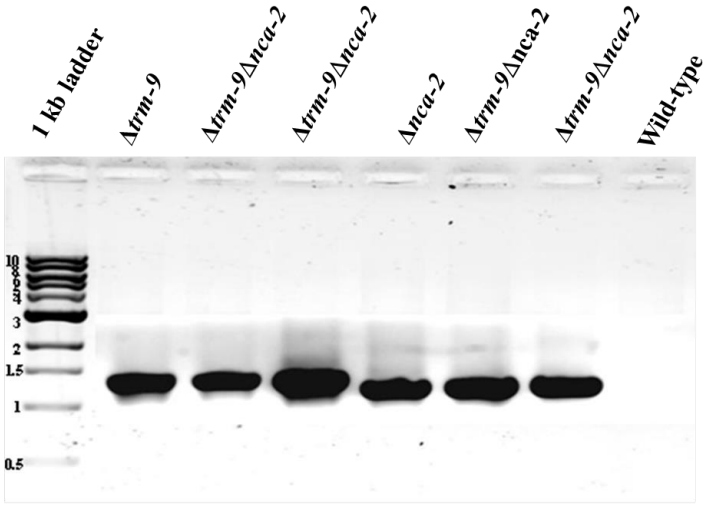

Supplementary Figure 2

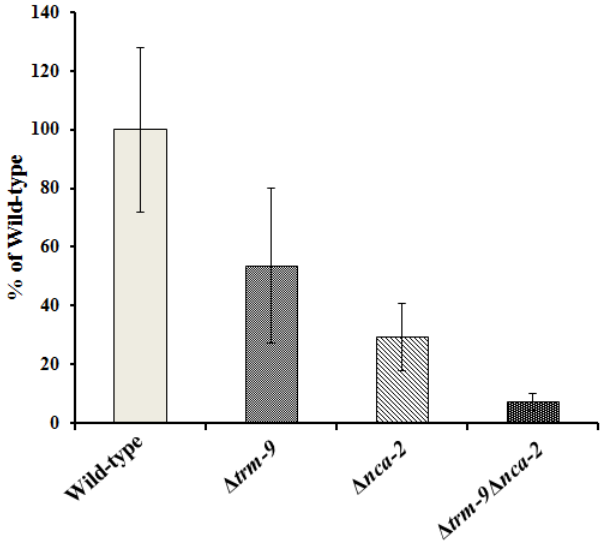

Supplementary Figure 3

A.

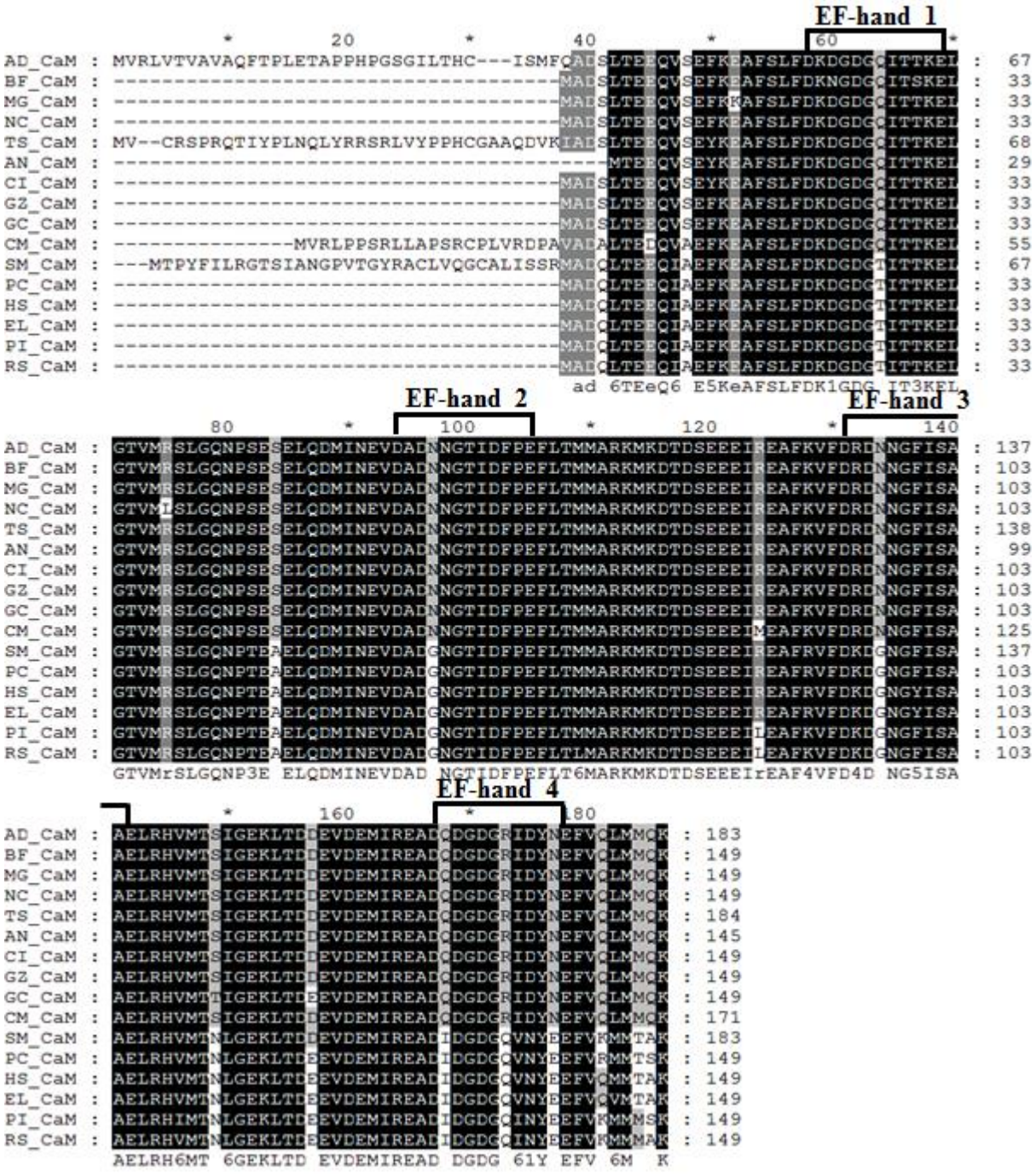

B.

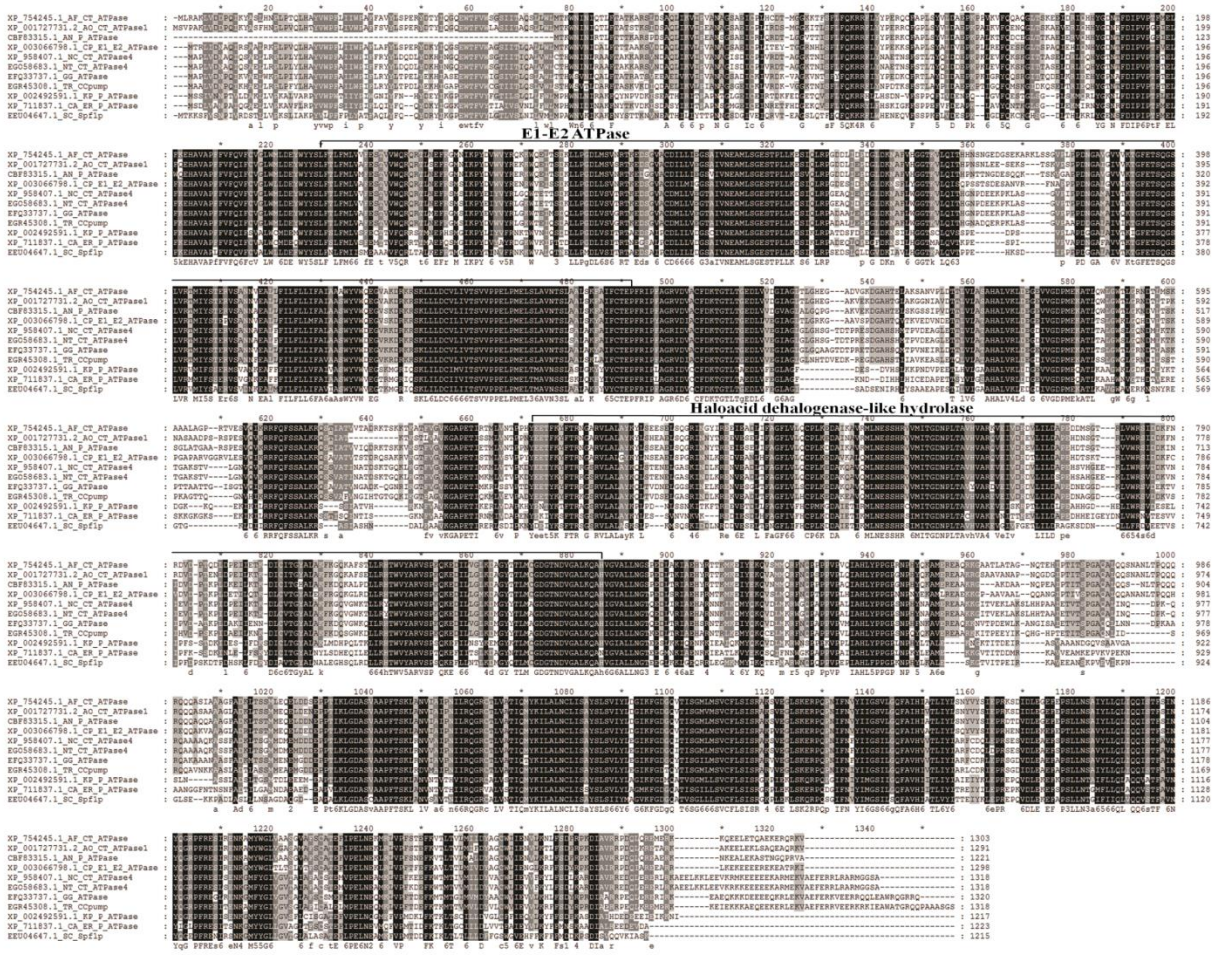

Supplementary Figure 4

A.

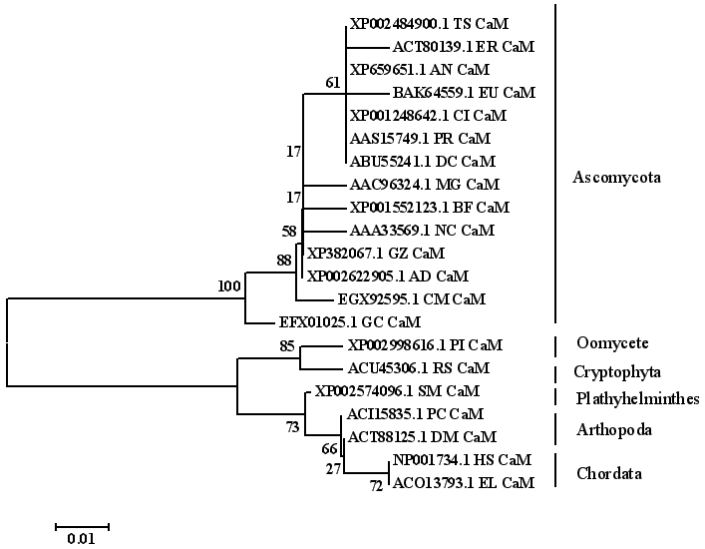

B.

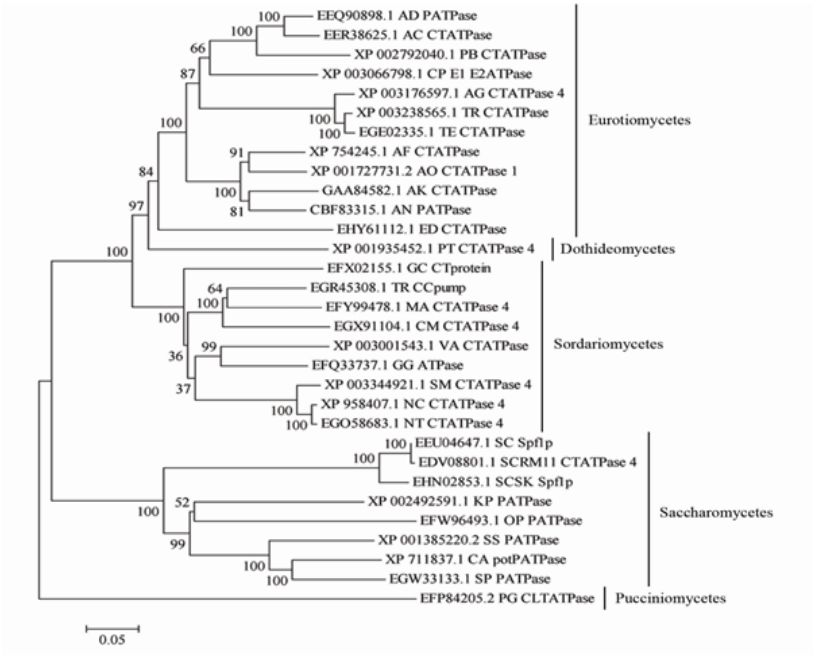

Supplementary Figure 5

A.

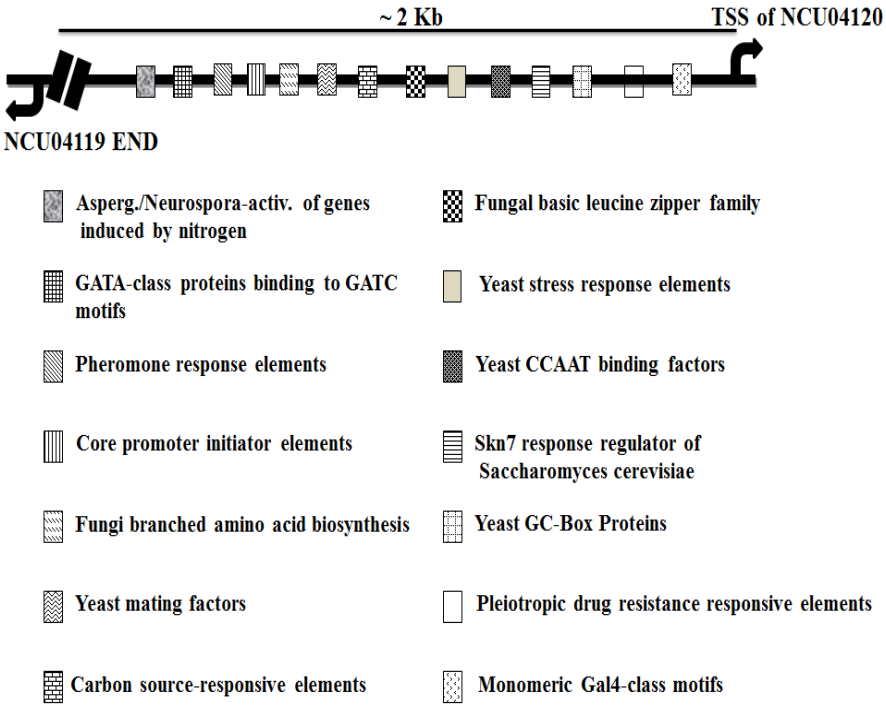

B.

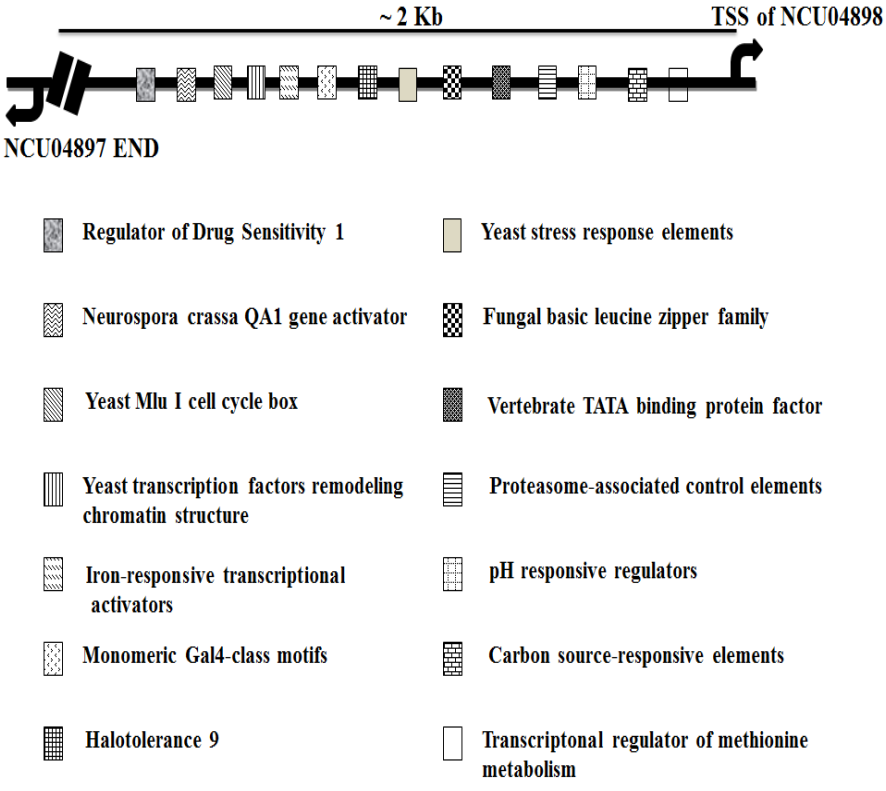

Supplementary Figure 6

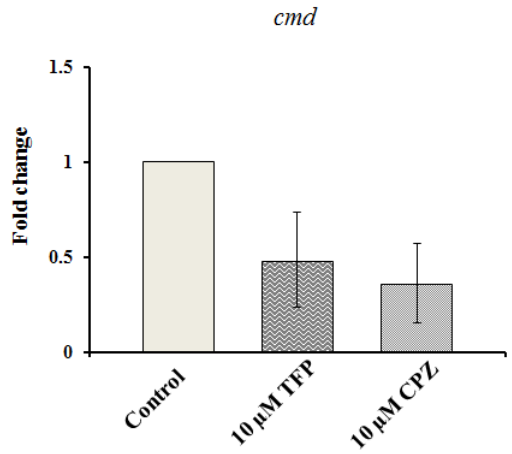

Supplementary Figure 7

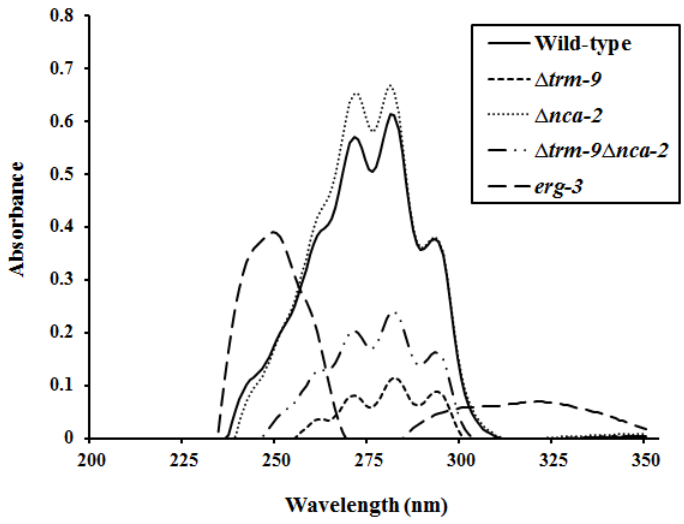

Supplementary Figure 8

A.

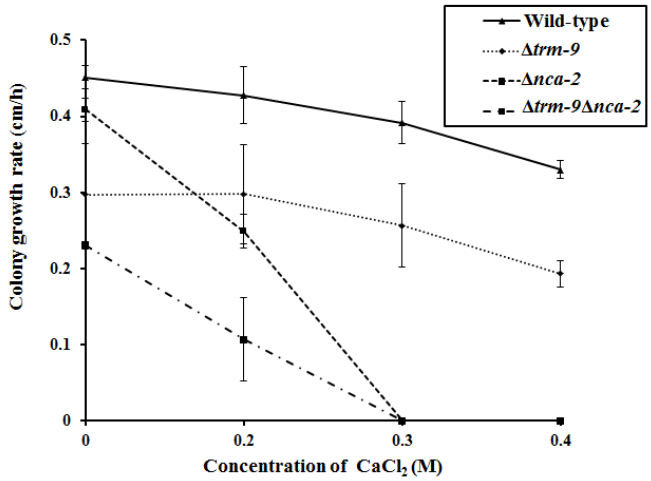

B.

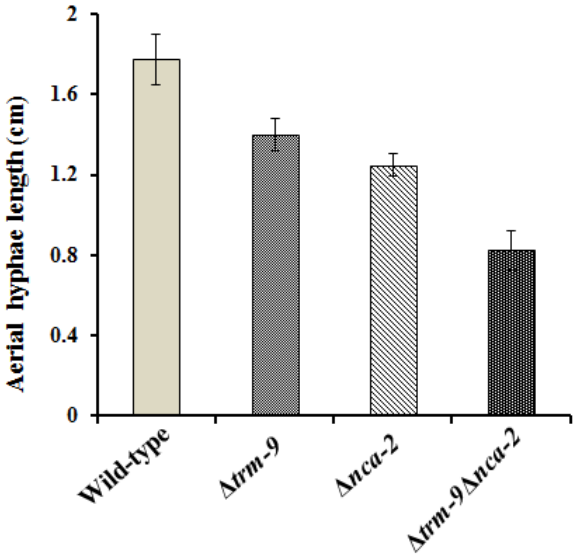

C.

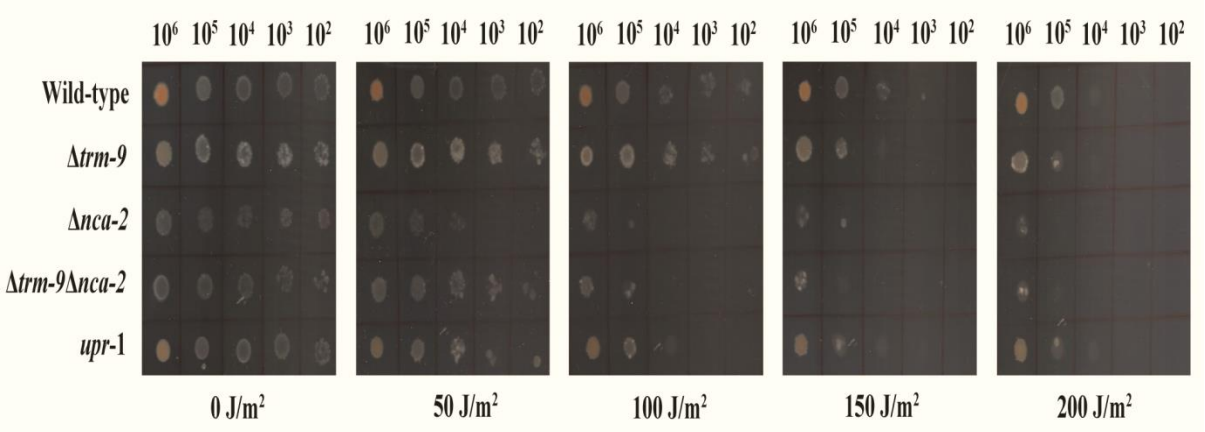

Arch Microbiol
DOI 10.1007/s00203-016-1319-0

ORIGINAL PAPER

The calmodulin gene in *Neurospora crassa* is required for normal vegetative growth, ultraviolet survival, and sexual development

Vijya Laxmi[1] · **Ranjan Tamuli**[1]

Received: 27 June 2016 / Revised: 2 November 2016 / Accepted: 7 November 2016

Abstract We isolated a *Neurospora crassa* mutant of the calmodulin (*cmd*) gene using repeat-induced point mutation and studied its phenotypes. The *cmd*^{RIP} mutant showed a defect in growth, reduced aerial hyphae, decreased carotenoid accumulation, a severe reduction in viability upon ultraviolet (UV) irradiation, and a fertility defect. Moreover, meiotic silencing of the *cmd* gene resulted in a barren phenotype. In addition, we also performed site-directed mutational analysis of the calcium/calmodulin-dependent kinase-2 (Ca^{2+}/CaMK-2), a target of the CaM protein encoded by the *cmd* gene. The *camk-2*^{S247A} and the *camk-2*^{T267A} mutants in a homozygous cross, or in a cross with a *Δcamk-2* mutant, displayed an intermediate phenotype, suggesting that serine 247 and threonine 267 phosphorylation sites of the Ca^{2+}/CaMK-2 are essential for full fertility in *N. crassa*. Therefore, CaM in *N. crassa* is required for normal vegetative growth, UV survival, and sexual development. Additionally, serine 247 and threonine 267 phosphorylation sites are important for the Ca^{2+}/CaMK-2 function.

Keywords Calcium signaling · Calcium/calmodulin-dependent protein kinases · Calmodulin · *Neurospora crassa* · Meiotic silencing · Repeat-induced point mutation

Communicated by Erko Stackebrandt.

Electronic supplementary material The online version of this article (doi:10.1007/s00203-016-1319-0) contains supplementary material, which is available to authorized users.

✉ Ranjan Tamuli
ranjantamuli@iitg.ernet.in; ranjan.tam@gmail.com

[1] Department of Biosciences and Bioengineering, Indian Institute of Technology Guwahati, Guwahati, Assam 781 039, India

Introduction

Calcium (Ca^{2+}) plays a central role as an intracellular signal in biological systems (Berridge 1987; Gadd 1994; Sanders et al. 2002; Davies and Terhzaz 2009). Ca^{2+} signaling is mediated by a number of proteins including a high-affinity Ca^{2+} sensor protein calmodulin (CaM) that regulates numerous cell functions in different organisms including the model filamentous fungus *Neurospora crassa* (Tamuli et al. 2013; Laxmi and Tamuli 2015). In *N. crassa*, only one CaM was isolated using affinity chromatography and identified based on its characteristic Ca^{2+}-dependent shift in electrophoretic migration, activation of bovine heart cAMP-phosphodiesterase (PDE), and characteristic peaks in an absorption spectrum (Ortega Perez et al. 1981; Cox et al. 1982; Capelli et al. 1993). The *N. crassa* CaM is somewhat less acidic than its vertebrate counterpart, and its amino acid composition is typical of plant CaM with the exception of lack of trimethyllysine and unusual high content of serine (Cox et al. 1982). The *N. crassa* CaM shows 85% sequence identity with the human CaM protein and is less potent in the activation of myosin light chain kinase than CaM from higher organisms (Cox et al. 1982; Melnick et al. 1993). CaM activates soluble adenylate cyclase, Ca^{2+}/CaM-dependent protein kinase (Ca^{2+}/CaMK), cyclic AMP phosphodiesterase, and protein phosphatase in *N. crassa* (Reig et al. 1984; Tuinen et al. 1984; Tellezinon et al. 1985; Higuchi et al. 1991).

CaM is an essential gene in *N. crassa*, therefore, its functions were investigated using the CaM antagonists, trifluoperazine (TFP), and chlorpromazine (CPZ). Inhibition of CaM using TFP and CPZ was resulted in a defect in vegetative and hyphal growth, shortening of period length of the conidiation rhythm, light-induced phase shifting, activation of chitin synthase enzyme, and sexual development in *N.*

Published online: 25 November 2016

crassa (Sadakane and Nakashima 1996; Suzuki et al. 1996; Suresh and Subramanyam 1997; Laxmi and Tamuli 2015).

CaM interacts with various proteins and enzymes including the Ca^{2+}/CaMK II, a Ser/Thr protein kinase, to amplify the Ca^{2+} signaling cascade. The Ca^{2+}/CaMK II contains a conserved N-terminal catalytic domain and a C-terminal regulatory domain containing overlapping autoinhibitory and Ca^{2+}/CaM-binding domains (Swulius and Waxham 2008; Kumar and Tamuli 2014). The autoinhibitory segment is positioned in the active site, sterically blocking access to its substrates. Binding of Ca^{2+}/CaM displaces the autoinhibitory segment by wrapping around kinase resulting in its activation (Hoffman et al. 2011). The Ca^{2+}/CaMK II can then lock itself into activated state by autophosphorylation on a conserved threonine residue (Thr 286) in the autoinhibitory segment that increases its affinity for CaM to about 1000-fold, which markedly reduces the dissociation rate of bound Ca^{2+}/CaM purified from rat brain (Meyer et al. 1992).

N. crassa contains four Ca^{2+}/CaMKs, and two kinases CAMK-1 and CAMK-2 were shown essential for full fertility (Kumar and Tamuli 2014). The *N. crassa* Ca^{2+}/CaMK-2 also contains a conserved kinase domain, and overlapping autoinhibitory and Ca^{2+}/CaM-binding domains like other Ca^{2+}/CaMK II homologs (Tamuli et al. 2011; Kumar and Tamuli 2014). However, due to essential requirement, detailed cellular roles of CaM and its interactions with target proteins including Ca^{2+}/CaMK-2 have remained elusive.

In this study, we generated *N. crassa* strains duplicated for the *cmd* gene cloned under the copper-responsive promoter *tcu-1* (P_{tcu-1}) to generate *cmd* mutant by repeat-induced point mutation (RIP), and to identify its critical amino acid resides (Cambareri et al. 1989; Lamb et al. 2013; Tamuli et al. 2016). We isolated a RIP-induced *cmd* mutant that showed a defect in morphology, growth, and carotenoid accumulation. In addition, we performed site-directed mutations of two putative phosphorylation sites and a residue in the CaM-binding domain of the CaMK-2, and identified an essential role of the serine 247 and threonine 267 phosphorylation sites for full fertility in *N. crassa*.

Materials and methods

Strains, media, growth conditions, transformation, sequencing, assay for carotenoid accumulation and ultraviolet sensitivity, and meiotic silencing

Media, growth, and crosses of Neurospora were essentially as described previously (Westergaard and Mitchell 1947; Davis and De Serres 1970). The *N. crassa* wild type, the *Δcmd* (hetrokaryon), and the other mutant strains used in this study were either obtained from the Fungal Genetics Stock Center (FGSC, Manhattan, KS) or generated in our laboratory (Table 1; McCluskey et al. 2010). The standard Vogel's media (VM; Vogel 1964) were routinely used for Neurospora growth, and growth media were supplemented with pantothenate (0.01 mg/ml; Murray and Perkins 1963; http://www.fgsc.net/methods/stanford.html) and bathocuproinedisulfonic acid (250 μM) where indicated. Antibiotics resistance was scored on medium containing 0.05% fructose, 0.05% glucose, and 2% sorbose (FGS) containing 2% bacto agar and supplemented with hygromycin B (220 μg/ml), basta (400 μg/ml), or nourseothricin (50 μg/ml) for the selection of progeny containing constructs with the selectable marker *hph*, *bar*, or *nat*, respectively (Tamuli et al. 2016). For basta selection, VM containing 0.5% L-proline in lieu of ammonium (NH_4NO_3) was also used. Transformation of *N. crassa* strains was performed using a BioRad Gene Pulser apparatus (BioRad Laboratories, CA, USA), and conditions for electroporation were 1.5 kV, 25 F, and 600 Ω (Margolin et al. 1997; Bhat et al. 2004). Sequencing was performed at the Genomics Core (UC Riverside, USA), or at the SciGenom Labs (Cochin, India) and Eurofins Genomics India Pvt. Ltd. (Bangalore, India) as indicated. Morphological studies, growth rate, aerial hyphae, hyphal morphology, carotenoid accumulation, and ultraviolet (UV) sensitivity assay were performed as described previously (Ryan et al. 1943; Zalokar 1954; Deka et al. 2011; Deka and Tamuli 2013; Kumar and Tamuli 2014; Laxmi and Tamuli 2015). Meiotic silencing assay was performed as described previously (Kumar and Tamuli 2014). The phenotypes of the crosses were examined on the petri plate lid under a microscope (Carl Zeiss, Germany) after 25 days and scored as fertile (produced thousands of ascospores), intermediate (produced few hundred ascospores) or barren (produced exceptionally few ascospores).

Construction of strains and generation of *cmd*^{RIP} mutant strains

The CaM (NCU04120) open reading frame (ORF) of 1016 bp was PCR amplified by using the primer pairs CMD-A-FOR and CMD-A-REV-GFP (Table 2) and cloned into the *Pac*I and *Sma*I restriction sites of pRS426PVG (P_{tcu-1}*::5xGly::V5::gfp*) vector (Ouyang et al. 2015) using the yeast strain FY834 and recombination cloning as described previously (Colot et al. 2006; Tamuli et al. 2016). Plasmid DNA isolated from the transformed yeast was used for transformation into *E. coli* DH5α ultracompetent cells, and plasmids isolated from these cells were confirmed by sequencing (Genomics Core, University of California Riverside). We isolated a plasmid construct P_{tcu-1}*::cmd::5xGly::V5::gfp* that was transformed into the *N. crassa* strain 51-IV-8a (Table 1). The initial heterokaryotic transformants were selected on sorbose medium (with VM containing 0.5% L-proline

Table 1 List of *Neurospora crassa* strains used in this study

Strain	Genotype	Reference
74-OR23-IVA	Wild type; *mat A*	FGSC 2489
ORS-SL6 a	Wild type; *mat a*	FGSC 4200
NCU04120	Δ*cmd::hph; mat a* (heterokaryon)	FGSC 11618
NCU09123	Δ*camk-1::hph; mat A*	FGSC 12547
NCU09123	Δ*camk-1::hph; mat a*	FGSC 12548
NCU02283	Δ*camk-2::hph; mat A*	FGSC 12449
NCU02283	Δ*camk-2::hph; mat a*	FGSC 12448
NCU06177	Δ*camk-3::hph; mat A*	FGSC 11536
NCU06177	Δ*camk-3::hph; mat a*	FGSC 11537
NCU09212	Δ*camk-4::hph; mat a*	FGSC 11545
17	Δ*camk-1::hph*Δ*camk-2::hph; mat a*	Kumar and Tamuli (2014)
21	Δ*camk-2::hph*Δ*camk-3::hph; mat A*	Kumar and Tamuli (2014)
Δ*Sad-1*	Δ*Sad-1::hph; mat A*	FGSC 8741
Δ*Sad-1*	Δ*Sad-1::hph; mat a*	FGSC 8740
51-IV-8a	Δ*rid-1::nat*; Δ*mus-51::hph; mat a*	Ouyang et al. (2015)
850	Δ*rid-1::nat*; Δ*pan-2::bar::*$P_{tcu\text{-}1}$*::cmd::V5::gfp; mat a*	This study
851	Δ*rid-1::nat*; Δ*pan-2::bar::*$P_{tcu\text{-}1}$*::cmd::V5::gfp; mat a*	This study
852	Δ*rid-1::nat*; Δ*pan-2:: bar::*$P_{tcu\text{-}1}$*::cmd::V5::gfp; mat a*	This study
853	Δ*rid-1::nat*; Δ*pan-2::bar::*$P_{tcu\text{-}1}$*::cmd::V5::gfp; mat a*	This study
854	Δ*rid-1::nat*; Δ*pan-2::bar::*$P_{tcu\text{-}1}$*::cmd::V5::gfp; mat a*	This study
24	Δ*pan-2::bar::*$P_{tcu\text{-}1}$*::cmd::V5::gfp; mat A*	This study
26	Δ*pan-2::bar::*$P_{tcu\text{-}1}$*::cmd*^{RIP}*::V5::gfp; mat A*	This study
38	Δ*pan-2::bar::*$P_{tcu\text{-}1}$*::cmd*^{RIP}*::V5::gfp; mat A*	This study
3	Δ*pan-2::bar::*$P_{tcu\text{-}1}$*::cmd*^{RIP}*::V5::gfp; mat A*	This study
6	Δ*rid-1::nat*; Δ*pan-2::bar::*$P_{tcu\text{-}1}$*::cmd*^{RIP}*::V5::gfp; mat a*	This study
9	Δ*pan-2::bar::*$P_{tcu\text{-}1}$*::cmd*^{RIP}*::V5::gfp; mat A*	This study
35	Δ*rid-1::nat*; Δ*pan-2::bar::*$P_{tcu\text{-}1}$*:: cmd*^{RIP}*::V5::gfp; mat a*	This study
50	Δ*rid-1::nat*; Δ*pan-2::bar::*$P_{tcu\text{-}1}$*::cmd*^{RIP}*::V5::gfp; mat a*	This study
55	Δ*pan-2::bar::*$P_{tcu\text{-}1}$*::cmd*^{RIP}*::V5::gfp; mat A*	This study
102	Δ*camk-2::hph; camk-2::bar; mat a*	This study
116	Δ*camk-2::hph; camk-2::bar; mat A*	This study
119	Δ*camk-2::hph; camk-2::bar; mat a*	This study
120	Δ*camk-2::hph; camk-2::bar; mat A*	This study
17	Δ*camk-2::hph; camk-2*^{S247A}*::bar; mat A*	This study
51	Δ*camk-2::hph; camk-2*^{S247A}*::bar; mat a*	This study
12	Δ*camk-2::hph; camk-2*^{T267A}*::bar; mat a*	This study
19	Δ*camk-2::hph; camk-2*^{T267A}*::bar; mat A*	This study
4	Δ*camk-2::hph; camk-2*^{L309D}*::bar; mat A*	This study
34	Δ*camk-2::hph; camk-2*^{L309D}*::bar; mat a*	This study
36	Δ*camk-2::hph; camk-2*^{L309D}*::bar; mat a*	This study
37	Δ*camk-2::hph; camk-2*^{L309D}*::bar; mat A*	This study
34-97-3	*upr-1; mat a*	Tamuli et al. (2006)

in lieu of NH_4NO_3) supplemented with basta (400 µg/ml) and pantothenate (0.01 mg/ml). Integration of the $P_{tcu\text{-}1}$*::cmd::5xGly::V5::gfp* construct at the *pantothenic acid-2* (*pan-2*) locus in the linkage group (LG) VI of the transformed strains was PCR verified using primers P_{tcu}-CaM-RIP-FP-3 and GFP-RV (Table 2). We crossed a heterokaryotic 51-IV-8a transformant strain, designated as 26-35-IV-8 of genotype [(Δ*rid-1::nat*; Δ*mus-51::hph mat a*) + (Δ*pan-2::bar::*$P_{tcu\text{-}1}$*::cmd::5xGly::V5::gfp; mat a*)], with the wild type; *mat A* strain, and isolated five homokaryotic strains (850, 851, 852, 853, and 854) containing the *cmd* construct in the *pan-2* locus (Table 1). We

Table 2 Primers used in this study

Primer	Sequence (5′→ 3′)
[a]CMD-A-FOR	ttcgcacacacatccccaaccaaccATGGTATGCTCATTCCTTATCTCGG
[b]CMD-A-REV-GFP	gttagggataggctttccgccgcctccgccCTTCTGCATCATGAGCTGGACGAAC
CaM-RIP-FP-1	ACCTCCATATCTACCACTTC
CaM-RIP-FP- 2	TCATCCACCACCAAGTTAGC
CaM-RIP-RP	GATCCCTTCACATCCGAATG
P_{tcu}-CaM-RIP-FP-3	TTGAGAACGAATCCTTCATC
GFP-RV	AACTTGTGGCCGTTTACGTC
[c]S247A-2283-F	GGCGCGGCGTC**G**C**G**GACAACGCC
[c]S247A-2283-R	GGCGTTGTCCG**C**G**A**CGCCGCGCC
[c]F-T267A-2283	GCCAAGCGCATG**G**C**C**GCCCACGAGG
[c]R-T267A-2283	CCTCGTGGGCGG**C**C**A**TGCGCTTGGC
[c]F-L309D-2283	AACTTTAATGCGAGAAGGACG**GAT**CATGCGGCTATCGATACAGTA
[c]R-L309D-2283	TACTGTATCGATAGCCGCATG**ATC**CGTCCTTCTCGCATTAAAGTT
3NCU2283F	GCAGCCGTGTCGATACAAAG
4NCU2283R	GTCAATGGTCAAGCACCTGC
16NCU02283F-HI	AGTACGAGATCGACGGAGGA
5HPHR	ATCCACTTAACGTTACTGAAATC
Seq-NCU02283F	CGTCGACATCTGGGCCTTGG
RT-NCU04120-F	GTGAGGCCTTCAAGGTGTTC
RT-NCU04120-R	CGTCATCAGTGAGCTTCTCG

[a,b] Sequences in lowercase in the primers CMD-A-FOR and CMD-A-REV-GFP are homologous to the sequences of P_{tcu-1} and the *5xGly::V5::gfp*, respectively, in the pRS426PVG/ptcu-1 vector (Ouyang et al. 2015)

[c] The target codon in the mutagenic primers is shown bold, and the nucleotides changed are underlined

generated these strains expressing the *cmd* gene under the P_{tcu-1} during our collaborative work at the Borkovich laboratory (UC Riverside, USA) in order to study the essential Ca^{2+}-signaling genes using a regulatable expression system (Tamuli et al. 2016). In these strains, induction and repression of the *cmd* gene are regulated, respectively, by the addition of bathocuproinedisulfonic acid (BCS), which is a copper chelator, and by addition of copper II sulfate ($CuSO_4$) that results in excess Cu^{2+}.

We obtained five homokaryotic strains of genotype Δ*rid-1::nat*; *Δpan-2::bar::*P_{tcu-1}*::cmd::V5::gfp; mat a* (strains 850, 851, 852, 853, and 854; Table 1) from the Borkovich laboratory and used further for generation of RIP mutants and for meiotic silencing assay. We performed the crosses involving the Δ*rid-1::nat*; Δ*pan-2::bar::*P_{tcu-1}*::cmd::v5::gfp; mat a* homokaryotic strains (strains 850 and 853; Table 1) with the wild type; *mat A* strain, and isolated two progenies (strains 24 and 26; Table 1) from the cross of the strain 850 with the wild type, and another progeny (strain 38; Table 1) from the cross of the strain 853 with the wild type. The strains 26 and 38 (Table 1) displayed slow growth phenotype in the initial screening (data not shown). Furthermore, we isolated the strain 35 (Table 1) from the cross of the strains 24 with 850, strains 3, 6, 9, and 50 (Table 1) from the cross of the strains 26 with 850, and the strain 55 from the cross of the strains 38 with 853 (Table 1) based on their initial slow growth phenotype (data not shown). Thus, we screened 208 progenies from these crosses and isolated eight strains (Supplementary Table 1) based on their initial slow growth phenotype (data not shown). These eight strains contain a tagged ectopic duplication of the *cmd* gene, containing an endogenous copy of the *cmd* gene in the LG V and its tagged ectopy copy at the *pan-2* locus in the LG VI. From these eight strains, a 1241-bp fragment of the *cmd* endogenous allele was PCR amplified using primer pairs CaM-RIP-FP-1 and CaM-RIP-RP, and a 1272-bp fragment of the tagged *cmd* construct in *pan-2* locus was PCR amplified using primer pairs P_{tcu}-CaM-RIP-FP-3 and GFP-RV, and PCR purified products were sequenced (SciGenom Labs, Cochin, India, and Eurofins Genomics India Pvt. Ltd. Bangalore, India) using the same pairs of primers used for the PCR amplification and the common primer CaM-RIP-FP-2 for sequencing of middle region of both endogenous and the ectopic copies of the *cmd* gene. The sequences of the cmd^{RIP} mutant alleles were aligned with the *cmd* gene sequence from the wild type to identify the mutations and deposited in GenBank with accession numbers KX009461-71 (Supplementary Table 1).

Site-directed mutagenesis of *camk-2* and transformation of *camk-2*^{S247A}, *camk-2*^{T267A} and *camk-2*^{L309D} constructs

The site-directed mutation of the *camk-2* was performed by using the pRK-2 (P_{T7}*::camk-2::bar*) construct (Kumar and Tamuli 2014). The mutagenic primers for site-directed mutation of the *camk-2* gene were designed by using QuikChange® Primer Design software (http://www.genomics.agilent.com/primerDesignProgram.jsp?&_requestid=247130). The procedure for generating the site-directed mutations was essentially as described in QuickChange® II site-directed mutagenesis protocol (Stratagene, CA, USA). Briefly, the mutational PCRs were performed using Phusion™ High-Fidelity DNA Polymerase (Finzymes, Finland) according to the manufacture's protocol, and mutagenic primer pairs S247A-2283-F and S247A-2283-R, F-T267A-2283 and R-T267A-2283, and F-L309D-2283 and R-L309D-2283 (Table 2) for the S247A, T267A, and L309D mutations, respectively, in the *camk-2* gene. The PCR products were digested with *Dpn*I restriction enzyme to digest the parental methylated and hemimethylated DNA template (unmutated) and then transformed into the *E. coli* DH5α (Hanahan 1985) ultracompetent cells for nick repair and plasmid isolation. The plasmid constructs pVL-2, pVL-3, and pVL-4 containing the *camk-2*^{S247A}, *camk-2*^{T267A}, and *camk-2*^{L309D} mutations, respectively, were isolated and confirmed by sequencing using the primer Seq-NCU02283F (Table 2; SciGenom Labs, Cochin, India, and Eurofins Genomics India Pvt. Ltd., Bangalore, India). The GenBank accession numbers for the *camk-2*^{S247A}, *camk-2*^{T267A}, and *camk-2*^{L309D} mutant alleles are KX021884, KX021885, and KX021886, respectively. The pVL-2, pVL-3, and pVL-4 plasmids were transformed into the Δ*camk-2::hph; mat A* recipient strain by electroporation as described above, and initial heterokaryotic transformants were selected on sorbose plate containing basta (400 μg/ml). We isolated four initial heterokaryotic transformants that were verified by PCR using primer pairs 3NCU02283F and 4NCU02283R (Table 2), and these strains were crossed with the Δ*camk-2::hph; mat a* mutant to generate the homokaryotic strain. From these crosses, 12 homokaryotic progenies were isolated (Table 1), and genotype of these progenies was verified by PCR (data not shown) using primers 3NCU02283F and 4NCU02283R (Table 2) for the site-directed mutant alleles, and primers 16NCU02283F-HI and 5HPHR (Deka et al. 2011; Table 2) for the Δ*camk-2::hph* allele as described previously (Kumar and Tamuli 2014).

Isolation of RNA and real-time PCR

RNA from *N. crassa* was isolated as described previously (http://www.fgsc.net/fgn37/sokol.html), and purity was determined by verifying that the A260/A280 ratio was two or more. One μg of total RNA was used to synthesize cDNA by using Verso cDNA Synthesis Kit (Thermo Scientific, MA, USA) according to the manufacture's protocol. Real-time PCR was performed in an ABI 7500 Fast Real-Time PCR System (Applied Biosystems, CA, USA) with the SYBR® Select Master Mix (Applied Biosystems, CA, USA) using 100 ng of cDNA and 10 mM each of primers RT-NCU04120-F and RT-NCU04120-R (Table 2) in a final reaction volume of 15 μl. The $2^{-\Delta\Delta C_T}$ quantification method (Livak and Schmittgen 2001) was used to calculate the fold change expression of the *cmd* gene, using the β-tubulin gene as an endogenous control and wild type as calibrator.

Results

Isolation of a *cmd*^{RIP} mutant that showed defects in growth, aerial hyphae development, carotenoid accumulation, ultraviolet survival, and fertility

We isolated eight *cmd*^{RIP} mutants (described in Materials and methods), and these mutants contained both conventional (G:C to A:T) and nonconventional RIP-induced mutations in the *cmd* alleles (Supplementary Table 1). However, only the Δ*pan-2::bar::*$P_{tcu\text{-}1}$*::cmd*^{RIP}*::V5::gfp; mat A* (26) mutant contained nonsynonymous substitutions in both the endogenous and ectopic copies of the *cmd* gene, and therefore, we used this mutant for subsequent studies. Sequence analysis revealed D57Y and Q148H mutations in the endogenous copy, and M1W and E8K mutations in the ectopic copy of the *cmd* gene in the Δ*pan-2::bar::*$P_{tcu\text{-}1}$*::cmd*^{RIP}; *mat A* (26) mutant (Supplementary Fig. 1). In addition, the CaM::V5::GFP fusion protein was expressed in *N. crassa* strains (Supplementary Table 1; Supplementary Fig. 2). The Δ*pan-2::bar::*$P_{tcu\text{-}1}$*::cmd*^{RIP}; *mat A* (26) mutant showed an abnormal colony morphology with matty growth (Fig. 1). In addition, the growth rates of the wild type, the Δ*pan-2::bar::*$P_{tcu\text{-}1}$*::cmd; mat a* (850) parental strain, and the Δ*pan-2::bar::*$P_{tcu\text{-}1}$*::cmd*^{RIP}; *mat A* (26) mutant were 0.37 ± 0.21, 0.32 ± 0.02, and 0.10 ± 0.07 cm h^{-1} ($n = 3$), respectively, suggesting a slow growth phenotype of the Δ*pan-2::bar::*$P_{tcu\text{-}1}$*::cmd*^{RIP}; *mat A* (26) mutant (Fig. 2). Moreover, the Δ*pan-2::bar::*$P_{tcu\text{-}1}$*::cmd*^{RIP}; *mat A* (26) mutant produced very short aerial hyphae and carotenoid accumulation in this mutant was reduced by fourfold (Fig. 3). In addition, the Δ*pan-2::bar::*$P_{tcu\text{-}1}$*::cmd*^{RIP}*; mat A* (26) mutant showed a severe sensitivity to UV irradiation (Fig. 4). The UV sensitivity of the Δ*pan-2::bar::*$P_{tcu\text{-}1}$*::cmd*^{RIP}; *mat A* (26) mutant was similar to the *upr-1* mutant, suggesting that CaM has a major role in UV-induced DNA damage repair process like the translesion DNA polymerase REV-3 encoded by the *upr-1* gene

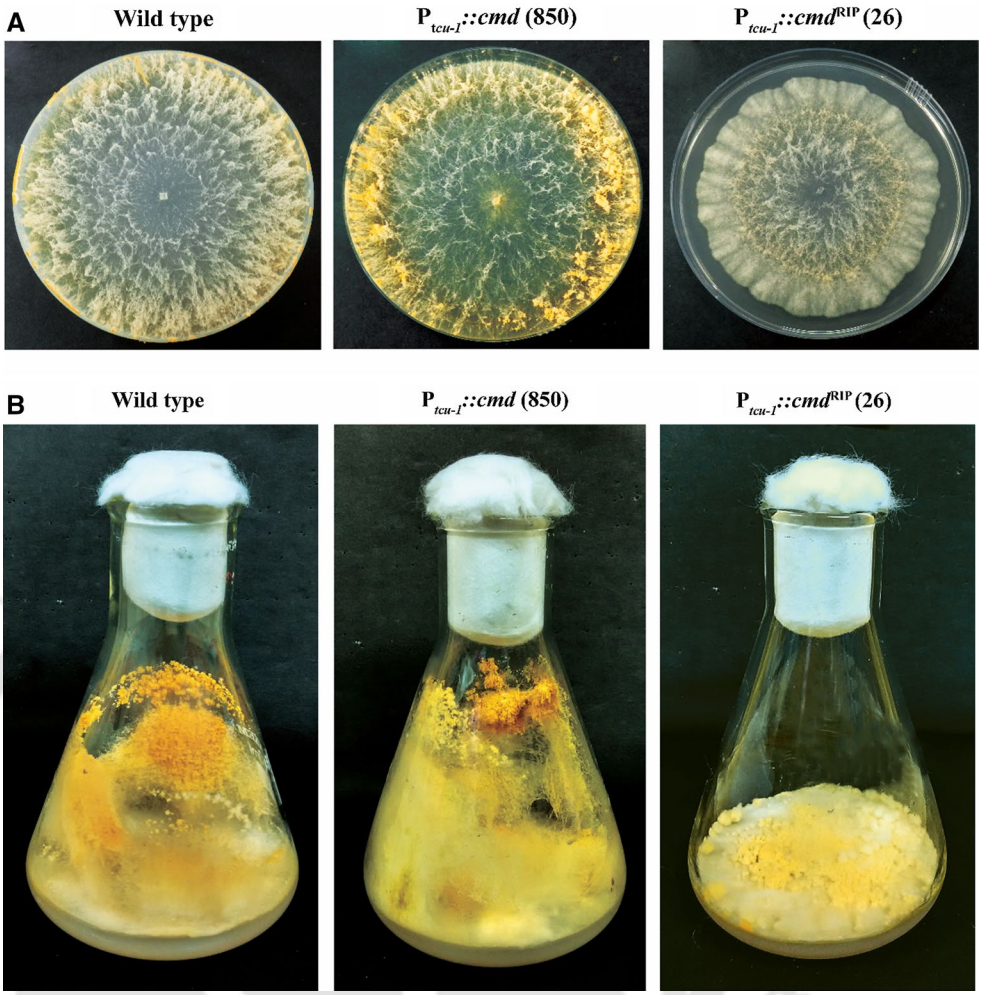

Fig. 1 Morphology of the *cmd*^{RIP} mutant. **a** Colony morphology. Wild type, P$_{tcu-1}$*::cmd::V5::gfp* (850) and P$_{tcu-1}$*::cmd*^{RIP}*::V5::gfp* (26) strains were cultured on VM agar plates supplemented with pantothenate (0.01 mg/ml) and BCS (250 μM). Strains were grown for 2 days at 30 °C in dark and 1 day in constant light at room temperature and photographed. **b** Growth in flask. The wild type, P$_{tcu-1}$*::cmd::V5::gfp* (850) and P$_{tcu-1}$*::cmd*^{RIP}*::V5::gfp* (26) strains were grown on VM agar plates supplemented with pantothenate (0.01 mg/ml) and BCS (250 μM) for 3 days at 30 °C in dark, followed by 3 days under constant light at room temperature and photographed

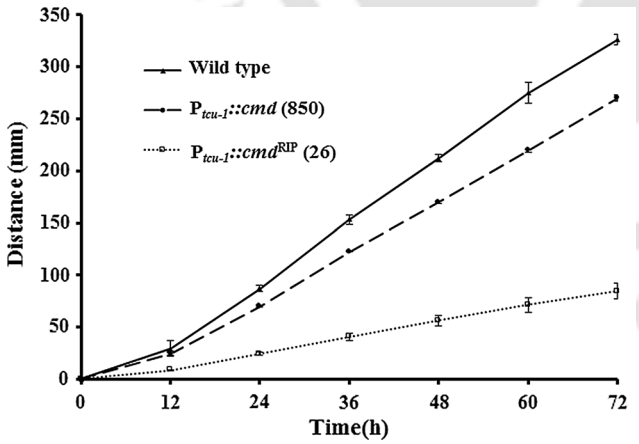

Fig. 2 The *cmd*^{RIP} mutant showed a slow growth rate. The *N. crassa* strains were grown in race tubes containing VM agar supplemented with pantothenate (0.01 mg/ml) and BCS (250 μM) and incubated at 30°C for 72 h. Each data point represents the mean of at least three independent experiments

(Sakai et al. 2002). Moreover, we observed a reduction in normal black ascospores and a significant increase in white ascospores in the crosses involving the Δ*pan-2::bar::* P$_{tcu-1}$*::cmd*^{RIP}; *mat A* (26) and the Δ*pan-2::bar::* P$_{tcu-1}$*::cmd*^{RIP}; *mat a* (35) mutants (data not shown).

Essential requirement of calmodulin for full fertility in *N. crassa*

We performed crosses involving strains engineered for inducing meiotic silencing of the *cmd* gene to understand its role in sexual development. The engineered Δ*pan-2::bar::*P$_{tcu-1}$*::cmd::V5::gfp* strains possess an endogenous *cmd* gene in the LG V and an ectopic copy of the *cmd* gene tagged with V5 and GFP under the P$_{tcu-1}$ in the *pan-2* locus in the LG VI (Fig. 5). The crosses involving the Δ*pan-2::bar::* P$_{tcu-1}$*::cmd::V5::gfp* strain with the wild type were barren (produced exceptionally few ascospores; Supplementary Table 2). However, crosses

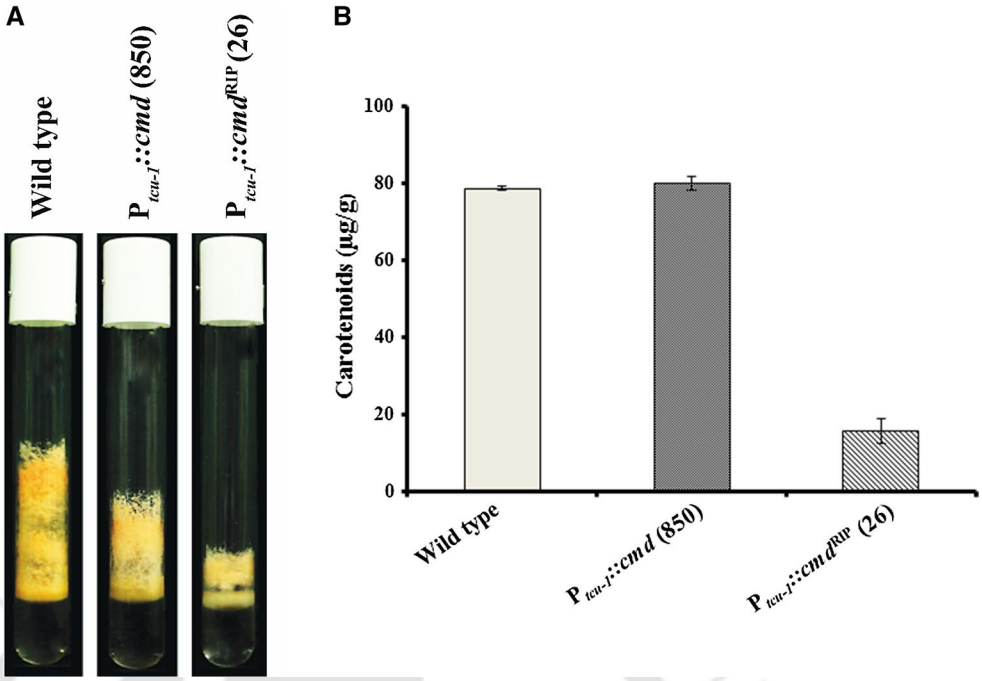

Fig. 3 Aerial hyphae growth and carotenoids accumulation in the *cmd*^{RIP} mutant. **a** Aerial hyphae growth. Wild type, $P_{tcu\text{-}1}$*::cmd::V5::gfp* (850) and $P_{tcu\text{-}1}$*::cmd*^{RIP}*::V5::gfp* (26) strains were grown on VM liquid medium supplemented with pantothenate (0.01 mg/ml) and BCS (250 µM). Cultures were grown for 3 days at 30 °C in dark and 4 days in constant light at room temperature and photographed. **b** Analysis of carotenoids content. Carotenoids content of wild type, $P_{tcu\text{-}1}$*::cmd::V5::gfp* (850) and $P_{tcu\text{-}1}$*::cmd*^{RIP}*::V5::gfp* (26) strains. Carotenoids were extracted and estimated in µg carotenoids per g of dry weight. Error bars show the standard errors calculated from the data for three independent experiments

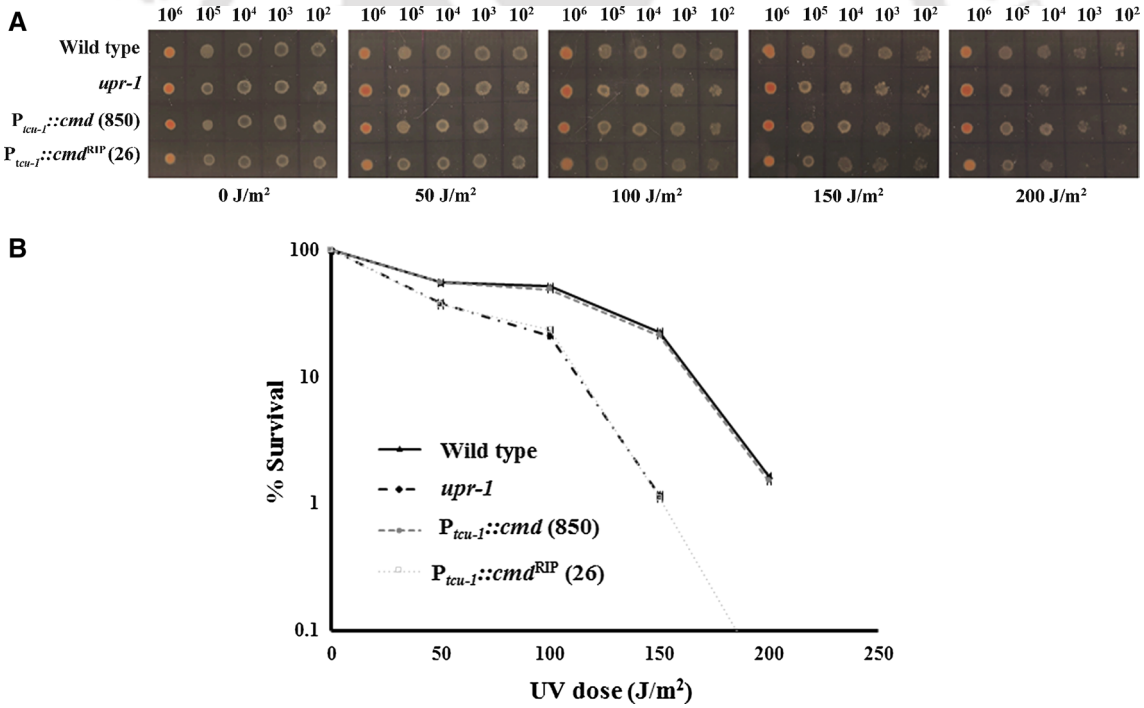

Fig. 4 UV survival assay of the *cmd*^{RIP} mutant. **a** Qualitative analysis of UV sensitivity. Approximately 10^5, 10^4, 10^3, 10^2, and 10^1 conidia were spotted from left to right on agar plates and irradiated with the indicated UV doses. The *upr-1* strain was used as a reference strain to compare the relative UV sensitivity of the $P_{tcu\text{-}1}$*::cmd*^{RIP}*::V5::gfp* (26) mutant. **b** Quantitative assay. Dose–response curves of the wild type, $P_{tcu\text{-}1}$*::cmd::V5::gfp* (850), $P_{tcu\text{-}1}$*::cmd*^{RIP}*::V5::gfp* (26) and the *upr-1* strain on exposure to UV irradiations. Each data point represents the mean of at least three independent experiments

homozygous for Δ*pan-2::bar::*$P_{tcu\text{-}1}$*::cmd::V5::gfp* were fertile phenotype (produced thousands of ascospores; Supplementary Table 2). In addition, crosses involving the Δ*pan-2::bar::*$P_{tcu\text{-}1}$*::cmd::V5::gfp* strain with the Δ*Sad-1* mutant, the semi-dominant suppressor of meiotic silencing, were fully fertile (Supplementary Table 2). These results

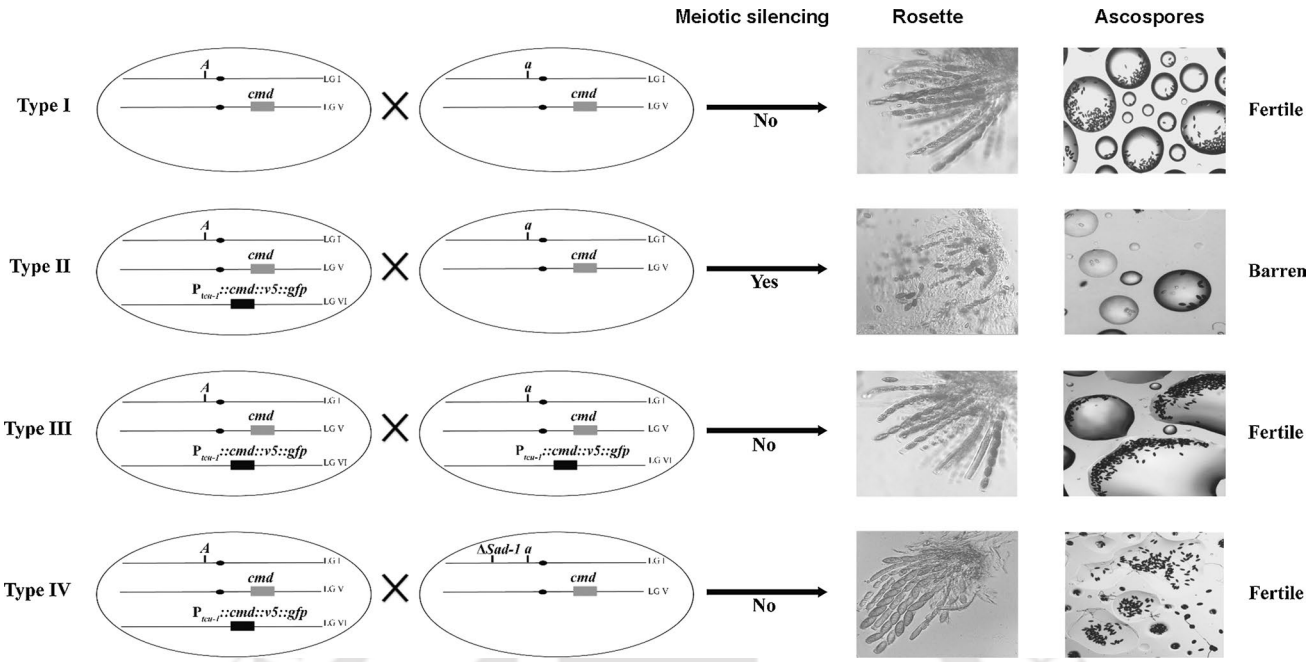

Fig. 5 Meiotic silencing assay of the *cmd* gene. Type 1 involves homozygous cross of the wild type strains of opposite mating type, each containing an endogenous *cmd* gene. Type 2 involves cross of $P_{tcu\text{-}1}$*::cmd::V5::gfp* strain with the wild type of opposite mating type. Type 3 is a homozygous cross of $P_{tcu\text{-}1}$*::cmd::V5::gfp* strains of opposite mating type. Type 4 involves cross of $P_{tcu\text{-}1}$*::cmd::V5::gfp* strain with Δ*Sad-1* of opposite mating type. Phenotype of the Type 2 cross was barren due to meiotic silencing of the *cmd* gene (the tagged ectopic *cmd* copy, $P_{tcu\text{-}1}$*::cmd::V5::gfp*, was unpaired). However, meiotic silencing was not occurred in both Type 3 (all copies of the *cmd* were paired in the homozygous cross) and Type 4 (due to the presence of the semi-dominant suppressor of meiotic silencing allele; Δ*Sad-1*) crosses, and therefore, these crosses were fully fertile. For each type of cross, representative images for a rosette of maturing asci and ejected ascospores on the lid of the petri dish examined under microscope are shown

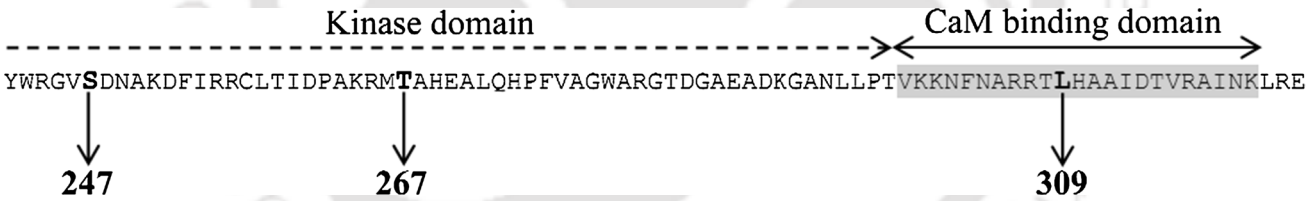

Fig. 6 Partial amino acid sequence of the CAMK-2 of *N. crassa.* The dash line and solid line represent the kinase domain and the CaM-binding region, respectively. The amino acid residues targeted for site-directed mutations are indicated with arrows

indicated meiotic silencing of the *cmd* gene in the heterozygous crosses, when a copy of the *cmd* gene remains unpaired, suggesting the requirement of CaM during meiosis for full fertility.

Site-directed mutational analysis of calcium-/calmodulin-dependent kinase-2 revealed two important residues serine 247 and threonine 267

To identify its important amino acid residues, we performed site-directed mutational analysis of Ca^{2+}/CaMK-2 that contains a catalytic and an overlapping autoinhibitory and Ca^{2+}/CaM-binding domains, and plays an essential role for full fertility in *N. crassa* (Deka et al. 2011; Kumar and Tamuli 2014). In the rat Ca^{2+}/CaM kinase II, autophosphorylation of threonine 286, the adjacent phosphorylation site to the CaM-binding domain (Lin et al. 1987), was found essential for the kinase to become autonomous (Schworer et al. 1988; Hanson et al. 1989). Furthermore, phosphorylation at threonine 286 was followed by the phosphorylation at serine 279 in the rat Ca^{2+}/CaM kinase II (Miller et al. 1988; Hanson et al. 1989). In *N. crassa*, the threonine 267 and serine 247, containing the $^{R}_{K}XX^{T}_{S}$ consensus (Kim et al. 1998), were identified as the potential autophosphorylation sites adjacent to the CaM-binding domain (Tamuli et al. 2011; Deka et al. 2011; Kumar and Tamuli 2014; Fig. 6). We

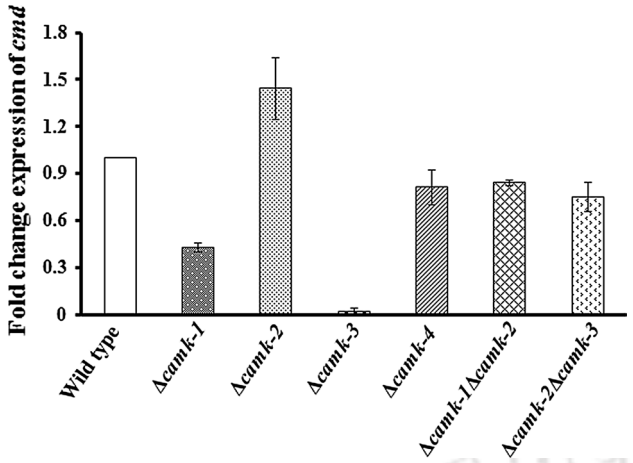

Fig. 7 Expression studies of the *cmd* gene using real-time PCR in the CaMKs knockout mutants. Fold change in expression profile of *cmd* gene in the wild type, and Δ*camk-1*, Δ*camk-2,* Δ*camk-3,* Δ*camk-4*, Δ*camk-1*Δ*camk-2*, and Δ*camk-2*Δ*camk-3* mutant strains. Fold change was calculated by $2^{-\Delta\Delta C_T}$ method, using wild type and β-tubulin as calibrator and endogenous control, respectively. Standard errors calculated from the data for two independent experiments are shown using error bars

generated *N. crassa* strains with S247A and T267A mutations in the putative phosphorylation sites in the catalytic domain, and L309D mutation in the CaM-binding domain of the CaMK-2 protein (Fig. 6). The homozygous crosses of the *camk-2*^{S247A} and the *camk-2*^{T267A} mutants or the crosses involving these mutants with the Δ*camk-2* mutant showed an intermediate phenotype (produced few hundreds of ascospores; Supplementary Table 3), suggesting an essential requirement of the serine 247 and threonine 267 phosphorylation sites for full fertility of *N. crassa*. However, the crosses homozygous for the *camk-2*^{L309D} mutant or its crosses with the Δ*camk-2* mutant were fertile (Supplementary Table 3), suggesting that the leucine 309 is dispensable for full fertility in *N. crassa*.

Expression analysis of the *cmd* gene in CaMKs single and double knockout mutant strains

We studied expression of *cmd* gene in the mutants for all the four known *camk* genes including the Δ*camk-1*Δ*camk-2* and Δ*camk-2*Δ*camk-3* double knockout mutants using real-time PCR (strains 17 and 21, Table 1; Kumar and Tamuli 2014). We found that the *cmd* gene was upregulated ~0.5-fold in Δ*camk-2* mutant and downregulated in the Δ*camk-1*, Δ*camk-3,* Δ*camk-4*, and in the double knockout mutants (Fig. 7). Fold change expression of the *cmd* gene was lowest in the Δ*camk-3* mutant. Therefore, expression of the *cmd* gene might compensate the absence of the *camk-2* gene product in *N. crassa*.

Discussion

In this study, we generated *N. crassa* strains to disrupt the *cmd* gene and identification of its critical amino acid residues using RIP, a gene silencing mechanism that causes multiple G:C to A:T mutations and methylation of remaining cytosine residues within the duplicated DNA sequences (Cambareri et al. 1989). The RIP-associated cytosine methylation can also spread into the adjacent flanking regions (Selker et al. 1993; Irelan and Selker 1997). We isolated eight RIP mutants containing both conventional (G:C to A:T) and nonconventional RIP mutations in the *cmd* gene, although, only one mutant was found to possess nonsynonymous substitutions in both copies of the *cmd* gene (Supplementary Table 1; Supplementary Fig. 1). However, we could not isolate a single progeny with in-frame stop codon within the *cmd* ORF, which further supports that the *cmd* gene is essential in *N. crassa*. Therefore, nuclei harboring a disrupted *cmd* gene could only be maintained in a heterokaryon form. The essential requirement of the *cmd* gene is also supported by the expression of the CaM^{RIP}::V5::GFP fusion protein that might be partially functional in the Δ*pan-2::bar::* P$_{tcu-1}$*:: cmd*^{RIP}*::V5::gfp; mat A* (26) mutant (Supplementary Fig. 2). Furthermore, the nonconventional RIP-induced mutations in the CaM could be due to the essential requirement of the sole *cmd* gene like the essential gene *poi-2* (*p*lenty *o*f *i*t) that also play a role during the vegetative growth and sexual development in *N. crassa* (Kim and Nelson 2005). Among the eight RIP-induced mutants, only the Δ*pan-2::bar::* P$_{tcu-1}$*::cmd*^{RIP}*::V5::gfp; mat A* (26) mutant contained mutations in both the copies of the *cmd* gene, with D57Y and Q148H mutations in the endogenous copy, and M1W and E8K mutations in the ectopic copy (Supplementary Table 1; Supplementary Fig. 1). The Δ*pan-2::bar::* P$_{tcu-1}$*::cmd*^{RIP}*::V5::gfp; mat A* (26) mutant showed a defect in colony morphology, reduce growth rate, aerial hyphae, and carotenoid accumulation (Figs. 1, 2, 3).

The Δ*pan-2::bar::*P$_{tcu-1}$*::cmd*^{RIP}*::V5::gfp; mat A* (26) mutant was severely sensitive to the UV irradiation like the *upr-1* mutant (Fig. 4). The *N. crassa* REV homolog genes *upr-1* (*ncrev3*), *mus-42* (*ncrev1*), and *mus-26* (*ncrev7*) play a role in DNA repair and UV mutagenesis through the bypass of (6-4) photoproducts (Sakai et al. 2002, 2003). Expression of *ncrev1* and *ncrev7* was found to be UV-inducible like the case of *upr-1* (Sakai et al. 2002, 2003). CaM mediates DNA repair by modulating the initial step of excision repair of UV-damaged DNA (Charp 1987) and H2AX phosphorylation in response to low-dose radiation exposure of RAW 264.7 macrophages (Smallwood et al. 2009). We found that the CaM protein has a role in UV-induced DNA damage repair process in *N. crassa*.

We also tested the requirement of the *cmd* gene during meiosis by performing crosses involving strains to induce meiotic silencing of the *cmd* gene (Fig. 5). We found that the crosses involving an unpaired copy of the *cmd* showed a barren phenotype, and this phenotype was suppressed both in the crosses homozygous for strains with an ectopic copy of the *cmd* gene, and in the heterozygous cross with the Δ*Sad-1* mutant (Supplementary Table 2). Therefore, in these crosses, meiotic silencing of the *cmd* gene was responsible for the barren phenotype, suggesting that the product of the *cmd* gene is essential during meiosis for full fertility in *N. crassa*. Meiotic silencing is a posttranscriptional gene silencing mechanism in *N. crassa*, where a gene not paired with a homolog in prophase I of meiosis generates a signal that transiently silences all sequences homologous to it by cleavage of the target mRNA (Shiu et al. 2001; Shiu and Metzenberg 2002). If any gene essential during meiosis is inserted ectopically into a wild type or innocuously marked strain and the resulting strain is crossed to wild type, this heterozygous cross should be barren. Therefore, meiotic silencing may provide insights into the function of genes necessary for meiosis, including genes for which a knockout construct would be lethal in vegetative phase of *N. crassa* (Shiu et al. 2001; Shiu and Metzenberg 2002).

We had also performed site-directed mutational analysis of CaMK-2 that was shown essential for full fertility in *N. crassa* to identify the key amino acid residues for fertility (Deka et al. 2011; Kumar and Tamuli 2014). CaMK-2 contains a kinase domain and overlapping autoinhibitory and CaM-binding domains (Deka et al. 2011; Kumar and Tamuli 2014). The CaMK-2 also contains nine potential serine/threonine autophosphorylation sites (Deka et al. 2011; Kumar and Tamuli 2014). We replaced two putative inhibitory autophosphorylation sites of CaMK-2 with nonphosphorylable alanine and examined its effects on fertility of *N. crassa*. In the rat Ca^{2+}/CaM kinase II, threonine 286, which is adjacent to the CaM-binding domain (Lin et al. 1987), autophosphorylation is indispensable for transition to an autonomous kinase (Schworer et al. 1988; Hanson et al. 1989). In the absence of autophosphorylation, such as in the T286L mutant, removal of Ca^{2+}/CaM results in a rapid deactivation of the kinase in COS cells (Hanson et al. 1989; Hanson and Schulman 1992). The initial phosphorylation at threonine 286 is followed by the phosphorylation at serine 279 in the rat Ca^{2+}/CaM kinase II (Miller et al. 1988; Hanson et al. 1989). In *N. crassa*, the threonine 267 and serine 247 are the potential autophosphorylation sites adjacent to the CaM-binding domain and contain the $^{R}_{K}XX^{T}_{S}$ consensus (Kim et al. 1998; Fig. 6). We found that crosses homozygous for the *camk-2*^{S247A} and *camk-2*^{T267A} mutants or cross of these mutants with the Δ*camk-2* mutant showed an intermediate phenotype, suggesting that the serine 247 and threonine 267 autophosphorylation sites are essential for full fertility in *N. crassa* (Supplementary Table 3). We also studied the effect of L309D mutation, located in the CaM-binding domain, of CaMK-2 in *N. crassa*. The CaM-binding sequences of the Ca^{2+}/CaM kinases usually contain basic and hydrophobic amino acid residues, but lack acidic amino acid residues (Colbran and Soderling 1990; Cruzalegui et al. 1992; Rhoads and Friedberg 1997; Tokumitsu et al. 2000). In the rat Ca^{2+}/CaMK kinase, mutations of three consecutive residues valine, lysine, and leucine to triple aspartic acid in the CaM-binding domain reduced the binding ability of Ca^{2+}/CaM, probably because of an intermolecular electrostatic repulsion (Tokumitsu et al. 1997, 2000). We found that the homozygous crosses of the *camk-2*^{L309D} mutant or its crosses with the Δ*camk-2* mutant were fully fertile (Supplementary Table 3), indicating that leucine 309 might be nonessential for CaMK-2 and CaM interaction, and dispensable full fertility of *N. crassa*.

Therefore, this study showed that the calmodulin gene has a role in vegetative growth, carotenoid accumulation, and UV survival, and fertility in *N. crassa*. Therefore, CaM is required for normal vegetative growth, survival in response to UV irradiation, and sexual development in *N. crassa.* The site-directed mutational analysis of CaMK-2 revealed that serine 247 and threonine 267 are important for full fertility in *N. crassa*. Expression analysis of the *cmd* gene in *camk* single and double mutants indicated their complex genetic interaction pattern. Future work will reveal molecular pathway of these genes function.

Acknowledgements The FGSC generously waived charges for the Neurospora strains. The FGSC was supported by NSF Grant BIR-9222772. VL was supported by a Research Fellowship from the Ministry of Human Resource Development (MHRD), Government of India (GoI). We thank Professor Katherine A. Borkovich (Department of Plant Pathology and Microbiology, Institute for Integrative Genome Biology, UC Riverside, CA, USA) for help in generating the *N. crassa* strains expressing the *cmd* gene under the P_{tcu-1}. We acknowledge partial financial supports from the IIT Guwahati, Department of Biotechnology, GoI (to RT; BT/PR3635/BCE/8/892/2012), the Indo-US Science and Technology Forum (to RT, 2013/30; http://www.iusstf.org/), and the National Institutes of Health (to KAB; http://www.nih.gov/).

References

Berridge MJ (1987) Inositol trisphosphate and diacylglycerol: two interacting second messengers. Annu Rev Biochem 56:159–193. doi:10.1146/annurev.bi.56.070187.001111

Bhat A, Tamuli R, Kasbekar DP (2004) Genetic transformation of *Neurospora tetrasperma*, demonstration of repeat-induced point mutation (RIP) in self-crosses and a screen for recessive RIP-defective mutants. Genetics 167:1155–1164. doi:10.1534/genetics.103.025171

Cambareri EB, Jensen BC, Schabtach E, Selker EU (1989) Repeat-induced G-C to A-T mutations in Neurospora. Science 244:1571–1575. doi:10.1126/science.2544994

Capelli N, Tuinen DV, Perez RO, Arrighi JF, Turian G (1993) Molecular cloning of a cDNA encoding CaM from *Neurospora crassa*. FEBS Lett 321:63–68. doi:10.1016/0014-5793(93)80622-2

Charp PA (1987) DNA repair in human cells: method for the determination of calmodulin involvement. Methods Enzymol 139:715–730. doi:10.1016/0076-6879(87)39122-0

Colbran RJ, Soderling TR (1990) Calcium/calmodulin-independent autophosphorylation sites of calcium/calmodulin-dependent protein kinase II. Studies on the effect of phosphorylation of threonine 305/306 and serine 314 on calmodulin binding using synthetic peptides. J Biol Chem 265:11213–11219

Colot HV, Park G, Turner GE, Ringelberg C, Crew CM, Litvinkova L, Weiss RL, Borkovich KA, Dunlap JC (2006) A high-throughput gene knockout procedure for Neurospora reveals functions for multiple transcription factors. Proc Natl Acad Sci USA 103:10352–10357. doi:10.1073/pnas.0601456103

Cox JA, Ferraz C, Demaille JG, Perez RO, van Tuinen D, Marme D (1982) Calmodulin from *Neurospora crassa*. General properties and conformational changes. J Biol Chem 257:10694–10700

Cruzalegui FH, Kapiloff MS, Morfin JP, Kemp BE, Rosenfeld MG, Means AR (1992) Regulation of intrasteric inhibition of the multifunctional calcium/calmodulin-dependent protein kinase. Proc Natl Acad Sci USA 89:12127–12131

Davies SA, Terhzaz S (2009) Organellar calcium signalling mechanisms in Drosophila epithelial function. J Exp Biol 212:387–400. doi:10.1242/jeb.024513

Davis RH, De Serres FJ (1970) Genetic and microbial research techniques for *Neurospora crassa*. Methods Enzymol 17:79–143. doi:10.1016/0076-6879(71)17168-6

Deka R, Kumar R, Tamuli R (2011) *Neurospora crassa* homologue of neuronal calcium sensor-1 has a role in growth, calcium stress tolerance, and ultraviolet survival. Genetica 139:885–894. doi:10.1007/s10709-011-9592-y

Deka R, Tamuli R (2013) *Neurospora crassa ncs-1*, *mid-1* and *nca-2* double-mutant phenotypes suggest diverse interaction among three Ca^{2+} -regulating gene products. J Genet 92:559–563

Gadd GM (1994) Signal transduction in fungi. In: Gow NAR, Gadd GM (eds) The growing fungus. Chapman and Hall, London, pp 183–210

Hanahan D (1985) Techniques for transformation of *E. coli*. In: Glover DM (ed) DNA cloning: a practical approach, 1st edn. IRL Press, Oxford, pp 109–135

Hanson PI, Schulman H (1992) Inhibitory autophosphorylation of multifunctional Ca^{2+}/calmodulin-dependent protein kinase analyzed by site-directed mutagenesis. J Biol Chem 267:17224–172161

Hanson PI, Kapiloff MS, Lou LL, Rosenfeld MG, Schulman H (1989) Expression of a multifunctional Ca^{2+}/calmodulin-dependent protein kinase and mutational analysis of its autoregulation. Neuron 3:59–70. doi:10.1016/0896-6273(89)90115-3

Higuchi S, Tamura J, Giri PR, Polli JW, Kincaid RL (1991) Calmodulin-dependent protein phosphatase from Neurospora crassa. Molecular cloning and expression of recombinant catalytic subunit. J Biol Chem 266:18104–18112

Hoffman L, Stein RA, Colbran RJ, Mchaourab HS (2011) Conformational changes underlying calcium/calmodulin-dependent protein kinase II activation. EMBO J 30:1251–1262. doi:10.1038/emboj.2011.40

Irelan JT, Selker EU (1997) Cytosine methylation associated with repeat-induced point mutation causes epigenetic gene silencing in *Neurospora crassa*. Genetics 146:509–523

Kim H, Nelson MA (2005) Molecular and functional analyses of *poi-2*, a novel gene highly expressed in sexual and perithecial tissues of *Neurospora crassa*. Eukaryot Cell 4:900–910. doi:10.1128/EC.4.5.900-910.2005

Kim YK, Li D, Kolattukudy PE (1998) Induction of Ca^{2+}-calmodulin signaling by hard-surface contact primes *Colletotrichum gloeosporioides* conidia to germinate and form appressoria. J Bacteriol 180:5144–5150

Kumar R, Tamuli R (2014) Calcium/calmodulin-dependent kinases are involved in growth, thermotolerance, oxidative stress survival, and fertility in *Neurospora crassa*. Arch Microbiol 196:295–305. doi:10.1007/s00203-014-0966-2

Lamb TM, Vickery J, Bell-Pedersen D (2013) Regulation of gene expression in *Neurospora crassa* with a copper responsive promoter. G3 (Bethesda) 3:2273–2280. doi:10.1534/g3.113.008821

Laxmi V, Tamuli R (2015) The *Neurospora crassa cmd, trm-9,* and *nca-2* genes play a role in growth, development, and survival in stress conditions. Genom Appl Biol 6:1–8. doi:10.5376/gab.2015.06.0007

Lin CR, Kapiloff MS, Durgerian S, Tatemoto K, Russo AF, Hanson P, Schulman H, Rosenfeld MG (1987) Molecular cloning of a brain-specific calcium/calmodulin-dependent protein kinase. Proc Natl Acad Sci USA 84:5962–5966

Livak KJ, Schmittgen TD (2001) Analysis of relative gene expression data using real-time quantitative PCR and the $2^{-\Delta\Delta C_T}$ method. Methods 25:402–408. doi:10.1006/meth.2001.1262

Margolin BS, Freitag M, Selker EU (1997) Improved plasmids for gene targeting at the *his-3* locus of *Neurospora crassa* by electroporation. Fungal Genet Newsl 44:34–36

McCluskey K, Wiest A, Plamann M (2010) The Fungal Genetics Stock Center: a repository for 50 years of fungal genetics research. J Biosci 35:119–126

Melnick MB, Melnick C, Lee M, Woodward DO (1993) Structure and sequence of the calmodulin gene from *Neurospora crassa*. Biochim Biophys Acta 1171:334–336. doi:10.1016/0167-4781(93)90079-S

Meyer T, Hanson PI, Stryer L, Schulman H (1992) Calmodulin trapping by calcium–calmodulin-dependent protein kinase. Science 256:1199–1202. doi:10.1126/science.256.5060.1199

Miller SG, Patton BL, Kennedy MB (1988) Sequences of autophosphorylation sites in neuronal type II CaM kinase that control Ca^{2+}-independent activity. Neuron 1:593–604. doi:10.1016/0896-6273(88)90109-2

Murray NE, Perkins DD (1963) Stanford Neurospora methods. Neurospora Newsl 4:21–25

Ortega Perez R, Van Tuinen D, Marmé D, Cox JA, Turian G (1981) Purification and identification of calmodulin from *Neurospora crassa*. FEBS Lett 133:205–208. doi:10.1016/0014-5793(81)80506-6

Ouyang S, Beecher CN, Wang K, Larive CK, Borkovich KA (2015) Metabolic impacts of using nitrogen and copper-regulated promoters to regulate gene expression in *Neurospora crassa*. G3 (Bethesda) 5:1899–1908. doi:10.1534/g3.115.020073

Reig JA, Tellezinon MT, Flawia MM, Torres HN (1984) Activation of *Neurospora crassa* soluble adenylate cyclase by calmodulin. Biochem J 221:541–543. doi:10.1042/bj2210541

Rhoads AR, Friedberg F (1997) Sequence motifs for calmodulin recognition. FASEB J 11:331–340

Ryan FJ, Beadle GW, Tatum EL (1943) The tube method of measuring the growth rate of Neurospora. Am J Bot 30:784–799

Sadakane Y, Nakashima H (1996) Light-induced phase shifting of the circadian conidiation rhythm is inhibited by calmodulin antagonists in *Neurospora crassa*. J Biol Rhythms 11:234–240. doi:10.1177/074873049601100305

Sakai W, Ishii C, Inoue H (2002) The *upr-1* gene encodes a catalytic subunit of the DNA polymerase zeta which is involved in damage-induced mutagenesis in *Neurospora crassa*. Mol Genet Genom 267:401–408. doi:10.1007/s00438-002-0671-8

Sakai W, Wada Y, Naoi Y, Ishii C, Inoue H (2003) Isolation and genetic characterization of the *Neurospora crassa REV1*

and *REV7* homologs: evidence for involvement in damage-induced mutagenesis. DNA Repair 2:337–346. doi:10.1016/S1568-7864(02)00223-9

Sanders D, Pelloux J, Brownlee C, Harper JF (2002) Calcium at the crossroads of signaling. Plant Cell 14:S401–S417. doi:10.1105/tpc.002899

Schworer CM, Colbran RJ, Keefer JR, Soderling TR (1988) Ca^{2+}/calmodulin-dependent protein kinase II. Identification of a regulatory autophosphorylation site adjacent to the inhibitory and calmodulin-binding domains. J Biol Chem 263:13486–13489

Selker EU, Fritz DY, Singer MJ (1993) Dense nonsymmetrical DNA methylation resulting from repeat-induced point mutation in Neurospora. Science 262:1724–1728. doi:10.1126/science.8259516

Shiu PK, Metzenberg RL (2002) Meiotic silencing by unpaired DNA: properties, regulation and suppression. Genetics 161:1483–1495

Shiu PK, Raju NB, Zickler D, Metzenberg RL (2001) Meiotic silencing by unpaired DNA. Cell 107:905–916. doi:10.1016/S0092-8674(01)00609-2

Smallwood HS, Lopez-Ferrer D, Eberlein PE, Watson DJ, Squier TC (2009) Calmodulin mediates DNA repair pathways involving H2AX in response to low-dose radiation exposure of RAW 264.7 macrophages. Chem Res Toxicol 22:460–470. doi:10.1021/tx800236r

Suresh K, Subramanyam C (1997) A putative role for calmodulin in the activation of *Neurospora crassa* chitin synthase. FEMS Microbiol lett 150:95–100. doi:10.1111/j.1574-6968

Suzuki S, Katagiri S, Nakashima H (1996) Mutants with altered sensitivity to a calmodulin antagonist affect the circadian clock in *Neurospora crassa*. Genetics 143:1175–1180

Swulius MT, Waxham MN (2008) Ca^{2+}/calmodulin-dependent protein kinases. Cell Mol Life Sci 65:2637–2657. doi:10.1007/s00018-008-8086-2

Tamuli R, Ravindran C, Kasbekar DP (2006) Translesion DNA polymerases Pol zeta, Pol eta, Pol iota, Pol kappa and Rev1 are not essential for repeat-induced point mutation in *Neurospora crassa*. J Biosci 31:557–564

Tamuli R, Kumar R, Deka R (2011) Cellular roles of neuronal calcium sensor-1 and calcium/calmodulin-dependent kinases in fungi. J Basic Microbiol 51:120–128. doi:10.1002/jobm.201000184

Tamuli R, Kumar R, Srivastava DA, Deka R (2013) Calcium signaling. In: Kasbekar DP, McCluskey K (eds) Neurospora: genomics and molecular biology. Caister Academic Press, Norfolk, pp 35–57

Tamuli R, Deka R, Borkovich KA (2016) Calcineurin subunits A and B interact to regulate growth and asexual and sexual development in *Neurospora crassa*. PLoS ONE 11:e0151867. doi:10.1371/journal.pone.0151867

Tellezinon MT, Ulloa RM, Glikin GC, Torres HN (1985) Characterization of *Neurospora crassa* cyclic AMP phosphodiesterase activated by calmodulin. Biochem J 232:425–430. doi:10.1042/bj2320425

Tokumitsu H, Wayman GA, Muramatsu M, Soderling TR (1997) Calcium/calmodulin-dependent protein kinase kinase: identification of regulatory domains. Biochemistry 36:12823–12827

Tokumitsu H, Muramatsu M, Ikura M, Kobayashi R (2000) Regulatory mechanism of Ca^{2+}/calmodulin-dependent protein kinase kinase. J Biol Chem 275:20090–20095. doi:10.1074/jbc.M002193200

Tuinen DV, Perez RO, Marme D, Turian G (1984) Calcium, calmodulin-dependent protein phosphorylation in *Neurospora crassa*. FEBS Lett 176:317–320. doi:10.1016/0014-5793(84)81187-4

Vogel HJ (1964) Distribution of lysine pathways among fungi: evolutionary implications. Am Nat 98:435–446

Westergaard M, Mitchell HK (1947) Neurospora V. A synthetic medium favoring sexual reproduction. Am J Bot 34:573–577. doi:10.2307/2437339

Zalokar M (1954) Studies on biosynthesis of carotenoids in *Neurospora crassa*. Arch Biochem Biophys 50:71–80. doi:10.1016/0003-9861(54)90010-7

The calmodulin gene in *Neurospora crassa* is required for normal vegetative growth, ultraviolet survival, and sexual development

Archives of Microbiology

Vijya Laxmi[1] and Ranjan Tamuli[1†]

[†]email: ranjantamuli@iitg.ernet.in, ranjan.tam@gmail.com

[1]Department of Biosciences and Bioengineering,

Indian Institute of Technology Guwahati,

Guwahati-781 039, Assam, India.

Supplementary Table 1 Sequence analysis of *cmd*^{RIP} mutant allele

cmd^{RIP} mutant strain	*cmd* allele	GenBank accession number (if any)	Total Number of nucleotides mutated	Altered amino acids
Δ*pan-2::bar::*P$_{tcu-1}$*::cmd*^{RIP}*::V5::gfp; mat A* (3)	*cmd* (endogenous)	-	None	None
	P$_{tcu-1}$*::cmd*^{RIP}*::V5::gfp* (ectopic)	KX009461	100	M1W, A2G, S4P, E8K, Q9R, K14R, S18P, F20L, K22R, D25E, I28F, V36A, M37L, G41A, N43T, E46K, E48D, V56A, D59N, T63P, I64F
Δ*rid-1::nat*; Δ*pan-2::bar::*P$_{tcu-1}$*::cmd*^{RIP}*::V5::gfp; mat a* (6)	*cmd* (endogenous)	-	None	None
	P$_{tcu-1}$*::cmd*^{RIP}*::V5::gfp* (ectopic)	KX009462	83	M1W, A2G, S4P, E8K, S11P, E12K, K14R, S18P, F20L,

				M37L, N43T, E46K, E48D, L49F, D59N, N61T, I64F, P67L
Δ*pan-2::bar::*P$_{tcu-1}$*::cmd*^{RIP}*::V5::gfp; mat A* (9)	*cmd*^{RIP} (endogenous)	KX009469	1	None
	P$_{tcu-1}$*::cmd*^{RIP}*::V5::gfp* (ectopic)	KX009463	98	M1W, A2G, E8N, Q9R, E12D, K14R, S18P, D25E, K31R, V36A, S39P, E46K, E48K, E55K, V56A, D59N, N61T, T63P
Δ*pan-2::bar::*P$_{tcu-1}$*::cmd*^{RIP}*::V5::gfp; mat A* (26)	*cmd*^{RIP} (endogenous)	KX009470	2	D57Y, Q148H
	P$_{tcu-1}$*::cmd*^{RIP}*::V5::gfp* (ectopic)	KX009464	11	M1W, E8K
	cmd (endogenous)	-	None	None

Δ*rid-1::nat*; Δ*pan-2::bar::*P$_{tcu-1}$*::cmd*^{RIP}*::V5::gfp; mat a* (35)	P$_{tcu-1}$*:: cmd*^{RIP}*::V5::gfp* (ectopic)	KX009465	97	M1W, A2G, S4P, E8K, E12D, K14R, S18P, D25E, I28F, T29P, T30P, K31R, L33F, T35P, M37L, L40W, N43T, E46K, E48D, M52L, N54T, I64F, P67L
Δ*pan-2::bar::*P$_{tcu-1}$*::cmd*^{RIP}*::V5::gfp; mat A* (38)	*cmd* (endogenous)	-	None	None
	P$_{tcu-1}$*:: cmd*^{RIP}*::V5::gfp* (ectopic)	KX009466	81	M1W, A2G, E8K, E12N, K14R, S18P, V36F, L40W, N43T, E48D, V56A,D59N, N61T, P67L, L70F
Δ*rid-1::nat*; Δ*pan-2::bar::*P$_{tcu-1}$*:: cmd*^{RIP}*::V5::gfp; mat a* (50)	*cmd* (endogenous)	-	None	None
	P$_{tcu-1}$*:: cmd*^{RIP}*::V5::gfp* (ectopic)	KX009467	121	M1W, A2G, D3N, E8K, E12N, K14R, S18P, K22R, D25E, I28F, T30P, E32D,

				L33F, M37W, R38P, N43T, E46K, E48N, L49F, D57N, D59N, N61T, T63P
Δ*pan-2::bar::*P$_{tcu-1}$*::cmd*^{RIP}*::V5::gfp; mat A* (55)	*cmd*^{RIP} (endogenous)	KX009471	1	None
	P$_{tcu-1}$*::cmd*^{RIP}*::V5::gfp* (ectopic)	KX009468	72	M1R, A2G, E8K, E12N, K14R, S18P, K31R, M37L, E46N, D57N, D59N

Supplementary Table 2 Phenotypes of crosses involving strains inducing meiotic silencing of *cmd*

Cross	Meiotic Silencing (Yes/No)	Phenotype
Wild type; *mat A* X Wild type; *mat a*	No	Fertile
Δ*Sad-1::hph; mat A* X Δ*Sad-1::hph; mat a*	No	Sterile
Δ*Sad-1::hph; mat A* X Wild type; *mat a*	No	Fertile
Δ*Sad-1::hph; mat a* X Wild type; *mat A*	No	Fertile
Δ*pan-2::bar::*P_{tcu-1}*::cmd::v5::gfp; mat a* (850) X Wild type; *mat A*	Yes	Barren
Δ*pan-2::bar::*P_{tcu-1}*::cmd::v5::gfp; mat a* (850) X Δ*Sad-1::hph; mat A*	No	Fertile
Δ*pan-2::bar::*P_{tcu-1}*::cmd::v5::gfp; mat A* (24) X Wild type; *mat a*	Yes	Barren
Δ*pan-2::bar::*P_{tcu-1}*::cmd::v5::gfp; mat A* (24) X Δ*Sad-1::hph; mat a*	No	Fertile
Δ*pan-2::bar::*P_{tcu-1}*::cmd::v5::gfp; mat a* (850) X Δ*pan-2:: bar::*P_{tcu-1}*::cmd::v5::gfp; mat A* (24)	No	Fertile
Δ*pan-2::bar::*P_{tcu-1}*::cmd::v5::gfp; mat a* (851) X Wild type; *mat A*	Yes	Barren
Δ*pan-2::bar::*P_{tcu-1}*::cmd::v5::gfp; mat a* (851) X Δ*Sad-1::hph; mat A*	No	Fertile
Δ*pan-2::bar::*P_{tcu-1}*::cmd::v5::gfp; mat a* (851) X Δ*pan-2::bar::*P_{tcu-1}*::cmd::v5::gfp; mat A* (24)	No	Fertile
Δ*pan-2::bar::*P_{tcu-1}*::cmd::v5::gfp; mat a* (852) X Wild type; *mat A*	Yes	Barren
Δ*pan-2::bar::*P_{tcu-1}*::cmd::v5::gfp; mat a* (852) X Δ*Sad-1::hph; mat A*	No	Fertile

Δ*pan-2::bar::*P$_{tcu-1}$*::cmd::v5::gfp; mat a* (852) X Δ*pan-2::bar::*P$_{tcu-1}$*::cmd::v5::gfp; mat A* (24)	No	Fertile
Δ*pan-2::bar::*P$_{tcu-1}$*::cmd::v5::gfp; mat a* (853) X Wild type; *mat A*	Yes	Barren
Δ*pan-2::bar::*P$_{tcu-1}$*::cmd::v5::gfp; mat a* (853) X Δ*Sad-1::hph; mat A*	No	Fertile
Δ*pan-2::bar::*P$_{tcu-1}$*::cmd::v5::gfp; mat a* (853) X Δ*pan-2::bar::*P$_{tcu-1}$*::cmd::v5::gfp; mat A* (24)	No	Fertile
Δ*pan-2::bar::*P$_{tcu-1}$*::cmd::v5::gfp; mat a* (854) X Wild type; *mat A*	Yes	Barren
Δ*pan-2::bar::*P$_{tcu-1}$*::cmd::v5::gfp; mat a* (854) X Δ*Sad-1::hph; mat A*	No	Fertile
Δ*pan-2::bar::*P$_{tcu-1}$*::cmd::v5::gfp; mat a* (854) X Δ*pan-2::bar::*P$_{tcu-1}$*::cmd::v5::gfp; mat A* (24)	No	Fertile

Supplementary Table 3 Phenotype of crosses involving *camk-2* mutants

Female parent	Male Parent	Phenotype
Wild type; *mat A*	Wild type; *mat a*	Fertile
Δ*camk-2::hph; mat A*	Δ*camk-2::hph; mat a*	Barren
Δ*camk-2::hph; camk-2::bar; mat a* (102)	Wild type; *mat A*	Fertile
Δ*camk-2::hph; camk-2::bar; mat a* (119)	Wild type; *mat A*	Fertile
Δ*camk-2::hph; camk-2::bar; mat A* (116)	Wild type; *mat a*	Fertile
Δ*camk-2::hph; camk-2::bar; mat A* (120)	Wild type; *mat a*	Fertile
Δ*camk-2::hph; camk-2::bar; mat a* (102)	Δ*camk-2::hph; mat A*	Fertile
Δ*camk-2::hph; camk-2::bar; mat a* (119)	Δ*camk-2::hph; mat A*	Fertile
Δ*camk-2::hph; camk-2::bar; mat A* (116)	Δ*camk-2::hph; mat a*	Fertile
Δ*camk-2::hph; camk-2::bar; mat A* (120)	Δ*camk-2::hph; mat a*	Fertile
Δ*camk-2::hph; camk-2::bar; mat A* (120)	Δ*camk-2::hph; camk-2::bar; mat a* (102)	Fertile
Δ*camk-2::hph; camk-2::bar; mat a* (102)	Δ*camk-2::hph; camk-2::bar; mat A* (116)	Fertile
Δ*camk-2::hph; camk-2::bar; mat a* (119)	Δ*camk-2::hph; camk-2::bar; mat A* (120)	Fertile
Δ*camk-2::hph; camk-2*^{S247A}*::bar; mat A* (17)	Wild type; *mat a*	Fertile
Δ*camk-2::hph; camk-2*^{S247A}*::bar; mat a* (51)	Wild type; *mat A*	Fertile
Δ*camk-2::hph; camk-2*^{S247A}*::bar; mat A* (17)	Δ*camk-2::hph; camk-2*^{S247A}*::bar; mat a* (51)	Intermediate
Δ*camk-2::hph; camk-2*^{S247A}*::bar; mat A* (17)	Δ*camk-2::hph; mat a*	Intermediate

Δ*camk-2::hph; camk-2*^{S247A}*::bar; mat a* (51)	Δ*camk-2::hph; mat A*	Intermediate
Δ*camk-2::hph; camk-2*^{T267A}*::bar ; mat a* (12)	Wild type; *mat A*	Fertile
Δ*camk-2::hph; camk-2*^{T267A}*::bar; mat A* (19)	Wild type; *mat a*	Fertile
Δ*camk-2::hph; camk-2*^{T267A}*::bar; mat a* (12)	Δ*camk-2::hph; camk-2*^{T267A}*::bar; mat A* (19)	Intermediate
Δ*camk-2::hph; camk-2*^{T267A}*::bar; mat a* (12)	Δ*camk-2::hph; mat A*	Intermediate
Δ*camk-2::hph; camk-2*^{T267A}*::bar; mat A* (19)	Δ*camk-2::hph; mat a*	Intermediate
Δ*camk-2::hph; camk-2*^{L309D}*::bar; mat A* (4)	Wild type; *mat a*	Fertile
Δ*camk-2::hph; camk-2*^{L309D}*::bar; mat A* (37)	Wild type; *mat a*	Fertile
Δ*camk-2::hph; camk-2*^{L309D}*::bar; mat a* (34)	Wild type; *mat A*	Fertile
Δ*camk-2::hph; camk-2*^{L309D}*::bar; mat a* (36)	Wild type; *mat A*	Fertile
Δ*camk-2::hph; camk-2*^{L309D}*::bar; mat A* (4)	Δ*camk-2::hph; camk-2*^{L309D}*::bar; mat a* (34)	Fertile
Δ*camk-2::hph; camk-2*^{L309D}*::bar; mat A* (37)	Δ*camk-2::hph; camk-2*^{L309D}*::bar; mat a* (34)	Fertile
Δ*camk-2::hph; camk-2*^{L309D}*::bar; mat A* (37)	Δ*camk-2::hph; camk-2*^{L309D}*::bar; mat a* (36)	Fertile
Δ*camk-2::hph; camk-2*^{L309D}*::bar; mat A* (4)	Δ*camk-2::hph; camk-2*^{L309D}*::bar; mat a* (36)	Fertile
Δ*camk-2::hph; camk-2*^{L309D}*::bar; mat A* (4)	Δ*camk-2::hph; mat a*	Fertile
Δ*camk-2::hph; camk-2*^{L309D}*::bar ; mat A* (37)	Δ*camk-2::hph; mat a*	Fertile
Δ*camk-2::hph; camk-2*^{L309D}*::bar; mat a* (34)	Δ*camk-2::hph; mat A*	Fertile
Δ*camk-2::hph; camk-2*^{L309D}*::bar; mat a* (36)	Δ*camk-2::hph; mat A*	Fertile

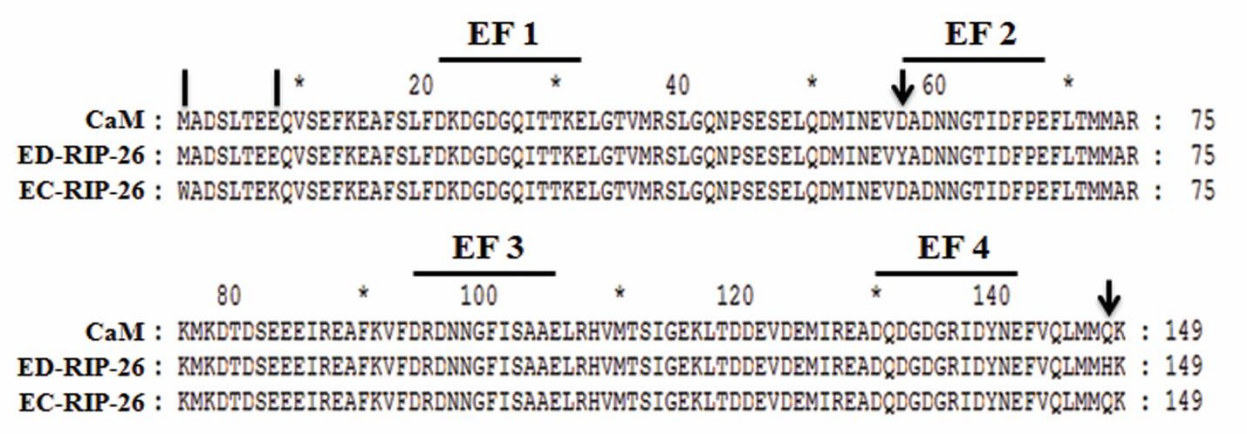

Supplementary Fig. 1 Alignment of the CaM protein sequence of the wild type and *cmd*^{RIP} mutant Δ*pan-2::bar::*P$_{tcu-1}$*:: cmd*^{RIP}*::V5::gfp; mat A* (26). The mutated amino acid residues in the endogenous (ED) and in the ectopic (EC) copies of the *cmd* gene are indicated by solid arrows and solid ticks, respectively, above the alignment. The horizontal lines above the alignment indicate the regions for the four EF-hand domains (EF1-4) in the CaM.

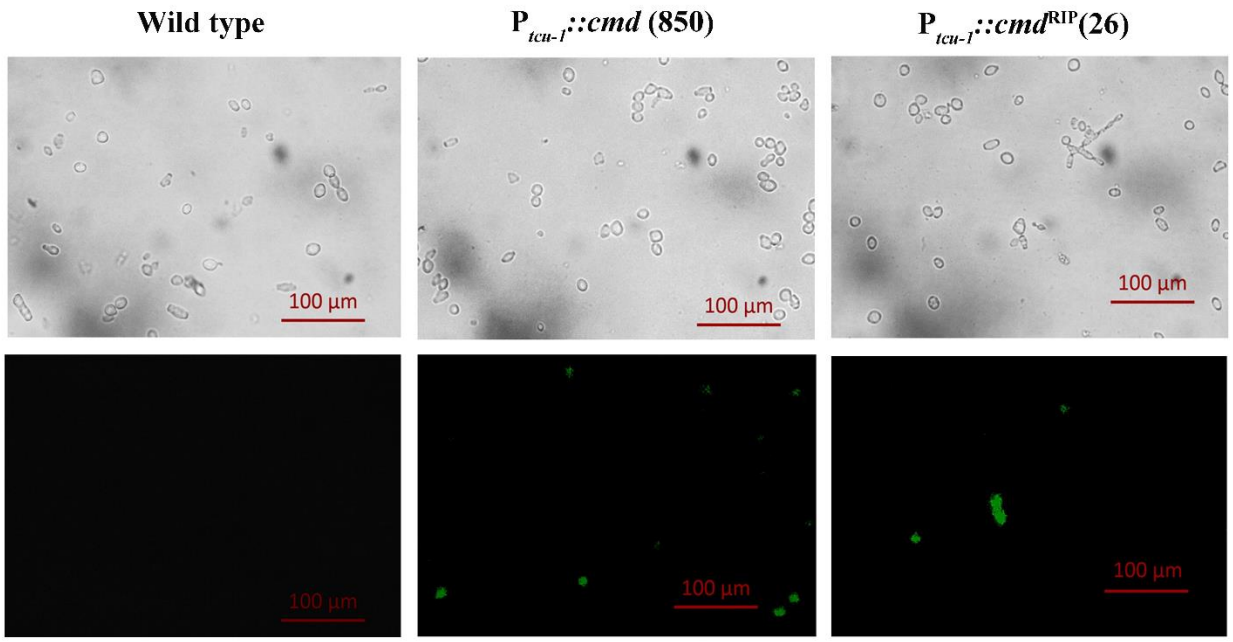

Supplementary Fig. 2 Expression of the CaM::V5::GFP protein under the P_{tcu-1} in *N. crassa* strains. The wild type, Δ*rid-1::nat*; Δ*pan-2::bar::*P_{tcu-1}*::cmd::V5::gfp; mat a* (850), and Δ*pan-2::bar::*P_{tcu-1}*:: cmd*^{RIP}*::V5::gfp; mat A* (26) strains were grown in 13 x 100 mm glass tubes containing VM agar supplemented with pantothenate (0.01 mg/ml) and BCS (250 µM), and grown for 3 days at 30°C in the dark followed by 4 days under constant light at room temperature. Conidia were harvested by using sterile water and analyzed by using a Trinocular inverted microscope (AxioVertA1FL, Carl Zeiss, Göttingen, Germany) with a 450–490 nm excitation filter and 515 nm emission filter and photographed with a CCD camera (ProgRess C5, JENOPTIK AG, Jena, Germany). Scale bar 100 µm.